Finn Aakre Haugen

Optimal Design, Operation and Control of an Anaerobic Digestion Reactor

Telemark University College

Faculty of Technology

PhD Dissertation:

Optimal Design, Operation and Control of an Anaerobic Digestion Reactor

Finn Aakre Haugen
Telemark University College, Norway

February 24, 2014

Contents

Controllers **171**

Preface

This dissertation is submitted for the academic degree of Philosophiae Doctor (PhD) in the PhD study programme *Process, Energy and Automation Engineering* at *Telemark University College* (TUC), Norway.

The dissertation consists of two main parts. Part I gives an introduction to the research project. Part II consists of a collection of scientific articles which have been published or submitted for publication, including the background and the methods of each article.

It is assumed that the reader of this dissertation has basic knowledge about anaerobic digestion, mechanistic mathematical modeling, automatic control, and state estimation.

I have accomplished the study as a Research Fellow in a 3/4 employment in parallel with a 1/4 academic employment at Telemark University College, starting Fall 2009.

The research project is focused on a real pilot anaerobic digestion reactor at a specific, typical Norwegian dairy farm, namely Foss farm, and a planned full-scale reactor at the farm. Although these are specific applications, I hope that the results can be useful also for other similar applications.

To make the results as easily available as possible, the scientific articles produced, are published, or submitted for publication, only in scientific journals providing Open Access publication, which means that the articles are freely available on the Internet.

My background is mainly in the field of engineering cybernetics, which includes mathematical modeling, estimation and control of dynamic systems. The field of biological systems, more specifically: anaerobic digestion, has been new to me. The research has been application oriented, aiming at improving design, operation and control of anaerobic digestion

processes using model-based methods from engineering cybernetics and optimization, regarding the specific application mentioned as an application example.

I am grateful to have had the opportunity to accomplish this PhD study. I have learnt a lot. Hopefully, I have given some contributions. And it has been great fun!

Finn Aakre Haugen
Porsgrunn, Norway
February 24, 2014

Acknowledgements

I am thankful to many:

Thanks to professor Bernt Lie who has been my main supervisor. His vast knowledge, good judgements, and critical questions have been of great value. Also, I appreciate the freedom and flexibility allowed me in planning my PhD study.

Thanks to professor Rune Bakke who has been my co-supervisor. Being the head of the research activities in bioengineering at TUC, he has been a key figure in my and others' research in this field at TUC. I have learnt a lot from his expertise. Thanks to him for always sharing time and knowledge.

Thanks to Knut Vasdal at Foss farm who has played an invaluable role in my work. He has built the AD reactor at the farm on which my work is based, and he has been maintaining and operating the reactor continuously. I have learnt a lot from his practical and theoretical knowledge about biological processes through our numerous discussions.

Thanks to Eivind Fjelddalen who has built and mounted the control cabinets and most of the instruments. It is impressive to experience his mastery in practical electronics and instrumentation.

Thanks to Jon Hovland at the Tel-Tek research institute in Porsgrunn, Norway, who has always provided useful inputs using his deep insight in bioengineering.

Thanks to Wenche Bergland who has organized and supervised the laboratory analysis at TUC from which I have got essential data for the mathematical modeling. Thanks to Mehrdad Torabzadegan who has organized and accomplished much of the laboratory analysis. Thanks also to Nora Cecilie I. Furuvik, Hildegunn Hegna Haugen, and Carlos Dinamarca for maintaining the laboratory facilities, and to the many students in the master study in Environmental Engineering at TUC who

have worked in the laboratory and reported the data meticulously. Furthermore, thanks to Shadi Attar, Marta Duenas Diez, and Bjørn Glemmestad for useful discussions.

Thanks to the head of my department, Randi Toreskås Holta, for encouragement and providing space in my ordinary working hours for concentrated work. Thanks also to the administration at TUC, in particular Lars André Tokheim and Inger Kristiansen who lead the academic and administrative activities of the PhD study at TUC professionally.

Thanks to Jing Liu and Sten Strömberg at Bioprocess Control, Lund, Sweden, for useful discussions and information in the beginning of my PhD study.

My warmest thanks to my dear wife, Hong, who has always given me much support for my work. The family life, with her and our children, Heidi, Henning, Ida, Inge, and Daniel, has made a solid base for my efforts. Nonetheless, the hours and days lost is a sacrifice. Thanks to my mother, Inger, for her persistent encouragement, and to my brother, Knut, for his interest and pertinent questions about my progress :-) Thoughts go to my father, Tarjei, and brother, Dag. It would have been nice if they were with us.

Finally, I am thankful to former professor Jens Glad Balchen, my teacher in basic systems and control at Norwegian Institute of Technology[1], for introducing me and thousands of other students into the fascinating and powerful field of engineering cybernetics. In many ways, my career is due to him.

---

[1] Now the Norwegian University of Science and Technology

Summary

A pilot anaerobic digestion (AD) reactor fed with animal waste at a typical Norwegian dairy farm is constructed, and a full-scale reactor is planned. These reactors are of the UASB (upflow anaerobic sludge blanket) type. The main aims of the research project based on these reactors can be stated with the following questions. *For the pilot reactor*: How to design a control system for controlling the methane gas production to its setpoint, and how to keep the reactor at safe conditions as defined in terms of concentration of volatile fatty acids? How to control the reactor temperature to its setpoint? How to design and implement a state estimator to estimate state variables of the anaerobic digestion process which can not be measured directly, for use in control and monitoring systems? *For the planned full-scale reactor*: How to determine the optimal design and operation of a full-scale reactor able to process all the available biological resources, i.e. animal waste? The approach taken to answer these questions is mainly model-based, using practical experiments on the pilot reactor to evaluate the proposed solutions.

The main results are as follows. A mechanistic dynamic anaerobic digestion model, named the modified Hill model, has been adapted to the pilot reactor using steady-state and dynamic data from on-line sensors and laboratory analysis. The model is based on material balances of the biodegradable volatile solids, volatile fatty acids, acid generating microbes, and methane generating microbes. The main output variable of the model is the methane gas flow. A dynamic model for the reactor temperature based on an energy balance of the liquid is adapted to the pilot reactor.

It is demonstrated both in simulations and practical experiments that the produced methane gas flow depends on the reactor temperature, indicating a need for feedback temperature control. Simulations and practical experiments show that both on-off control and industry-standard PI control is appropriate for temperature control. Simulations indicate that feedforward control based on measurement of the ambient and influent

temperatures can improve the control substantially. The Skogestad method is the favoured open loop controller tuning method, while the Relaxed Ziegler-Nichols tuning method is the favoured closed loop tuning method compared with both the standard Ziegler-Nichols tuning method and the Tyreus-Luyben tuning method. Simulations indicate that for control system stability it is safe to tune the PI temperature controller at minimum flow.

The produced power is proportional to the produced methane gas flow, at fixed conditions. Therefore, a constant power production can be obtained by controlling the methane flow control to a setpoint. Conditions for safe operation of the reactor in terms of a maximum gas production, which corresponds to a maximum feed rate, are found using steady-state responses of dynamic simulations, taking into account the upper limit of the volatile fatty acids concentration recommended in the literature, namely 0.8 g/L. Both simulations and practical experiments indicate that both the on-off controller and the PI controller are viable controllers for methane gas flow control. The Skogestad method and the proposed Relaxed Ziegler-Nichols tuning method are the favoured controller tuning methods. Simulations show that for control system stability is is safe to tune the PI controller at the lowest feed rate.

A state estimator, also denoted a soft sensor, is implemented in the form of the Unscented Kalman Filter (UKF) algorithm based on the modified Hill model and using the continuous measurement of methane gas flow. The UKF also uses the measured reactor temperature and the known feed flow. The UKF estimates continuously the four model state variables of the modified Hill model, and an augmented state variable which is here the concentration of volatile solids of the influent. The Unscented Kalman Filter (UKF) algorithm is selected instead of the well-known Extended Kalman Filter as it can be used without any linearization of the nonlinear model.

Various model-based control systems have been designed using the modified Hill model and the UKF: One is a predictive control system aiming at controlling the methane gas flow to a setpoint which may be varied, e.g. due to changing produced power demands. Simulations indicate that, with a setpoint profile which is known in advance, the setpoint tracking performance of a predictive control system is considerably better comparing with PI control, which is as expected. With disturbance changes not known in advance, the disturbance compensation is not much better with predictive control compared with PI control, which also is as expected since no controller can take any predictive action for such disturbances. A successful practical application of the predictive controller

on the real pilot reactor is presented. Also, a predictive controller aiming at retaining the reactor at an operating point where the volatile fatty acids (VFA) concentration has a maximum allowable value, is designed, and compared with PI control based on feedback from VFA estimated with the UKF. Simulations indicate the PI control system and the predictive controller have similar performance, but the PI controller is much simpler. The VFA control system is not yet tested on the real reactor.

Optimal design and operation of the planned full-scale reactor are determined using optimization algorithms based on steady state simulations of the modified Hill AD model combined with models of the reactor temperature and heat exchanger temperatures based on energy balances. Maximum available feedstock is 6 m^3/d dairy waste. Three alternative optimization problems are solved: Maximization of produced methane gas flow, minimization of reactor volume, and maximization of power surplus. Constraints of the optimization problems are an upper limit of the VFA concentration, and an upper limit of the feed rate corresponding to a normal animal waste production at the farm. The most proper optimization problem appears to be minimization of the reactor volume, assuming that the feed rate is fixed at its upper limit and that the VFA concentration is at its upper limit. The optimal result is a power surplus of 49.8 MWh/y, a hydraulic retention time of 6.1 d, and a reactor temperature of 35.9 °C, assuming heat recovery with an heat exchanger, and perfect reactor heat transfer insulation. It is shown that the optimal solutions, i.e. the power surplus, are improved if the ratio of the solids (biomass) retention time (SRT) to the hydraulic retention time (HRT) is increased. Although not studied in this research project, this ratio may be increased by adding granules to the reactor.

Both in reactor temperature control and methane gas flow control, the original Ziegler-Nichols closed loop PI tuning settings give poor control system stability. To improve the stability, a modification of the PI settings is proposed based on a combination of the Skogestad tuning formulas for "integrator plus time-delay" processes and the ultimate gain and ultimate period from the Ziegler-Nichols tuning procedure. The modified settings are here denoted the Relaxed Ziegler-Nichols PI settings.

Part I – INTRODUCTION

Background of the research project

Aims at the national level in Norway

The Norwegian Government's Report to the Parliament (Stortingsmelding) no. 39, 2008-2009, *The Climate Changes – Agriculture as a Part of the Solution* (in Norwegian: *Klimaendringene – landbruket en del av løsningen*) states as an aim to use 30 percent of the animal waste for biogas production within year 2020. Research that is relevant to this aim is conducted at Telemark University College (TUC) and other Norwegian institutions.

In particular, TUC participates in the research project *Biogas Reactor Technology for Norwegian Agriculture* granted by the Norwegian Research Council (Norsk Forskningsråd)[2]. Some excerpts from the project description which relates to my own research are as follows: "In order to reduce the greenhouse gas emissions, much of the manure in Norway should be treated by anaerobic digestion (AD).... Increased loading is also possible if the process parameters are monitored online, making it possible with early and adequate response to environmental changes. The development and use of new sensor technology and process controlling system is another important part of the project. Effective UASB AD reactors equipped with advanced process control systems might be connected to the already existing farm infrastructure. These biofilm reactors have low investment cost and can operate at smaller farms. This technology is further developed for implementation in Norwegian agriculture."

My research, documented by this dissertation, attempts to contribute to the issues in the excerpt above. The specific research aims, and the approach taken, are stated later in the present part of the dissertation. Below, some key issues from the above excerpt are discussed.

---

[2]Project number: 208019. Project period: 2011–2015.

Why anaerobic digestion of animal waste?

A number of arguments in the favour of anaerobic digestion of animal waste, compared with no special treatment, i.e. using the waste as fertilizer directly and without any collection of biogas from the untreated waste, are:

1. **Energy and power production**: Methane gas (CH_4) is a product of anaerobic digestion of the waste, and can be combusted to release energy. Under ideal conditions, the energy contents of methane gas is 9.95 kWh/m^3, at standard temperature and pressure (STP). The produced energy can be used for heating and power generation, Deublein & Steinhauser (2010).

2. **Reduction of greenhouse gas emissions**: Animal waste releases CH_4, N_2O (nitrous oxide gas or laughing gas), and CO_2 (carbondioxide) gas into the atmosphere. According to the Norwegian Government's Report to the Parliament (Stortingsmelding) no. 34, 2006-2007, *Norwegian Climate Politics (Norsk klimapolitikk),* in Norway, approximately 9% of the total release of climate gases measured as CO_2 equivalents are due to activities in the agricultural sector. Of these 9%, slightly less than 50% is CH_4 gas release, and slightly less than 50% is N_2O gas release. Of the CH_4 gas release, approximately 13% is due to storage and dispersion of animal waste, while most of the remaining part (85%) is due to the natural digestion in the livestock. According to the *Fourth Assessment Report (AR4) of the Intergovernmental Panel on Climate Change (IPCC)*, 2007, the 100 year Global warming potential (GWP) of CH_4 is 25 times that of CO_2, and the GWP of N_2O is 298 times that of CO_2.

   Anaerobic digestion of animal waste can contribute to a reduction of these climate gas releases, by reducing CH_4 and by reducing N_2O. By AD of fresh waste, the direct release of CH_4 from the waste is of course reduced. Furthermore, roughly 76% of the carbon in the fed substrate is bound in (the total of) the CH_4 and CO_2 gases produced by the AD process, Deublein & Steinhauser (2010). The combustion of CH_4 produces H_2O and CO_2. The N_2O release may be reduced if the AD process effluent is inserted into the soil, where the inorganic nitrogen compounds, as NH_3 and NH_4-N, are converted into nitrate, a good fertilizer. If not inserted into the soil, NH_3 will be released, to produce N_2O, a strong greenhouse gas.

3. **Possibility of production of good fertilizer**: The AD process effluent is not necessarily a good fertilizer. It has actually a higher

concentration of inorganic nitrogen than that of the influent, due to the AD process degradation of proteins and amino-acids, Deublein & Steinhauser (2010). Indeed, laboratory analysis of samples taken from the pilot reactor studied in this project shows that the concentration of NH_4-N is larger in the effluent than in the influent: In the period January 9 – April 18, 2013, the average concentration of NH_4-N of 10 samples of the effluent is 1119 mg/L, while the average concentration of 10 samples of the influent in the same period is 841 mg/L. Furthermore, there is hardly no reduction of the odor in the effluent compared to that of the influent.

Although not the focus of this dissertation, it is here appropriate to point to the successful post-treatment of the AD process effluent which is implemented at Foss Biolab, cf. Figure 6. The effluent is fed to a nitrification reactor where oxygen is introduced to convert the inorganic nitrogen compounds, NH_3 and NH_4-N, into nitrate, NH_3O-, which is a good fertilizer. Furthermore, the emission of N_2O is reduced since N_2O is generated in a chemical reaction of NH_3, and the fertilizer is almost odorless.

Why UASB reactors?

Two commonly used types of AD reactors are:

- **CSTR** (Continuous stirred tank reactor), Tchobanoglous et al. (2003). In an ideal CSTR, the substrate and the biomass, or micro-organisms, are completely mixed. Thus, the hydraulic retention time (HRT) and the biomass retention time, commonly represented as the solids retention time (SRT) are equal. i.e. their ratio is equal to one:

$$\text{CSTR: } \frac{\text{SRT}}{\text{HRT}} = 1 \tag{1}$$

- **UASB reactors**, invented in the Netherlands by Lettinga and co-workers, Lettinga et al. (1980). In these reactors, the SRT is larger than the HRT:

$$\text{UASB reactors: } \frac{\text{SRT}}{\text{HRT}} > 1 \tag{2}$$

Figure 1 shows the principal construction of the UASB reactor used at Foss farm in this research project. The key characteristic of UASB reactors is the dense granulated sludge bed which retains the microorganisms, and
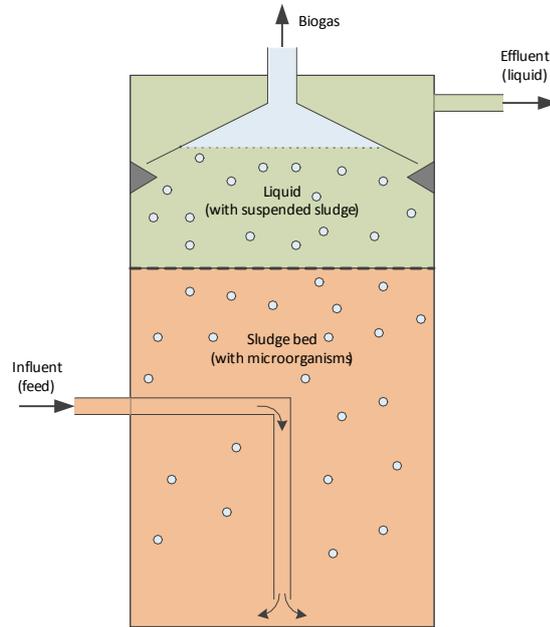
Figure 1: Principal construction of the UASB reactor used at Foss farm in this research project.

prevents them from being washed out of the reactor with the effluent. The formation of the granulated sludge is due to flocculation and gravity. There is no need for agitation of the sludge other than what is caused by the gas formation and the feed flow. Since the SRT is larger than the HRT for UASB reactors, their reactor volume can be made smaller, or, alternatively, their loading (feeding) rate can be higher compared with CSTRs.

As an illustration of the difference between CSTR and UASB reactors, design of the full-scale reactor, similar to the design made in Article no. 5, is accomplished. The minimum reactor volume, $V_{\min}$, is found from the requirement that the VFA concentration, S_{vfa}, is not exceeding 0.8 g/L which is a critical limit for safe, or "healthy", reactor operation, cf. Article no. 5. Three cases are considered, characterized by their different SRT/HRT ratio values. In Table 1, the SRT/HRT ratios are adjusted variables (optimization variables), underlined to distinguish them from variables having fixed values, while the volume is the objective, shown in frames. The ratio value of 2.9 for one of the UASB cases is the same value as is estimated for the real pilot reactor studied in this research project. The ratio value of 20 is an assumed possible maximum value, cf. Article no. 5. The reactor temperature, T_{reac}, and feed rate, F_{feed}, are fixed at the values shown in Table 1. In the table, also the methane gas production,

F_{meth}, is shown.[3] $V_{\min}$ is found from the steady state of dynamic simulations based on the modified Hill AD model, cf. Article no. 5.

Table 1: Minimum reactor volume for three different cases described in the text.

	Unit	**CSTR**	**UASB**	**UASB**
SRT/HRT	d/d	<u>1</u>	<u>2.9</u>	<u>20</u>
S_{vfa}	g/L	0.8	0.8	0.8
T_{reac}	°C	38	38	38
F_{feed}	m^3/d	4.2	4.2	4.2
F_{meth}	m^3/d	20.8	20.8	20.8
$\boxed{V_{\min}}$	m^3	$\boxed{74.0}$	$\boxed{25.6}$	$\boxed{3.8}$

Table 1 shows that $V_{\min}$ depends largely on the SRT/HRT ratio. The higher ratio, the smaller $V_{\min}$. Of course, constructional costs, and the power needed for daily operation of the reactor, are smaller if the reactor volume is smaller. This illustrates one important benefit of using UASB reactor comparing with using a CSTR.

How to design the UASB reactors?

Assuming that the whole amount the animal waste produced continuously at the farm, is to be fed to the reactor, what is the optimal reactor size? Here, "optimal" can be defined in a number of ways, for example, maximum methane gas production, or minimum reactor volume, or maximum power surplus taking into account the power needed to operate the reactor. A mathematical model of the reactor is very useful for reactor design. Model-based reactor design of a full-scale reactor at Foss farm is discussed in Article no. 6.

Why monitoring and control?

The importance of monitoring and control is explained briefly in the following:

Monitoring:

---

[3]F_{meth} is the same in all the cases because S_{vfa} has the same value in all of the cases and the concentrations of the methane producing microorganisms are the same in all of the cases.

- *Online measurements:* Monitoring in the form of online measurements can prevent shutdown of the reactor due to abnormal situations, for example feed or gas blockings.

- *State estimation:* Monitoring can be in the form of a state estimator, or soft sensor, which calculate online state variables that are not measured, using a combination of a proper mathematical model of the AD process and online measurement of one of more AD process output variables, typically biogas flow. Of course, only those variables which are included in the model can be estimated. In the mathematical model used in this project – the modified Hill model – the variables which can be estimated are the concentrations [g/L] of

  - biodegradable volatile solids,
  - volatile fatty acids (VFA),
  - acidogens (acid generating microbes), and
  - methanogens (methane generating microbes).

  Also the concentration of volatile solids in the reactor influent is estimated in this project. Among the above variables, the VFA concentration is the most important one because a high value indicate that the reactor has "poor health", as discussed in Article no. 3. Online measurement of the VFA concentration is possible, Madsen et al. (2011), but hardly a viable option for the applications in focus of this dissertation. State estimation of the pilot reactor is described in Article no. 4.

Control:

- *Biogas production control*: Under ideal conditions, the energy contents of methane gas at standard temperature and pressure (STP) is 9.95 kWh/m^3. Therefore, a specific power production by the reactor can be obtained by controlling the biogas flow to the corresponding setpoint using feedback control. To this end, industry standard controllers, like on-off and PI controllers, can be used. Improved control can be obtained with predictive control which is model-based control. On-off and PI biogas control are discussed in Article no. 3, while predictive control is discussed in Article no. 4.

- *Reactor temperature control*: Both simulations and experiments on the real pilot reactor indicate that both the dynamic and steady state methane gas production depend on the reactor temperature. Consequently, to operate the reactor under well-defined and fixed conditions, the reactor temperature must

be controlled to a proper setpoint. Reactor temperature control is discussed in Article no. 2.

Aims of the research project and the approach taken

Aims

The main aims of this research project are as follows. For the real pilot reactor and the planned full-scale reactor:

- How to design a control system for controlling F_{meth} to a setpoint, or, alternatively, to keep the reactor at safe conditions as defined in terms of S_{vfa}? Furthermore, there is a need for a control system to retain the reactor temperature at a setpoint.

- How to design and implement a state estimator to estimate state variables of the AD process which can not be measured directly, for use in control and monitoring systems?

- How to determine the optimal design and operation of a full-scale reactor able to process all the available biological resources, i.e. animal waste?

Approach

The approach taken to reach these aims is mainly model-based, see Figure 2. The mathematical model encapsulates only a part, of course, of the real process, which here is the AD reactor including the AD process taking place in the contents of the reactor, the reactor itself as a thermal system, auxiliary systems, e.g. pumps and heat exchanger for preheating the influent. With a model at hand, model-based tools are available for solving various problems. In this research project, models are used as follows:

- Control:
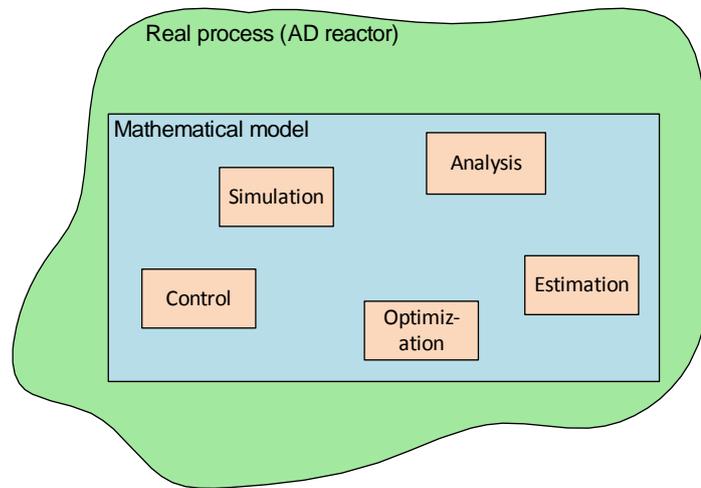
Figure 2: Illustration of the approach taken in this project.

    – Model-based PI controller tuning, articles 2, 3, 6, and 7.

    – Predictive control which inherently uses a process model to calculate optimal control signals, article 4.

- Estimation using the Kalman Filter algorithm, article 4.

- Optimization of design and operation, article 5.

- Analysis: In this project, models are used to analyze control systems in terms of stability margins of control systems, all articles except number 5.

- Simulations have been used for testing of control systems and state estimators in all articles about control and estimation, all articles.

Description of the biological and technical systems

Foss Biolab

The pilot AD reactor and the planned full-scale reactor are at Foss farm, Skien, Norway. The laboratory which includes the pilot reactor at the farm is denoted Foss Biolab. Figure 3 shows the farm, Figure 4 shows a part of the laboratory, and Figure 5 shows the control cabinet and the PC running the monitoring and control program.

Figure 3: Foss farm, Skien, Norway.

Figure 4: At Foss Biolab: The AD reactor is behind the nitrification reactor to the right in the picture.

Process description

The AD reactor is a part of the biological plant at Foss Biolab. Figure 6 shows a Piping & Instrumentation Diagram (P&ID) of the plant.

Input to the plant is dairy manure diluted with 25% water and filtered, and outputs are high quality fertilizer and biogas consisting of 70–75% methane. The plant is monitored and controlled with a PC running LabVIEW. The main parts of the plant are as follows (numbers refer to Figure 6).

1. A reservoir for raw dairy manure with approximately 25% added water.

2. A sieve (separator), a rotary filter designed by staff at Foss Biolab, to separate the manure into two fractions of similar total solid mass: > 70 % of the volume is wet fraction, and < 30 % is dry fraction.

3. A high rate UASB reactor fed with filtered cow manure as substrate for production of energy-rich biogas that contains mainly methane. Effective reactor volume is approximately 250 L. Figure 1 shows the construction of the reactor at Foss farm used in this research project.

Figure 5: Control cabinet, and PC running National Instruments LabVIEW software for monitoring and control.

4. A 200 L nitrification reactor fed with AD reactor effluent to produce high quality liquid fertilizer and pellets fertilizer from formed foam. The nitrification reactor is not included in this research project.

The present reactor has been in operation since April 2012, while a previous similar reactor was in operation from August 2011 until April 2012.

Monitoring and control system

Figure 7 shows a block diagram of the reactor and the monitoring and control system. The different parts of the block diagram are described in the following.

Sensors

FT-1: AD reactor effluent flow sensor (home-made) based on measuring the frequency of automatic effluent charge and discharge of a cup of
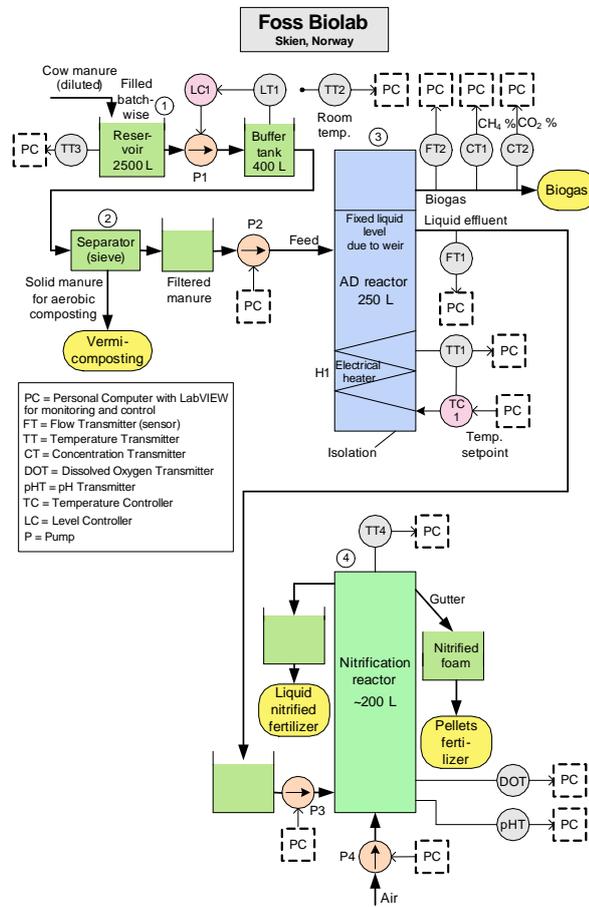
Figure 6: Piping & Instrumentation Diagram (P&ID) of the biological process line of the pilot plant at Foss Biolab.

fixed volume.

FT-2: Thermal biogas flow sensor.

CT-1: Infrared (IR)-based CH_4 gas concentration sensor.

CT-2: Infrared (IR)-based CO_2 gas concentration sensor.

TT-1: Pt100 reactor temperature sensor.

TT-2: Pt100 biolab room temperature sensor.

Actuators

P-1: A voltage controlled peristaltic pump which is operated using Pulse-width modulation (PWM). Figure 8 illustrates the principle of
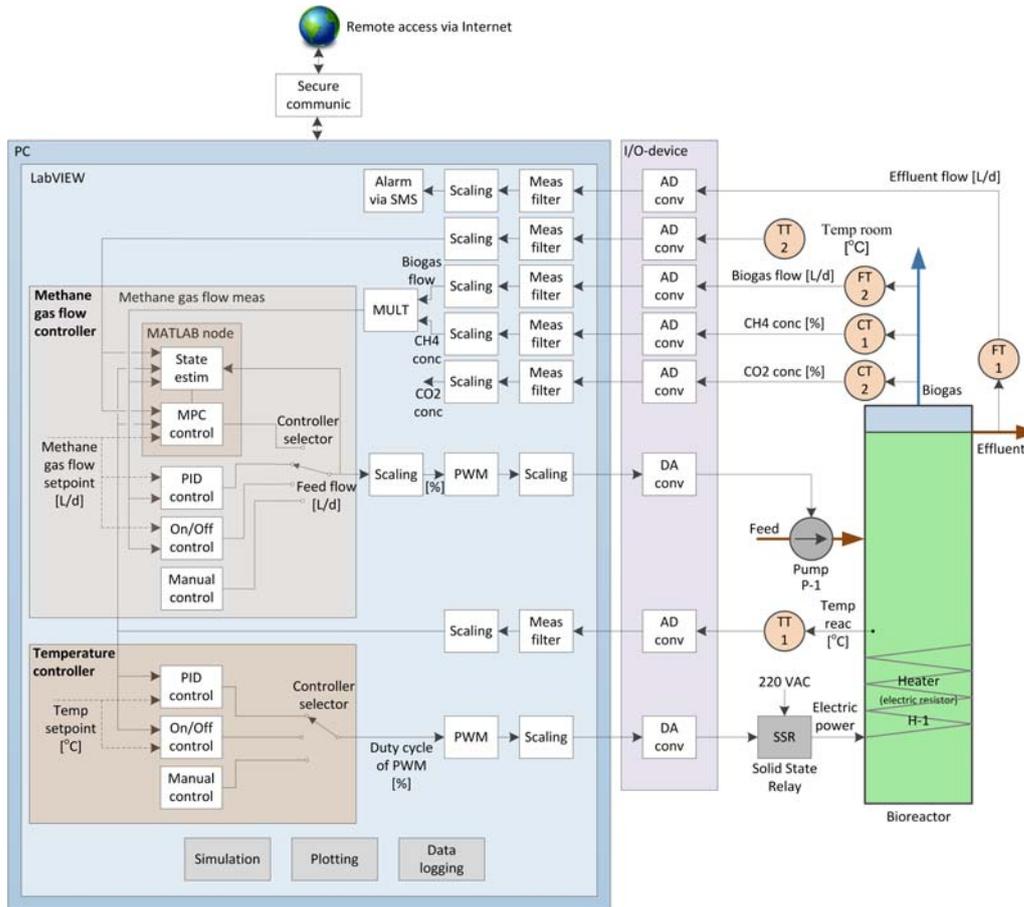
Figure 7: Monitoring and control system for the pilot AD reactor.

PWM. With PWM an approximately continuous or smooth control signal is obtained using factual binary control.

In the present application, the methane gas flow controller generates $F_{\text{feed}}^{\text{demand}}$, and the corresponding duty cycle, D, which is used as input to the PWM element, is calculated. The PWM element, which is implemented with the Square Wave Point-by-Point function in LabVIEW, sets the feed flow to $F_{\text{feed}_{\text{on}}}$ lasting for time T_{on} during the fixed duty cycle period, T_{p}, according to the value of D. In the mean, F_{feed} becomes approximately equal to $F_{\text{feed}}^{\text{demand}}$ if T_{p} is small compared to the time-constant of the process to be controlled, as is the case here. In the present application the PWM parameters are as follows: Fixed cycle time of 700 s, on-value of control signal corresponding to 714 L/d, and off-value corresponding to zero L/d.

There are several benefits of using PWM control compared with analog control: The calibration of the pump is needed only at one
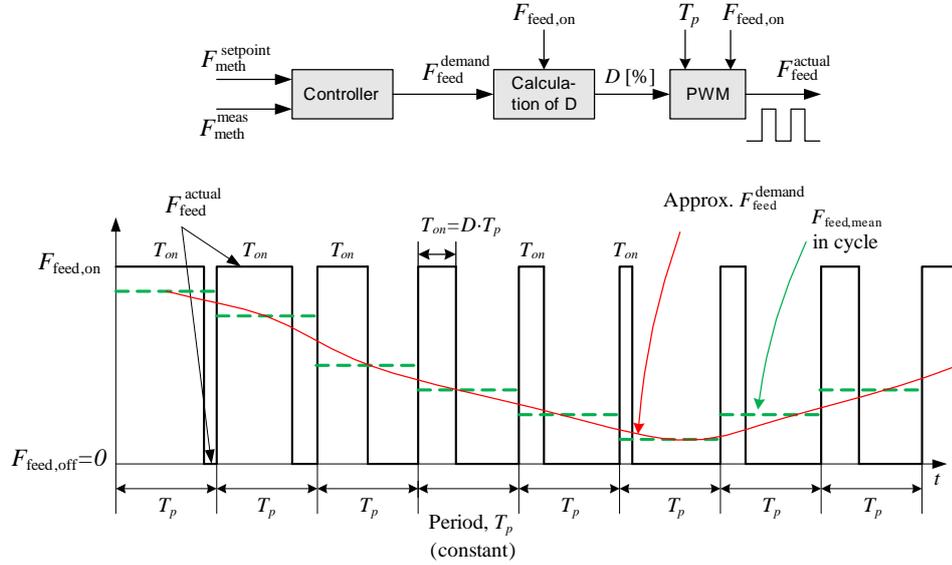
Figure 8: The principle of pulse width modulation (PWM).

flow rate, $F_{\text{feed}_{\text{on}}}$. And, as observed, PWM also reduces the frequency of blockings in the feed pipeline.

H-1: An electrical heater which is controlled using PWM. The heater comprises an electrical resistor wound around the reactor inside the thermal insulation jacket. The maximum power delivered by the heater is 200 W. The PWM cycle time is 30 sec which is neglibile compared to the dynamics of the temperature control loop. The control signal (in percent) calculated by the temperature controller is the duty cycle of the PWM element. The PWM output signal controls the SSR (solid state relay) on-off.

I/O-device

Low-cost USB-based I/O-devices (National Instruments) are used to connect the PC to the sensors and actuators. Control and measurement signals are analog voltages. So-called current loops are used to convert measurement signal originally in the form of a milliampere signal to a voltage signal.

Computer and software

The computer program for monitoring and control is running on a laptop PC which is connected to the Internet. The program is implemented with LabVIEW, but some computational demanding parts are implemented in MATLAB Nodes. Figure 9 shows the part of the front panel of the LabVIEW program where the user can select among a large number of tabs containing adjustable parameters.
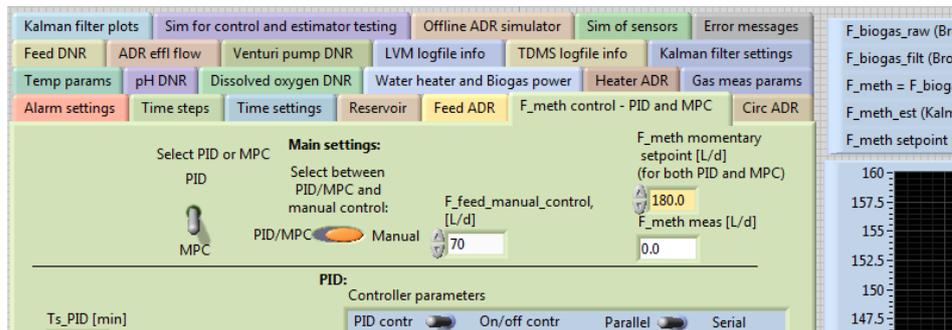
Figure 9: Part of front panel of LabVIEW program for monitoring and control.

The main parts of the LabVIEW program are described below (referring to Figure 9).

Measurement filters are used to smooth measurement noise. The filters are time-constant filters programmed from scratch in LabVIEW. The time-constants are adjusted for appropriate noise filtering without removing important process information. For temperature measurements a time-constant of 10 min is used, for biogas flow measurement a time-constant of 0.2 d is used, and for gas concentration a time-constant of 1 h is used.

Scalings are transformation of measurement signals (voltages) to the pertinent physical units, e.g. deg C, L/d, etc.

Methane gas flow control: An automatic methane gas flow control system is implemented. The methane flow measurement is obtained by multiplying the biogas flow measurement and methane concentration measurement, cf. Figure 2.1. Several control functions are implemented: On-off control; Industrial PID control (proportional+integral+derivative); MPC (Model-based predictive control) based on Hill's model (1983), including a state estimator

(Kalman Filter), and manual control. Results with PID and MPC control are summarized in the next section.

The gas flow controller manipulates the feed pump P-1 which is operated using PWM (Pulse-Width Modulation) with a fixed cycle time of 10 min. The PWM is implemented with a Square Wave function in LabVIEW on which the duty cycle (percentage of on-time relative to a fixed period) is adjustable. PWM control has several important practical benefits compared with analog control: The calibration of the pump is needed only at one flow, namely the maximum flow rate (i.e. the flow with PWM signal in the On-state), and it is therefore easier to obtain any flow (in average) within the minimum and the maximum flow ranges. PWM operation of the pump seems to reduce the number of blockings in the feed pipeline.

Reactor temperature control: An automatic reactor temperature control system is implemented. Several control functions are implemented: Manual control, on/off control (thermostat control), PID control. The temperature is measured with a Pt100-sensor.

The controller manipulates the heat supplied to the reactor. The heat is provided by an electrical coil in the form of a resistor wound about the reactor. The control signal from the temperature controller sets the duty cycle of a PWM element with a fixed cycle time of 60 seconds. The PWM elements turns an SSR element (Solid State Relay) on or off thereby turning the 220 VAC across the heating coil on or off.

Data logging: Measurement and control signals are written every 15 minutes to log files in both text-format (CSV format) for use in MATLAB and binary format (TDMS files) for use in the Diadem data analysis tool (National Instruments).

Simulation: An off-line simulator of the AD process is implemented. The underlying mathematical model is based on Hill's model (1983), with some modifications. Model parameters are estimated offline using data in logfiles and from laboratory analysis. The user can adjust any model parameter and select any simulator time interval.

Alarm via sms: Automatic alarm submission via sms is implemented with e-mail functions in LabVIEW. The e-mail message is forwarded to by an external service[4]. The alarm condition here is blocking as detected by the effluent flow sensor. Automatic alarming has eliminated situations with no-feed to the reactor due to blockings.

---

[4]by Ipipi

Remote access: A secure communication between the PC and the Internet facilitates remote access to the screen and the file system on the lab PC[5]. Data files can be downloaded any time. The LabVIEW program can even be modified from a computer anywhere on the Internet. The remote access has been of great practical help in this project.

Laboratory analysis

In this research project, the volatile solids (VS) and volatile fatty acids (VFAs) concentrations of both the reactor influent and effluent are used for mathematical modeling. Their values are obtained from standard laboratory analysis methods as described briefly below.

VS: Three parallel tests for each sample. The samples are dried in an oven at 105 °C for approximately one day. Then, the (dried) samples are combusted in a furnace at 550 °C for 2 hours. The VS concentration in g/L is calculated as the weight lost during the combustion divided by the sample volume.

VFAs: Two parallel tests for each sample. The samples are centrifuged for 30 min, and then filtered. The samples are diluted with deionized water, then added to small vials together with formic acid, capped, and stored in a refrigerator until measurement is done. The VFA concentrations in g/L are measured by a gas chromatograph (GC) using three injections from each of the parallels.

---

[5] by LogMeIn

Contributions by this dissertation

1. Adaptation of a mechanistic dynamic model, based on material balances, of the AD processes in a bioreactor fed with dairy waste using a combination of steady state experimental (real) steady state data and dynamic data from online sensors and laboratory analysis. (Article no. 1.)

2. Demonstrating that the temperature dependency of Hashimoto et al. (1981) in the modified Hill AD process model represents precisely the dynamic response in methane gas flow due to temperature changes for a real reactor. (Article no. 1.)

3. Demonstrating that industrial standard controllers such as on-off controllers and PI controllers are viable controllers for controlling the produced methane gas flow and the reactor temperature of an AD reactor. (Articles nos. 2 and 3.)

4. Demonstration of how nonlinear predictive control can be implemented in a computer application in which LabVIEW and MATLAB are efficiently combined. (Article no. 4.)

5. Demonstrating how nonlinear predictive control can be applied to an AD process. (Article no. 4.)

6. Demonstrating that the Unscented Kalman Filter can be successfully applied to an AD process. (Article no. 4.)

7. Definition of alternative optimization objectives for optimal design and operation of an AD reactor fed with dairy waste. Solving the optimization problems using the model of the AD processes, which are based on material balances, and the model of the reactor temperature, which is based on energy balance. Demonstrating that the simple and intuitive brute force optimization method is sufficient

for solving the aforementioned optimization problems. (Article no. 5.)

8. Design of the Relaxed Ziegler-Nichols closed loop tuning method which is shown to improve both the original Ziegler-Nichols PI settings and the Tyreus-Leuben PI settings. (Article no. 6.)

9. Development of a procedure to estimate the phase margin for simulated and practical nonlinear control systems directly from experiments. (Article no. 6.)

Conferences attended

During my PhD study I have participated at the following relevant conferences:

17th Nordic Process Control Workshop, Denmark Technical University, Lyngby, 2012. Poster: *State Estimation of a Pilot Anaerobic Digestion Reactor.*

IWA World Conference on Water, Climate and Energy 2012, Dublin, May, 2012. Oral presentation: *Mathematical Modelling for Planning Optimal Operation of a Biogas Reactor for Dairy Manure.*

13th World Congress on Anaerobic Digestion, Santiago de Compostela, Spain, June, 2013. Poster: *Modelling and Control of a Pilot Anaerobic Digestion Reactor.*

11th IWA conference on Instrumentation, Control and Automation, Narbonne, France, September, 2013. Poster: *An advanced and flexible computer-based system for monitoring and control of a pilot bioreactor.*

The articles, posters and powerpoint presentations produced for these conferences are not presented in this dissertation since the main results presented there are included in the scientific articles, or in the section entitled *Background and methods* preceding each of the articles.

Future work

The present research project may be succeeded with the following work:

Adapting more comprehensive models to the reactor, for e.g. simulation-based analysis, state estimation using a Kalman Filter (as in Article 4), and optimization (as in Article 5). With more comprehensive models than the modified Hill model used in the present research project, additional variables, e.g. pH, alkalinity, CO_2, H_2, and NH_3 can be studied. These variables may be important in AD processing of e.g. swine waste and co-digestion of animal waste and food waste. Several possible models are evaluated in Article 1. Among these, the following two models appear as most attractive: The model by Hill & Barth (1977), and the ADM1 model by Batstone et al. (2002).

Mathematical modeling of the nitrification reactor which succeeds the AD reactor, cf. Figure 6. By combining that model with a proper model of the AD reactor, cf. the item above, a model of the complete biological plant may be obtained, to be used for e.g. analysis, (optimal) design and state estimation.

Economical analysis revealing the economical feasibility of the AD processing of the waste, possibly combined with nitrification.

Abbreviations and nomenclature for Part I

The abbreviations and nomenclature presented in the following apply to the present part, Part I, of the dissertation. For each of the articles in Part II, the abbreviations and nomenclature are given in the article.

Abbreviations

AD = Anaerobic digestion.

AD = Analog-digital.

BVS = Biodegradable volatile solids.

CSTR = Continuous stirred tank reactor.

DA = Digital-analog.

GC = Gas chromatograph.

GHG = Greenhouse gases.

GWP = Global warming potential.

HRT = Hydraulic retention time.

IAE = Integral of absolute value of control error.

I/O = Input/output.

IPCC = Intergovernmental panel on climate change.

LS = Least squares.

MPC = Model-based predictive controller.

STP = Standard temperature and pressure; 0 ºC, 1 bar.

ODE = Ordinary differential equation.

PID = Proportional plus integral plus derivative (control).

PWM = Pulse-width modulator.

SSE = Sum of squared errors.

SRT = Solids retention time.

SSR = Solid state relay.

UASB = Upflow anaerobic sludge blanket.

VFA = Volatile fatty acids.

VS = Volatile solids.

Nomenclature

CH_4 is methane.

CO_2 is carbondioxide.

F_{feed} [m^3/d] is influent or feed flow or load rate, assumed equal to effluent flow (constant volume).

F_{meth} [L CH$_4$/d] is methane gas flow.

NH_3 is ammonia.

NH_4- is ammonium.

NH_3O- is nitrate.

N_2O is nitrous oxide gas or laughing gas.

S_{bvs} [g BVS/L] is concentration of BVS in reactor.

S_{vfa} [g VFA/L] is concentration of VFA acids in reactor.

T_{reac} [°C] is reactor temperature.

X_{acid} [g acidogens/L]: Concentration of acidogens.

X_{meth} [g methanogens/L]: Concentration of methanogens.

Bibliography

Bala, B. K. & Satter, M. A. (1991), 'System dynamics modelling and simulation of biogas production systems', *Renewable Energy, Pergamon Press* **1**(5/6), 723–728.

Batstone, D. J., Keller, J., Angelidaki, I., Kalyuzhnyi, S. V., Pavlovstahis, S. G., Rozzi, A., Sanders, W. T. M., Siegrist, H. & Vavilin, V. A. (2002), *Anaerobic Digestion Model No. 1, Scientific and Technical Report 15*, IWA Publising.

Davison, A. C. & Hinkley, D. V. (1997), *Bootstrap Methods and their Application*, Cambridge University Press.

Deublein, D. & Steinhauser, A. (2010), *Biogas from Waste and Renewable Resources*, Wiley.

Edgar, T. F., Himmelblau, D. & Lasdon, L. (2001), *Optimization of Chemical Processes*, McGraw-Hill.

Grüne, L. & Pannek, J. (2011), *Nonlinear Model Predictive Control*, Springer-Verlag, London.

Haber, R., Bars, R. & Schmitz, U. (2011), *Predictive Control in Process Engineering*, Wiley-VCH.

Hashimoto, A. G., Chen, Y. R. & Varel, V. H. (1981), 'Theoretical aspect of anaerobic fermentation: State-of-the-art', *Livestock Waste: A Renewable Resource. American Society of Agricultural Engineers* .

Haugen, F. (2012), 'The Good Gain method for simple experimental tuning of PI controllers', *Modeling, Identification and Control* **33**(4), 141–152.

Haugen, F. (2013), 'Air heater',
`http://home.hit.no/~finnh/air_heater`.

Haugen, F., Bakke, R., Vasdal, K. & Bergland, W. (2013), 'Foss Biolab',
`http://fossbiolab.no`.

Hill, D. T. (1983), 'Simplified monod kinetics of methane fermentation of animal wastes', *Agric. Wastes* **5**.

Hill, D. T. & Barth, C. L. (1977), 'A dynamic model for simulation of animal waste digestion', *J. Water Pollution Control Federation* **49**(10).

Julier, S. J. & Uhlmann, J. K. (1997), 'A new extension of the Kalman Filter to nonlinear systems', *Int. Symp. Aerospace/Defense Sensing, Simul. and Controls* **3**.

Lettinga, G., van Velsen, A. F. M., Hobma, S. W., de Zeeuw, W. & Klapwijk, A. (1980), 'Use of the upflow sludge blanket (USB) reactor concept for biological wastewater treatment, especially for anaerobic treatment', *Biotechnology and Bioengineering* **22**(4), 699–734.

Maciejowski, J. (2002), *Predictive Control with Constraints*, Prentice-Hall.

Madsen, M., Holm-Nielsen, J. B. & Esbensen, K. H. (2011), 'Monitoring of anaerobic digestion processes: A review perspective', *Renewable and Sustainable Energy Reviews* **15**, 3141–3155.

Simon, D. (2006), *Optimal State Estimation*, Wiley.

Skogestad, S. (2004), 'Simple analytic rules for model reduction and PID controller tuning', *Modeling, Identification and Control* **25**(2), 85–120.

Tchobanoglous, G., Burton, F. G. & Stensel, H. D. (2003), *Wastewater Engineering: Treatment and Reuse*, Metcalf and Eddy, McGraw Hill.

Tyreus, B. D. & Luyben, W. L. (1992), 'Tuning PI Controllers for Integrator/Dead Time Processes', *Ind. Eng. Chem* **31**(31).

Ziegler, J. & Nichols, N. (1942), 'Optimum settings for automatic controllers', *Trans. ASME* **64**(3), 759–768.

Part II – SCIENTIFIC ARTICLES

List of articles

Article 1 – Adapting a Dynamic Mathematical Model to a Pilot Anaerobic Digestion Reactor (page 37).

Published in *Modeling, Identification and Control*, 34 (2), 2013.

Authors: Finn Haugen, Rune Bakke, and Bernt Lie.

Article 2 – Temperature Control of a Pilot Anaerobic Digestion Reactor (page 63).

Published in *Modeling, Identification and Control*, 34 (3), 2013.

Authors: Finn Haugen, Rune Bakke, and Bernt Lie.

Article 3 – On-off and PI Control of Methane Gas Production of a Pilot Anaerobic Digestion Reactor (page 85).

Published in *Modeling, Identification and Control*, 34 (3), 2013.

Authors: Finn Haugen, Rune Bakke, and Bernt Lie.

Article 4 – State Estimation and Model-based Control of a Pilot Anaerobic Digestion Reactor (page 105).

Submitted to *Journal of Control Science and Engineering* October 28, 2013. Accepted after revision February 12, 2014. In press per February 23, 2014.

Authors: Finn Haugen, Rune Bakke, and Bernt Lie.

Article 5 – Optimal Design and Operation of a UASB Reactor for Dairy Cattle Manure (page 143)**.**

Submitted to *Computers and Electronics in Agriculture* November 6, 2013. Revised version (based on reviewer's comments) resubmitted February 10, 2014.

Authors: Finn Haugen, Rune Bakke, Bernt Lie, Jon Hovland, and Knut Vasdal.

Article 6 – Relaxed Ziegler-Nichols Closed Loop Tuning of PI Controllers (page 171).

Published in *Modeling, Identification and Control*, 34 (2), 2013.

Authors: Finn Haugen and Bernt Lie.

Article 1 – Adapting a Dynamic Mathematical Model to a Pilot Anaerobic Digestion Reactor

Authors: Finn Haugen, Rune Bakke and Bernt Lie.

Authors' roles in the article: Finn Haugen: Main ideas, implementation, and writing. Rune Bakke (co-supervisor) and Bernt Lie (supervisor): Discussions, comments, and proof readings.

Background and methods of the article

Background

In this research project, mechanistic dynamic models are used for estimation (monitoring), control, and optimization of design and operation of AD reactors. Design and results of applications are presented in the articles constituting this dissertation. Obviously, the selection of a proper model is crucial. Several model candidates are discussed in the paper. For the ultimate model selection, the following generic rule is applied: "Among appropriate model candidates, select the simplest one." The selection is the model in Hill (1983). This model assumes a CSTR reactor which implies that the solids or biomass retention time (SRT) is equal to the hydraulic retention time (HRT). However, since the present reactor is a UASB reactor, the model should be modified to include the possibility of SRT being larger than HRT. A motivation for this is given in Article no. 5,

where it is shown that the ratio of SRT to HRT is a very important
parameter in optimization of design and operation of AD reactors.

The resulting model is denoted the modified Hill model, consisting of four
nonlinear differential equations representing the material balances of
biodegradable volatile solids, volatile fatty acids, acid generating microbes
(acidogens), and methane generating microbes (methanogens). The model
can predict the methane gas flow produced in the reactor.

The simplicity of the modified Hill is beneficial in the applications in the
present research project. In more demanding applications, this relatively
simple model is inadequate. Alternative, more complex models are
discussed in the article.

Also, a dynamic model for the reactor temperature based on an energy
balance of the liquid phase of the reactor, is adapted using experimental
data. This model is useful for testing reactor temperature control systems
and for optimization of reactor design and operation taking power surplus
into account.

Methods

The method of adaptation of the modified Hill model to the real reactor is
as follows: Using experimental data from a proper approximate steady
state operating point, the assumed unknown model parameters, except
one, are calculated from the steady state version of the dynamic Hill model
obtained by setting the time-derivatives to zero, thereby obtaining a set of
algebraic model equations. The number of unknown parameters equals the
number of equations, so the solution is easily obtained, manually. Then,
the remaining parameter, which is a yield factor in the formula for
methane gas flow, is estimated using the nonlinear least squares method,
i.e. optimization, to tune the pertinent parameter by adapting dynamic
simulations to dynamic operational data.

The principle of model adaptation applied here, where an optimization
method (least squares), dynamic simulations and experimental dynamic
data are combined, appears to be a powerful model adaptation method.
The method also avoids any model manipulation since the dynamic model,
i.e. its set of differential equations, is used in its original form.

The quality of the parameter estimates is analyzed as follows: The
standard deviation of the parameter estimates is calculated with
bootstrapping with parametric simulation, Davison & Hinkley (1997),

where the standard deviations are calculated from simulations where the laboratory data are perturbed with random noise similar to the observed noise or variations. Furthermore, the sensitivity of the parameter estimates are expressed with relative sensitivity of the estimates to assumed changes in observed data used for the estimation.

The dynamic model for the reactor temperature is derived from energy balance of the liquid, assuming homogeneous conditions. The model comprises one single differential equation, the same as presented in basic mathematical modeling courses. Still, the model is able to predict the temperature precisely. The only unknown model parameter is the heat transfer coefficient of the reactor walls. Three different methods are applied to estimate this parameter, namely (1) the least squares method using the static model assuming steady state (static) conditions, (2) the LS method using the dynamic model where the unknown parameter is adjusted until the difference between the measured and the simulated temperature is minimized in the LS sense, and (3) nonlinear LS where the model includes also a lag in the form of a time constant which is estimated, and, hence, there are two parameters to be estimated. The third method gives the best estimate in as evaluated with the SSE index (sum of squared errors) the estimated from experimental data.

Supplementary material: Causal diagram

This section shows a causal diagram of the modified Hill model, regarded as supplementary material to Article no. 1.

Figure 10 shows a causal diagram for modified Hill's model presented in the article. The diagram is principally similar to the causal diagram in Bala & Satter (1991). While not displaying the mathematical relations in detail, the causal diagram may help understanding the interactions taking place in the AD reactor, as far as the model is representative, of course. The "inventories" represent mathematical integrators or accumulators with the "level" representing the pertinent state variable. An *increase* is represented by a plus sign, while a *reduction* is represented by a minus sign. The ($\cdot$) symbol represents mathematical functions according to the mathematical model.

The dynamics of microorganisms (acidogens and methanogens) are slower than the dynamics of the BVS and VFA which is indicated in Figure 10.

To illustrate the information conveyed by the causal diagram, assume that
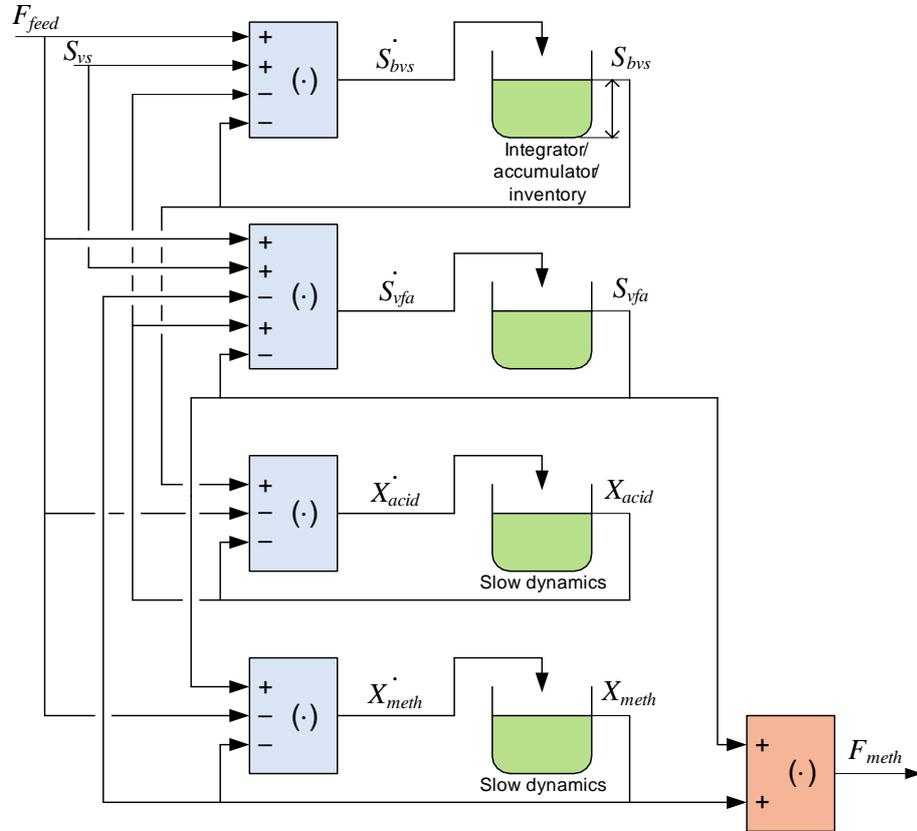
Figure 10: A causal diagram for Hill's model showing the qualitative impacts that the various variables have on other variables. The level of the "inventories" or "tanks" represent the state variables.

the reactor initially is at steady-state with operating point data as shown in Table 12 in the article, and that F_{feed} then is changed as a step. Figure 11 shows the simulated responses due to this step. Comparing these responses with the causal diagram:

- Simulation shows that the transient response in S_{bvs} increases, which is in accordance with the positive input to the upper functional block in Figure 10.

  Eventually S_{bvs} flattens and becomes constant. This can be explained by the negative feedback from S_{bvs} to its time-derivative in the causal diagram: When S_{bvs} increases, the rate of change of S_{bvs} decreases. Physically explained, when S_{bvs} increases, more BVS leaves the reactor.

- The transient response in S_{vfa} increases, which is in accordance with
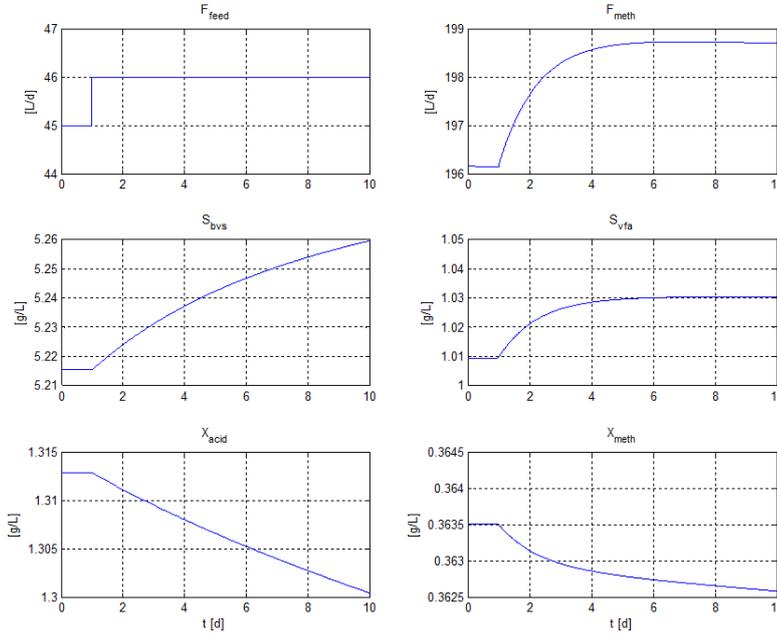
Figure 11: Simulated responses due to a step change of F_{feed}.

the positive input to the second functional block. This increase and eventual flattening of S_{vfa} can be explained in the same way as for S_{bvs} above.

- The transient response in X_{acid} decreases, which is in accordance with the negative input to the third functional block. Physically, the decrease is due to a part of the acidogens being washed out from the reactor due to the increased effluent flow caused by the increased influent flow.

  Eventually the reduction of X_{acid} decreases. X_{acid} flattens and becomes constant which is due to increased S_{bvs} which in itself causes a growth of acidogens, and this growth counteracts the increased washout.

- The transient response in X_{meth} decreases, which is in accordance with the negative input to the bottom functional block. Physically, the decrease is due to a part of the methanogens being washed out from the reactor due to the increased effluent flow caused by the increased influent flow.

  Eventually the reduction of X_{meth} decreases. X_{meth} flattens and becomes constant which is due to increased S_{vfa} which in itself causes

a growth of methanogens, and this growth counteracts the increased washout.

- F_{meth} increases which is due to the increased S_{vfa}. Actually, X_{meth} decreases, slowly, which in itself causes a reduction of F_{meth}. However, the increase of S_{vfa} is larger than the decrease of X_{meth}, and therefore the net effect is an increase of F_{meth}.

Adapting Dynamic Mathematical Models to a Pilot Anaerobic Digestion Reactor

Finn Haugen   Rune Bakke   Bernt Lie

Telemark University College, Kjolnes ring 56, 3918 Porsgrunn, Norway. E-mail contact:
{*finn.haugen,rune.bakke,bernt.lie*}*@hit.no*

Abstract

A dynamic model has been adapted to a pilot anaerobic reactor fed diary manure. Both steady-state data from online sensors and laboratory analysis and dynamic operational data from online sensors are used in the model adaptation. The model is based on material balances, and comprises four state variables, namely biodegradable volatile solids, volatile fatty acids, acid generating microbes (acidogens), and methane generating microbes (methanogens). The model can predict the methane gas flow produced in the reactor. The model may be used for optimal reactor design and operation, state-estimation and control. Also, a dynamic model for the reactor temperature based on energy balance of the liquid in the reactor is adapted. This model may be used for optimization and control when energy and economy are taken into account.

Keywords: Anaerobic digestion, bioreactor, biogas, mathematical modeling.

1. Introduction

1.1. Anaerobic digestion of animal wastes

Anaerobic digestion (AD) of animal wastes can produce biogas with methane to be used as an energy source, and a liquid effluent containing valuable nutrients. Moreover, AD reduces methane emission, odours and contaminants. AD bioreactors are effective as they allow for relatively high load rates (feed rates) and small reactor volumes. AD reactors may become unstable, i.e. a persistent decrease of gas production, because of inhibitory effects on methane-forming microorganisms due to large concentrations of volatile fatty acids (VFA) and ammonia and too low pH. Instability can also occur because of washout of microbes when the feed (load) rate is too large.

Various theoretical and practical aspects of AD processes are described in e.g. Tchobanoglous et al. (2003) and Deublein and Steinhauser (2010). A presentation of AD of animal wastes (dairy, beef, poultry, and swine) is provided e.g. by Husain (1998).

1.2. Possible applications of mathematical models

Foss Biolab, Haugen et al. (2012), is a pilot biological plant at Foss dairy farm in Skien, Norway, for nutrient and energy recovery from animal waste. The aims of this paper are to adapt a dynamic mathematical model of the anaerobic digestion (AD) processes of the reactor in the plant able to predict the methane gas flow produced in the reactor, and to adapt a dynamic model able to predict the reactor temperature.

Possible applications of a mathematical model of the AD processes in the reactor are as follows.

- *Analysis of the dynamic and steady-state behaviour of the AD processes* primarily based on simulations. Using simulations can provide process insight which would otherwise be practically difficult to obtain.

- *Optimal design and operation of a full-scale reactor*, i.e. designing optimal reactor size and calculating optimal feed rate according to proper optimization criteria, Edgar et al. (2001).

- *Design of state estimators*, also denoted soft-sensors, which are algorithms calculating the state of the process continuously, Simon (2006). The most common state estimation algorithm is the Kalman Filter which exists in different versions. A state estimator is an essential part of model-based predictive controllers, see below. It may also be used as a soft-sensor on its own as a substitute for real measurements.

- *Model-based tuning of industry-standard PID controllers* (Proportional + Integral + Derivative), Seborg et al. (2004), for biogas flow control to keep the produced biogas flow at or close to a given setpoint.

- *Design and implementation of model-based predictive controllers* (MPCs), Grüne and Pannek (2011), for biogas flow control.

Possible applications of a mathematical model of the reactor temperature are:

- *Optimal reactor design and operation taking energy and economy into account.* A combination of the AD process model and the reactor temperature model will be necessary to solve this optimization problem.

- *Tuning a temperature controller for the reactor.*

1.3. Outline of this paper

Section 2 gives a description of the pilot AD reactor at Foss Biolab. Section 3 describes adaptation of a dynamic mathematical model of the AD process to the reactor. Section 4 describes mathematical modelling of the reactor temperature. A discussion is given in Section 5, and conclusions are given in Section 6. Nomenclature including abbreviations is given in Appendix A. Laboratory analysis methods for relevant components are described in Appendix B. For easy reference, a summary of the modified Hill's model adapted to the pilot reactor is given in Appendix C.

MATLAB (by The MathWorks, Inc.) has been used as computational tool for this paper.

2. The AD reactor

2.1. Overview

Figure 1 shows a Piping & Instrumentation Diagram (P&ID) of the biological process plant at Foss dairy farm. Input to the plant is dairy manure diluted with 25% water and filtered, and outputs are fertilizer and biogas consisting of 70-75% methane. The plant is monitored and controlled with a PC running LabVIEW. The main parts of the plant are as follows (numbers refer to Figure 1).

1. A reservoir for raw dairy manure with approximately 25% added water.

2. A sieve to separate the manure into two fractions of similar total solid mass: > 70 % of the volume is wetter fraction, and < 30 % is dryer fraction. The dryer fraction is used for vermicomposting.

3. A high rate anaerobic digestion reactor fed filtered cow manure as substrate for production of energy-rich biogas that contains mainly methane. The effective reactor volume is approximately 250 L.

4. A nitrification reactor of approximately 200 L fed AD reactor effluent to produce liquid fertilizer and pellets fertilizer from formed foam.

This paper concerns the AD reactor in the process line.

The present reactor has been operational since April 2012, while a previous similar reactor was in operation from August 2011 until April 2012.

2.2. Instrumentation

Below is a list of the instrumentation used with the AD reactor depicted in Figure 1. The encircled numbers refer to the diagram in Figure 1.

PC is a laptop PC running the computer program for monitoring and control implemented in LabVIEW. The PC is connected to sensors and actuators via USB-based I/O-devices.

P2: A voltage controlled peristaltic pump which is operated using pulse-width modulation (PWM) with a fixed cycle time of 10 min.
There are several benefits of using PWM control compared with analog control: The calibration of the pump is needed only at one flow, namely the maximum flow rate (i.e. the flow with PWM signal in the On state), and it is therefore easier to obtain any flow (in average) within the minimum and the maximum flow ranges. PWM may also reduce blocking in the feed pipeline.

FT-1: AD reactor effluent flow sensor (home-made) based on measuring the frequency of effluent charging and discharging of a cup of fixed volume.

FT-2: Thermal biogas flow sensor.

The sensor output is normal litres of gas at NTP (Normal Temperature and Pressure), i.e. temperature 0 °C and pressure 1.013 bar.
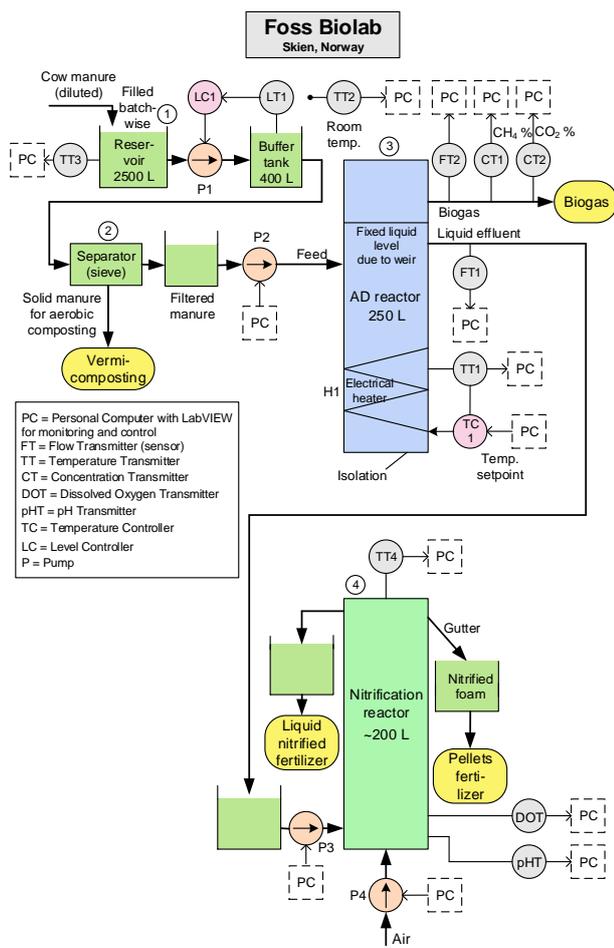
Figure 1: *Piping & Instrumentation Diagram (P&ID) of the biological process line of the pilot plant at Foss Biolab, Skien, Norway. This paper concerns the AD reactor.*

The raw measurement signal from this sensor is quite noisy with an observed standard deviation of approximately 14 L/d (litres per day) which is approximately 2% of the upper range limit (URL) which is 720 L/d. To smooth the noise, a lowpass filter with time-constant of 0.2 d is implemented in the LabVIEW program.

CT-1: Infrared (IR)-based CH_4 gas concentration sensor.

To smooth the measurement signal from this sensor, a first-order lowpass filter with time-constant of 1 h (hour) is implemented in the LabVIEW program.

CT-2: Infrared (IR)-based CO_2 gas concentration sensor.

The measurement signal is filtered with a lowpass filter with time-constant of 1 h.

TT-1: Pt100 reactor temperature sensor.

Filter: Lowpass filter with time-constant of 10 min.

TT-2: Pt100 biolab room temperature sensor.

Filter: Lowpass filter with time-constant of 10 min.

TC-1: Reactor temperature controller which is operated as an On-Off controller (i.e. thermostat controller). The controller is an industrial stand-alone temperature controller.

H-1: Electrical heater for the AD reactor which is controlled using the built-in PWM option in TC-1. The heater comprises an electrical resistor wound around the reactor inside the thermal insulation jacket.

2.3. Available data

Data used for model adaptation are offline-data from laboratory analysis and online-data from sensors.

Samples for laboratory analysis have been taken regularly from the reactor since August 2011, following sampling guidelines given by Esbensen and Paasch-Mortensen (2010). A number of different variables characterizing the reactor influent and effluent are analyzed. Among these, concentration of volatile solids (VS) and concentration of total volatile fatty acids (VFA) are used for model adaptation in the present study.

Online-data include feed flow (load rate), reactor temperature, ambient (air) and feed temperature (assumed to be the same and therefore measured with one sensor), biogas flow, and methane gas concentration. The latter two provide methane gas flow.

3. Adaptation of a mathematical model to the AD reactor

3.1. Selection of dynamic model

Several dynamic mathematical models for AD processes exist. Overviews of such models are given by e.g. Gavala et al. (2003), Lyberatos and Skiadas (1999), and Stromberg (2010).

3.1.1. Model selection criteria

For our purposes, cf. Section 1.2, a model is searched for according to the following criteria:

1. The model must be able to predict the produced biogas. However, it is sufficient that methane gas flow is predicted since the useful energy content of the gas is related to the methane content only.

2. The model should be relatively simple since it is to be used in a real-time implementation of a state estimator and a model-based controller. Relatively simple models are preferable since they may be easier to adapt and maintain.

3. The model should be able to represent the temperature dependency of the dynamics of the AD process. This is because the reactor may be operated at different temperatures, although the mesophile condition which is about 35°C is assumed to give the optimal temperature condition for the methane-producing micro-organisms, or methanogens, Tchobanoglous et al. (2003). Optimality in terms of cost may imply a temperature being different from 35°C.

3.1.2. Model candidates

A number of candidates of model for AD of dairy manure were considered in the light of the above criteria. Below is a summarized characterization of these models.

- *Andrews and Graef (1971):*

  – Model characteristics: The model is general, and does not assume any particular type of organic substrate. Substrate: Acetic acid. Hydrolysis step is not included. Biological reaction includes only convertion of volatile acids to CO_2 and CH_4 by only one type of microbes, namely methanogenic microbes. pH between 6 and 8 is assumed. Temperature 38 °C is assumed.

  – State variables (there are five): Concentration of substrate; Concentration of methanogens; Concentration of dissolved CO_2 in liquid phase; Partial pressure of CO_2 in gas phase; Alkalinity.

  – Gas predicted by the model: CH_4 gas flow; CO_2 gas flow; Biogas flow as sum of these gas flows.

- *Hill and Barth (1977):*

  – Model characteristics: The model is general for animal waste, and is validated using experimental data from reactors fed poultry waste and swine waste. Hydrolysis step is included. Model parameters are expressed as Arrhenius-based functions of temperature.

  – State variables (9): Concentration of volatile matter; Concentration of soluble organics; Concentration of volatile acids in the form of acetate; Concentration of acidogens ("acid-formers"); Concentration of methanogens ("methane-formers"); Concentration of dissolved CO_2 in liquid phase; Partial pressure of CO_2 in gas phase; Concentration of $NH_4{}^+$ in liquid phase; Partial pressure of NH_3 in gas phase; Concentration of cations (other than ammonia and hydrogen);

  – Gas predicted by the model: CH_4 gas flow; CO_2 gas flow; NH_3 gas flow; Biogas flow as sum of these gas flows.

- *Hill (1983):*

  – Model characteristics: The model applies to waste from poultry, beef, dairy, or swine with two parameters – the biodegradability constant and the acidity constant – being unique for each of these wastes. Substrate: Volatile solids (VS). A certain fraction of the fed VS is assumed biodegradable. Hydrolysis step is not included. Model is validated using experimental data with all four wastes mentioned above. Applicable temperature range is 20°C – 60°C based on the temperature-dependency of the maximum reaction rates according to Hashimoto et al. (1981).

  – State variables (4): Concentration of biodegradable volatile solids (BVS); Concentration of volatile fatty acids (VFA) as acetate; Concentration of acidogens; Concentration of methanogens;

  – Gas predicted by the model: CH_4 gas flow.

- *Husain (1998):*

  – Model characteristics: Husain (1998) presented Hill's model (1983) with more details regarding chemical reactions. Husain also changed some of the model parameter values, and expressed the death rates of the acidogens and metanogens as VFA-based Monod functions instead of relating the death rates to the maximum reaction rates as Hill did.

  – State variables (4) are as in Hill's model.

  – Gas predicted by the model as in Hill's model.

- *Batstone et al. (2002):*

  – Model characteristics: This model is known as ADM1 (Anaerobic Digestion Model No. 1). ADM1 is a general, complex AD model

which describes biochemical and physico-chemical processes. The biochemical steps include disintegration, extracellular hydrolysis, acidogenesis, acetogenesis, and methanogenesis. The physico-chemical equations describe ion association and dissociation, and gas-liquid transfer.

In a representation of ADM1 in Rosen et al. (2006) consisting of solely differential equations there are 35 state variables representing various concentrations, and approximately 100 parameters.

Temperature-dependent parameters are expressed as Arrhenius-type functions of temperature.

The ADM1 model is very stiff as the dynamics of pH and hydrogen are relatively fast. The stiffness poses numerical challenges for implementation in e.g. MATLAB/SIMULINK, Rosen et al. (2006). One solution to the stiffness problem is to replace the stiff state variables by algebraic states calculated by a numerical solver at each simulation time step, Rosen et al. (2006), and hence the model becomes a DAE model (differential algebraic equations).

– State variables (35): Monosaccharides; Amino acids; Long chain fatty acids; Valerate; Butyrate; Propionate; Acetate; Hydrogen gas; Methane gas; Inorganic carbon; Inorganic nitrogen; Soluble inerts; Composites; Carbohydrates; Proteins; Lipids; Degraders (seven) for sugar, amino acid, long chain fatty acids, valerate & butyrate, propionate, acetate, and hydrogen; Particulate inerts; Cations; Anions; Ion states (six) for valerate, butyrate, propionate, acetate; bicarbonate, and ammonia; CH_4 gas; CO_2 gas; H_2 gas.

– Gas predicted by the model: CH_4 gas flow; CO_2 gas flow; H_2 gas flow; Biogas flow as sum of these gas flows.

- *Zaher et al. (2009):*

  – Model characteristics: The model applies to dairy waste and includes hydrolysis, acidogenesis, methanogenesis – hydrogenotrophic and acetotrophic. The model is validated against different real batch processes with continuous mixing, operating at 35°C.

  – State variables (15): Concentration of the following microbial groups: Acidogens; Acetotrophic methanogens; Hydrogenotrophic

methanogens; Concentration of the following materials: Biosolids (particulate substrate); Degradable substrate (as sugars); Volatile fatty acids (as acetate); Hydrogen; Carbondioxide; Methane; Bicarbonate; Ammonium; Phosphates; Moisture (water); Protons (H+); Cations.

– Gas predicted by the model: Biogas flow (the individual gas components are however not stated explicitly in Zaher et al. (2009).

3.1.3. Selection of the ultimate model

In the light of the criteria for model selection presented in Section 3.1.1 Hill's model, Hill (1983), is selected as the ultimate model as it satisfies all the criteria and because it is simpler than comparable models, see below. Support for this selection is found in the evaluations of various AD models made by Stromberg (2010) and Husain (1998) where they conclude favourably about this model.

Brief evaluations of the other models presented above in the light of our selection criteria are given in the following.

The model by Andrews and Graef (1971) is not selected because it is validated only at the fixed temperature 38°C. Also, we see it as drawback that it contains only one type of microorganisms while two or more types are very common in more modern models.

The model by Hill and Barth (1977) is attractive for our purposes, but is not selected here because it is more complicated than Hill's model, Hill (1983). However, this model may be selected in future projects.

The model presented by Husain (1998) is basically the selected Hill's model.

The ADM1 model, Batstone et al. (2002), is not selected because it is very complex, and because numerical challenges may be expected in an online (real-time) implementation of state estimators and model-based controllers. Lyseng et al. (2012) adapted ADM1 quite successfully to our pilot reactor in the AQUASIM simulation tool, Reichert (1998), however with poor predictions of produced biogas as the reactor temperature was changed (simulated and measured experimental gas production were clearly different).

The model by Zaher et al. (2009) is not selected here because it is relatively complex, and the model parameters are not presented with any temperature dependency. Also, it would be necessary to modify the model originally made for batch AD processes to make it applicable to our bioreactor which has a continuous load rate.

3.2. Hill's AD model

The reasons for selecting Hill's model, Hill (1983), as the ultimate model to be adapted to the pilot bioreactor at Foss Biolab are given in Section 3.1. Hill's original model is presented in Section 3.2.1. A modified Hill's model which is the model adapted to the AD reactor at Foss Biolab is described in Section 3.2.2.

3.2.1. The original Hill's model

Figure 2 shows the steps of the AD process on which Hill's model is based. The alphabetic identificators used in Figure 2 refer to the model equations presented in the present section.
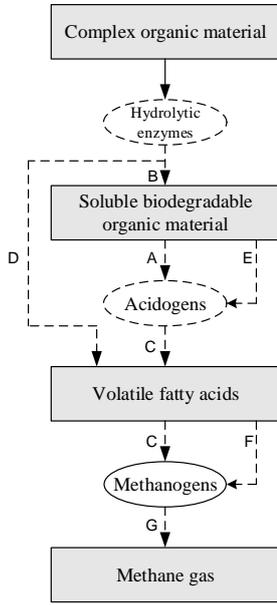

Figure 2: *The anaerobic digestion steps forming the basis of Hill's model. The alphabetic indicators refer to Hill's model, eqs. (1)-(10). The symbols resemble those in Zaher et al. (2009).*

Hill's model comprises eqs. (1)-(10) below, but a few changes are made in the symbols to make the model more readable and to have symbols which are in more compliance with symbols in other AD models. The differential equations stem from mass balances of the pertinent components. Homogeneous conditions are assumed.

The alphabetic identificators written in parentheses in the following refer to the flow diagram in Figure 2.

Defining that portion of the raw waste which can serve as substrate (A):

$$S_{bvs_{in}} = B_0 S_{vs_{in}} \qquad (1)$$

Defining that portion of the biodegradable material which is initially in the acid form (B):

$$S_{vfa_{in}} = A_f S_{bvs_{in}} \qquad (2)$$

Mass balance of biodegradable volatile solids (C):

$$\dot{S}_{bvs} = (S_{bvs_{in}} - S_{bvs}) \frac{F_{feed}}{V} - \mu \frac{1}{Y} X_{acid} \qquad (3)$$

Mass balance of VFA (D):

$$\dot{S}_{vfa} = (S_{vfa_{in}} - S_{vfa}) \frac{F_{feed}}{V}$$
$$+ \mu \frac{1-Y}{Y} X_{acid} - \mu_c \frac{1}{Y_c} X_{meth} \qquad (4)$$

Mass balance of acidogens (E):

$$\dot{X}_{acid} = \left(\mu - K_d - \frac{F_{feed}}{V} \right) X_{acid} \qquad (5)$$

Mass balance of methanogens (F):

$$\dot{X}_{meth} = \left(\mu_c - K_{dc} - \frac{F_{feed}}{V} \right) X_{meth} \qquad (6)$$

Methane gas flow rate (gas production) (G):

$$F_{meth} = V \mu_c k_{meth} \frac{1-Y_c}{Y_c} X_{meth} \qquad (7)$$

The reaction rates are as follows:

$$\mu = \mu_m \frac{1}{\frac{K_s}{S_{bvs}} + 1 + \frac{S_{vfa}}{K_i}} \qquad (8)$$

$$\mu_c = \mu_{mc} \frac{1}{\frac{K_{sc}}{S_{vfa}} + 1 + \frac{S_{vfa}}{K_{ic}}} \qquad (9)$$

The maximum reaction rates μ_m, μ_{mc} are functions of the reactor temperature as follows, Hashimoto et al. (1981):

$$\mu_m (T_{reac}) = \mu_{mc} (T_{reac}) = 0.013 T_{reac} - 0.129 \qquad (10)$$
$$(20°\text{C} < T_{reac} < 60°\text{C})$$

The death rates are set to one tenth of the maximum reaction rates:

$$K_d = 0.1 \mu_m \qquad (11)$$

$$K_{dc} = 0.1 \mu_{mc} \qquad (12)$$

Although Hill's model is selected as the ultimate model, we are motivated to implement a few changes to the model as explained in Section 3.2.2.

3.2.2. Modified Hill's model

Differences from the original Hill's model

In our study the following changes are made to the original Hill's model presented in Section 3.2.1. The resulting model is referred to as "the modified Hill's model".

- Parameters k_1, k_2, k_3, and k_5, replace the original parameters (yields) $1/Y$, $(1-Y)/Y$, $1/Y_c$, and $k_{meth}(1-Y_c)/Y_c$. Parameters k_1, k_2 and k_5 are estimated from experimental data, except k_3 which is calculated from the parameter values in the original Hill's model.

- The Haldane functions in the reaction rates μ and μ_c in Hill's original model, eqs. (8) and (9), are replaced with the simpler Monod functions:

$$\mu = \mu_m \frac{S_{bvs}}{K_s + S_{bvs}} \qquad (13)$$

$$\mu_c = \mu_{mc} \frac{S_{vfa}}{K_{sc} + S_{vfa}} \qquad (14)$$

This makes the calculations with the model in the context of parameter estimation easier. Using Monod functions is consistent with the comparable model by Simeonov et al. (1996).

- The death rates, eqs. (11) and (12), are replaced with constant parameters:

$$K_d = 0.02 \ [1/\text{d}] \qquad (15)$$

$$K_{dc} = 0.02 \ [1/\text{d}] \qquad (16)$$

which is in accordance with ADM1, Batstone et al. (2002). This simplifies the model.

- In the original Hill's model the retention time of the biomass (here: acidogens and methanogens) is equal to the hydraulic retention time (HRT):

$$T_{hr} = \frac{V}{F_{feed}} = \text{HRT} \qquad (17)$$

The retention time of the biomass is larger than the hydraulic retention time in up-flow sludge bed reactors such as applied here, where biomass is retained by gravity, Tchobanoglous et al. (2003). The retention time ratio b is here introduced. The retention time of the biomass, which is denoted the solids retention time (SRT), is assumed to be b times the hydraulic retention time:

$$T_{br} = bT_{hr} = \frac{bV}{F_{feed}} = \frac{V}{F_{feed}/b} = \text{SRT} \qquad (18)$$

where the term $V/(F_{feed}/b)$ expresses that the biomass flow out of the reactor is smaller than the flow of organic matter.

In the original Hill's model it is implicitly assumed that $b = 1$. Eq. (18) makes the model coherent with the standard ADM1 model, Batstone et al. (2002), in this respect though the SRT is represented differently (as an independent parameter) in ADM1. Eq. (18) is in accordance with the representation of SRT in e.g. Zaher et al. (2003) and Bernard et al. (2001).

Model equations in the modified Hill's model

Defining that portion of the raw waste which can serve as substrate:

$$S_{bvs_{in}} = B_0 S_{vs_{in}} \qquad (19)$$

Defining that portion of the biodegradable material which is initially in the acid form:

$$S_{vfa_{in}} = A_f S_{bvs_{in}} \qquad (20)$$

Mass balance of biodegradable volatile solids:

$$\dot{S}_{bvs} = (S_{bvs_{in}} - S_{bvs}) \frac{F_{feed}}{V} - \mu k_1 X_{acid} \qquad (21)$$

Mass balance of total VFA (see comment below):

$$\dot{S}_{vfa} = (S_{vfa_{in}} - S_{vfa}) \frac{F_{feed}}{V} \\ + \mu k_2 X_{acid} - \mu_c k_3 X_{meth} \qquad (22)$$

Mass balance of acidogens:

$$\dot{X}_{acid} = \left(\mu - K_d - \frac{F_{feed}/b}{V} \right) X_{acid} \qquad (23)$$

Mass balance of methanogens:

$$\dot{X}_{meth} = \left(\mu_c - K_{dc} - \frac{F_{feed}/b}{V} \right) X_{meth} \qquad (24)$$

Methane gas flow rate (gas production):

$$F_{meth} = V \mu_c k_5 X_{meth} \qquad (25)$$

where the reaction rates, with Monod kinetics, are as follows:

$$\mu = \mu_m \frac{S_{bvs}}{K_s + S_{bvs}} \qquad (26)$$

$$\mu_c = \mu_{mc} \frac{S_{vfa}}{K_{sc} + S_{vfa}} \qquad (27)$$

The maximum reaction rates μ_m, μ_{mc} are functions of the reactor temperature as in the original Hill's model, eq. (10), repeated here for easy reference:

$$\mu_m (T_{reac}) = \mu_{mc} (T_{reac}) = 0.013 T_{reac} - 0.129 \qquad (28)$$
$$(20°\text{C} < T_{reac} < 60°\text{C})$$

Above it is assumed that VFA is total VFA consisting mainly of propionate, butyrate, valerate, and acetate, Batstone et al. (2002). Acetate is the main VFA component, and it is used in aceticlastic methanogenesis which is the main methane-generating process. Methane is also generated in hydrogenotrophic methanogenesis. Hydrogen is generated from various components including the VFA components propionate, butyrate and valerate. To include effects of the hydrogenotrophic methanogenesis, S_{vfa} in our model represents total VFA and not only acetate.

Figure 3 shows an overall block diagram displaying the variables and parameters of the modified Hill's model eqs. (19)-(28).
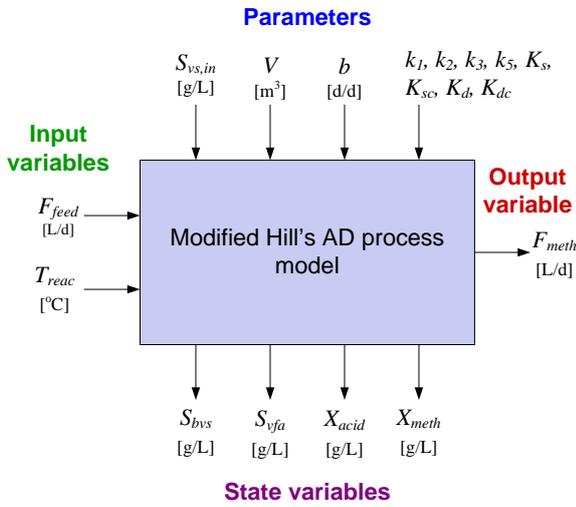

Figure 3: *Overall block diagram with variables and parameters of the modified Hill's model (19)-(28).*

In Section 3.3.3 about parameter estimation the steady-state (or static) version of the dynamic model is needed. The steady-state model is obtained by setting the time-derivatives in the above differential equations equal to zero.

3.3. Adaptation of modified Hill's model to the AD reactor

In the the following subsections, 3.3.1-3.3.3, the modified Hill's model, eqs. (19)-(28), is adapted to the AD reactor ADR2. In Section 3.3.1 are presented parameter values found in literature references or known by design. In Section 3.3.2 values of some of the parameters are calculated from a laboratory test. In Section 3.3.3 the remaining unknown parameters, and unknown values of two of the state variables (namely the

methanogens and acidogens concentrations) in a pertinent steady-state operating point, are estimated from time-series of laboratory data and time-series from on-line sensors. In Section 3.3.4 the temperature dependency of the estimated model is demonstrated.

3.3.1. Known parameters in modified Hill's model

Table 1 shows parameters which are assumed to have known values.

Table 1: Parameters with known values. (Units are listed in Appendix A.2.)

$k_3 = \frac{1}{Y_c} = 31.7$	Hill (1983)
$K_d = 0.02$	Batstone et al. (2002)
$K_{dc} = 0.02$	Batstone et al. (2002)
$k_{meth} = 0.5$	Hill (1983)
$K_{sc} = 3$	Husain (1998)
$V = 250$	Reactor design

3.3.2. Parameters in modified Hill's model calculated from laboratory test

Parameters B_0 and A_f are found from a laboratory test as described below. Their values are shown in Table 2.

Table 2: Parameters assumed to have known values

$A_f = 0.69 \, \frac{\text{g VFA/L}}{\text{g BVS/L}}$	Cf. comment in text
$B_0 = 0.25 \, \frac{\text{g BVS/L}}{\text{g VS/L}}$	Cf. comment in text

- B_0 defines the ratio between BVS and VS in the feed:

$$S_{bvs_{in}} = B_0 S_{vs_{in}} \qquad (29)$$

It is assumed that a proper value of B_0 can be found from the following specific long-term test. At time t_0 = July 12, 2011 a fresh sample of the subtrate was put into an incubator having constant temperature of 35 °C.

The biogas production was registered regularly until time t_1 = Sept. 25, 2011 which is the time where the biogas production became virtually zero. The VS concentration, here denoted $S_{vs_{in}}$, of the substrate was measured at times t_0 and t_1, cf. Table 3.

Since the biogas production is zero at t_1 it is concluded that the biodegradable part of the substrate is completely degraded at t_1. Thus, in the long-term test,

$$S_{bvs_{in}} = S_{vs_{in}}(t_0) - S_{vs_{in}}(t_1) \qquad (30)$$

Table 3: Long-term test to find parameter B_0

Time	$S_{vs_{in}}$	Biogas prod.
t_0 = July 12, 2011	29.25	Non-zero
t_1 = Sept. 25, 2011	21.92	Zero

From eq. (29) the following value of B_0 is obtained:

$$B_0 = \frac{S_{bvs_{in}}}{S_{vs_{in}}} = \frac{S_{vs_{in}}(t_0) - S_{vs_{in}}(t_1)}{S_{vs_{in}}(t_0)}$$

$$= \frac{29.25 - 21.92}{29.25} = 0.25 \frac{\text{g BVS/L}}{\text{g VS/L}} \qquad (31)$$

- A_f defines the ratio between VFA and BVS in the feed:

$$S_{vfa_{in}} = A_f S_{bvs_{in}} \qquad (32)$$

It is assumed that a proper value of A_f can be found from the approximate steady-state operating point around June 10, 2012 which is used for estimation of the model parameters (except parameter k_5 which is estimated from dynamic responses) using the steady-state version of the dynamic model. The pertinent values needed to calculate A_f are shown in Table 4. From eqs. (29) and (32),

$$A_f = \frac{S_{vfa_{in}}}{S_{bvs_{in}}} = \frac{S_{vfa_{in}}}{B_0 S_{vs_{in}}} \qquad (33)$$

$$= \frac{5.23}{0.25 \cdot 30.4} = 0.69 \frac{\text{g VFA/L}}{\text{g BVS/L}} \qquad (34)$$

Table 4: Data used to calculate parameter A_f

Time	$S_{vs_{in}}$	$S_{vfa_{in}}$
t_0 = 10. June 2012	30.4	5.23

3.3.3. Estimation of unknown parameters and variables in modified Hill's model using real data

Parameters and variables to be estimated

The following parameters and variables in the modified Hill's model, eqs. (19)-(28), are to be estimated:

$$k_1, k_2, k_5, K_s, b, X_{acid}, X_{meth}. \qquad (35)$$

In the model k_1, k_2, k_5, K_s, and b appear as parameters, while X_{acid} and X_{meth} are state variables. It is necessary to estimate X_{acid} and X_{meth} since their values are not known.

Identifiability

Before trying to estimate parameters and variables, their structural identifiability should be determined, Dochain and Vanrolleghem (2001). Structural identifiability concerns the possibility to give a unique value to the unknown parameters and variables, and this property can be assessed with a number of alternative methods, e.g. the method of Generating series which is based on calculating Lie derivatives, or by analyzing the uniqueness of the parameters of the Laplace based transfer function of a linearized version of the (nonlinear) model. However, for the estimation method used, see below, the structural identifiability is obvious since independent analytical expressions for the pertinent parameters and variables using steady-state data are obtained, except for one parameter, namely k_5, which is found by optimization using dynamic data. Hence a rigorous structural identifiability assessment is not necessary and therefore not accomplished here.

Method of parameter estimation

Yield-parameter k_5 is a crucial model parameter since it is directly related to the methane gas flow rate, cf. eq. (25). It is decided to estimate k_5 using nonlinear least squares (NLS) estimation based on optimization using iterated simulations of the modified Hill's model. The simulations are based on the explicit Euler method implemented with for-loops in MATLAB. The optimization problem is to minimize the difference between real (measured) and simulated F_{meth} in the least squares sense over a specific time interval which is from $t = 66$ d to 95 d in Figure 4. ($t = 0$ corresponds to April 19, 2012.)

The iterations (including simulations) are executed automatically by the optimization solver.[1]

From $t = 72.3$ d the methane gas flow is being controlled by a feedback controller manipulating the feed pump. The noise in gas flow measurement seen in Figure 4 is due to blockings and power outages. Because of the feedback control, this noise imposes noise in the feed flow, via the controller.

Before each of these simulations is started (automatically by the optimization solver) the six parameters/variables k_1, k_2, K_s, b, X_{acid}, and X_{meth} are calculated from the steady-state version of the dynamic model (19)-(28) using steady-state operational data at a specific operating point assuming intially that k_5 has a "guessed" value which is set equal to the value in eq. (7) of Hill's original model:

$$k_{5_{guess}} = k_{meth} \frac{1 - Y_c}{Y_c} = 15.4 \qquad (36)$$

Table 5 shows values of inputs and states in the pertinent steady-state operation point which is $t = 66$ d in Figure 4. ($t = 0$ = April 19, 2012.)

[1] The optimization solver is the lsqnonlin function in MATLAB.
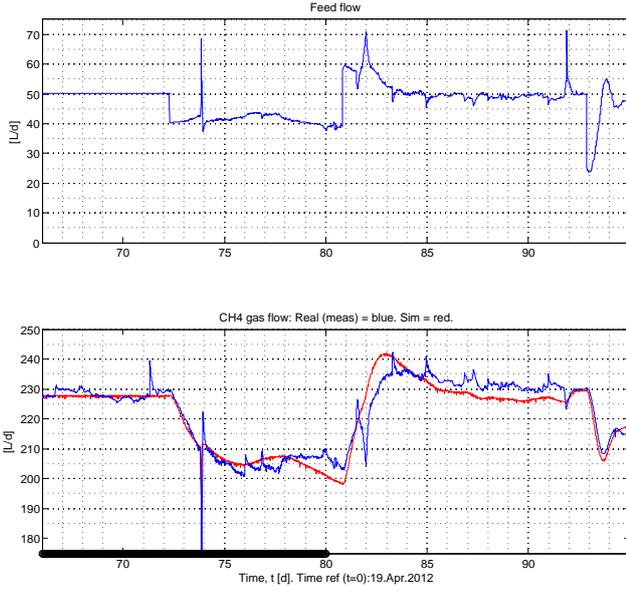
Figure 4: *Upper plot: Measured feed flow. Lower plot: Measured (blue) and simulated (red) methane gas flow.*

Table 5: Values of inputs and states in the steady-state operation point ($t = 66$ d; $t = 0 = 19$. April 2012) used for model adaption. Units are listed in Appendix A.2.

Variables	Comments
$F_{feed} = 50$	Applied by feed pump
$T_{reac} = 35$	Sensor reading
$S_{bvs_{in}} = 32.4$	Lab analysis
$S_{bvs} = 5.81$	Lab analysis
$S_{vfa} = 1.13$	Lab analysis
$F_{meth} = 227.9$	Sensor reading

The formulas for calculating the above mentioned six parameters/variables, namely k_1, k_2, K_s, b, X_{acid}, X_{meth}, from the steady-state version of the dynamic model (19)-(28) are given below.

- b is calculated from the steady-state version (i.e. the time-derivative term is set to zero) of eqs. (24) and (27) to give

$$b = \frac{\frac{F_{feed}}{V}}{\mu_{mc}\frac{S_{vfa}}{S_{vfa}+K_{sc}} - K_{dc}} \qquad (37)$$

- K_s is calculated from the steady-state version of eqs. (23) and (26) to give

$$K_s = S_{bvs}\left(\frac{\mu_m}{K_d + \frac{F_{feed}}{bV}} - 1\right) \qquad (38)$$

- X_{meth} is calculated from the steady-state version of eq. (25) to give

$$X_{meth} = \frac{F_{meth}}{V\mu_c k_5} \qquad (39)$$

- X_{acid} is calculated with

$$X_{acid} = r_{am}X_{meth} \qquad (40)$$

Here, r_{am} is (in the steady-state calculations) set to

$$r_{am} = 3.4 \qquad (41)$$

as it was observed in simulations for various feed rates with the original Hill's model with parameters from Husain (1998) that the ratio X_{acid}/X_{meth} varied only slightly around 3.4. However, this ratio is not necessarily 3.4 after the estimation procedure is finished.

- k_1 is calculated from the steady-state version of eqs. (19) and (26) to give

$$k_1 = \frac{(S_{bvs_{in}} - S_{bvs})F_{feed}}{V\mu X_{acid}} \qquad (42)$$

- k_2 is calculated from the steady-state version of eqs. (22), (26) and (27) to give

$$k_2 = \frac{\mu_c k_3 X_{meth} - (S_{vfa_{in}} - S_{vfa})\frac{F_{feed}}{V}}{\mu X_{acid}} \qquad (43)$$

The simulations used in the optimization (to estimate k_5) are based on the dynamic model (19)-(28). In the simulated model a lag of time-constant equal to

$$\theta_{lag} = 0.2 \text{ d} \qquad (44)$$

is included. This time-constant represents the lowpass filter used in the real system at Foss Biolab to smooth the noisy biogas flow measurement, cf. Section 2.2.

Figure 5 illustrates the estimation method used to estimate the parameters/variables (35). In this figure, p is the parameter to be estimated which is

$$p = k_5 \qquad (45)$$

In Figure 5, the measured output (time series) is

$$y_{meas} = F_{meth_{meas}} \qquad (46)$$

and inputs (time series) are

$$u = [F_{feed}, T_{reac}] \qquad (47)$$

The output of the optimization objective function f (and this output is to be minimized) is the sum of
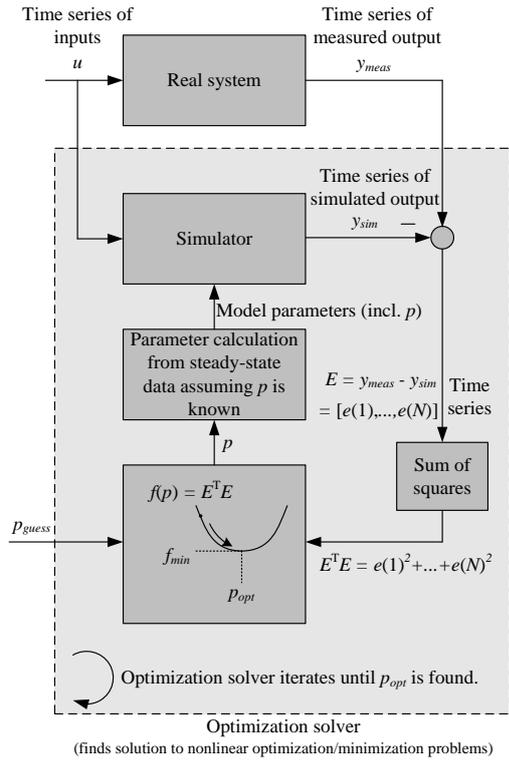
Figure 5: *The estimation of parameter vector $p = k_5$ is based on optimization (minimization) using iterated simulations.*

squares of prediction errors over the estimation time interval:

$$f(M, p) = SSE_{e_{pred}} \tag{48}$$

$$= \sum_{k=1}^{N} [e_{pred}(t_k)]^2 \tag{49}$$

$$= E_{pred}^T E_{pred} \tag{50}$$

E_{pred} is the time-series (vector) of prediction errors:

$$E_{pred} = [e_{pred}(t_1), \ldots, e_{pred}(t_N)]^T \tag{51}$$

where N is the number of time-steps in the estimation time interval. In the present application, $e_{pred}(t_k)$ is

$$e_{pred}(t_k) = F_{meth_{meas}}(t_k) - F_{meth_{sim}}(t_k) \tag{52}$$

where $F_{meth_{meas}}$ is measured reactor methane flow, and $F_{meth_{sim}}$ is simulated F_{meth}.

In eq. (48), M represents the model comprising eqs. (19)-(28).

The optimal (best) estimate of p is the value of p which minimizes $SSE_{e_{pred}}$:

$$p_{est} = p_{opt} : \min_p SSE_{e_{pred}} \tag{53}$$

Results

In the time interval 80-95 d in Figure 4, the simulated F_{meth} based on the estimated model is plotted together with real F_{meth}. The simulation runs with initial state equal to the real state at $t = 66$ d. In this time interval the maximum difference between the simulated F_{meth} and the real F_{meth} is approximately 10 L/d while the maximum gas flow is approximately 235 L/d. It seems that the adapted modified Hill's model is able to predict the produced methane gas quite well.

Figure 6 shows in the upper plots real values (from laboratory analysis) and simulated values of the state variables S_{bvs} and S_{vfa} together with the respective real concentrations in the feed.
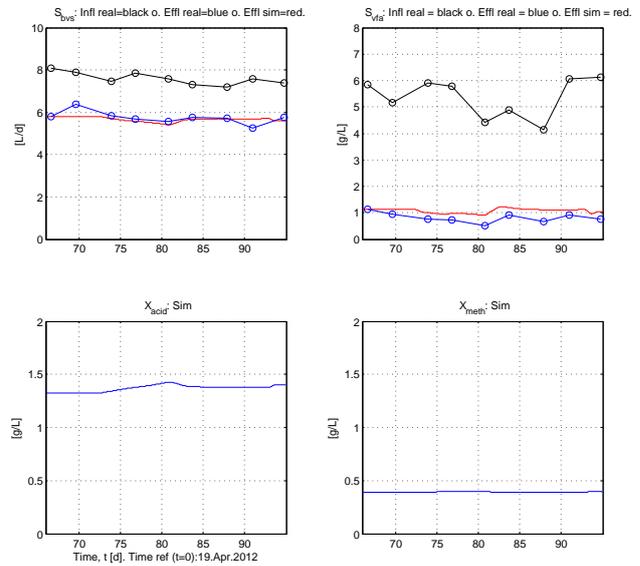
Figure 6: *Upper plots: Real values (from laboratory analysis) and simulated values of the state variables S_{bvs} and S_{vfa} together with the respective real concentrations in the feed. Lower plots: Simulated values of the state variables X_{acid} and X_{meth} for which we do not have laboratory analysis data.*

The lower plots show simulated values of the state variables X_{acid} and X_{meth} for which no laboratory analysis data are available.

Table 6 shows the values of the estimated variables and parameters together with standard deviations (σ), both absolute and relative, obtained with simulations as described later in the present section.

Uncertainty of estimates in terms of standard deviation

Uncertainty in the estimates can be expressed by the variability of the estimates. The variability may be calculated in a number of ways, e.g.:

Table 6: Values of estimated variables and parameters, and absolute and relative standard deviations (σ). Units are listed in Appendix A.2. The standard deviations are found from bootstrapping simulations as described in the present section.

Estimates	Abs σ	Rel σ [%]
$b = 2.90$	0.030	$\frac{0.030 \cdot 100}{2.90} = 1.0$
$K_s = 15.5$	0.24	1.5
$k_1 = 3.89$	0.11	2.8
$k_2 = 1.76$	0.058	3.3
$k_5 = 26.3$	0.27	1.0
$X_{acid} = 1.32$	0.024	1.8
$X_{meth} = 0.39$	0.0070	1.8

- Calculation of the covariance of the parameter estimation error from Fisher's Information Matrix which involves numerical or analytical calculation of model output sensitivities (i.e. calulation of partial derivatives, or linearization) with respect to model parameters, Dochain and Vanrolleghem (2001). With a complex model analytical sensitivies may be calculated using computer tools for symbolic mathematics.

  A possible alternative way of calculating the parameter estimation error covariances is with the calculation of so-called sigma points using the nonlinear model directly, without any linearization, as in the Unscented Kalman Filter, Simon (2006).

- Bootstrapping with parametric simulation, Davison and Hinkley (1997), which involves running a large number of simulations where the pertinent input data used in the estimation are varied randomly according to an assumed probability distribution which (should) resemble the actual distribution of the real data used in the estimation. (Bootstrapping with parametric simulation resembles Monte Carlo simulations.) The parameter uncertainty can then be assessed from the observed variations of the estimates in the simulations typically in terms of standard deviation of the variation.

The method of bootstrapping is selected since this method is relatively straightforward and applicable.

Table 7 lists three quantities used as input data in the parameter estimation. These quantities are varied randomly and independently in the bootstrapping simulations. These quantities represent the steady-state operating point used in the parameter estimation, as explained above in the present section. Table 7 shows the pertinent standard deviations (σ) calculated from a number of laboratory analysis data sets taken over several weeks in the summer of year 2012. This time interval includes the steady-state operating point, namely day 66, see Figure 4). In the simulations it is assumed that their probability distributions are Gaussian.

Table 7: Standard deviations of quantities which are varied (randomly) in bootstrapping with parametric simulation used to assess variations of estimated parameters.

$\sigma_{S_{vs_{in}}}$ [g/l]	$\sigma_{S_{bvs}}$ [g/l]	$\sigma_{S_{vfa}}$ [g/l]
0.253	0.256	0.0119

The resulting standard deviations of the estimates found from the bootstrapping simulations are shown in Table 6. Note that these standard deviatons express only the variations in the estimates due to variations in the three quantities given in Table 7. There are several other factors which contribute to the (total) uncertainty of the estimates, as model structure errors and systematic measurement errors.

Sensitivity of estimates with respect to assumptions

It is informative to assess the sensitivity of the estimates with respect to assumptions for the estimation method. The relative sensitivity of parameter p to parameter a is defined as

$$S_{p,a} = \frac{\frac{\partial p}{p}}{\frac{\partial a}{a}} \approx \frac{\frac{\Delta p}{p_0}}{\frac{\Delta a}{a_0}} = \frac{\frac{p_1 - p_0}{p_0}}{\frac{a_1 - a_0}{a_0}} \qquad (54)$$

where p_0 and a_0 are nominal values. p_0 is a parameter shown in Table 6. a_0 is a parameter shown in Table 2 or Table 5. p_1 and a_1 are respective values after a change is made in a.

Table 8 shows relative sensitivities as found by perturbing parameters a_i with a 10% positive additive change and observing the corresponding change in the estimated parameter p. For example, $S_{b,B_0} = -0.62$ in Table 8 means that a 10% additive increase in the assumed value of B_0 causes an additive change in the estimated b of $-0.62 \cdot 10\% = -6.2\%$.

Note that X_{acid} and X_{meth} in Table 8 are actually estimated values for the steady-state operating point, and serve as initial values in the simulations which are run as a part of the estimation of parameter k_5 using optimization. Thus the simulated responses in X_{acid} and X_{meth} varies with time, see Figure 6.

None of relative sensitivities shown in Table 8 has extreme values. Hence it is concluded that the relative sensitivities do not demand a change of the assumed values of the pertinent a-parameters.

Table 8: Relative sensitivities $S_{a,b}$

$p \downarrow, a \rightarrow$	$S_{vs_{in}}$	A_f	B_0	K_d
b	0	0	0	0.30
K_s	0	0	1	0
k_1	1.3	-1.5	-0.62	-0.066
k_2	2.6	1.7	1.7	0.28
k_5	-1.7	-1.5	-1.5	-0.066
X_{acid}	2.0	1.7	1.7	0.066
X_{meth}	2.0	1.7	1.7	0.066

3.3.4. Temperature dependency

In the modified Hill's model (as in the original model) the reaction rates, eqs. (26) and (27), depend on the reactor temperature T_{reac}, cf. (28). In the model adaption made in Section 3.3.3 T_{reac} was kept constant at 35 °C. Simulations with modified Hill's model, though not shown here, indicate that a change in T_{reac} gives a dynamic response in F_{meth}. We do not have experimental results with varying T_{reac} for reactor ADR2 which is used in the present study. However, experimental results exist for reactor ADR1 which was in use at Foss Biolab from August 17, 2011 until April 19, 2012. It is fair to assume that the temperature dependency as expressed in Hill's model holds equally well for ADR2 as for ADR1 since the physical appearances of the two reactors are similar and the operation and feed (manure from the same dairy livestock) are similar.

Figure 7 shows responses in F_{meth} due to changes in T_{reac} and F_{feed} for the reactor ADR1.

During the time period shown in Figure 7 both T_{reac} and the feed flow F_{feed} were changed, but only the variations caused by the temperature change are of interest here. The simulations are based on a mathematical model adapted to ADR1 using the same method for model adaptation as is used for model adaptation to ADR2 as described in Section 3.3.3.

As seen in Figure 7, T_{reac} was increased twice:

- At time $t = 60.5$ d: From approximately 24°C to approximately 30°C.

- At time $t = 67.5$ d: From approximately 30°C to approximately 35°C.

These temperatures are in the mesophilic range. The changes were implemented as step-wise changes of the temperature setpoint in the temperature controller TC1, cf. Figure 1.

Since the simulated F_{meth} and the real F_{meth} plotted in Figure 7 show similar responses, it can be concluded that eq. (28) represents the temperature dependency of the real reactor quite accurately, at least in the mesophilic temperature range.
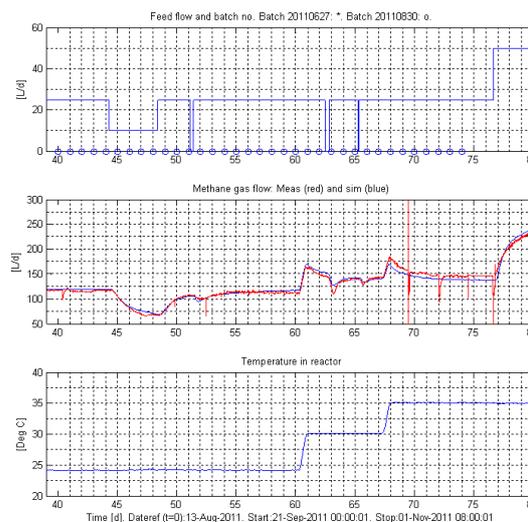

Figure 7: *Reactor ADR1: Responses in F_{meth} (middle) due to changes in T_{reac} (lower) and F_{feed} (upper).*

4. Reactor temperature model

The reactor temperature T_{reac} is actually a (dynamic) state variable although it is assumed to be a parameter in the modified Hill's model, cf. eq. (28). In some situations it is useful to have a dynamic model describing the dynamic behaviour of T_{reac}, e.g. in optimization of the reactor design and operation where energy and economical cost are taken into account, and in model-based tuning of a temperature controller for the reactor. A dynamic model describing T_{reac} is now derived and adapted the model to the real bioreactor (ADR2).

T_{reac} depends on a number of variables and parameters, e.g. the manipulated supplied power to the electrical heater for the reactor, the temperature of the reactor feed, the feed flow rate, etc. It is reasonable to assume that T_{reac} can be modelled with an energy balance for the liquid of the reactor. Due to the mixing which takes place in the reactor it is assumed that there are homogeneous conditions in the reactor. The energy balance can be written as

$$\frac{dT_{reac}}{dt} = \frac{1}{c\rho V}[P_{heat}$$
$$+ c\rho F_{feed}\left(T_{feed} - T_{reac}\right) \quad (55)$$
$$+ G\left(T_{room} - T_{reac}\right)]$$

The liquid in the reactor is assumed having the same thermal characteristics as water. All model parameters in eq. (55) except the thermal conductivity G are assumed known, cf. Table 9.

Table 9: Assumed known parameters of reactor temperature model.

$c = 4200$ J/(kg K)
$\rho = 1000$ kg/m^3
$V = 250$ L

All variables and parameters in eq. (55) are assumed to have SI units, although some are presented in different units in the present section.

Measured time series of all variables in eq. (55), i.e. T_{reac}, P_{heat}, F_{feed} and T_{room}, are available. F_{feed} is constantly 55 L/d. T_{room} varies between 12.7 °C and 15.8 °C with mean value 13.7 °C. T_{feed} is assumed to be equal to T_{room}.

G is estimated from experimental data. Three alternative methods are applied:

1. **Least squares (LS) method with static model**: By assuming that all variables, including T_{reac}, in eq. (55) have constant values, dT_{reac}/dt can be set to zero. Solving the resulting static model for G gives

$$G = \frac{-P_{heat} - c\rho F_{feed}(T_{feed} - T_{reac})}{T_{room} - T_{reac}} \quad (56)$$

from which G can be estimated with the LS method.

2. **LS method with dynamic model**: The model (55) is linear in the unknown parameter G:

$$G = \frac{1}{T_{room} - T_{reac}}[c\rho V \frac{dT_{reac}}{dt} \quad (57)$$
$$- P_{heat} - c\rho F_{feed}(T_{feed} - T_{reac})]$$

Here, dT_{reac}/dt is calculated using simple numerical differentiation[2]:

$$\frac{dT_{reac}}{dt} = \frac{T_{reac}(t_{k+1}) - T_{reac}(t_k)}{T_s} \quad (58)$$

G is estimated from eq. (57) with the LS method.

3. **Nonlinear least squares (NLS) method with dynamic model and additional lag**: It is assumed that the original model (55) describes the dynamic properties of T_{reac}. It is also assumed that there may be additional dynamic phenomena due to energy capacitance in the heating element (the coil) and in the reactor wall. Furthermore, a measurement filter in terms of a discrete-time algorithm resembling a time-constant system with time-constant $T_f = 600$ s is actually in operation

---

[2]We used the `diff` function in MATLAB.

in the AD reactor. This filter also adds dynamics to the temperature behaviour. To obtain a total model able to represent these additional dynamics, the original model (55) is augmented with the following general "lag model" incorporating time-constant dynamics:

$$\frac{dT_{reac_{lag}}}{dt} = \frac{(T_{reac} - T_{reac_{lag}})}{\theta_{temp}} \quad (59)$$

where θ_{temp} [d] is a time-constant. One motivation for this augmentation is the expectation that the estimation of G in eq. (55) will be improved if also θ_{temp} in eq. (59) is estimated. Thus, both G and θ_{temp} are estimated. The measured temperature is now represented with $T_{reac_{lag}}$, while T_{reac} is actually unknown which makes it difficult to apply the ordinary LS method for estimation. Instead, NLS estimation is used based on optimization using iterated simulations. The procedure is the same as was used to estimate parameter k_5 in the modified Hill's model, cf. Section 3.3.3. Therefore, Figure 5 applies, but with the following changes. The measured output is

$$y_{meas} = T_{reac_{meas}} \quad (60)$$

and inputs (time series) are

$$u = [P_{heat}, T_{room}, T_{feed}] \quad (61)$$

where $T_{room} = T_{feed}$. The prediction error, $e_{pred}(t_k)$, is

$$e_{pred}(t_k) = T_{reac_{meas}}(t_k) - T_{reac_{lag_{sim}}}(t_k) \quad (62)$$

where $T_{reac_{lag_{sim}}}$ is simulated $T_{reac_{lag}}$.

The model used in the iterated simulations executed by the optimization function consists of the differential equations (55) and (59).

The parameter vector to be estimated is

$$p = \begin{bmatrix} G \\ \theta_{temp} \end{bmatrix} \quad (63)$$

The following guessed (initial) parameter values for the estimation are used:

$$p_{guessed} = \begin{bmatrix} G_{guessed} \\ \theta_{temp_{guessed}} \end{bmatrix} = \begin{bmatrix} 1.0 \cdot 10^5 \text{ (J/d)K} \\ 1.0 \text{ d} \end{bmatrix} \quad (64)$$

The guessed value of $G_{guessed}$ stems from some calculations made with the previous AD reactor (ADR1).

Table 10: Results of estimation of G with different estimation methods

Method	G	θ_{temp}	SSE	RMSE
	[(J/d)/K]	[d]	[K^2]	[K]
1. LS static	$1.88 \cdot 10^5$	–	23.4	0.38
2. LS dyn	$2.11 \cdot 10^5$	–	18.7	0.34
3. NLS dyn&lag	$1.96 \cdot 10^5$	0.023	11.1	0.26

Estimated parameters and performance indices with the above three methods of estimation of G are shown in Table 10.

To check the quality of the estimates, both SSE (sum of squared error) which is defined by eq. (48), and RMSE which is the Root Mean Squared Error index, Varmuza and Filzmoser (2009), are calculated:

$$\text{RMSE} = \sqrt{\frac{1}{N} \sum_{k=1}^{N} [e_{pred}(t_k)]^2} \qquad (65)$$

SSE is the same function as is used to solve the NLS estimation problem, but it does not have the same unit as the prediction error, e. RMSE resembles the standard deviation, and it has the same unit as the production error, e. Therefore, RMSE may be more useful than SSE as a performance index for model validation, while SSE is more useful in solving estimation (optimization) problems since it is a square function, Varmuza and Filzmoser (2009).

Figure 8 shows simulated T_{reac} for three cases of parameter estimation, cf. Table 10, together with real (measured) T_{reac}, P_{heat}, and $T_{room} = T_{feed}$. (The oscillations in P_{heat} are due to the On/Off control signal from the temperature controller.) The respective time intervals of the timeseries of data used for estimation in the three cases are shown in the upper plot in Figure 8.

Notes to the plots in Figure 8:

- Around $t = 161.4$ d and 161.9 d the changes in the measured T_{reac} appears *earlier* than the changes in P_{heat} assumed to cause the changes in T_{reac}. The sampling time is $T_s = 15$ min $= 0.0104$ d, which is in the same range as of the periods of the changes of P_{heater}.

- The simulated T_{reac} is clearly larger than the measured T_{reac} between $t = 160.6$ and 161.0 d. The difference may be due to disturbances for which the controller compensates by increasing the (average) P_{heater}. These disturbances are not due to the observed reduction of T_{room} since the actual values of T_{room} are used in the simulation. We can not identify these disturbances, but they may be unknown variations in T_{feed}.
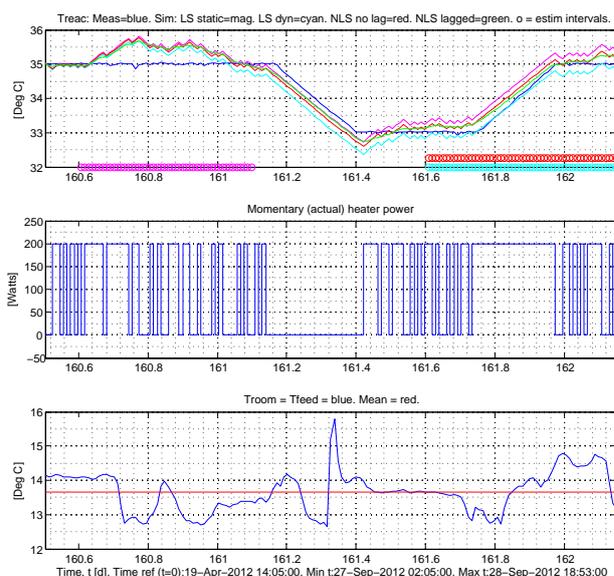

Figure 8: *Upper plot: Real (measured) and simulated T_{reac}, and time intervals for estimation (marked 'o'). Middle plot: Real P_{heat}. Lower plot: $T_{room} = T_{feed}$.*

The results shown in Table 10 and Figure 8 show no large difference between the three estimation methods used here, and all of the simulated responses of T_{reac} resembles quite well the measured T_{reac}. Still, the best result is obtained with the third method (NLS with augmented dynamic model). Hence, the ultimate estimated value of G is selected as

$$G = 1.96 \cdot 10^5 \text{ (J/d)K} \qquad (66)$$

The thermal time-constant, $\theta_{thermal}$, can now be calculated from the model (55). Using the pertinent numerical values for the parameters,

$$\theta_{thermal} = \frac{c\rho V}{c\rho F_{feed} + G} \qquad (67)$$

$$= \frac{4200 \cdot 1000 \cdot 0.25}{4200 \cdot 1000 \cdot 0.055 + 1.96 \cdot 10^5} \qquad (68)$$

$$= 2.46 \text{ d} \qquad (69)$$

In some applications of the thermal model derived in the present section, for example in optimization of reactor design and operation where thermal energy is taken into account, it will be sufficient to use only the main part of the model. The main part is given by eq. (55). However, in temperature controller tuning more appropriate controller parameter values can be expected by taking into account also the lag-model (59).

5. Discussion

The modified Hill's model which has been adapted to the pilot bioreactor fed dairy manure is a relatively simple model compared with alternative models since the model does not contain neither ammonia, alkalinity, nor pH as variables. These variables are more important in reactors fed manure from swine or poultry because their values may have higher impact on the stability of such reactors.

The modified Hill's model is assumed to be sufficiently accurate as a basis for optimal reactor design and operation, state-estimation and control for a reactor fed dairy manure where the main output is the produced methane gas flow. In applications requiring a prediction of hydrogen or carbondioxide gas production alternative models must be used.

The parameters B_0 (biodegradability constant) and A_f (acidity constant) are estimated from data from one experiment only. Ideally, more experimental data should have been used.

In the original Hill's model, Haldane functions are used in the reaction rates. Instead, Monod functions are used, mainly to simplify model adaptation. These simplifications have support in some literature references.

In the orignal Hill's model, the solids residence time and the hydraulic residence time were assumed to be equal. In our study, this assumption caused problems with the model adaptation (results are not shown here), while assuming different residence times, related with a proportionality factor, worked well.

The dynamic model based on energy balance describing the temperature in the liquid phase of the bioreactor assumes homogeneous conditions in the reactor. A model with acceptable accuracy was adapted under this idealized assumption. However, the model adaptation was improved by including an additional time-constant lag in the model. This lag can be regarded as a representation of inhomogeneous conditions, or spatial variations, in the reactor.

6. Conclusions

A dynamic model has been adapted to a pilot anaerobic reactor fed dairy manure using steady-state and dynamic operational data. The model is a modification of a model originally developed by Hill (1983). The model is based on material balances, and comprises four state variables, namely biodegradable volatile solids, volatile fatty acids, acidogens, and methanogens. Simulations compared with measured methane gas flow indicate that the model is able to predict the methane gas flow produced in the reactor.

The steady-state data used for the model adaptation are feed flow (loading rate), reactor temperature, methane gas flow, and laboratory analysis values of influent and effluent VS and VFA concentrations at one specific steady-state operating point. The dynamic data used are feed flow, reactor temperature and methane gas flow over a time-interval of 15 days.

Also, a dynamic model for the reactor temperature based on an energy balance of the liquid is adapted to the pilot reactor. The model is able to predict the reactor temperature. A combination of this model and the model of the the anaerobic processes can be useful in optimization of reactor design and operation when energy production and economical costs are taken into account. Furthermore, this model can be used for temperature controller tuning.

Acknowledgments

A. Nomenclature

A.1. Abbreviations

AD = Anaerobic digestion

ADM1 = Anaerobic Digestion Model No. 1

ADR1 = Anaerobic digestion reactor 1 which was in use at Foss Biolab from 17. August 2011 until 19. April 2012

ADR2 = Anaerobic digestion reactor 1 which has been in use at Foss Biolab from 19. April 2012

BVS = Biodegradable volatile solids

HRT = Hydraulic retention time

LS = Least squares

MPC = Model-based predictive control

NLS = Nonlinear least squares

PWM = Pulse-width modulation

RMSE = Root mean squared error

SSE = Sum squared error

VFA = Volatile fatty acids

VS = Volatile solids

A.2. Nomenclature of model of AD processes

The nomenclature is in alphabetical order.

A_f [(g VFA/L)/(g BVS/L)] is acidity constant.

b [d/d] is retention time ratio.

B_0 [(g BVS/L)/(g VS/L)] is biodegradability constant.

F_{feed} [L/d] is influent or feed flow or load rate, assumed equal to effluent flow (constant volume).

F_{meth} [L CH$_4$/d] is methane gas flow.

k_1 [g BVS/(g acidogens/L)] is a yield constant.

k_2 [g VFA/(g acidogens/L)] is a yield constant.

k_3 [g VFA/(g methanogens/L)] is a yield constant.

k_5 [L/g methanogens] is a yield constant.

K_i [g VFA/L] is VFA inhibition constant for acidogens.

K_{ic} [g VFA/L] is VFA inhibition constant for methanogens.

K_s [g BVS/L] is Monod half-velocity constant for acidogens.

K_{sc} [g VFA/L] is Monod half-velocity constant for methanogens.

K_d [d^{-1}] is specific death rate of acidogens.

K_{dc} [d^{-1}] is specific death rate of methanogens.

μ [d^{-1}] is reaction (growth) rate of acidogens.

μ_c [d^{-1}] is reaction (growth) rate of methanogens.

μ_m [d^{-1}] is the maximum reaction rate for acidogens.

μ_{mc} [d^{-1}] is the maximum reaction rate for methanogens.

σ_y is standard deviation of signal y.

$S_{p,a}$ is relative sensitivity of parameter p with respect to parameter a.

S_{vfa} [g VFA/L] is concentration of VFA acids in reactor.

$S_{vfa_{in}}$ [g VFA/L] is concentration of VFA in biodegradable part of influent.

S_{bvs} [g BVS/L] is concentration of BVS in reactor.

$S_{bvs_{in}}$ [g BVS/L] is concentration of BVS in influent.

$S_{vs_{in}}$ [g VS/L] is concentration of volatile solids in influent.

T_{reac} [°C] is reactor temperature.

θ_{bio} [d] is time-constant of lag in methane gas responses.

V [L] is effective reactor volume.

X_{acid} [g acidogens/L] is concentration of acidogens.

X_{meth} [g methanogens/L] is concentration of methanogens.

Y [g acidogens/g BVS] is yield coefficient of acidogens.

Y_c [g methanogens/g VFA] is yield coefficient of methanogens.

A.3. Nomenclature of model of reactor temperature

The nomenclature is in alphabetical order.

c [J/(kg K)] is specific heating capacity of reactor liquid.

G [(J/d)/K] is thermal conductivity.

P_{heat} [J/d] is supplied power to electrical heater.

ρ [kg/m^3] is density of reactor liquid.

T_{feed} [°C] is temperature of reactor feed.

T_{room} [°C] is air (ambient) temperature.

θ_{temp} [d] is time-constant of lag in temperature responses.

θ_{therm} [d] is the thermal time-constant calculated from the energy balance of the reactor.

V [m^3] is effective volume of reactor liquid.

B. Laboratory analysis methods

Below is a description of the methods of laboratory analysis of the components in the bioreactor influent and effluent used in the mathematical modeling presented in this paper.

- **VS**: Three parallel tests for each sample. The samples are dried in an oven at 105°C for approximately one day. Then, the (dried) samples are combusted in a furnace at 550°C for 2 hours. The VS concentration in g/L is calculated as the weight lost during the combustion divided by the sample volume.

- **VFAs**: Two parallel tests for each sample. The samples are centrifuged for 30 min, and then filtered. The samples are diluted with deionized water, then added to small vials together with formic acid, capped, and stored in a refrigerator until measurement is done. The VFA concentrations in g/L are measured by a gas chromatograph (GC) using three injections from each of the parallels.

Other components analyzed, but not used in the modeling in this paper are tCOD, sCOD, ammonia, TS, TSS, VSS, pH, and alkalinity (measured as calcium carbonate).

C. Summary of modified Hill's model

For easy reference, the modified Hill's model, eqs. (19)-(28), adapted to the AD reactor ADR2 at Foss Biolab in Section 3.3, is summarized in this appendix. The modified Hill's model is originally presented in Section 3.2.2. Nomenclature is defined in Appendix A. Parameter values are given in Table 11.

Defining that portion of the raw waste which can serve as substrate:

$$S_{bvs_{in}} = B_0 S_{vs_{in}} \tag{70}$$

Defining that portion of the biodegradable material which is initially in acid form:

$$S_{vfa_{in}} = A_f S_{bvs_{in}} \tag{71}$$

Mass balance of biodegradable volatile solids:

$$\dot{S}_{bvs} = (S_{bvs_{in}} - S_{bvs}) \frac{F_{feed}}{V} - \mu k_1 X_{acid} \tag{72}$$

Mass balance of total VFA:

$$\dot{S}_{vfa} = (S_{vfa_{in}} - S_{vfa}) \frac{F_{feed}}{V} + \mu k_2 X_{acid} - \mu_c k_3 X_{meth} \tag{73}$$

Mass balance of acidogens:

$$\dot{X}_{acid} = \left(\mu - K_d - \frac{F_{feed}/b}{V} \right) X_{acid} \tag{74}$$

Mass balance of methanogens:

$$\dot{X}_{meth} = \left(\mu_c - K_{dc} - \frac{F_{feed}/b}{V} \right) X_{meth} \tag{75}$$

Methane gas flow rate (gas production):

$$F_{meth} = V \mu_c k_5 X_{meth} \tag{76}$$

where the reaction rates, with Monod kinetics, are as follows:

$$\mu = \mu_m \frac{S_{bvs}}{K_s + S_{bvs}} \tag{77}$$

$$\mu_c = \mu_{mc} \frac{S_{vfa}}{K_{sc} + S_{vfa}} \tag{78}$$

where the maximum reaction rates are functions of the reactor temperature as follows:

$$\mu_m(T_{reac}) = \mu_{mc}(T_{reac}) = 0.013 T_{reac} - 0.129 \tag{79}$$
$$(20°C < T_{reac} < 60°C)$$

Table 11: Parameters in Hill's model adapted to AD reactor at Foss Biolab

$A_f = 0.69$
$b = 2.90$
$B_0 = 0.25$
$k_1 = 3.89$
$k_2 = 1.76$
$k_3 = 31.7$
$k_5 = 26.3$
$K_d = 0.02$
$K_{dc} = 0.02$
$K_s = 15.5$
$K_{sc} = 3$
$V = 250$

In analysis of reactor dynamics and stability and in design of some types of state estimators and controllers it may be necessary to define a proper steady-state operation point. A steady-state operating point can be found from e.g. a simulation by reading off the value of the state variables at steady-state. One example of a steady-state operating point is given in Table 12.

References

Andrews, J. F. and Graef, S. P. Dynamic modeling and simulation of the anaerobic digestion process.

Table 12: Values of inputs and states in one example of a steady-state operation point.

$F_{feed} = 45$ L/d
$T_{reac} = 35$ °C
$S_{vs_{in}} = 30.2$ g/L
$S_{bvs} = 5.2155$ g/L
$S_{vfa} = 1.0094$ g/L
$X_{acid} = 1.3128$ g/L
$X_{meth} = 0.3635$ g/L
$F_{meth} = 196.1560$ L CH_4/d

In: Anaerobic Biological Treatment Processes. R.F. Gould (ed.). *Advances in Chemistry Series, Amer. Chem. Soc, Washington D. C.*, 1971. 105:126–162. doi:10.1021/ba-1971-0105.ch008.

Batstone, D. J., Keller, J., Angelidaki, I., Kalyuzhnyi, S. V., Pavlovstahis, S. G., Rozzi, A., Sanders, W. T. M., Siegrist, H., and Vavilin, V. A. *Anaerobic Digestion Model No. 1, Scientific and Technical Report 15.* IWA Publising, 2002.

Bernard, O., Hadj-Sadok, Z., Dochain, D., Genovesi, A., and Steyer, J. Dynamical Model Development and Parameter Identification for an Anaerobic Wastewater Treatment Process. *Biotechnology and Bioengineering*, 2001. 75(4). doi:10.1002/bit.10036.

Davison, A. C. and Hinkley, D. V. *Bootstrap Methods and their Application.* Cambridge University Press, 1997. doi:10.1017/CBO9780511802843.

Deublein, D. and Steinhauser, A. *Biogas from Waste and Renewable Resources.* Wiley, 2010.

Dochain, D. and Vanrolleghem, P. *Dynamical Modelling and estimation in Wastewater Treatment Processes.* IWA Publishing, 2001.

Edgar, T. F., Himmelblau, D., and Lasdon, L. *Optimization of Chemical Processes.* McGraw-Hill, 2001.

Esbensen, K. and Paasch-Mortensen, P. *Process sampling: Theory of sampling – the missing link in process analytical technologies. In Bakeev, K. (ed): Process Analytical Technology.* Wiley, 2010. doi:10.1002/9780470689592.ch3.

Gavala, H. N., Angelidaki, I., and Ahring, B. K. Kinetics and modeling of anaerobic digestion process. *Advances in Biochemical Engineering/Biotechnology, Springer-Verlag*, 2003. 81.

Grüne, L. and Pannek, J. *Nonlinear Model Predictive Control.* Springer-Verlag, London, 2011. doi:10.1007/978-0-85729-501-9.

Hashimoto, A. G., Chen, Y. R., and Varel, V. H. Theoretical Aspect of Anaerobic Fermentation: State-Of-The-Art. *Livestock Wastes: A Renewable Resource, American Society of Agricultural Engineers*, 1981.

Haugen, F., Bakke, R., Vasdal, K., and Bergland, W. Foss Biolab. *http://fossbiolab.no*, 2012.

Hill, D. T. Simplified Monod kinetics of methane fermentation of animal wastes. *Agric. Wastes*, 1983. 5:1–16. doi:10.1016/0141-4607(83)90009-4.

Hill, D. T. and Barth, C. L. A dynamic model for simulation of animal waste digestion. *J. Water Pollution Control Federation*, 1977. 49(10).

Husain, A. Mathematical models of the kinetics of anaerobic digestion – A selected review. *Biomass and Bioenergy*, 1998. 14(5/6).

Lyberatos, G. and Skiadas, I. V. Modeling of anaerobic digestion - A review. *Global Nest: the Int. J.*, 1999. 1(2):63–76.

Lyseng, B. C., Bergland, W., Botheju, D., Haugen, F., and Bakke, R. Biogas reactor modelling with ADM1. *Telemark Open Research Archive (TEORA), Norway, http://teora.hit.no/dspace/handle/2282/1311*, 2012.

Reichert, P. *AQUASIM 2.0. User Manual. Technical report.* Swiss Federal Institute for Environmental Science and Technology (EAWAG), 1998.

Rosen, C., D., Gernaey, K. V., Pons, M. N., and Jeppsson, U. Implementing ADM1 for plant-wide benchmark simulations in Matlab/Simulink. *Water Science & Technology, IWA Publishing*, 2006. 54(4):11–19.

Seborg, D. E., Edgar, T. F., and Mellichamp, D. A. *Process Dynamics and Control, 2. Ed.* Wiley, 2004.

Simeonov, I., Momchev, V., and Grancharov, D. Dynamic modeling of mesophilic anaerobic digestion of animal waste. *Water Research*, 1996. 30(5):1087–1094. doi:10.1016/0043-1354(95)00270-7.

Simon, D. *Optimal State Estimation.* Wiley, 2006.

Stromberg, S. *Development and Evaluation of Numerical Models for Anaerobic Digestion.* M.Sc. thesis. Lund Univ., Sweden, 2010.

Tchobanoglous, G., Burton, F. G., and Stensel, H. D. *Wastewater Engineering: Treatment and Reuse.* Metcalf and Eddy, McGraw Hill, 2003.

Varmuza, K. and Filzmoser, P. *Introduction to Multi-variable Statistical Analysis in Chemometrics*. CRC Press, Taylor & Francis Group, 2009.

Zaher, U., Pandey, P., and Chen, S. A simple elemental continuity based model application to study the anaerobic microbial activity for the treatment of dairy manure. *Appl. Math. Modelling*, 2009. 33.

Zaher, U., Rodríguez, J., Franco, A., and Vanrolleghem, P. A. Application of the IWA ADM1 model to simulate anaerobic digester dynamics using a concise set of practical measurements. In *IWA Conference on Env. Biol. – Advancement on Water and Wastewater Applications in the Tropics*. Kuala Lumpur, Malaysia, 2003.

Article 2 – Temperature Control of a Pilot Anaerobic Digestion Reactor

Authors: Finn Haugen, Rune Bakke and Bernt Lie.

Authors' roles in the article: Finn Haugen: Main ideas, implementation, and writing. Rune Bakke (co-supervisor) and Bernt Lie (supervisor): Discussions, comments, and proof readings.

Background and methods of the article

Background

Both theoretical results, i.e. simulations based the modified Hill model derived in Article no. 1, and experiments on the real pilot reactor indicate that both the dynamic and steady state methane gas production depends clearly on the reactor temperature. Assuming that it is desirable to operate the reactor under well-defined conditions, the reactor temperature must be controlled to a proper setpoint. According to Tchobanoglous et al. (2003), 35 °C is a typical temperature at mesophilic conditions. Due to inevitable disturbances – variations in influent and ambient temperatures – a feedback temperature control system is necessary, otherwise the temperature may drift too far away from the desired temperature.

Both the on-off controller and the proportional plus integral (PI) controller are appropriate temperature controllers for the reactor. The main benefit of the on-off controller is its simplicity – it can be used virtually without

any tuning. Its drawback is the inevitable sustained oscillations. The benefit of the PI controller is that it gives smooth control with ideally zero steady state control error. Its drawback is that the controller parameters, which are the controller gain and the integral time, requires tuning to ensure proper control system stability. In this project, the PI controller is selected as the ultimate temperature controller.

Methods

In this article, all controller functions and controller tunings are tested on a simulator based on the temperature model derived in Article no. 1, before implementation on the real reactor, thereby saving time and effort.

For PI controller tuning, both open loop tuning methods and closed loop tuning methods are available. It is shown both theoretically and practically that open loop tuning with the Skogestad method, Skogestad (2004), works well on the reactor.

Furthermore, it is shown that closed loop tuning with the well-known Ziegler-Nichols method, Ziegler & Nichols (1942), is unsuccessful. Applying the well-known Tyreus-Luyben modifications of the Ziegler-Nichols settings, Tyreus & Luyben (1992), are also not successful. The unsuccessful tunings can be explained by the process time delay being considerably smaller than the time delay. Motivated by these unsuccessful tuning methods, improved PI settings are derived, reported in Article no. 6.

To analyze the control systems for different controller settings, standard frequency response measures are calculated. The stability margins, i.e. the gain margin and the phase margin, and the closed loop response time which is estimated as the inverse of the amplitude crossover frequency (the bandwidth), are calculated with the margin() function of MATLAB. The frequency response is calculated from transfer functions. The practical control system is not analyzed, except its dynamical (transient) responses are observed to evaluate qualitatively the control system stability.

Temperature Control of a Pilot Anaerobic Digestion Reactor

Finn Haugen   Rune Bakke   Bernt Lie

Telemark University College, Kjolnes ring 56, 3918 Porsgrunn, Norway. E-mail contact:
{*finn.haugen,rune.bakke,bernt.lie*}*@hit.no*

Abstract

Results of analysis and design and implementation of a temperature control system for a practical pilot anaerobic digestion (AD) bioreactor fed with dairy waste are presented. A dynamic model of the reactor temperature is used as the basis for theoretical results, including simulations. Controller functions include on-off control, proportional plus integral (PI) control, and feedforward control. Various PI controller tuning methods are compared. The need for adaptivity of PI settings is investigated. Results for a simulated full-scale reactor are given.

Keywords: Anaerobic digestion, bioreactor, biogas, temperature control, PI control, on-off control, feedforward control.

1. Introduction

The main aim of this paper is to present the results of analysis and design and implementation of a temperature control system for a practical pilot anaerobic digestion (AD) bioreactor fed with dairy waste. The bioreactor is a part of the biological plant for nutrient and energy recovery at Foss Biolab, Skien, Norway. A description of the plant and the monitoring and control system can be found in Haugen et al. (2013a) and Haugen et al. (2013b). Results of analysis and design of a temperature control system for a hypothetical full-scale reactor is also included.

This paper focuses on feedback control with on-off control and PI control (proportional + integral), and feedforward control. An advanced alternative to these traditional control methods is MPC (model-based predictive control) which is possible to use for the present reactor control since a fairly accurate dynamic reactor temperature model exists and the crucial variables are measured. However, MPC is not included in this paper since the temperature setpoint is constant and disturbances as ambient temperature changes can be

compensated for effectively using the aforementioned control methods. However, MPC may be the preferred control method in applications where the setpoint (profile) is changing, and in applications where the trade-off between small control error and smooth control actions should be directly adjustable by the user.

The outline of this paper is as follows. A process description is given in Section 2. In Section 3, rationales of bioreactor reactor temperature control are given. On-off temperature control is described in Section 4. Smooth control with PI control is covered in Section 5. Model-based and model-free feedforward control of a simulated reactor are described in Section 6. Results for temperature control of a full-scale reactor are provided in Section 7. A discussion is given in Section 8, and conclusions are given in Section 9. A dynamical mathematical model used for analysis and simulation is presented in Appendix A. Abbreviations and nomenclature are given in Appendix B.

Energy recovery design, e.g. using relatively warm reactor liquid effluent to preheat cold influent, and using biogas combustion to heat the reactor, is not covered in this paper. Energy recovery and other issues in

optimal reactor design and operation will be addressed in future publications.

MATLAB and SIMULINK (MathWorks, Inc.) are used for numerical computations and simulations based on the models described in Section A. The software of the real temperature control system is implemented in LabVIEW (National Instruments, Inc.).

2. Process description

Figure 1 depicts the temperature control system.
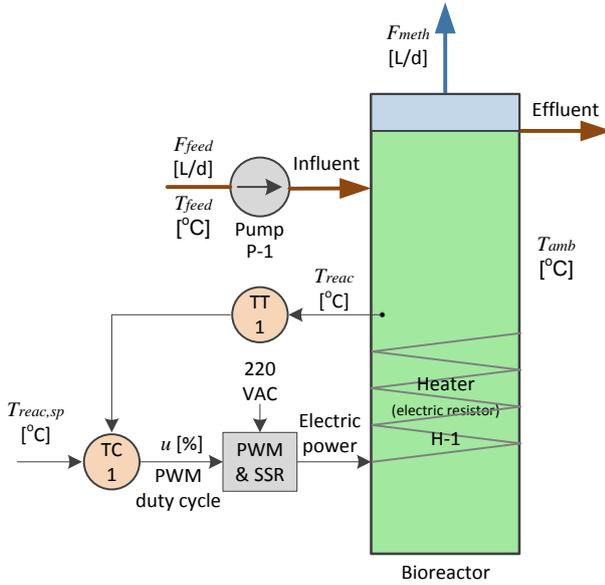
Figure 1: *Temperature control system for AD reactor.*

The feed temperature, T_{feed}, is assumed to be the same as the ambient – here: room – temperature, T_{amb}, since the feed resides for several days in an intermediate storage in the room where the reactor is placed.

Detailed information about the system components are given in the following.

Reactor is cylindrical with 250 L effective liquid volume. Height (0.40 m) is 5 times reactor diameter (2.00 m). Gas volume is assumed negligible compared to liquid volume.

TT-1 is a Pt100 reactor temperature sensor. It has an accuracy of approximately ± 0.3 °C. The repeatability is not known.

The temperature measurement signal is noisy. It is assumed that the noise, n, is a random stochastic signal with zero mean value. From a representative unfiltered measurement time-series,

$$\sigma_n = 0.0829 \text{ °C} \qquad (1)$$

TC-1 is the temperature controller implemented in LabVIEW (National Instruments) running on a PC. The available controller functions are manual control, PID control, and on-off control. The time-step of the control loop is 2 s.

H-1 is an electrical heater for the AD reactor which is controlled using pulse-width modulation (PWM) option in TC1. The heater comprises an electrical resistor wound around the reactor inside the thermal insulation jacket. The maximum power delivered by the heater is 200 W.

PWM is a pulse-width modulation element implemented with the Square Wave Point-by-Point function in LabVIEW. The PWM element operates with a fixed cycle time of 30 sec which is negligible compared to the dynamics of the temperature control loop. The control signal (in percent) calculated by the temperature controller is the duty cycle of the PWM element. PWM control emulates analog control.

SSR is a solid state relay (semiconductor) which is turned on-off with a voltage (5/0 V) corresponding to the state of the PWM element (on-off) which controls the SSR. The SSR switches the 220 VAC mains voltage onto/off the heater.

A secure communication between the PC and the Internet with the LogMeIn software facilitates remote access to the computer screen and to the file system on the lab PC.

3. Rationales of bioreactor temperature control

In the following, rationales of bioreactor temperature control are given in terms of temperature dependency of methane production and temperature disturbance compensation.

3.1. Temperature dependency of methane production

For a bioreactor, the produced methane flow depends on the reactor temperature, T_{reac}. The temperature dependency is expressed in e.g. Hill's model of AD of animal wastes, Hill (1983). In Hill's model the maximum reaction rate, μ_{max}, of the acid-generating microorganisms – acidogens – and the methane-generating microorganisms – methanogens – is temperature-dependent. This dependency is represented by the following linear function, Hashimoto

et al. (1981):

$$\mu_{\max}\left(T_{\mathrm{reac}}\right) = 0.013T_{\mathrm{reac}} - 0.129 \tag{2}$$
$$(20\ ^{\circ}\mathrm{C} < T_{\mathrm{reac}} < 60\ ^{\circ}\mathrm{C})$$

In the ADM1 model (Anaerobic Digestion Model No. 1), Batstone et al. (2002), the temperature dependency of a number of model parameters is expressed in terms of Arrhenius-like functions.
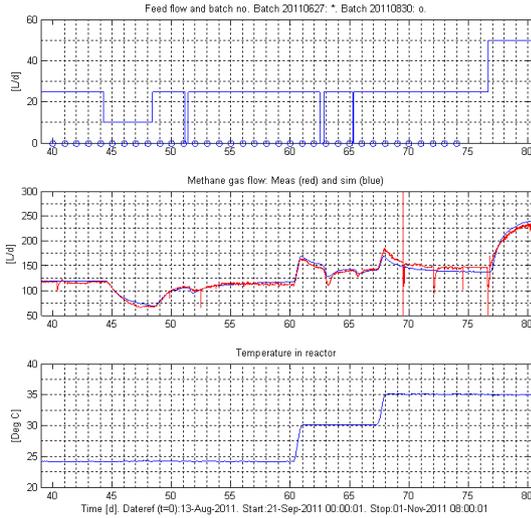

Figure 2: *Reactor ADR1: Responses in F_{meth} (middle) due to changes in T_{reac} (lower) and F_{feed} (upper). For F_{meth}: Measured is blue. Simulation is red. [This plot also appears in Haugen et al. (2013a)].*

As an illustration of the dependence of F_{meth} on T_{reac}, Figure 2 shows measured (and simulated) time-series in F_{meth} due to changes in T_{reac} and in F_{feed} for the reactor ADR1 which was in use at Foss Biolab from August 17, 2011 until April 19, 2012. The rest of the present paper focuses on reactor ADR2 which has been in use from April 19, 2012. However, it is assumed that the temperature dependency holds equally well for ADR2 as for ADR1 since the physical appearances of the two reactors are similar and the operation and feedstock (waste from the same dairy livestock) are similar.

During the time interval in Figure 2 both T_{reac} and the feed flow F_{feed} were changed, but only the variations caused by the temperature change is of interest here. T_{reac} is increased twice (implemented as step-wise changes of the temperature control setpoint):

- At time $t = 60.5$ d (days): From 24ºC to 30ºC.

- At $t = 67.5$ d: From 30ºC to 35ºC.

Figure 2 illustrates clearly the dependence of F_{meth} on T_{reac}.

The simulations of F_{meth} shown in Figure 2 are based on the modified Hill's model adapted to ADR1. Adaptation of modified Hill's model to ADR1 is not published. (Model adaptation to ADR2 is presented in Haugen et al. (2013a).)

The temperature effect on gas production is a result of gas solubility changes, reduced microbial growth rates, and stress caused by the temperature transition, Tchobanoglous et al. (2003).

Tchobanoglous *et al.* state that methanogens are sensitive to temperature changes, and that these microbes should not be excited to temperature variations larger than $\pm\ 0.5\ ^{\circ}\mathrm{C}$. Consequently, a temperature control system should be designed to be able to keep the temperature offset from the specified temperature setpoint less than $\pm\ 0.25\ ^{\circ}\mathrm{C}$.

Tchobanoglous *et al.* also point out that most AD processes are designed for operation at mesophile conditions, i.e. at temperatures in the range 30-38 ºC. While it is important to determine the optimal reactor temperature, this is not address in the present paper, but instead in a forthcoming paper based on theoretical optimization methods applied to mathematical models of the AD reactor.

The most important disturbances acting on the reactor temperature are

- the ambient temperature, T_{amb},

- the temperature of the feed flow, T_{feed} (assumed to be the same as T_{amb} for the practical reactor),

- the feed flow, F_{feed}.

3.2. Disturbance compensation

A well operating temperature control system will compensate for changes in these disturbances automatically. To demonstrate the importance of temperature control, Figure 3 shows the responses in T_{reac}, u, and T_{amb} with (automatic) control with and without control for reactor ADR2. The setpoint, T_{sp}, is 30ºC. In the period from $t = 389.25$ to 389.96 d the temperature is controlled automatically with a PI controller. In this period the control error, which is the difference between T_{sp} and T_{reac}, is within ± 0.05 K. In the period from $t = 389.96$ to 390.75 d the control system is deactivated; The reactor is operated with open loop control, or "blind" control with a constant control signal, $u = 39.8\%$, which is actually the average value over a time interval of 1 d with automatic control. Figure 3 shows that with open loop control, T_{reac} tends to drift

away from T_{sp}, due to inevitable variations in T_{amb}. Due to external demands about operation of the reactor, the controller was switched back to automatic mode at $t = 390.75$ d. At that point of time the offset from the setpoint had increased to approximately 0.18 °C, i.e. the slope is approximately -1 °C/d. If this decrease continues the temperature will deviate from its setpoint by the maximum deviation of 0.25 °C after 0.25 d = 6 h (hours).
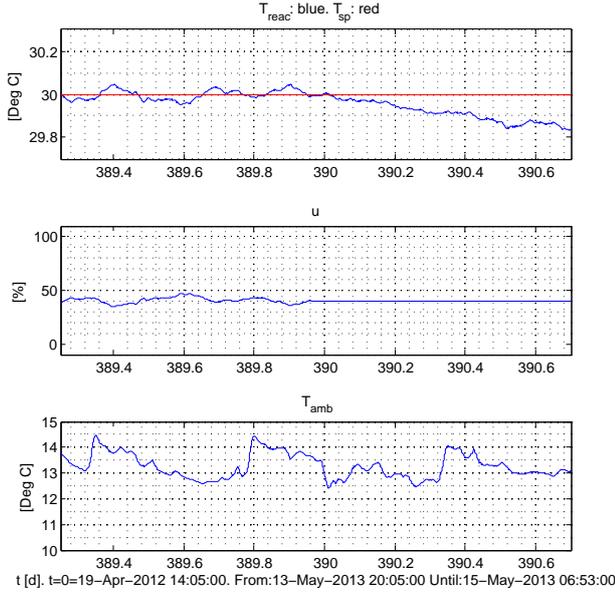

Figure 3: *Responses on the real reactor (ADR2): $t = 389.25$-389.80 d: Automatic closed loop (feedback) temperature control. $t = 389.80$-390.75 d: Open loop control, or "blind" control.*

4. On-off control

The on-off controller can be regarded as the simplest feedback controller available. The controller function is

$$u = \left\{ \begin{array}{l} u_{on} \text{ for } e \geq d_e \\ u_{off} \text{ for } e < -d_e \end{array} \right\} \qquad (3)$$

where e is control error:

$$e = T_{sp} - T_{reac} \qquad (4)$$

and d_e an adjustable dead-band to avoid switching of u due to (measurement) noise in e. Noise-triggered switching is also counteracted using a measurement lowpass filter with a properly adjusted time-constant, τ_f, to attenuate the noise properly. In the present application, $\tau_f = 10$ min, found by trial-and-error, and $d_e = 0$.

Simulations

Figure 4 shows simulated responses of T_{reac} and u with $T_{sp} = 30$ °C. T_{amb} is set to 17 °C which is representative for the room temperature in the real experiment reported below. $u_{on} = 100\%$. $u_{off} = 0\%$. The time interval of the plot is 0.32 d which is the same as for the real time-series plotted in Figure 4.

From the simulated time-series:

- $P_u = 0.055$ d = 79.2 min.

- Amplitude of oscillation of T_{reac} is 0.04 °C.

- $|e|_{max} = 0.07$ °C.

- $\mu_e = T_{sp} - \mu_{T_{reac}} = -0.016$ °C.
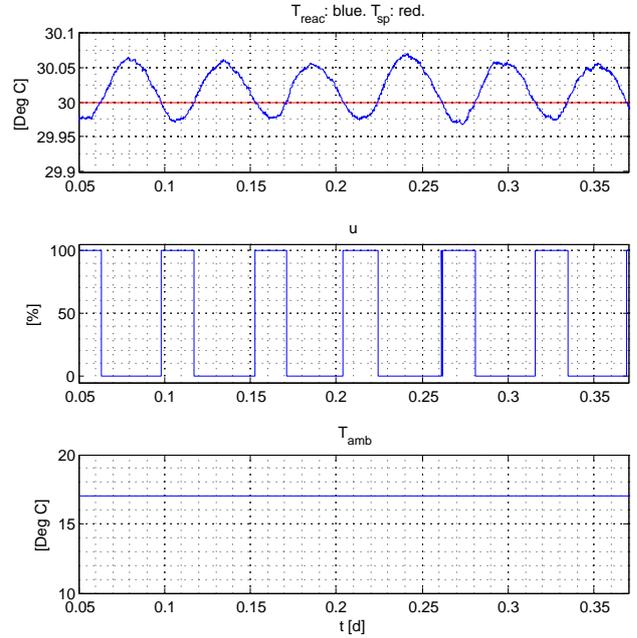
Figure 4: *Simulated time-series for the reactor with on-off temperature control. Random measurement noise is included.*

Practical results

Figure 5 shows experimental T_{reac}, T_{sp}, u, and T_{amb}. From the experimental time-series:

- $P_u = 0.045$ d = 64.8 min.

- Amplitude of oscillation of T_{reac} is 0.05 °C.

- $|e|_{max} = 0.07$ °C.

- $\mu_e = T_{sp} - \mu_{T_{reac}} = -0.019$ °C.
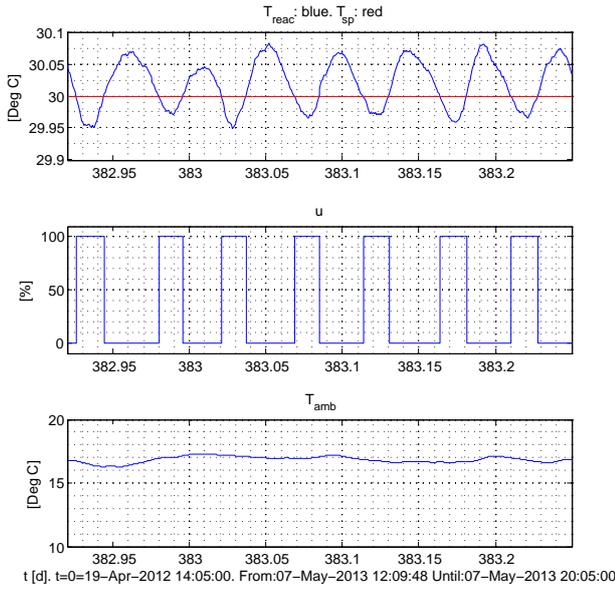
Figure 5: *Real time-series for the reactor with on-off temperature control. T_{reac} is filtered with time-constant 10 min. The sampling time-step of time-series is 15 min.*

Comments and conclusions

- The simulated responses are in good accordance with the real responses, which indicates that the dynamic model used for simulation is quite accurate.

- For the real responses: $|e|_{\max} \approx 0.07$ °C is acceptable. Also, $\mu_e = 0.019$ °C is acceptable. The oscillatory behaviour of T_{reac} is acceptable since the variation is within ± 0.25 °C.

- The on-off behaviour of the control signal, u, is also acceptable in our application since the actuator is an electrical heater with no moving parts. However, in applications with a mechanical actuator like a pump or valve used to manipulate the flow of e.g. hot water or steam, smooth or continuous control with PI(D) control may be preferred, cf. Section 5.

5. PID control

5.1. Controller function

PID control is prevalent in industrial applications, Seborg et al. (2004). The PID controller provides smooth control as opposite to on-off control. The PID controller used in this paper is based on discretization of the following continuous-time PID controller:

$$u = u_{\text{man}} + K_c e + \frac{K_c}{\tau_i} \int_0^t e\left(\tau\right) d\tau + K_c \tau_d \dot{e} \qquad (5)$$

The discretization is based on the implicit Euler method with time-step $\tau_s = 2$ s.

Typically, the derivative term provides control stability and agility, but it also propagates measurement noise which may cause too noisy control signal. In the present application, representative time-series of the raw (unfiltered) temperature measurement show a control signal standard deviation of 1.3 K with PI control and 4.5 K with PID control. Although the actuator in the present application is an electrical heater with no moving parts so the control noise can not make any mechanical problems, it was decided to not use the derivative term. This decision is made to increase the relevancy of controller tuning results in the present paper to systems with mechanical actuators.

A great number of controller methods for tuning controller parameters exist, Seborg et al. (2004), O'Dwyer (2003). Selected open loop controller tuning methods applied to the reactor are presented in Section 5.3, while applications of selected closed loop methods are presented in Section 5.4. Summaries of tuning results are given in Section 5.2.

5.2. Summary of results with various tuning methods

Sections 5.2.1 and 5.2.2 below summarize the results of controller tuning for the simulated temperature control system and for the real system, respectively. Tuning details are in Sections 5.3 and 5.4.

5.2.1. Simulated temperature control system

Table 1 summarizes the results for the simulated temperature control system based on the model presented in Appendix A.1. The table shows controller settings, GM (gain margin), phase margin (PM), and the closed-loop response-time τ_r [d] which is calculated as the inverse of the bandwidth which is here defined as the amplitude crossover frequency, ω_c [rad/d]:

$$\tau_r = \frac{1}{\omega_c} \qquad (6)$$

τ_r indicates the speed of the response of the control system due to a setpoint step change. τ_r is approximately the time-constant of the control system. The above frequency response characteristics are based on the transfer functions model in Appendix A.2.

Seborg et al. (2004) recommend the following ranges for the stability margins, where the lower limits can be

Table 1: Results with various PI tuning methods for simulated temperature control system: S = Skogestad. ZN = Ziegler-Nichols. R-ZN = Relaxed Ziegler-Nichols.

Method	K_c [%/K]	τ_i	GM	PM [deg]	τ_r [d]
S	152	0.080 d = 6912 s	7.76 = 17.8 [dB]	40.5	0.038
ZN	716	0.046 d = 3960 s	1.32 = 2.39 [dB]	6.4	0.012
Rx-ZN ($k_r = 4$)	203	0.138 d 11880 = s	6.5 = 16.2 [dB]	47.8	0.031

regarded as critical:

$$1.7 = 4.6 \text{ dB} \leq \text{GM} \leq 4.0 = 12.0 \text{ dB} \qquad (7)$$

and

$$30^{\text{o}} \leq \text{PM} \leq 45^{\text{o}} \qquad (8)$$

5.2.2. Real temperature control system

Table 2 summarizes the controller settings for the real temperature control system.

Table 2: Results with various PI tuning methods for the real temperature control system: S = Skogestad. ZN = Ziegler-Nichols. R-ZN = Relaxed Ziegler-Nichols.

Method	K_c [%/K]	τ_i
S	149	0.080 d = 6912 s
ZN	573	0.038 d = 3240 s
Rx-ZN ($k_r = 4$)	162	0.113 d = 9720 s

5.3. Open-loop controller tuning

5.3.1. Introduction

There are many open loop controller tuning methods available, for example the Ziegler and Nichols open loop method, Ziegler and Nichols (1942), Direct Synthesis methods including the Lambda tuning method, Seborg et al. (2004), Internal Model Control (IMC) methods, Seborg et al. (2004), the Hägglund-Åstrøm Robust Tuning method, Hägglund and Åstrøm (2002),

and the SIMC method (Simple IMC) by Skogestad (2004), here denoted the Skogestad method.

The Ziegler and Nichols open loop method has no adjustable settings, and typically give very fast control but with relatively small stability margins. The Hägglund-Åstrøm method has no adjustable settings. The IMC, Lambda, and the Skogestad method each has one tuning parameter which determines the closed loop time constant, and typically for these methods the setpoint step responses are without oscillations indicating relatively large stability margins.

It is convenient to use a tuning method. This leaves out the Ziegler and Nichols open loop method and the Hägglund-Åstrøm method. Among the remaining candidates, the Skogestad method is selected as we are not aware of important benefits with the other methods over the Skogestad method. It is evaluated favourably in Haugen (2010) comparing with a number of open loop methods, and closed loop methods.

5.3.2. The Skogestad method (SIMC method)

Skogestad (2004) has developed PID controller tuning formulas for a number of processes given by their transfer functions. As shown in Appendix A.2, the reactor can be represented by a transfer function comprising a dominant time-constant term representing the energy balance of the reactor liquid with some additional lag. In controller tuning, it is safe regarding control system stability to assume that this lag is a time-delay of the same amount as the lag, Skogestad and Postlethwaite (2007). Thus, it is safe to use the Skogestad PI tuning formulas for the following "time-constant with time-delay" model of the reactor:

$$\frac{\Delta T_{\text{reac}}(s)}{\Delta u(s)} = \frac{K}{\tau_{\text{reac}}s + 1}e^{-\tau_{\text{delay}}s} \qquad (9)$$

For this type of process, Skogestad designates a PI controller. As pointed out in Haugen and Lie (2013), cf. also DiRuscio (2010), the Skogestad PI tuning formulas for eq. (9) become identical with the tuning formulas for the following "integrator with time-delay" process which approximates eq. (9) in the transient phase:

$$\frac{\Delta T_{\text{reac}}(s)}{\Delta u(s)} = \frac{K_{i_p}}{s}e^{-\tau_{\text{delay}}s} \qquad (10)$$

where

$$K_{i_p} = \frac{K}{\tau_{reac}} \qquad (11)$$

The Skogestad PI settings for the process model eq.

(10) become

$$K_c = \frac{1}{K_{i_p} \left(\tau_c + \tau_{\text{delay}} \right)} \quad (12)$$

$$= \frac{1}{2 K_{i_p} \tau_{\text{delay}}} \quad (13)$$

$$\tau_i = 2 \left(\tau_c + \tau_{\text{delay}} \right) \quad (14)$$

$$= 4 \tau_{\text{delay}} \quad (15)$$

Comments: In eqs. (13) and (15), Skogestad's rule-of-thumb $\tau_c = \tau_{\text{delay}}$ are used. The factor 2 in eq. 14 and 4 in eq. 15 are due to the modification of the τ_i setting introduced in Haugen and Lie (2013) to give faster disturbance compensation, while retaining acceptable stability margins. In Skogestad's original settings, the factors are 4 and 8, respectively.

The process parameters K_{i_p} and τ_{delay} can be found experimentally, or from a model, as explained in the following.

Estimating τ_{delay} from an experimental response

Figure 6 shows the response in the T_{reac} due to a step change in the control signal, u, from 62% to 82%, hence a step amplitude of $\Delta u = 20\%$.
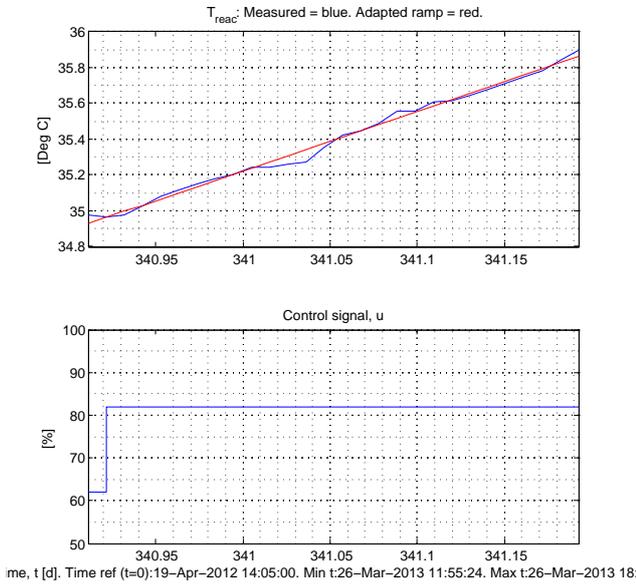

Figure 6: *The response in T_{reac} (upper plot, blue) due to a step change in the control signal, u, (lower diagram) from 62% to 82% ($\Delta u = 20\%$), and the ramp-wise response (upper plot, red) adapted to T_{reac}. (The sampling time of the data is 15 min = 0.0104 d.)*

The measurement filter which is normally in use, is bypassed in this experiment to obtain parameter values that are independent of the filter dynamics. Figure 6 also shows (in red colour) the ramp-like response adapted to the real T_{reac}. The slope of this ramp-like response determines parameter K_{i_p}, as explained below.

From the response shown in Figure 6 which is without measurement filtering, a lag of approximately 0.01 d can be observed. Under normal operation of the reactor a measurement filter of time-constant 15 min = 0.0069 d is used. Thus, the total lag is approximately 0.01 + 0.0069 = 0.0169. Furthermore, the sampling time of the data shown in Figure 6 is 15 min = 0.0104 d which adds uncertainty to the estimation of the aforementioned lag of 0.01 d. Consequently, a total lag, τ_{lag}, is estimated visually as

$$\tau_{\text{lag}} \approx 0.02 \text{ d} \quad (16)$$

The estimate eq. (16) is in good accordance with the lag estimated with a nonlinear least square method as 0.023 d in Haugen et al. (2013a). There, the lag was estimated at a lower feed rate, namely 45 L/d, while the feed rate in the present study is 65 L/d.

As argued in the beginning of the present section,

$$\tau_{\text{delay}} = \tau_{\text{lag}} = 0.02 \text{ d} \quad (17)$$

Estimating K_{i_p} from an experimental response

K_{p_i} can be found as the normalized initial slope of the step response in the reactor temperature:

$$K_{i_p} = \frac{S}{\Delta u} \quad (18)$$

where S is slope and Δu is amplitude of step change of u. A step response test can be accomplished during a few hours, while it may take several days to obtain K_{p_i} from eq. (11) if K and τ_{reac} are estimated from a step response since the (theoretical) τ_{reac} for the reactor is typically several days (in the operating point defined in Table 6 it is 2.24 d).

For the present reactor, K_{p_i} is found as follows. Figure 6 shows (in red colour) the ramp-like step response adapted to the real T_{reac} over the time-interval $t_0 = 340.94 - 341.20$ d using the following assumed model for this ramp:

$$T_{\text{reac}}^{\text{ramp}} = a \left(t - t_0 \right) + b \quad (19)$$

where t [d] is time. The coefficients a and b are estimated with the least squares method. However, only a is of interest here. It is estimated as

$$a_{est} = 3.35 \text{ K/d} \quad (20)$$

Now, K_{i_p} can be calculated from eq. (11):

$$K_{i_p} = \frac{S}{\Delta u} = \frac{a}{\Delta u} \tag{21}$$

$$= \frac{3.35 \text{ K/d}}{20\%} \tag{22}$$

$$= 0.168 \text{ (K/d)}/\% \tag{23}$$

Calculating K_{i_p} from the reactor model

K_{i_p} can be calculated from eq. (18) where K and τ_{reac} can be calculated from the transfer function derived from the energy balance of the reactor, cf. Appendix A.2. From eq. (11), using eqs. (53) and (54),

$$K_{i_p} = \frac{K}{\tau_{reac}} = \frac{K_u}{c\rho V} \tag{24}$$

$$= \frac{2 \text{ (W = J/s)}/\% \cdot 86400 \text{ s/d}}{4200 \text{ J/(kgK)} \cdot 1000 \text{ kg/m}^3 \cdot 0.25 \text{ m}^3}$$

$$= 0.165 \text{ (K/d)}/\% \tag{25}$$

which agrees very well with the experimental value in eq. (23).

Simulations

The PI settings are calculated with K_{p_i} given by eq. (24) and τ_{delay} given by eq. (17). The PI settings are shown in Table 1. Figure 7 shows simulations of the control system. The responses indicate acceptable stability. The stability margins shown in Table 1 have acceptable values, though GM is large.

Practical results

PI settings are calculated with eqs. (13)-(15) with K_{p_i} given by eq. (23) and τ_{delay} given by eq. (17). The resulting settings are shown in Table 2. Figure 8 shows responses on the real reactor with these settings.

With the above Skogestad PI settings the standard deviation of T_{reac} (10 min time-constant filter) over 20 days is 0.015 K. The mean of T_{reac} is very close to its setpoint. The variations of T_{reac} are within approximately ± 0.05 °C.[1]

Comments and conclusions

With the Skogestad tuning method:

- The tuned control loop shows good stability.

- The tuning experiment does not involve any trial-and-error, i.e. iterations are not needed, which is beneficial from a practical point of view.

---

[1]Due to external demands for the operation of the reactor, $T_{reac_{sp}} = 25$°C in the pertinent time-series, while $T_{reac_{sp}}$ is varied around 35°C in Figure 8.
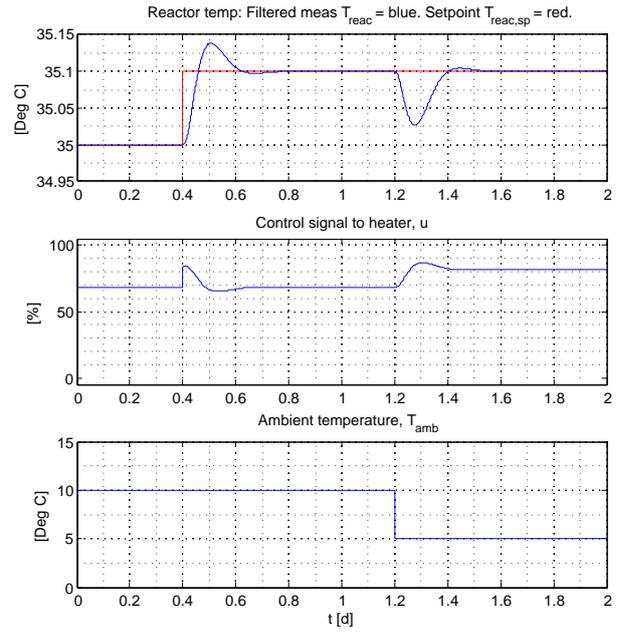
Figure 7: *Simulations of temperature control system with the Skogestad PI settings.*

5.4. Closed loop controller tuning

5.4.1. Introduction

Closed loop tuning methods are applied with the controller in place (in the loop). The following closed loop methods are considered:

- The well-known Ziegler-Nichols (ZN) closed loop method, Ziegler and Nichols (1942), with Åström-Hägglund's relay-method, Åstrøm and Hägglund (1995) to find the ultimate gain and period. (Section 5.4.2.)

- The Relaxed Ziegler-Nichols (R-ZN) closed loop PI tuning method, proposed by Haugen and Lie (2013). This method is based on the same experiments as in the ZN (closed loop) method, but relaxes the PI settings to obtain a smoother control signal and to improve the stability compared with the original ZN method. The method is based on a combination of the Skogestad method and the ZN closed loop method. (Section 5.4.3.)

- The Tyreus-Luyben method, Tyreus and Luyben (1992), which is, probably, the best known method to modify the ZN closed loop PI settings to obtain more relaxed control. However, it is shown by Haugen and Lie (2013) that the R-ZN method is beneficial compared with the Tyreus-Luyben
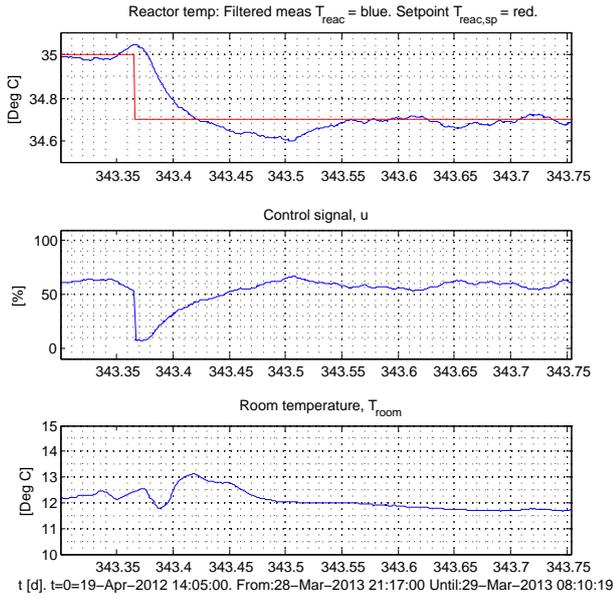
Figure 8: *Real time-series for reactor with PI temperature controller tuned with the Skogestad method.*

method. These benefits are confirmed in simulations of the reactor (detailed results are not shown here).

- The Good Gain method, Haugen (2012), which has similarities with the ZN method. Sustained oscillation in the tuning phase is avoided, and in addition the final stability of the control system is typically improved comparing with the ZN method. However, the method can be used reliably only if the noise and disturbances affecting the process measurement is small to make it possible to read off the tuning parameter T_{ou} (time from overshoot to undershoot after a setpoint step with a P controller). On the real reactor the noise and disturbances are so prevalent that the Good Gain method is not applicable. This problem is confirmed in simulations containing realistic noise (responses are not shown).

5.4.2. The ZN closed loop method based on relay tuning

Åstrøm and Hägglund (1995) suggest a relay or on-off controller to replace the P controller in the tuning phase of the ZN closed loop (or Ultimate Gain) method, Ziegler and Nichols (1942), thereby avoiding the trial-and-error procedure since the oscillations come automatically. The ultimate controller gain is

calculated as

$$K_{c_u} = \frac{4A}{\pi E} \quad (26)$$

where A is the amplitude of the on-off control signal. If $u_{on} = 100\%$ and $u_{off} = 0\%$, as in our application, A is 50%. E is the amplitude of the oscillations in the process measurement.

The PI controller settings are

$$K_c = 0.45 K_{c_u} = 0.45 \frac{4A}{\pi E} \quad (27)$$

$$\tau_i = \frac{P_u}{1.2} \quad (28)$$

where P_u is the period of the oscillation.

Due to external demands it was necessary to operate the reactor at approximately 30 °C in the experiments with the ZN method, while 35 °C was used in experiments with the Skogestad method.

Simulations

The simulations with on-off controller shown in Figure 4 are the basis for relay tuning. From the simulations, $E = 0.04$ K and $P_u = 0.055$ d. Furthermore, $A = 50\%$. This gives PI settings as shown in Table 1, where also stability margins, and response-time are shown. The resulting stability margins, cf. Table 1, are very small. Although not shown here, simulations show oscillatory responses, with little damping.

Practical results

The real responses with on-off controller shown in Figure 5 are used for relay tuning. From the responses, $E = 0.05$ K and $P_u = 0.045$ d. Furthermore, $A = 50$ %. This gives

$$K_{c_u} = \frac{4 \cdot 50}{\pi \cdot 0.05} = 1273 \ \%/\text{K} \quad (29)$$

The resulting PI settings are calculated with eqs. (27)-(28) to give PI as shown Table 2. Figure 9 shows responses on the real reactor.

Comments and conclusions

- Both the model and the real system shows poor stability. This poor stability is actually typical when the ZN tuning is applied to a process where there is a small or no pure time-delay, as is the case here.

- It is concluded that the ZN closed loop method is inappropriate for tuning the temperature controller.
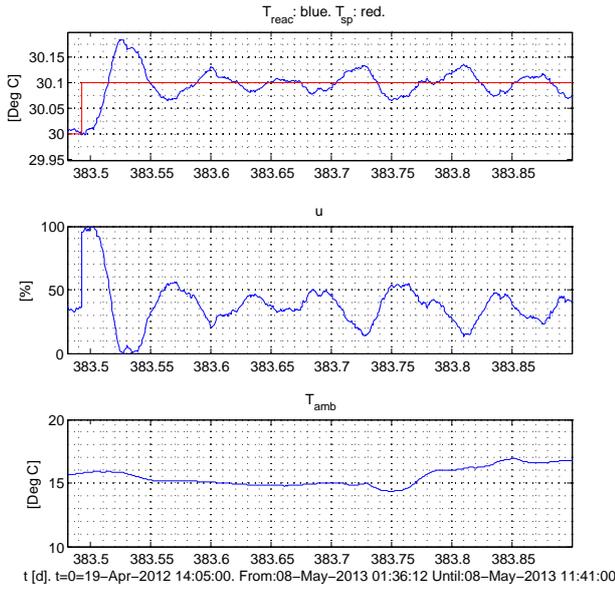
Figure 9: *Real time-series for reactor with PI temperature controller tuned with relay-based ZN method.*

5.4.3. Relaxed ZN PI tuning

Relaxed ZN PI settings, as proposed by Haugen *et al.* (2012b), are calculated from the ultimate gain, K_{c_u}, and the ultimate period, P_u, found from e.g. relay oscillations:

$$K_c = \frac{2}{\pi \left(k_r + 1\right)} K_{c_u} \tag{30}$$

and

$$\tau_i = \frac{k_r + 1}{2} P_u \tag{31}$$

where k_r is a parameter determined by the user to obtain a proper closed loop system time-constant,

$$\tau_c = k_r \tau_{\text{delay}} \tag{32}$$

where τ_{delay} is the process time-delay. $k_r = 1$ kan be regarded as the default value. With $k_r = 1$ eq. (32) is the same as Skogestad's rule-of-thumb: $\tau_c = \tau$. Enhanced relaxed control can be obtained with $k_r > 1$.

Haugen *et al.* (2013b) recommend $k_r = 1$ in eqs. (30)-(31) if the process has a dominating lag or integrator, due to energy or material balance, plus a noteable time-delay, and $k_r = 4$ if the process has zero or neglible time-delay, but some lag, in addition to the dominating lag or integrator. The bioreactor has a dominating lag – approximately an integrator – due to the energy balance of the liquid, and an additional relatively small lag due to dynamics in the heater and the reactor wall. There is also a relatively small lag due to

the measurement filter. A physical reason for a clear pure time-delay is not obvious. Thus, k_r is set to 4 in the PI settings given by eqs. (30)-(31), giving

$$K_c = 0.13 K_{c_u} \tag{33}$$

and

$$\tau_i = 2.5 P_u \tag{34}$$

Simulations

Using $K_{c_u} = 1273$ %/K and $P_u = 0.055$ d, cf. Section 5.4.2, gives PI settings as shown in Table 1. The resulting stability margins are relative large, cf. Table 1. However, it is decided not to retune the controller since the settings shown in Table 1 are safe regarding control system stability, and the PM value of 47.8° is actually close to (but outside) the non-critical limit of 45°. Simulation (not shown here) show well damped responses, coherent with large stability margins. Also, $k_r = 1$ is tried, but the phase margin is relatively small (17.1°), as expected.

Practical results

$k_r = 4$ is used in eqs. (33)-(34) with $K_{c_u} = 1273$ %/K and $P_u = 0.045$ d from Section 5.4.2. The resulting PI settings are shown in Table 2. Figure 10 shows responses on the real reactor with these PI settings. (The PI settings with $k_r = 4$ were applied just before the setpoint step.) The responses indicate acceptable stability. Also, $k_r = 1$ is applied on the real reactor, but responses (not shown here) indicate poor stability.

Comments and conclusions

- Both theoretical analysis, i.e. simulations (though not shown here) and stability margins, and practical results indicate successful controller tuning using enhanced R-ZN settings with $k_r = 4$. The stability margins are large, cf. Table 1, and the simulated and real responses are smooth.

- R-ZN settings with $k_r = 1$ are not recommended here.

5.5. Control system robustness against process parameter changes

5.5.1. Introduction

The transfer function model of the temperature control system presented in Appendix A.2 forms a good basis for a stability robustness analysis of the control system. It is assumed that the controller is a PI controller tuned with the Skogestad method at one specific operating point. The Skogestad model-based PI settings formulas
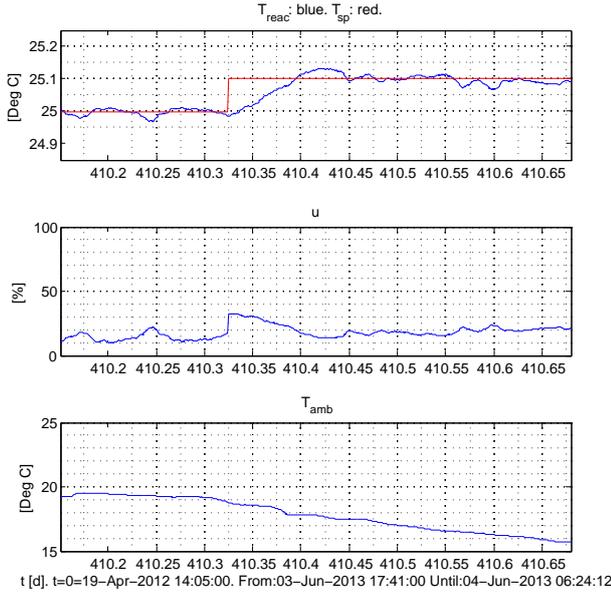
Figure 10: *Real responses in the temperature control system with enhanced R-ZN PI settings with $k_r = 4$.*

also make a good basis for adaptation of the PI settings if known changes of model parameters occur.

The PI settings are given by eqs. (13) and (15). Assuming K_{i_p} is given by eq. (24), the PI settings become

$$K_c = \frac{1}{2K_{i_p}\tau_{\text{delay}}} = \frac{c\rho V}{2K_u\tau_{\text{delay}}}$$

$$\tau_i = 4\tau_{\text{delay}}$$

In the following subsections the control system robustness against changes in parameters assumed most apt to changes, is discussed. The changes are:

- Changes in the feed flow, F_{feed}.

- Changes in the reactor lag, τ_{lag}.

The impact that changes in these two parameters have on the dynamic properties of the control system is analysed. To this end, it is assumed that the controller, which is assumed a PI controller, is tuned with the Skogestad method as in Section 5.3.2.

5.5.2. Changes in feed flow

The tuning is based on the process having "integrator with time-delay" dynamics, cf. Section 5.3.2. These settings are valid as long as the time-constant is larger than four times the time-delay, and this assumption is always valid for a practical reactor – even with a

varying F_{feed}. As an example, assume the relatively high value $F_{\text{feed}} = 87$ L/d which is the feed flow which gives the maximum methane gas flow in steady state as calculated from Hill's model adapted to the present bioreactor by Haugen et al. (2013a). The reactor time-constant is then

$$\tau_{reac} = \frac{c\rho V}{c\rho F_{\text{feed}} + G} \quad (35)$$

$$= \frac{4200 \cdot 1000 \cdot 0.25}{4200 \cdot 1000 \cdot \frac{87}{1000} + 1.96 \cdot 10^5} \quad (36)$$

$$= 1.87 \text{ d} \quad (37)$$

which is much more than four times the effective lag of 0.02 d used as a time-delay in the Skogestad tuning method. So, the above PI settings, which are independent of F_{feed}, apply even if F_{feed} has its largest value. Obviously, they also apply for the smallest resonable value of F_{feed} since a small value makes a relatively large value of τ_{reac}. In other words, the stability of the control loop is essentially independent of F_{feed} since the assumptions of Skogestad's PI tuning rules remain valid.

Assuming that variations of F_{feed} are the only parameter variations which affect the reactor dynamics, it is concluded that there is no need for adjusting the PI settings as functions of the varying F_{feed}. This is also confirmed in simulations.

5.5.3. Changes in lag or time-delay

Although the transfer function model presented in Appendix A.2 does not contain any pure time-delay transfer function, it is useful to assume that such a time-delay is present since the time-delay margin is a safe (conservative) estimate of the lag margin. It can be shown, see e.g. Haugen and Lie (2013), that the time-delay margin (increase), $\Delta\tau$, can be calculated from the phase margin, PM, with eq. (38) below. Inserting numbers related to PI controller tuning with the Skogestad method given in Table 1, yields the results given in eq. (40) below.

$$\Delta\tau \text{ [d]} = \frac{\text{PM [deg]} \cdot \frac{\pi}{360} \text{ [rad/deg]}}{\omega_b \text{ [rad/d]}} \quad (38)$$

$$= \frac{40.8 \text{ [deg]} \cdot \frac{\pi}{360} \text{ [rad/deg]}}{26.3 \text{ [rad/d]}} \quad (39)$$

$$= 0.0135 \text{ d} = 19.5 \text{ min} \quad (40)$$

One implication of this value of $\Delta\tau$ is that stability problems may occur if the measurement filter time-constant, τ_f, is increased by an amount approximately 19.5 min. If it is necessary to increase τ_f, it should be accompanied by an equal increase in τ_{delay} used in the Skogestad tuning formulas, eqs. (13) and (15).

6. Feedforward control

6.1. Introduction

Feedforward control can compensate very effectively for variations in process disturbances, Seborg et al. (2004). The following variables are regarded as disturbances acting on the bioreactor here regarded as a thermal system: T_{amb}, T_{feed}, and F_{feed}.

Figure 11 shows the structure of a temperature control system for the bioreactor with both feedforward and feedback control.
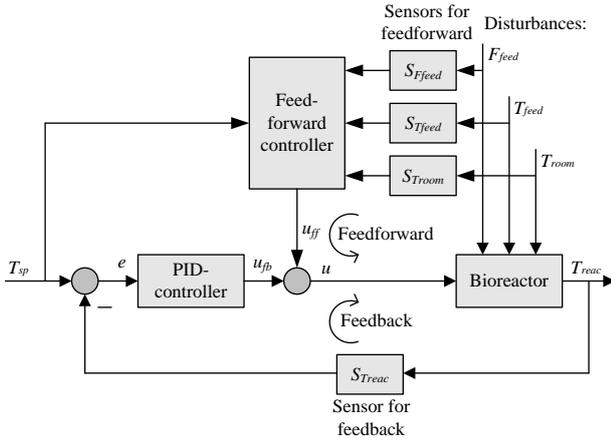

Figure 11: *Temperature control system for the bioreactor with both feedforward and feedback control.*

The total control signal is calculated as the sum of the feedback and feedback control terms:

$$u = u_{\mathrm{fb}} + u_{\mathrm{ff}} \qquad (41)$$

Results presented in previous sections indicate that for the reactor studied, feedback control is sufficient to keep the reactor temperature close to the setpoint. Hence, there is hardly any need for feedforward control. However, in other cases with severe, varying disturbances due to e.g. large ambient temperature variations, feedforward control may give a substantial improvement of the control. It will be shown how to design feedforward control for the present bioreactor, and the results should be transferable to other reactors or similar thermal systems.

In the following respective sections, two alternative feedforward controllers are developed:

- Model-based feedforward controller using a phenomenological model, i.e. an energy balance of the reactor.

- Model-free feedforward controller using steady-state operational data only.

Simulation results are shown in the following. However, no practical results are shown since feedforward control is not implemented on the real system.

6.2. Model-based feedforward control

The feedforward controller can be designed from the process model, eq. (46), as follows: First, the reactor temperature T_{reac} is substituted by its setpoint T_{sp}. Then the resulting model is solved for the control variable u, now denoted u_{ff}, to get the feedforward controller:

$$
\begin{aligned}
u_{\mathrm{ff}} = \; & \tfrac{1}{K_u}[c\rho V \dot{T}_{sp} \\
& - c\rho F_{\mathrm{feed}}\left(T_{\mathrm{feed}} - T_{\mathrm{sp}}\right) \\
& - G\left(T_{\mathrm{amb}} - T_{\mathrm{sp}}\right)]
\end{aligned}
\qquad (42)
$$

which can be implemented assuming all parameters and variables on the right-side of eq. (42) are known apriori or from measurements, which is a realizable assumption here.

Simulations

The feedforward controller, eq. (42), is applied to a simulated reactor having model parameter values as shown in Table 6. The setpoint is constant. $T_{\mathrm{amb}} = T_{\mathrm{feed}}$ (as in all subsequent simulations) is varied as a sinusoid of amplitude 10 °C with a period of 1 d, which assumed a representative variation if the reactor is outdoors, and with mean value 15 °C. In the simulation, T_{amb} pass through a lag of time-constant 0.01 d before it enters the contents of the reactor. This lag is meant to represent additional thermal dynamics of a real reactor. However, this lag is not included in the feedforward controller. Hence, a (relatively small) model error is included.

Figure 12 shows responses with and without feedforward control. Both cases include feedback PI control with the controller tuned with the Skogestad method with $K_c = 152$ %/°C and $T_i = 6912$ s.

Table 3 shows analysis results. $|e|_{\mathrm{max}}$ is the maximum control error. The IAE index is calculated from $t = 0.5$ to 5 d.

Table 3: Results for temperature control with and without feedforward control, but with feedback PI control in both cases.

| Feedforward?	$|e|_{\mathrm{max}}$	IAE
Without	0.0892	0.256
With	0.0056	0.016
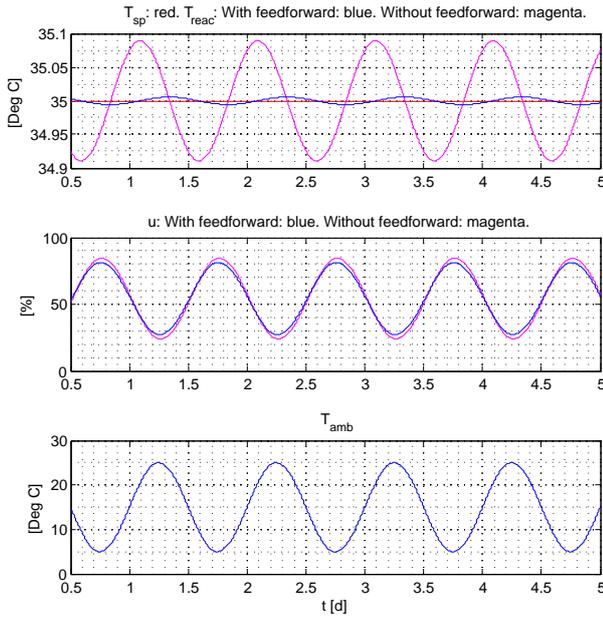
Figure 12: *Simulation of temperature control with and without feedforward control, with feedback PI control in both cases.*

Note: When the feedforward controller is active, it is necessary to set the output range of the PI controller to cover both positive and negative values to make the PI controller be able to compensate for the imperfect feedforward control signal, which is due to model error, with both positive and negative values. If the output range is only positive, the compensation may be insufficient, and the result may be a nonzero steady state control. If the output range of the PI controller can cover positive values only, an alternative solution is to subtract a proper negative constant, e.g. 20%, from the PI control signal, thereby forcing the PI control signal to become positive.

Comments and conclusions

- Feedforward control improves the control performance considerably.

- The simulations show that the control signal time-series appears very similar in feedback (only) control and in feedforward control, indicating that the "timing" of the control action is crucial for good control performance, and good timing is provided by feedforward control.

- The reason why there is a nonzero control error with feedforward control is the inclusion of the assumed realistic thermal dynamics in terms of a lag

of 0.01 d. Without this model error, the control error would have been zero with feedforward control.

6.3. Model-free feedforward control

A feedforward controller may be designed from steady-state operational data. It is assumed here that $T_{amb} = T_{feed}$ is the most important varying disturbance for our reactor. T

- For each of N distinct values of the disturbance, T_{amb}, observe the value of the control signal u which gives approximately zero steady state control error. This may be done during PI(D) feedback control. Typically, feedback control is used together with feedforward control, so no extra effort is needed to run the feedback control here. The result is a table of corresponding values of T_{amb} and u_s (steady-state value).

- Use table lookup, i.e. some interpolation method, to calculate the instantaneous feedforward control signal u_{ff} from the instantaneous measured T_{amb}.

This is an approximate design method since it is based on only steady-state data, but it can improve the disturbance compensation substantially. If the disturbance is a so-called input disturbance, i.e. the disturbance enters the process dynamically at the same "position" as the control variable does, the model-free feedforward may perform as well as the model-based feedforward. This is the case in the simulation example described below.

Simulations

Table 4 shows the corresponding steady-state values of $T_{amb} = T_{feed}$ and u found under steady-state conditions with PI control (subindex "s" means steady-state). The conditions are the same as in the simulation in Section 6.2. The simulated responses with model-free feedforward is virtually indistinguishable from the results with model-based feedforward shown in Figure 12 and Table 3.

Table 4: $N = 5$ corresponding values of $T_{amb} = T_{feed}$ and u.

T_{amb_s} [°C]	u_s [%]
5	81.4
10	67.9
15	54.3
20	40.7
25	27.1

7. Temperature control of a full-scale reactor

Reactor description

In this section results for the pilot reactor presented in previous sections are applied to a simulated full-scale reactor having the same form of mathematical model as for the pilot reactor, cf. Appendix A, with the following parameter and operational values:

- The reactor volume is $V = 10$ m³. This size is assumed representative for reactors at farms using animal waste as feed.

- The reactor is assumed rectangular with height, H, and depth, D, being equal, and width, W, being twice the depth, as is approximately the case for anaerobic baffle reactors (ABR).[2] From the known volume, $H = D = W/2 = 1.71$ m.

- The area-specific heat conductivity is same as for pilot reactor. Hence, the heat conductivity of full-scale reactor is $G_{\text{fs}} = GA_{\text{fs}}/A_{\text{pilot}} = 2.08 \cdot 10^6$ (J/d)K. G is conductivity of pilot reactor. A_{fs} and A_{pilot} are conductive areas of the respective reactors. A_{pilot} is calculated from the given volume and design of the pilot reactor, cf. Section 2 (detailes not given here). Assuming for simplicity that all areas are conductive, A_{fs} is calculated as $10H^2$.

- The reactor lag is guessed as $\tau_{\text{lag}} = 0.05$ d, while it is 0.01 d for the pilot.

- The temperature measurement filter time-constant is as for pilot reactor, $\tau_f = 10$ min $= 0.0069$ d.

- An extreme operating point, with maximum power demand, is assumed: Temperature setpoint is $T_{\text{sp}} = 38$ °C. Ambient temperature is $T_{\text{amb}} = -20$ °C. Temperature of liquid feed is $T_{\text{feed}} = 0$ °C. Feed flow $F_{\text{feed}} = 1000$ L/d giving hydraulic retention time HRT $= 10000$ L/10000 L/d $= 1$ d.

- Using the extreme operating point (above) in the static version of the dynamic energy balance eq. (46), and allowing for 50% design margin, the maximum power to be delivered by the electrical heater is 29.8 kW.

- The controller output, u, is in unit of kW, not percent as for the pilot.

---

[2]An ABR reactor of this size is being constructed at Skoglund farm, Porsgrunn, Norway.

The main specification of the temperature control system is:

- The control error is limited, cf. Section 3:

$$|e| \leq 0.25 \text{ °C} = E \qquad (43)$$

The following conditions are assumed for simulation and analysis: $T_{\text{sp}} = 38$ °C, $T_{\text{feed}} = 0$ °C, $F_{\text{feed}} = 10000$ L/d. T_{amb} is assumed sinusoidal with period 1 d, assumed to represent a relatively large, still realistic, outdoor temperature variation:

$$T_{\text{amb}}(t) = -10\text{°C} + 10\text{°C} \cdot \sin\left(\frac{2\pi}{1 \text{ d}}t\right) \qquad (44)$$

where t is time [d]. Table 5 summarizes the results of simulations and analysis for different controllers and controller settings. The results are commented in the following.

Table 5: Results with three different controllers. R-ZN PI = PI controller with R-ZN settings. S PI = PI tuned with Skogestad settings. On-off = On-off controller.

	R-ZN PI	S PI	On-off
K_c	9.6	4.3	N/A
τ_i[min]	463	328	N/A
$|e|_{\text{max}}$ [°C]	0.026	0.065	0.34
μ_e [°C]	0	0	0.10
$|S(j\omega_1)|$	0.35 $= -9.1$ dB	0.88 $= -1.1$ dB	N/A
GM	7.3	15.1	N/A
PM	38.2º	43.0º	N/A

Simulations

Simulations have been run, but plots are not shown here, with the following three controllers:

- PI controller tuned with the R-ZN method with tuning parameter $k_r = 4$, cf. Section 5.4.3.

- PI controller tuned with the Skogestad method, cf. Section 5.3.2.

- On-off controller, cf. Section 4.

Frequency response analysis

Figure 13 shows for each of the two PI controller settings, a Bode plot of the magnitude of the sensitivity function of the control loop, $S(j\omega) = S(j2\pi f) = 1/[1 + L(j2\pi f)]$ where L is the loop transfer function defined in Appendix A.2.
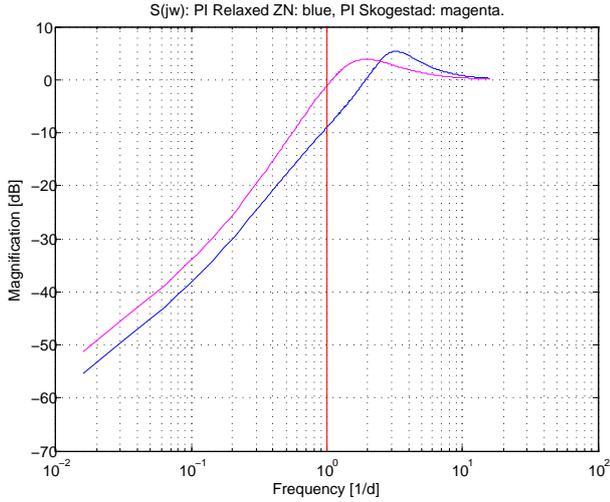
Figure 13: *Bode plot of the magnitude of the sensitivity function of the control loop for two different PI controller settings.*

The frequency $f_1 = 1$ d^{-1} is the frequency of the sinusoidal T_{amb} in the simulations. The $|S|$-plot shows how much the response in the process output variable due to a sinusoidal process disturbance is reduced by using feedback control, compared with no feedback control, Seborg et al. (2004). The smaller the value of $|S(j2\pi f_j)|$, the more effective the feedback disturbance compensation for a sinusoidal disturbance of frequency f_j [d^{-1}]. If $|S(j2\pi f_j)| \approx 1 = 0$ dB, the feedback makes no difference compared with open loop control (constant control signal).

Let $H_d(s)$ be the open loop transfer function from T_{amb} to T_{reac}. $H_d(s)$ can be calculated from eq. (46). $|H_d(j2\pi f_j)|$ expresses the self-regulation of the reactor for sinusoidal T_{amb} of frequency f_j [d^{-1}]. Assume $f_j = 1$ d$^{-1} = f_1$, corresponding to eq. (44). Calculations show that $|H_d(j2\pi f_1)| \approx 0.0079$ for F_{feed} between the assumed large value of 10 m^3/d and small value of 1 m^3/d. Hence, without feedback control, the amplitude of T_{reac} is $0.0079 \cdot 10$ ºC $= 0.079$ ºC which satisfies ineq. (43) if no other disturbances exist. However, in practice, feedback control is needed to compensate for static or low-varying disturbances.

Comments and conclusions

- The values of GM and PM indicate that the stability is acceptable with both PI settings.

- The Bode plot in Figure 13, and Table 5, shows that with Skogestad PI settings, $|S(j2\pi f_1)| = 0.88$. This indicates that the feedback control loop reduces the impact of the assumed sinusoidal T_{amb}

on T_{reac} by only 12%. With the R-ZN settings the reduction is far better, namely 65%.

- Inequality (43) is not satisfied with the on-off controller due to a permanent mean offset from setpoint. However, ineq. (43) may be satisfied if the value of u_{on} is reduced.

- Assume that the ineq. (43) is not satisfied with PI control. An attempt to optimize the controller tuning can be made using loop-shaping, Skogestad and Postlethwaite (2007), or optimization methods, Edgar et al. (2001). The controller settings must satisfy the following requirement:

$$|S(j2\pi f_1)| \, |H_d(j2\pi f_1)| \, A_{T_{\text{amb}}} \leq E \qquad (45)$$

where $A_{T_{\text{amb}}}$ is the maximum amplitude of T_{amb}, e.g. 10ºC, E is given by ineq. (43), and f_1 is the frequency [d^{-1}] of the sinusoidal T_{amb}, here assumed 1 d^{-1}.

Also, activating the derivative term should be considered to reduced the control error.

- The control error may be reduced considerably with feedforward control, cf. Section 6. Model-based feedforward is implemented on the simulated full-scale reactor with the aforementioned result, but responses are not shown here. However, the results above indicate that feedback PI control is sufficient.

8. Discussion

Model accuracy

For the pilot reactor, the practical performance of the reactor temperature control systems with on-off control and with PI control is in good accordance with the theoretical performances as seen in simulations. This indicates that the mathematical models used are sufficiently accurate to be used for analysis, design, and simulations. The accuracy of the models in the present study motivates for use of models for design of planned reactors having different physical dimensions.

The present reactor is heated by an electrical resistor wound around the reactor inside the thermal insulation jacket. If the reactor is heated differently, e.g. by heating the influent, we think that just simple modifications of the model are necessary.

Sensor accuracy

According to technical specifications the reactor temperature sensor, a Pt100 sensor, has an accuracy of approximately $\pm$ 0.3 ºC in the pertinent temperature

range. In various experiments that are conducted in this study, the observed temperature responses vary less than this accuracy. Although we have no data for the repeatability of the sensor, the good accordance between measured and simulated responses indicate that the repeatability is sufficient for us to rely on the temperature measurements.

9. Conclusions

It is demonstrated that the produced methane gas flow depends clearly on the bioreactor temperature. Moreover, according to literature references, methane-generating microbes should not be exposed to temperature changes larger than 0.5 °C in amplitude. Thus, the temperature should be controlled to a setpoint with a maximum control error of ± 0.25 °C.

On-off feedback control may be used for temperature control, given that the on-off operation is acceptable, which may not be the case with a mechanical actuator. The mean control error (offset) from the setpoint is typically non-zero. The maximum control error may be unacceptable.

A PI controller can be tuned successfully with the Skogestad method and with the R-ZN tuning method. The original ZN closed loop method is not appropriate because of poor resulting stability.

The robustness of the PI control system is investigated assuming model-based Skogestad PI settings. The PI settings are independent of the feed flow, so the tuning is robust against feed flow variations. Frequency response analysis shows a time-delay margin of approximately 20 minutes which is here assumed a safe value.

Both model-based feedforward controller designed from the energy balance of the reactor, and a model-free controller using table lookup on operational data, are applied to a simulated reactor, with almost identical performances. Comparing with only feedback control, feedforward control improves the temperature control considerably.

A temperature control system for a simulated full-scale reactor is simulated. The self-regulation of the reactor is sufficient to limit the impact on the reactor temperature by an assumed large sinusoidal daily variation of the ambient temperature. In practice, feedback control is needed to compensate for static or low-varying disturbances.

Acknowledgments

A. Mathematical models

A.1. Phenomenological reactor model

A mathematical model describing the dynamic behaviour if the reactor temperature, T_{reac}, is developed by Haugen *et al.* (2013a). The model is based on an energy balance for the liquid of the reactor. The liquid is assumed having the same thermal characteristics as water. Homogeneous conditions due to proper mixing are assumed. The model is as follows:

$$
\begin{aligned}
\dot{T}_{reac} = \frac{1}{c\rho V}[&P_{heat} \\
&+ c\rho F_{\text{feed}}\left(T_{\text{feed}} - T_{\text{reac}}\right) \\
&+ G\left(T_{\text{amb}} - T_{\text{reac}}\right)]
\end{aligned}
\tag{46}
$$

The supplied electrical power, P_{heat}, is proportional to the control signal:

$$
P_{heat} = K_u u
\tag{47}
$$

Model parameter values are given in Table 6. G is estimated from experimental data by Haugen *et al.* (2013a). The value of F_{feed} is as in experiments.

Table 6: Parameters of reactor temperature model.

$c = 4200$ J/(kg K)
$\rho = 1000$ kg/m^3
$V = 250$ L
$G = 1.96 \cdot 10^5$ (J/d)K
$K_u = 2$ W/%
$F_{\text{feed}} = 65$ L/d
$\tau_{\text{lag}} = 0.01$ d

Unless otherwise stated, it is assumed that

$$
T_{\text{feed}} = T_{\text{amb}}
\tag{48}
$$

In practice, some lag can be observed in the temperature. This lag is probably due to energy capacitance in the reactor wall and it also accounts for imperfect mixing in the reactor. The following time-constant model is used to represent the lag:

$$
\dot{T}_{reac_{\text{lag}}} = \frac{\left(T_{\text{reac}} - T_{reac_{\text{lag}}}\right)}{\tau_{\text{lag}}}
\tag{49}
$$

Figure 6 shows the response in T_{reac_lag} due to a step in the control signal, u. From this response the lag is estimated visually with the value given in Table 6.

A.2. Transfer functions model of the temperature control system

For simplicity, the same symbol is here used for a variable in both the Laplace domain and in the time-domain.

Figure 14 shows a block diagram of a transfer functions model of the control system. This model is used as the basis for the frequency response analysis in Section 5.
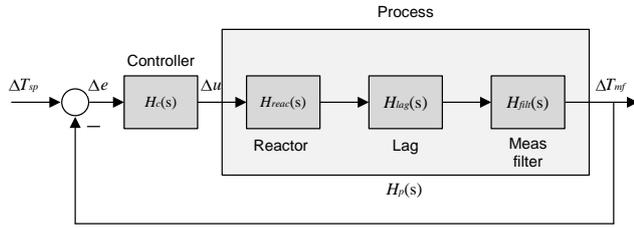
Figure 14: *Block diagram of a transfer functions model of the control system.*

Loop transfer function

From Figure 14,

$$L(s) = H_c(s) \underbrace{H_{reac}(s)\, H_\mathrm{lag}(s)\, H_\mathrm{filt}(s)}_{H_p(s)} \qquad (50)$$

The individual transfer functions of eq. (50) are defined in the following.

Controller transfer function

Assuming PI controller,

$$\frac{\Delta u(s)}{\Delta e(s)} = K_c \left(1 + \frac{1}{\tau_i s} \right) = H_c(s) \qquad (51)$$

Process transfer function

From eq. (46) and eq. (48),

$$\frac{\Delta T_\mathrm{reac}(s)}{\Delta u(s)} = \frac{K}{\tau_{reac} s + 1} = H_{reac}(s) \qquad (52)$$

where

$$K = \frac{K_u}{c\rho F_\mathrm{feed} + G} \qquad (53)$$

$$\tau_{reac} = \frac{c\rho V}{c\rho F_\mathrm{feed} + G} \qquad (54)$$

Lag transfer function

From the lag model, eq. (49),

$$\frac{\Delta T_{reac_\mathrm{lag}}(s)}{\Delta T_\mathrm{reac}(s)} = \frac{1}{\tau_\mathrm{lag} s + 1} = H_\mathrm{lag}(s) \qquad (55)$$

Filter transfer function

The raw temperature measurement, T_mr, which here is the same as T_{reac_lag}, is quite noisy and is therefore filtered with a time-constant filter having the following transfer function model:

$$\frac{\Delta T_\mathrm{mf}(s)}{\Delta T_\mathrm{mr}(s)} = \frac{1}{\tau_f s + 1} = H_\mathrm{filt}(s) \qquad (56)$$

where τ_f is the filter time-constant. For the present reactor, τ_f is set to 10 min.

Note: Above, T_mf represents the filtered measured reactor temperature. However, in most sections in this paper, it is practical to use symbol T_reac for filtered measured reactor temperature.

B. Abbreviations and nomenclature

B.1. Abbreviations

AD: Anaerobic digestion

GM: Gain margin

HRT: Hydraulic retention time

IMC: Internal model control

MPC: Model-based predictive control

PID: Proportional + integral + derivative

PM: Phase margin

PWM: Pulse-width modulation

R-ZN: Relaxed Ziegler-Nichols

SSR: Solid-state relay

TC: Temperature controller

TT: Temperature transmitter (-sensor)

ZN: Ziegler-Nichols

B.2. Nomenclature

Variables and parameters in alphabetic order:

c [J/(kg K)]: Specific heating capacity of liquid.

d_e [K] deadband of on-off controller.

e [K]: Control error (setpoint minus measurement).

F_{feed} [L/d]: Influent or feed flow or load rate, assumed equal to effluent flow (constant volume).

F_{meth} [L CH$_4$/d]: Methane gas flow.

G [(J/d)K]: Thermal conductance of reactor.

G_{he} [(J/d)K]: Thermal conductance of heat exchanger.

k_r: Adjustable parameter in the R-ZN controller tuning method.

K_c [%/K]: Controller gain.

K_u [W/%]: Actuator or heater gain.

τ_c [s] or [min] or [d]: Closed-loop time-constant in the Skogestad controller tuning method.

τ_d [s] or [min] or [d]: Derivative time.

τ_{delay} [s] or [min] or [d]: Time-delay.

τ_f [s] or [min] or [d]: Measurement filter time-constant.

τ_i [s] or [min] or [d]: Integral time.

τ_{lag} [d]: Lag time-constant.

μ [d^{-1}]: Reaction (growth) rate of acidogens.

μ_c [d^{-1}]: Reaction (growth) rate of methanogens.

μ_m [d^{-1}]: Maximum reaction rate of acidogens.

μ_{mc} [d^{-1}]: Maximum reaction rate of methanogens.

ρ [kg/m^3]: Density of reactor liquid.

T_{mf} [°C]: Filtered measurement signal.

T_{mr} [°C]: Raw (non-filtered) measurement signal.

T_{reac} [°C]: Reactor temperature.

T_{sp} [°C]: Setpoint of reactor temperature.

u [%]: Control signal.

u_{fb} [%]: Feedback control term.

u_{ff} [%]: Feedforward control term.

u_{man} [%]: Manual control signal.

V [L]: Effective reactor volume.

References

Åstrøm, K. J. and Hägglund, T. *PID Controllers: Theory, Design and Tuning*. ISA, 1995.

Batstone, D. J., Keller, J., Angelidaki, I., Kalyuzhnyi, S. V., Pavlovstahis, S. G., Rozzi, A., Sanders, W. T. M., Siegrist, H., and Vavilin, V. A. *Anaerobic Digestion Model No. 1, Scientific and Technical Report 15*. IWA Publising, 2002.

DiRuscio, D. On Tuning PI Controllers for Integrating Plus Time Delay Systems. *Modeling, Identification and Control*, 2010. 31(4):145–164. doi:10.4173/mic.2010.4.3.

Edgar, T. F., Himmelblau, D., and Lasdon, L. *Optimization of Chemical Processes*. McGraw-Hill, 2001.

Hägglund, T. and Åstrøm, K. J. Revisiting the Ziegler-Nichols Tuning Rules for PI Control. *Asian J. Of Control*, 2002. 4:364–380.

Hashimoto, A. G., Chen, Y. R., and Varel, V. H. Theoretical aspect of anaerobic fermentation: State-of-the-art. *Livestock Waste: A Renewable Resource. American Society of Agricultural Engineers*, 1981.

Haugen, F. Comparing PI tuning methods in a real benchmark temperature control system. *Modeling, Identification and Control*, 2010. 31:79–91. doi:10.4173/mic.2010.3.1.

Haugen, F. The Good Gain method for simple experimental tuning of PI controllers. *Modeling, Identification and Control*, 2012. 33(4):141–152. doi:10.4173/mic.2012.4.3.

Haugen, F., Bakke, R., and Lie, B. Adapting dynamic mathematical models to a pilot anaerobic digestion reactor. *Modeling, Identification and Control*, 2013a. 34(2):35–54. doi:10.4173/mic.2013.2.1.

Haugen, F., Bakke, R., Vasdal, K., and Bergland, W. Foss Biolab. http://fossbiolab.no, 2013b.

Haugen, F. and Lie, B. Relaxed Ziegler-Nichols Closed Loop Tuning of PI Controllers. *Modeling, Identification and Control*, 2013. 34(2):83–97. doi:10.4173/mic.2013.2.4.

Hill, D. T. Simplified monod kinetics of methane fermentation of animal wastes. *Agric. Wastes*, 1983. 5. doi:10.1016/0141-4607(83)90009-4.

O'Dwyer, A. *Handbook of Controller Tuning Rules*. Imperial College Press, 2003. doi:10.1142/p277.

Seborg, D. E., Edgar, T. F., and Mellichamp, D. A. *Process Dynamics and Control*. John Wiley and Sons, 2004.

Skogestad, S. Simple analytic rules for model reduction and PID controller tuning. *Modeling, Identification and Control*, 2004. 25(2):85–120. doi:10.4173/mic.2004.2.2.

Skogestad, S. and Postlethwaite, I. *Multivariable Feedback Control: Analysis and Design*. Wiley, 2007.

Tchobanoglous, G., Burton, F. G., and Stensel, H. D. *Wastewater Engineering: Treatment and Reuse*. Metcalf and Eddy, McGraw Hill, 2003.

Tyreus, B. D. and Luyben, W. L. Tuning PI Controllers for Integrator/Dead Time Processes. *Ind. Eng. Chem*, 1992. 31(31).

Ziegler, J. and Nichols, N. Optimum settings for automatic controllers. *Trans. ASME*, 1942. 64(3):759–768. doi:10.1115/1.2899060.

Article 3 – On-off and PI Control of Methane Gas Production of a Pilot Anaerobic Digestion Reactor

Authors: Finn Haugen, Rune Bakke and Bernt Lie.

Authors' roles in the article: Finn Haugen: Main ideas, implementation, and writing. Rune Bakke (co-supervisor) and Bernt Lie (supervisor): Discussions, comments, and proof readings.

Background and methods of the article

Background

This article assumes that a setpoint of the methane gas flow produced by an AD reactor is specified. It is shown how the actual methane gas flow can be retained at this setpoint using feedback control despite various process disturbances. A specified gas flow setpoint may stem from a specified net power production since, under ideal conditions, the energy contents of methane gas at standard temperature and pressure (STP) is 9.95 kWh/m^3. It should be noted that with methane gas flow control, the volumetric feed rate, which is here the control variable, will vary somewhat due to inevitable disturbances like variations in the feed composition.

Methods

In this article it is assumed that the controllers are standard process controllers, namely the on-off controller and the PI controller, using the feed rate as control variable. The control systems are tested in simulations based on the modified Hill model presented in Article no. 1. The Skogestad method, which is an open loop method, and the Relaxed Ziegler-Nichols closed loop method, which is presented in Article no. 6, are tuned both on a simulator and on the real reactor. The two tuning methods give approximately the same PI settings. The Skogestad method is ranged as the best method as it requires less tuning time, and because it is easier to change the PI settings at known changes in the process dynamics. Skogestad's method is successfully applied to the real reactor.

To analyze the simulated control systems for different controller settings, both performance and stability robustness measures are calculated. As performance measures, the IAE index (Integral of Absolute value of control Error), both for setpoint changes and for disturbance changes, and the closed loop response time are calculated from simulations and from the crossover frequency of the open loop frequency response, respectively. As stability robustness measures, the gain margin and the phase margin are calculated from the open loop frequency response. The frequency response is calculated from a linearized model with the margin() function of MATLAB. The practical control system is not analyzed, except its dynamical (transient) responses are observed to evaluate qualitatively the control system stability.

On-off and PI Control of Methane Gas Production of a Pilot Anaerobic Digestion Reactor

Finn Haugen   Rune Bakke   Bernt Lie

Telemark University College, Kjolnes ring 56, 3918 Porsgrunn, Norway. E-mail contact: {finn.haugen,rune.bakke,bernt.lie}@hit.no

Abstract

A proposed feedback control system for methane flow control of a real pilot anaerobic digestion reactor fed with dairy waste is designed and analyzed using the modified Hill model, which has previously been adapted to the reactor. Conditions for safe operation of the reactor are found using steady-state responses of dynamic simulations, taking into account the upper limit of the VFA concentration recommended in the literature. The controllers used are standard process controllers, namely the on-off controller and the PI controller. Several PI controller tuning methods are evaluated using simulations. Two methods are favoured, namely the Skogestad method, which is an open loop method, and the Relaxed Ziegler-Nichols closed loop method. The two methods give approximately the same PI settings. Still, the Skogestad method is ranged first as it requires less tuning time, and because it is easier to change the PI settings at known changes in the process dynamics. Skogestad's method is successfully applied to a PI control system for the real reactor. Using simulations, the critical operating point to be used for safe controller tuning is identified.

Keywords: Anaerobic digestion, bioreactor, gas flow control, on-off control, PI control, feedback.

1. Introduction

This paper attempts to answer the following questions related to a real pilot upflow anaerboic sludge blanket (UASB) reactor fed with dairy waste: What are the benefits and drawbacks of feedback, or closed loop, control of the produced methane flow compared to using open loop control, i.e. a constant feed rate? Assuming the use of standard process controllers, namely on-off and proportional-integral (PI) control, how does the control systems perform? How should the PI controller be tuned? Some of these questions are addressed using both simulations and practical experiments, while some are addressed only using simulations.

The pilot plant

The reactor is a part of a pilot biological plant for nutrient and energy recovery named Foss Biolab, situated at Foss farm, Skien, Norway. Input to the plant is dairy waste diluted with 25% water and filtered with a sieve, and outputs are fertilizer and biogas consisting of 70-75% methane. The reactor temperature is kept fixed at its setpoint with an automatic temperature control system, Haugen et al. (2013b). A description of the plant, including its monitoring and control system, is provided in Haugen et al. (2013c).

Anaerobic digestion (AD) of animal wastes

AD of animal wastes can produce biogas with methane to be used as an energy source, and a liquid effluent containing valuable nutrients. Moreover, AD reduces methane emission, odours and contaminants. AD bioreactors are effective as they allow for relatively high load rates (feed rates) and small reactor volumes. Various theoretical and practical aspects of AD processes are described e.g. in Tchobanoglous et al. (2003)

and Deublein and Steinhauser (2010). A presentation of AD of animal wastes, from dairy, beef, poultry, and swine, is provided e.g. in Husain (1998).

Literature review of reactor control

Bernard et al. (2001b) have implemented a model-based adaptive linearizing controller and a fuzzy controller designed to maintain the intermediate alkalinity (VFA, volatile fatty acids) and the total alkalinity within specified limits to ensure stable process conditions and avoid VFA accumulation despite organic load disturbances. The so-called AM2 model, Bernard et al. (2001a), is used for design and simulation.

Puñal et al. (2003) have designed an automatic fuzzy logic-based control system to maintain the online measured VFA concentration at a proper setpoint.

Méndez-Acosta et al. (2005) have designed a model-based controller for maintaining the COD (chemical oxygen demand) of the reactor effluent at its setpoint, using the AM2 model, Bernard et al. (2001a).

Méndez-Acosta et al. (2010) have designed a multivariable control system for controlling the concentration of VFA in the reactor to its setpoint using the feed rate, and controlling the total alkalinity to its setpoint using the addition of an alkali solution.

In neither of the ablove control systems, the biogas flow is controlled. Focus is on reactor stability rather than on energy production (1 Nm^3 methane at NTP = 9.95 kWh). In the papers referred below, the biogas flow is controlled.

Strömberg (2010) have identified, using simulations, three controllers for AD processes to be the most suitable ones for maximizing gas production while being able to react properly to process disturbances due to variations in pH, ammonia, and concentration in the reactor feed. The simulations are based on the ADM1 model, Batstone et al. (2002). All of the controllers have the feed rate as control variable (controller output). The controllers resemble an expert system, with logics (if-clauses) in the control function. A short description of these controllers follows.

The extremum-seeking variable gain controller by Liu et al. (2006) has the structure of a cascade control system where the primary loop implements biogas flow control, and the secondary loop implements pH control to stabilize pH.

In the disturbance monitoring controller by Steyer et al. (1999), disturbances in the form of pulses are added to the feed rate, and from the gas flow response the feed rate is adjusted to obtain maximum production. Pulsing is stopped if measured pH is below a critical value.

In the hydrogen-based variable gain controller by Rodriguez et al. (2006), online measurements of methane and hydrogen concentrations of the biogas are measured online are used by the controller for approaching a preset maximum methane gas flow. The controller is based on a relation between hydrogen concentration and effluent COD (Chemical Oxygen Demand) concentration as found from the ADM1 model, Batstone et al. (2002).

Strömberg et al. (2013) note that no uniform tuning method could be derived to tune the three controllers. Instead, the controllers were tuned by first running a large number of simulations to become familiar with the controller performances, and then the parameters were tuned manually.

Paper outline

This paper is organized as follows. Section 2 gives a short description of the proposed methane gas flow control system. Section 3 covers on-off control. Section 4 covers PI control, including an analysis of the control system robustness against process parameter changes. A discussion is given in Section 5, and conclusions are given in Section 6. Appendix A describes mathematical models used, and abbreviations and nomenclature are given in Appendix B.

Computing tools

MATLAB and SIMULINK (MathWorks, Inc.) are used for numerical computations and simulations. The algorithms of the real control system are implemented in LabVIEW (National Instruments, Inc.) running on a laptop PC.

2. The proposed methane flow control system

2.1. Control system objective

As is clear from the control systems referred in Section 1, there are alternative objectives for reactor control, i.e. obtaining a specified VFA concentration, or alkalinity, or obtaining a specified biogas production.

For the present reactor, the control objective is proposed as follows: F_{meth} is maintained at its setpoint, $F_{\mathrm{meth_{sp}}}$, assuming safe operation conditions, defined below.

Generally, the specific value of $F_{\mathrm{meth_{sp}}}$ may be calculated as the solution of a model-based optimization problem with a proper optimization criterion, e.g. maximum gas production, or economic optimization where power loss, energy prices, and value of money are taken into account. However, formulation of the

optimization problem is not discussed further in the present paper, but in a forthcoming paper.

2.2. Selection of control variable

F_{meth} is the process output variable to be controlled. An obvious candidate control variable is F_{feed} as it has a clear impact on F_{meth}. Also T_{reac}, which in the present reactor is controlled to its setpoint using a feedback control system, has a clear impact on F_{meth}, cf. Haugen et al. (2013b). Therefore, T_{reac} is a candidate as control variable. However, as pointed out in Tchobanoglous et al. (2003), T_{reac} should be kept ideally constant, variations within ± 0.5 °C being acceptable, to avoid stressing the methane-generating microorganisms (methanogens). Therefore, T_{reac} is not considered a usable control variable.

2.3. Implementation of the control system

In the methane gas flow control systems studied in the present paper, F_{feed} is the control variable while F_{meth} is the process output variable. Figure 1 shows the structure of the methane flow control system.
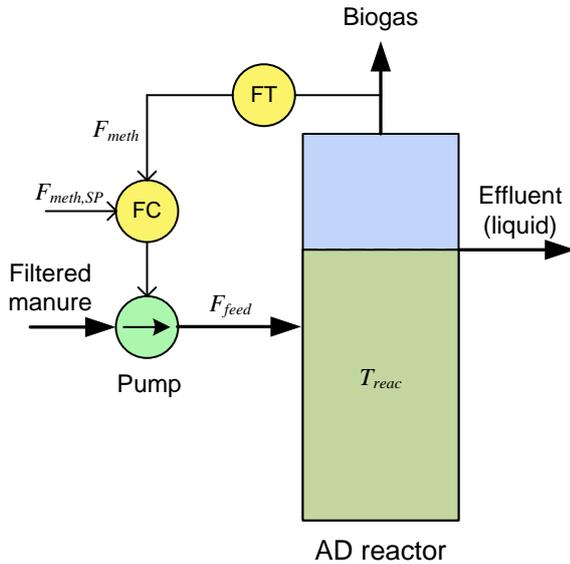
Figure 1: *Methane flow control system.*

The control signal from the gas flow controller, FC, acts on the feed pump (actuator) which is assumed to provide the feed flow, F_{feed}, demanded by the controller. The controller adjusts F_{feed} based on the control error which is the difference between the F_{meth} measurement and its setpoint. This measurement is provided by sensor FT. In practice, this measurement

is obtained by multiplying the online biogas flow measurement from a thermal gas flow sensor and the online methane concentration measurement from an IR-based sensor. The raw measurement signals are smoothed in filters which are described in Appendix A.3.

The gas flow controller manipulates the peristaltic feed pump using PWM (Pulse-Width Modulation). It is found that proper PWM settings are as follows: Fixed cycle time of 700 sec, on-value of control signal corresponding to 714 L/d, and off-value corresponding to zero L/d. Two factual benefits of using PWM control compared with analog control are (1) the calibration of the pump is needed only at the on-state of the flow rate, and (2) blockings in the feed pipeline are reduced.

2.4. Control functions

The controllers reviewed in Section 1 can be regarded as non-standard process controllers (though it can be claimed that a fuzzy logic controller is a standard controller). For the present reactor, it is proposed to use standard process controllers as on-off controllers and PI controllers, which are relatively simple controllers. For the latter there are many tuning procedures available, but there is no guarantee that any method gives successful PI settings. In this paper, several tuning methods are tested to identify the most suitable methods.
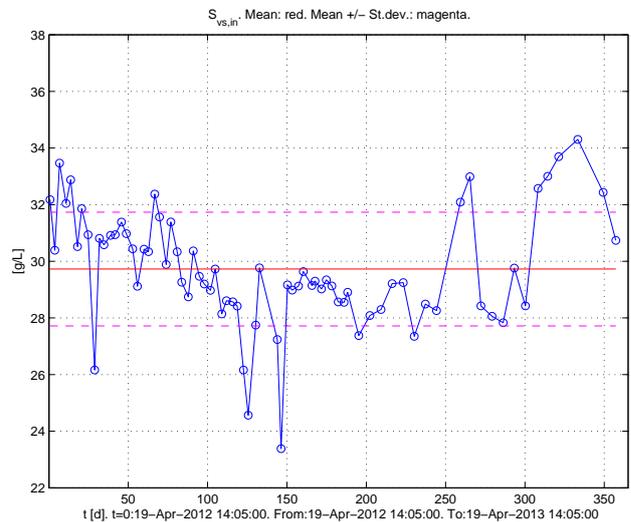
Figure 2: *Plot of $S_{\text{vs}_{\text{in}}}$ from laboratory analysis over one year. Mean value: $\mu_{S_{\text{vs}_{\text{in}}}} = 29.7$ g/L. Standard deviation: $\sigma_{S_{\text{vs}_{\text{in}}}} = 2.0$ g/L.*

In general, feedforward control can be a very efficient control method to compensate for severe dis-

143

turbances, assuming that these disturbances are measured continuously or are estimated continuously using a soft-sensor, e.g. a Kalman Filter algorithm, Dochain (2008), Simon (2006). For the present pilot reactor, variations in the volatile solids (VS) concentration of the feed, $S_{\mathrm{vs}_{\mathrm{in}}}$ [g/L], are regarded as the most important disturbance acting on F_{meth}. Figure 2 shows a plot of $S_{\mathrm{vs}_{\mathrm{in}}}$ over a period of one year. The largest change between the samples occurs around $t = 150$ d, and is approximately $\Delta S_{\mathrm{bvs}_{\mathrm{in}}} = 6$ g/L.

A simulation is here used to indicate the response in F_{meth} due to a change in $S_{\mathrm{bvs}_{\mathrm{in}}}$. It is assumed that the change is a step of amplitude 6 g/L. F_{meth} is controlled with a PI controller tuned with the Skogestad method, cf. Section 4.4.1. Figure 3 shows simulated responses of the control system due to a step change in $S_{\mathrm{vs}_{\mathrm{in}}}$. (The response due to a step change in the setpoint of F_{meth} at $t = 5$ d, is relevant in Section 4.4.1.)
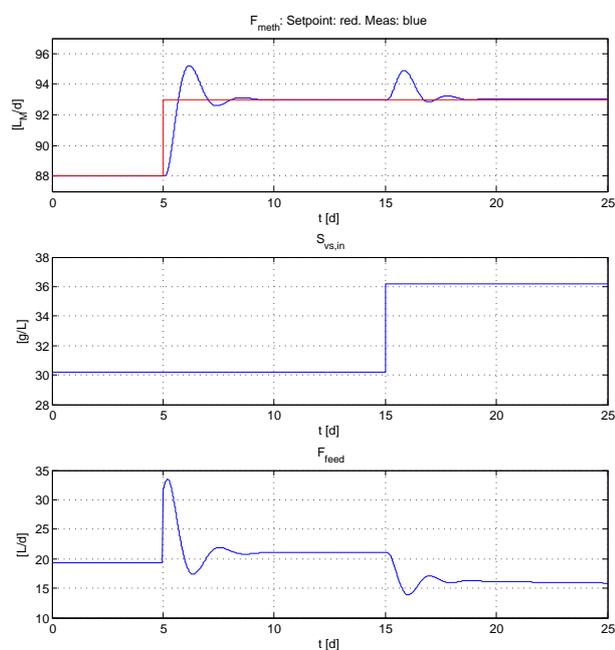

Figure 3: *Simulated responses of the control system due to a setpoint step and a disturbance step in $S_{vs_{in}}$. The PI controller is tuned with the Skogestad method.*

The maximum transient offset of F_{meth} from the setpoint is 1.9 L CH_4/d, which volume-normalized is 1.9 L CH_4/d/250 L = 0.0075 L CH_4/d/L. Assuming this transient offset is acceptable in a practical application, feedforward control is not needed.

Assuming the offset due to the variations in $S_{\mathrm{vs}_{\mathrm{in}}}$ is problematic, there is still a practical problem about implementing feedforward control because of the lack of appropriate online sensors. A soft-sensor for $S_{\mathrm{vs}_{\mathrm{in}}}$ is an alternative, but is here regarded an advanced method, and is therefore not discussed in the present paper. Using a soft-sensor for $S_{\mathrm{vs}_{\mathrm{in}}}$ is relevant for model-based control, to be addressed in a forthcoming paper.

2.5. Safe reactor operation and attainable operating points

Hill et al. (1987) have found, from a comprehensive study of literature reporting operational data for reactors fed with swine and beef waste, and confirmed by their own laboratory experiments, that $S_{\mathrm{vfa}} = 0.8$ g/L is a good indicator of the reactor health. $S_{\mathrm{vfa}} \geq 0.8$ g/L indicates an impending reactor failure, i.e. a reduction of methane production, while $S_{\mathrm{vfa}} \leq 0.8$ g/L indicates that the reactor is operated successfully, i.e. that the reactor is healthy. Hill *et al.* found that also the proprionic to acetic acid (P/A) ratio is a good indicator. However, this ratio can not be calculated from the mathematical model used in this paper, and therefore, the analysis here is not based on this ratio.

Hill *et al.* did not use dairy waste in their analysis since reliable data for such waste were not available. Nevertheless, it is here assumed that the aforementioned limit applies approximately also for reactors fed with dairy waste. A support for this assumption is that the validated AD reactor model by Hill (1983) has the same parameters describing the AD process for dairy, swine, poultry, and beef waste, except for parameters expressing the fraction of the organic feed that is degradable, but the AD process dynamics are independent of the latter parameters.

There are several alternative AD process indicators and control parameters. Angelidaki et al. (1993) identify e.g. ammonia as an important parameter for AD process control, particularly for animal waste rich on ammonia. Bernard et al. (2001b) reports that the internal alkalinity to total alkalinity ratio is an important indicator, and control parameter. According to Tchobanoglous et al. (2003), a pH level lower than 6.8 is inhibitory on the methanogenesis. These importance of monitoring and controlling these, and other, parameters, depends on the type of fed substrate, e.g. food waste, industrial waste, etc. However, from the literature, the ammonia content is relatively small and therefore hardly inhibitory for dairy waste (but it is for swine and poultry waste), the alkalinity is relatively large and not subject to large variations, and the buffer capacity is high implying that a proper pH level is maintained. Thus, VFA remains the main AD process parameter to be used here.

It is assumed that the reactor is represented by the modified Hill model which is adapted to the pilot re-
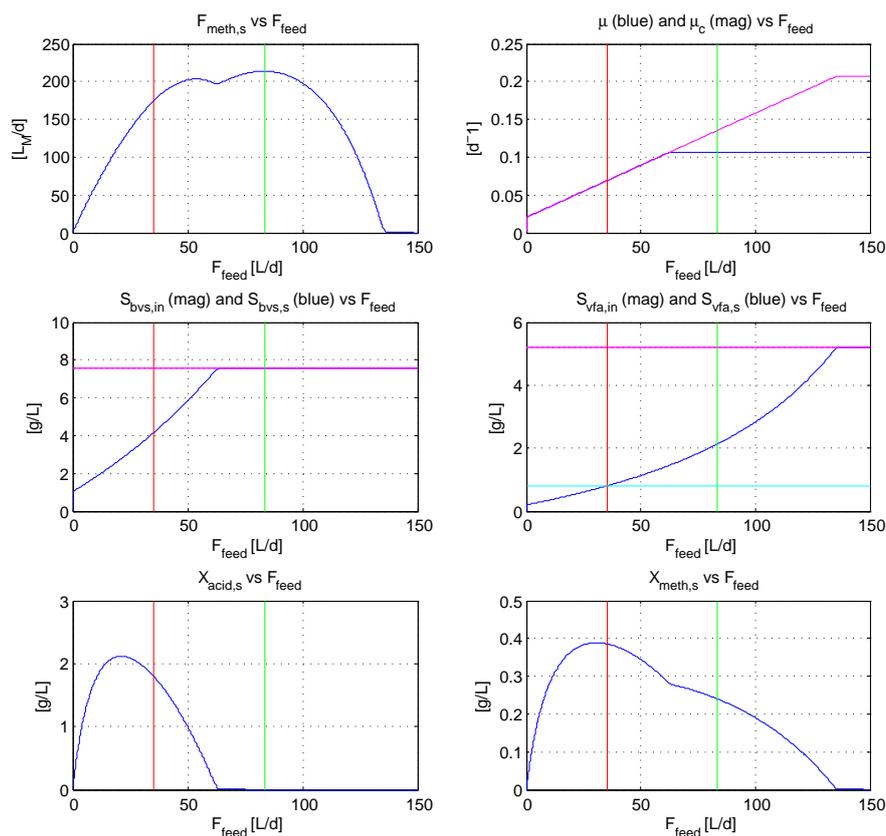
Figure 4: *Simulated static (steady-state) values of a number of variables versus F_{feed} (constant) at $T_{\text{reac}} = 35$ °C. Vertical and horizontal lines are explained in the text.*

actor by Haugen et al. (2013a). The model contains e.g. a Monod-based rate-limiting effect of high VFA concentration on conversion of VFA to methane, and it can predict washout of biomass, i.e. of acidogens and methanogens.

Figure 4 shows simulated static (steady-state) responses to a range of constant feed rates (F_{feed}). T_{reac} is 35 °C which is typical for AD reactors. The global, unconstrained maximum of F_{meth_s} is found as 214 L CH_4/d which is obtained with $F_{\text{feed}} = 83.4$ L/d, represented with right green vertical lines in Figure 4. However, at this operating point, X_{acid_s} is virtually zero, which is coherent with the middle left plot showing that $S_{\text{bvs}_{\text{in}}}$ is not being degraded. Therefore, this unconstrained maximum is not regarded as a viable operating point.

In Figure 4, the cyan horizontal line in the S_{vfa} plot represents $S_{\text{vfa}} = 0.8$ g/L. At this value, $F_{\text{feed}} = 35.3$ L/d, which is represented by red vertical lines in the plots. At this feed flow, $F_{\text{meth}_s} = 174$ L CH_4/d which is then the maximum attainable F_{meth_s} under safe conditions. The corresponding hydraulic retention time

(HRT) of the reactor is $174/35.3 = 4.9$ d.

Assume that the controller output range, i.e. the range of F_{feed}, is restricted by the user to ensure safe operating conditions. To continue the above example, assume that the upper limit of F_{feed} is set to 35.3 L/d which, according to the model, corresponds to $F_{\text{meth}_s} = 174$ L CH_4/d. The setpoint is set to $F_{\text{meth}_{sp}} = 174$ L CH_4/d. Assume that for the practical reactor, the factual F_{meth_s} that is obtained with $F_{\text{feed}} = 35.3$ L/d, is less than 174 L CH_4/d. Then, obviously, the steady-state control error is non-zero. To obtain zero steady-state error, either the upper limit of F_{feed} should be set higher than 35.3 L/d, or $F_{\text{meth}_{sp}}$ should be set smaller than 174 L CH_4/d, of which the latter alternative is the safest.

2.6. Comparing feedback control with open loop control

To demonstrate the effect of F_{meth} control, Figure 5 shows experimental time-series of F_{meth} and F_{feed}, and T_{reac}, with (automatic) control and without control.

It is clearly demonstrated that F_{meth} drifts less with control than without control. F_{meth} remains close to $F_{\mathrm{meth_{sp}}}$ even after the setpoint is changed. In the case of feedback control, F_{feed} is of course varying, while it is constant in open loop control. T_{reac} is actually different in the two cases, but it is assumed the difference between the two cases is independent of the temperature difference.
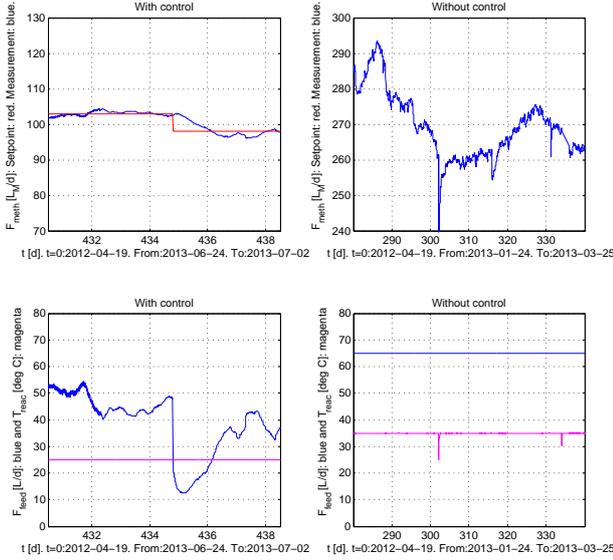

Figure 5: F_{meth} and F_{feed}, and T_{reac}, for the real reactor, with (automatic) control and without control. (The length of each of the time intervals for these two cases are different.)

If the drift of F_{meth} is acceptable when a constant F_{feed} is used, feedback control may be superfluous.

3. On-off control

The on-off controller can be regarded as the simplest feeedback controller available, Johnson (2000). It can be used without any tuning, except deciding the on-value and the off-value of the controller output. With on-off control the control system oscillates, and typically, the offset of the mean value of the control error from the setpoint is non-zero.

The on-off controller function can be defined as

$$u = \begin{cases} u_{\mathrm{on}} & \text{for } e \geq d_e \\ u_{\mathrm{off}} & \text{for } e < -d_e \end{cases} \tag{1}$$

where e is the control error,

$$e = F_{\mathrm{meth_{sp}}} - F_{\mathrm{meth}} \ [\mathrm{L\ CH_4/d}] \tag{2}$$

and d_e is an adjustable dead-band to avoid switching of u due to (measurement) noise in e. u_{on} and u_{off} are constant control signal levels. In applications with the pilot reactor, $d_e = 0.5$ L CH$_4$/d.

Table 1 summarizes a number of settings and absolute and volume-normalized characteristics found from simulated and experiments on the real reactor further described in the following.

Table 1: Settings and steady-state characteristics for simulated and practical experiments with on-off control.

Characteristics	Units	Sim	Real
u_{on}	[L CH$_4$/d]	45	45
u_{off}	[L CH$_4$/d]	5	5
F_{meth}	[L CH$_4$/d]	88	88
T_{reac}	[$^{\mathrm{o}}$C]	25	25
P_u	[d]	1.16	1.1
A_e	[L CH$_4$/d]	3.3	2.0
A_e/V	[L CH$_4$/d]	0.013	0.008
$|e|_{\mathrm{max}}$	[L CH$_4$/d]	4.2	2.2
$|e|_{\mathrm{max}}/V$	[L CH$_4$/d]	0.017	0.009
μ_e	[L CH$_4$/d]	-1.0	-0.2
μ_e/V	[L CH$_4$/d]	-0.0041	$-8.0 \cdot 10^{-4}$

Simulations

In simulations, though not displayed here, $F_{\mathrm{meth_{sp}}}(t)$ has the typical form of a sinusoidal oscillation, while $u(t)$ is a square wave.

Responses of the real reactor

Figure 6 shows F_{meth} from an experiment with on-off control on the real reactor.

Comments and conclusions

- The period, P_u, of the simulated and real oscillations are approximately equal which indicates that the dynamics of the reactor is well captured by the model. However, the amplitude of the oscillations differ by a factor of approximately 1.7. It is not clear what is the model error that causes this difference.

- For the real reactor, $|e|_{\mathrm{max}} \approx 2.2$ L CH$_4$/d, or normalized: $|e|_{\mathrm{max}}/V \approx 0.009$ L CH$_4$/d/L, is probably acceptable.

- For both the simulated and real reactor the mean control error are nonzero, but probably acceptable for both the simulated and the real reactor.
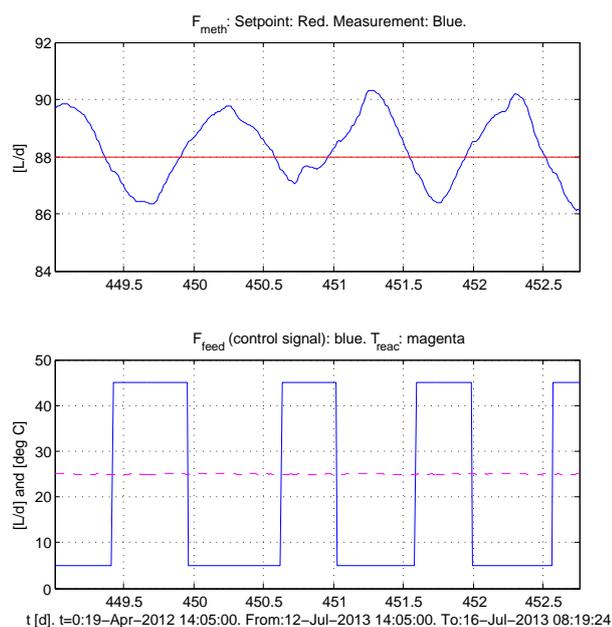
Figure 6: *Experimental F_{meth} with on-off methane gas flow control.*

- The on-off behaviour of the control signal, and hence the feed flow, may be acceptable in practical applications. Actually, it is observed that for the present reactor, discontinuous feeding reduces the frequency of the blockings.

4. PID control

4.1. Controller function

PID control is prevalent in industrial applications. The PID controller provides smooth control as opposed to on-off control, but its parameters must be tuned to fit the dynamics of the process to be controlled. The applied PID controller is based on Euler backward discretization of the following continuous time PID controller, with time-step $\tau_s = 2$ s:

$$u(t) = u_{\mathrm{man}} + K_c e(t) + \frac{K_c}{\tau_i} \int_0^t e\left(\tau\right)\, d\tau + K_c \tau_d \dot{e}(t) \quad (3)$$

Typically, the derivative term may provide control stability and agility, but is nevertheless often deactivated, i.e. $\tau_d = 0$, in practical applications because of its problematic propagation of measurement noise causing a noisy control signal. For the pilot reactor, it is decided to not use the derivative term.

4.2. Selection of controller tuning methods

It is of interest to compare different PI(D) tuning methods to arrive at a conclusion about recommended methods. The following methods are applied to the simulated reactor, and some of them are applied to the real reactor: Among open loop methods, the SIMC method (Simple IMC), Skogestad (2004), here denoted the Skogestad method, is selected. Comparing it with the famous Ziegler and Nichols open loop method, Ziegler and Nichols (1942), the Skogestad method benefits by having an adjustable parameter. Furthermore, the Skogestad method includes tuning formulas for various types of process dynamics. Other well-known open loop methods are the Lambda tuning method and the Internal Model Control (IMC) methods, Seborg et al. (2004), but it is not clear whether these methods have important benefits compared with the Skogestad method.

Among closed loop tuning methods, the famous Ziegler Nichols (ZN) closed loop method is applied, although it is expected to give small stability margins. As an alternative, the Relaxed Ziegler Nichols (R-ZN) method proposed by Haugen and Lie (2013) is tested. The Tyreus and Luyben (TL) method, Tyreus and Luyben (1992), is probably the best known method to modify the ZN closed loop PI settings to obtain more relaxed control. However, the R-ZN method compares favourably with the TL method, cf. Haugen *et al.*, (2013d). Therfore, the TL method is not tested here.

4.3. Summary of results

Table 2 gives a summary of results for a simulated reactor based on the model presented in Appendix A, and for the real reactor. The table shows controller settings, the gain margin (GM), the phase margin (PM), and the closed-loop response-time, τ_r [d], which is estimated as

$$\tau_r = \frac{1}{\omega_c} \quad (4)$$

τ_r is approximately the time-constant of the control system. The above frequency response characteristics are based on the transfer functions model described in Appendix A.3, except for the tuning method denoted "Skogestad with estimated transfer function" where the frequency response characteristics is based on the estimated transfer function. Seborg *et al.* (2004) present the following ranges of the stability margins:

$$1.7 = 4.6 \text{ dB} \leq \text{GM} \leq 4.0 = 12.0 \text{ dB} \quad (5)$$

and

$$30^{\mathrm{o}} \leq \text{PM} \leq 45^{\mathrm{o}} \quad (6)$$

Comments to Table 2:

Table 2: Results with various PI tuning methods for simulated and for real reactor.

Method	K_c [(L/d)/ (LCH$_4$/d)]	τ_i [d]	GM	PM [deg]	τ_r [d]
Sim: Skogestad	2.46	0.92	3.2 = 10.0 [dB]	32.3	0.39
Real: Skoge.	4.89	1.24	N/A	N/A	N/A
Sim: ZN	3.45	0.97	2.3 = 7.2 [dB]	25.6	0.30
Sim: R-ZN	2.44	1.16	3.4 = 10.7 [dB]	37.5	0.40
Real: R-ZN	5.00	1.16	N/A	N/A	N/A
Sim: Optimal	2.12	1.04	3.8 = 11.6 [dB]	38.0	0.44
Real: Skoge. with estim. transf. func.	13.5	0.54	2.8 = 8.9 [dB]	37.4	0.25

- The values of K_c for the simulated reactor are roughly half of the values for the real reactor, while the values of τ_i differ little. The variation in K_c is of course due to modeling errors. Actually, the modified Hill model was adapted to various time-series from time intervals relevant to controller tuning, but with no significant changes in the pertinent model parameters, nor in K_c. From this it can be concluded that using a phenomenological mathematical model as the basis for tuning a controller for the real reactor, is dubious. However, for the present reactor, the difference in values of K_c is safe.

- The PI settings calculated from the estimated process transfer function have approximately double the value of K_c and half the value of τ_i comparing with the respective settings found by the Skogestads method and the R-ZN method applied directly to the real reactor, and thus, the former settings are expected to give more aggressive control. Due to practical obstacles, the PI settings found from the estimated process transfer function have not been applied to the real reactor, so it is not known if they are applicable on the real reactor, or not.

4.4. Applications of controller tunings

4.4.1. Skogestad tuning

Simulations and real experiments indicate that the reactor dynamics can be characterized approximately as "time-constant with time-delay" with a time-constant of a few days and a time-delay of a few hours. As pointed out in Haugen and Lie (2013), the Skogestad method, with a proposed justified reduction of the integral time setting, gives the following PI settings for processes where the time-delay is less than one eighth of the time-constant, which is the case for the pilot reactor:

$$K_c = \frac{1}{2K_{i_p}\tau_{\text{delay}}} \quad (7)$$

$$\tau_i = 4\tau_{\text{delay}} \quad (8)$$

where K_{i_p}, the integrator gain, and τ_{delay}, the (apparent) time-delay, can be found from a simple process step response. K_{i_p} can be calculated as

$$K_{i_p} = \frac{S}{\Delta F_{\text{feed}}} \quad (9)$$

where ΔF_{feed} [L/d] is the applied step amplitude, and S [(L CH$_4$/d)/d] is slope of the time-delayed ramp-formed response in F_{meth}.

Simulations

K_{i_p} and τ_{delay} are found from an open-loop step response where F_{feed} is changed as a step of amplitude $\Delta F_{\text{feed}} = 1$ L/d. From the step response shown in Figure 7, where the red line is the "time-delayed ramp" step response of the assumed integrator with time-delay, $S = 0.883$ (L CH$_4$/d)/d and $\tau_{\text{delay}} = 0.23$ d. This gives $K_{p_i} = S/\Delta F_{\text{meth}} = 6.6/20 = 0.33$ [(L CH$_4$/d)/(L/d)]/d. The resulting PI settings and frequency response characteristics calculated from the linear model presented in Appendix A.3 are presented in Table 2. The stability margins are within the acceptable limits given by ineqs. (5)-(6).

Figure 3 shows simulated responses of the control system due to a setpoint step and a disturbance step in $S_{\text{vs}_{\text{in}}}$.

Responses of the real reactor

Figure 8 shows the response in F_{meth} due to a step in F_{feed} from 39 L/d to 19 L/d, i.e. the step amplitude is $\Delta F_{\text{feed}} = -20$ L/d. A negative step is used because the initial value of F_{feed} is relatively large. From the step response, $\tau_{\text{delay}} = 0.31$ d and $S = -6.6$ (L CH$_4$/d)/d are estimated. The resulting PI settings are shown in Table 2.
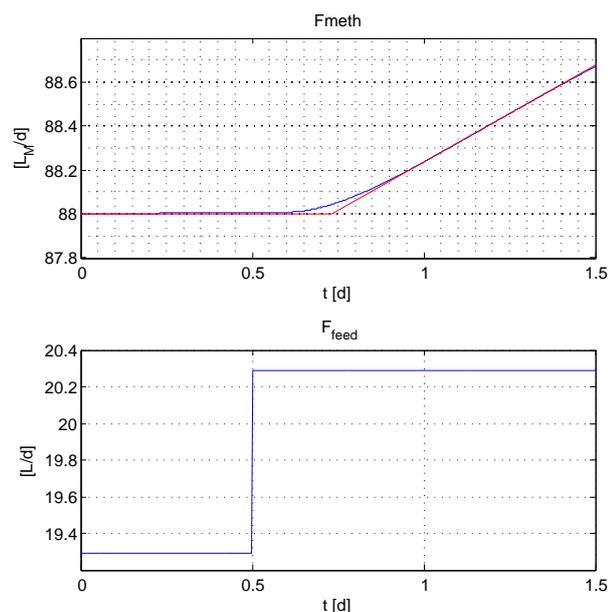
Figure 7: *Simulated open-loop step response where F_{feed} is changed as a step of amplitude* 1 *L/d.*

Figure 8: *Open-loop step response for the real reactor.*

Figure 9 shows responses on the real reactor with the above PI settings. There is no indication of poor stability. The relatively large response in F_{meth} between $t = 446.0$ and 446.5 d is assumed being due to a disturbance.

Comments and conclusions

- The Skogestad PI tuning method, here used as an open loop step response method, gives good results.

- The step response test can be accomplished within approximately half a day which is considerably shorter than e.g. relay-based tuning methods which may require more than two days, cf. Section 4.4.2.

4.4.2. Ziegler-Nichols PI tuning based on relay oscillations

Åstrøm and Hägglund (1995) suggested a relay or on-off controller to replace the P controller in the tuning phase of the ZN closed loop method, thereby avoiding the trial-and-error procedure since the oscillations come automatically. During the relay tuning the control signal becomes a square wave. Assuming the oscillation in the process output is (approximately) sinusoidal, as is the case with the present reactor, the

ultimate gain, K_{c_u}, is calculated as

$$K_{c_u} = \frac{4A_u}{\pi A_e} \qquad (10)$$

where A_u is the amplitude of the on-off control signal, and A_e is the amplitude of the control error and the process output. For a PI controller, the ZN settings are $K_c = 0.45 K_{c_u}$ and $\tau_i = P_u/1.2$ where P_u is the period of the oscillation.

Results

Using simulations with on-off controller (not shown) as the basis for relay tuning, gives $A_u = (45 - 5)/2 = 20$ L/d, $A_e = 3.3$ L$_M$, $P_u = 1.16$ d. The resulting PI settings are shown in Table 2 together with control system characteristics. The phase margin (PM) is 25.6° which is less than the lower limit in eq. (6). Simulations, not shown here, confirm relatively small stability margins as responses are oscillatory. It was decided not to use the Ziegler-Nichols method with the real reactor since the theoretical results are not satisfactory.

4.4.3. Relaxed Ziegler-Nichols PI tuning

The Relaxed Ziegler-Nichols (R-ZN) PI tuning method is proposed by Haugen and Lie (2013) to give more relaxed control, i.e. improved stability, compared with
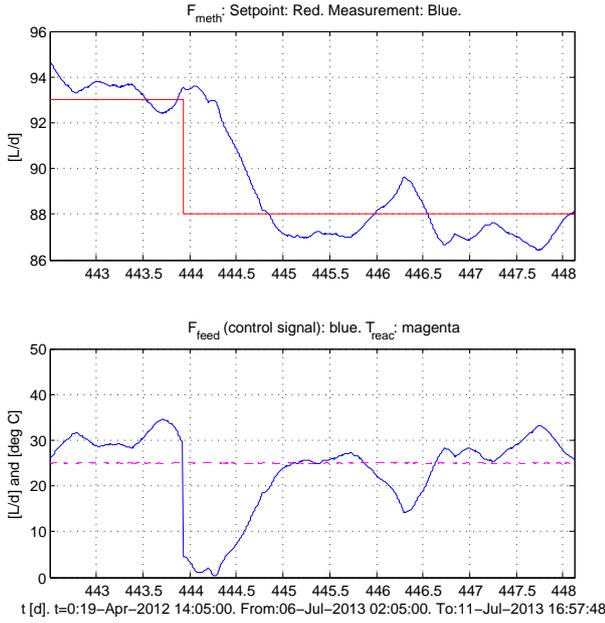
Figure 9: *Responses on the real reactor with PI methane flow controller tuned with Skogestad's method.*

the ZN closed loop method. The PI settings are:

$$K_c = \frac{2}{\pi (k_r + 1)} K_{c_u} \overset{k_r=1}{=} 0.32 K_{c_u} \qquad (11)$$

$$\tau_i = \frac{k_r + 1}{2} P_u \overset{k_r=1}{=} P_u \qquad (12)$$

where K_{c_u} and P_u can be found from relay oscillations. The tuning parameter k_r can be used for enhanced relaxation. Simulations with the modified Hill model, Haugen et al. (2013a), indicate that the default value $k_r = 1$ works well with the present pilot reactor.

Simulations

PI settings are calculated from simulated relay oscillations, not shown here. Table 2 shows the resulting PI settings, and control system characteristics. The stability margins have acceptable values. Since these PI settings differ little from those found with the Skogestad method in Section 4.4.1, simulations with R-ZN settings are not shown here (Figure 3 shows responses with Skogestad PI settings).

Practical results

The relay oscillations shown in Figure 6 are used as the basis for the PI controller tuning. The on and off values of the controller are $F_{\text{feed}_{\text{on}}} = 45$ L/d and $F_{\text{feed}_{\text{off}}} = 5$

L/d, respectively, giving $A_u = (45 - 5)/2 = 20$ L/d. From the oscillations, $A_e = 2.0$ L/d and $P_u = 1.1$ d. The resulting PI settings are shown in Table 2. Since these settings differ little from those found with the Skogestad method, cf. Section 4.4.1, it was decided not to perform separate experiments on the real reactor with R-ZN settings.

Comments and conclusions

- Both simulations and real experiments indicate successful controller tuning using the R-ZN method. The PI settings become close to those obtained with the Skogestad method, which is not a surprise since this method is designed from a combination of the Skogestad method and the ZN method.

- The Skogestad method is here favoured compared with the R-ZN method, due to the following observations: Firstly, the Skogestad method has a shorter tuning phase, namely approximately 0.7 d, cf. Figure 8, while the tuning phase of the R-ZN method is 2-3 days. Secondly, in the Skogestad method, retuning the controller in the case of a known process parameter change, e.g. an increase of the apparent τ_{delay} due to an increased filter time-constant, can be accomplished without performing any new experiment. With the R-ZN method, a new experiment is needed.

4.4.4. Optimal PI tuning based on the modified Hill model

In this method, PI controller parameter vector $p_c = [K_c, \tau_i]$ is tuned at a specific operating point to minimize the objective function $f_{\text{obj}}(p_c)$,

$$\min_{p_c} f_{\text{obj}}(p_c) \text{ s.t. } C \qquad (13)$$

(s.t. is "subject to"). C represents constraints. The following $f_{\text{obj}}(p_c)$ is here proposed:

$$f_{\text{obj}}(p_c) = \int_{t_1}^{t_2} (|e| + R|\dot{u}|) \, dt \qquad (14)$$

where e is the control error, $\dot{u} = \dot{F}_{feed}$ is the rate of change of the control signal, and R is a user-selected cost coefficient. With $R = 0$, eq. (14) is identical to the well-known IAE index, Seborg et al. (2004). The larger R, the more cost of control signal variations, and smoother, but also slower, control actions can be expected. Having only one parameter, R, to be tuned is a much easier tuning problem than having two parameters, K_c and τ_i. Furthermore, R has an intuitive interpretation. Many alternative objective functions are

possible, e.g. quadratic functions instead of absolute values, frequency response-based functions, etc. Equation (14) is here selected since it is an enhancement of the IAE index. A quadratic objective function was tested, but no benefits were identified compared to the selected function.

In eq. (13), C is a constraint on the stability margins in terms of $|S(j\omega)|_{\max}$, where $S(s) = 1/[1 + L(s)]$, where $L(s) = H_c(s)H_{AD_m}(s)$ is the loop transfer function. $H_{AD_m}(s)$ is given by eq. (25). The acceptable range of $|S(j\omega)|_{\max}$ is set as [1.2, 2.0], according to Seborg *et al.* (2004). However, this constraint was not active at the optimal solution (its value was 1.87).

$f_{obj}(p_c)$ is calculated from simulations with the (nonlinear) modified Hill model, Haugen et al. (2013a). The simulator is based on numerical integration of the differential equations using the Euler explicit numerical method implemented in native for-loops in a MATLAB script.[1]

The optimization problem is here solved using "brute force" (BF), i.e. $f_{obj}(p_c)$ is calculated over a grid of equidistant values of K_c and τ_i defined in respective arrays (MATLAB), and the optimal p_c is found by searching the matrix of stored values of f_{obj} for the minimum. This gives a global, approximate solution.

If a more precise value is desired, either BF optimization can be repeated but with the new grid cells covering the original grid cells containing the global optimum candidate, or a local optimizer, Edgar et al. (2001), can be applied with the global optimum candidate as the initial guess.[2] Both these alternatives were tested, with approximately the same optimum, but the repeated BF method being considerably easier to implement.

Application to simulated reactor

In eq. (14), $t_1 = 0$ d, and $t_2 = 5$ d. The reactor is initially in steady-state. $F_{meth_{sp}}$ is constant (88 L/d). At $t = 1$ d, $S_{vs_{in}}$ is increased as a step of amplitude 2 g/L. The arrays of K_c and τ_i are equidistant with 100 elements each. By trial-and-error, a proper value of R is found as 0.3. Table 2 shows the resulting optimal PI settings. The stability margins and response-time as calculated from the linear model presented in Appendix A.3. The stability margins have acceptable values. Figure 10 shows a simulation with the optimal PI settings, indicating acceptable stability.

---

[1] Comparing with implementation of the simulator in SIMULINK, the computational time is reduced by a factor of about 100 with for-loops.

[2] One example of a local optimizer is MATLAB's fmincon function.
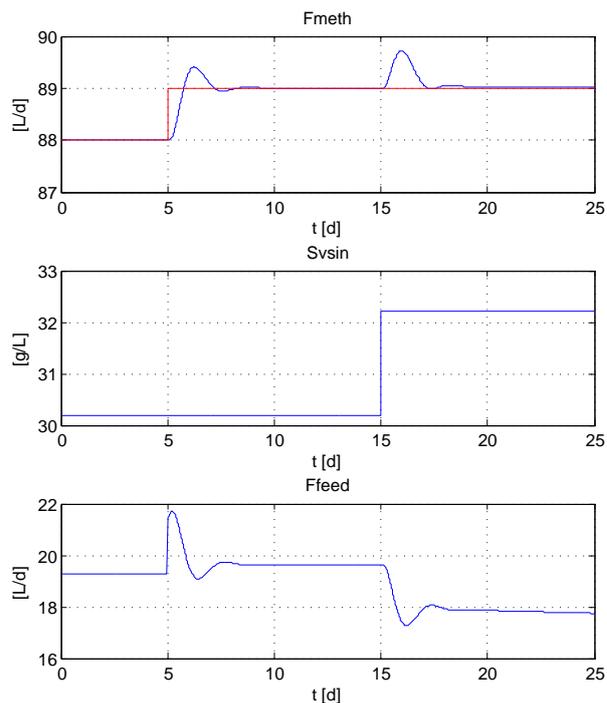
Figure 10: *Simulation of control system with optimal PI settings.*

Comments

- The optimal PI settings do not differ much from those found with the Skogestad method and the R-ZN method.

- Optimal tuning has not been applied to the real reactor. However, the optimal PI settings found from simulations will probably work well on the real reactor since K_c is smaller than K_c found from the Skogestad method applied to the real reactor, and the values of τ_i do not differ much.

- Optimal tuning is a flexible tuning method since it allows for alternative types of models and alternative objective functions.

4.4.5. PI tuning using estimated transfer function

Figure shows real F_{meth} and F_{feed}, and simulated F_{meth} using the real F_{feed}, over time interval of 4 d.

The simulation is based on transfer function $H_p(s)$ estimated from the shown real F_{meth} and F_{feed}. $H_p(s)$ is estimated using the n4sid function in MATLAB with automatic detection of the best model order[3], and using the delayest function to estimate the time-delay

---

[3] Using input argument NX = 'best'.
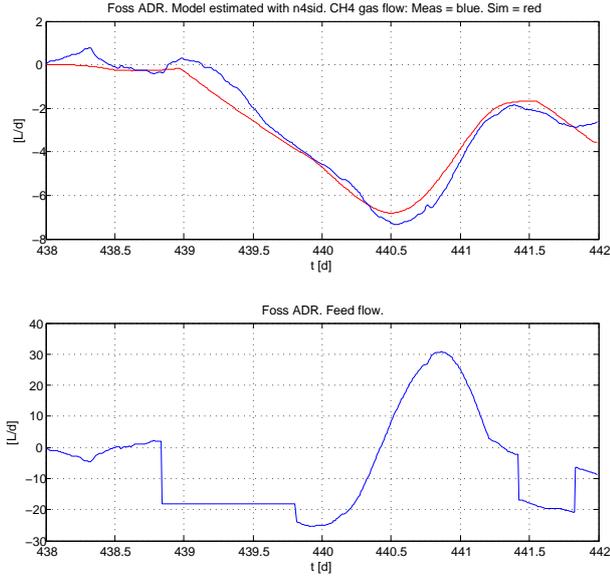
Figure 11: *Real and simulated F_{meth}.*

used in n4sid. The resulting estimate becomes

$$H_p(s) = \frac{1.15}{4.21s + 1} e^{-0.135s} = \frac{K_e}{\tau_e s + 1} e^{-\tau_{d_e} s} \quad (15)$$

Models estimated from other time-series do not differ much from eq. (15). Among the large number of controller tuning methods which can be used for eq. (15), the Skogestad method is selected. Since τ_{d_e} is considerably smaller than τ_e, the Skogestad PI setting for "integrator with time-delay" processes given in Section 4.4.1 with $K_{p_{i_e}} = K_e/\tau_e = 0.27$ [(L CH$_4$/d)/(L/d)]/d can be applied. The resulting PI settings are given in Table 2. The PI control system with eq. (15) as controlled process has stability margins of GM = 2.8 = 8.9 dB and PM = 37.4º, which are within the acceptable ranges ineqs. (5)-(6).

K_c and τ_i found here are, respectively, larger and smaller compared with the values found using the Skogestad method in Section 4.4.1 applied directly to the real reactor, cf. 2. This is due to $\tau_{d_e} = 0.135$ d being smaller than the time-delay of 0.31 d, and to the integral gain $K_{p_{i_e}} = 0.27$ [(L CH$_4$/d)/(L/d)]/d being smaller than $K_{p_i} = 0.33$ [(L CH$_4$/d)/d]/(L/d) found in Section 4.4.1.

4.4.6. Conclusions about PI tuning method

From the results in the above sections, the Skogestad method is favoured among the various tuning methods due to the following benefits. The step response experiment is simple, and the experimental period is short which is an important benefit with slow processes such as bioreactors. Known changes in the (apparent) time-delay can be accounted for in the PI(D) settings without new experiments. The control agility can easily be adjusted via the closed loop time-constant. The method can be applied without any prior mathematical model. Finally, the method has proven, in the present and in other application, to give good tuning results.

The R-ZN PI tuning method also works well, and can be expected to give tuning results similar to the Skogestad method. However, accomplishing the former method may take 3 or more times longer time compared with the Skogestad method. Furthermore, known changes in the (apparent) time-delay are not easily accounted for, without a new tuning.

4.5. Control system robustness against process parameter changes

4.5.1. Introduction

Figure 12 shows the static (steady-state) F_{meth}, here denoted $F_{\mathrm{meth_s}}$, as a function of constant F_{feed} for three different T_{reac} found by simulations with the modified Hill model, Haugen et al. (2013a).
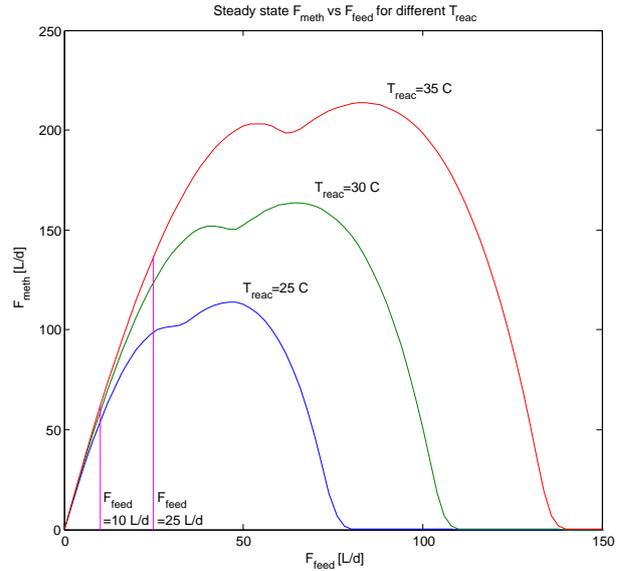
Figure 12: *Steady-state F_{meth} as a function of constant F_{feed} for different T_{reac}.*

The static process gain is defined as

$$K_p = \frac{\partial F_{\mathrm{meth_s}}}{\partial F_{\mathrm{feed}}} \quad (16)$$

K_p is the slope of the curve in Figure 12. Depending on F_{feed}, K_p is positive, zero or negative. In Figure 12 it can be seen that for a given T_{reac}, there is a maximum

achievable $F_{\mathrm{meth_s}}$, which defines the feasible setpoint of F_{meth}.

4.5.2. Dependency on T_{reac}

To illustrate temperature dependency, the operating point value is set to $F_{\mathrm{feed_{op}}} = 5$ L/d, and the response in $\Delta F_{\mathrm{meth}}(t)$, which is the deviation from the operating point due to a step change of F_{feed} of amplitude $\Delta F_{\mathrm{feed}} = 1$ L/d, is simulated for $T_{\mathrm{reac}} = 25$ °C and 35 °C. Figure 13 shows $\Delta F_{\mathrm{meth}}(t)$ simulated with the linearized model presented in Appendix A.2. The simulations indicate that the dynamics of the reactor is faster the larger T_{reac}. To quantify the agility of the dynamics, the 63% response time, resembling the time-constant, is approximately 7.5 d with $T_{\mathrm{reac}} = 25$ °C and approximately 4.1 d with $T_{\mathrm{reac}} = 35$ °C.
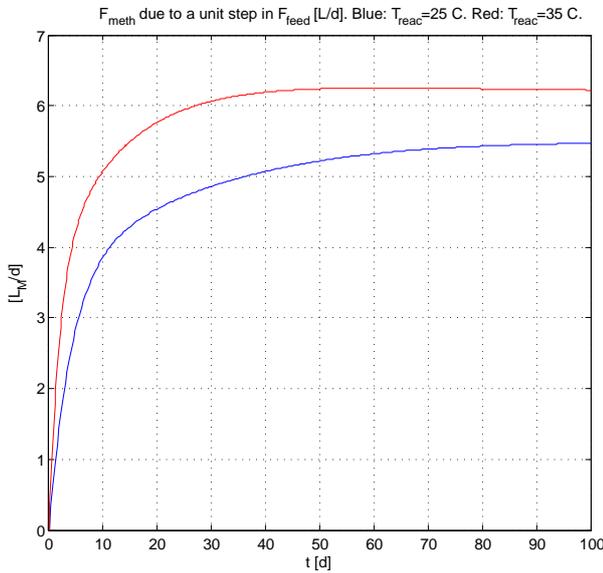
Figure 13: $\Delta F_{\mathrm{meth}}(t)$ *due to a step change of* F_{feed} *of amplitude 1 L/d at* $T_{\mathrm{reac}} = 25$ *°C and* 35 *°C.*

4.5.3. Dependency on F_{feed}

For illustration, T_{reac} is set to 35 °C. Figure 14 shows simulated $\Delta F_{\mathrm{meth}}(t)$ for a number of different values of $F_{\mathrm{feed_{op}}}$ due to a step change of amplitude 1 L/d of F_{feed} from $F_{\mathrm{feed_{op}}}$. The simulations show that the dynamics of $\Delta F_{\mathrm{meth}}(t)$ varies substantially with $F_{\mathrm{feed_{op}}}$.

4.5.4. Detecting critical operating point for controller tuning

Here, focus is on finding the critical operating point with respect to control system stability. PI control is
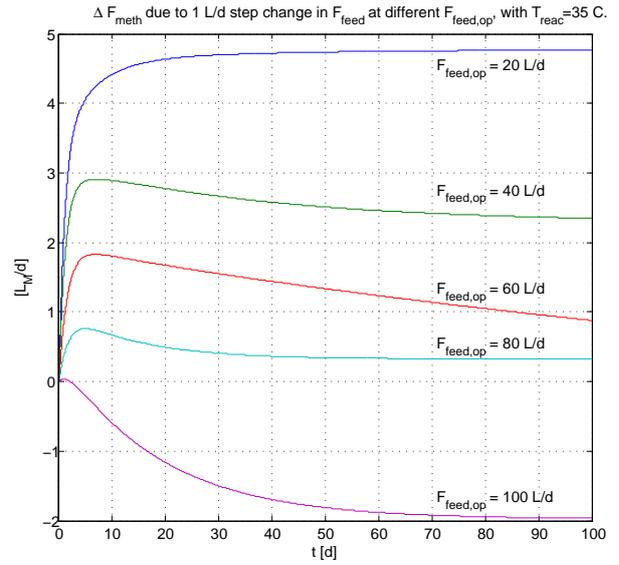
Figure 14: *Simulated* $\Delta F_{\mathrm{meth}}(t)$ *for a number of different values of* $F_{\mathrm{feed_{op}}}$ *due to a step change of amplitude* 1 *L/d of* F_{feed} *from* $F_{\mathrm{feed_{op}}}$. $T_{\mathrm{reac}} = 35$ *°C.*

assumed. Assume that the controller will have fixed settings. If a controller is tuned at the critical operating point, the control system will remain stable in any other operating point. On the other hand, if the controller is tuned at a non-critical operating point, the control system may become unstable at other operating points.

Some alternatives to using fixed controller settings to handle varying process dynamics are:

- Continuous adaptive tuning based on continuous estimation of a transfer function model, Åstrøm and Wittenmark (1994).

- Gain scheduling – experimental with table-lookup, or model-based, Seborg et al. (2004).

Implementation of experimental Gain scheduling is straightforward. T_{reac} and F_{feed} may be used as input variables to the table, and the PI settings are the output variables. Each of the PI settings can be found experimentally using e.g. the Skogestad method. However, implementation of the above mentioned alternatives are not designed nor analyzed here.

For the analysis of the control system stability the transfer function model of the methane flow control system presented in Appendix A.3 is used. The analysis is accomplished as follows: A PI controller is tuned using the R-ZN method (with tuning parameter $k_r = 1$) at one specific operating point which is

here denoted the basic operating point: ($F_{\text{feed}} = 10$ L/d, $T_{\text{reac}} = 25$ °C). In this tuning method the ultimate gain, K_{c_u}, and the ultimate period, P_u, are needed to calculate PI settings K_c and τ_i. In the tuning, $K_{c_u} = 1$ and $\tau_i = \infty$ initially. Then, $K_{c_u} = \text{GM}$ and $P_u = 2\pi/\omega_{180}$ where ω_{180} [rad/d] is the gain margin crossover frequency. The PI settings are used at different operating points, and the stability margins, namely the gain margin, GM, and the phase margin, PM, are calculated from the transfer function model.

From the results, a conclusion is made in the following about what is the critical operating point for controller tuning, and an attempt is made to explain the results using the (nonlinear) mathematical reactor model.

Table 3 summarizes the results. The fixed PI settings found at the basic operating point are $K_c = 1.29$ (L CH$_4$/d)/(L/d), and $\tau_i = 0.91$ d. The upper left cell of Table 3 represents the basic operating point.

Table 3: Stability margins of the methane control system at various operating points. The upper left cell is the basic operating point.

T_{reac} [°C]	$F_{\text{feed}} = 10$ [L/d]	$F_{\text{feed}} = 25$ [L/d]
25	**GM** = **5.3** **PM** = **38.8**°	GM = 7.6 PM = 42.3°
30	GM = 3.3 PM = 35.5°	GM = 3.5 PM = 39.0°
35	GM = 2.4 PM = 30.0°	GM = 2.3 PM = 30.8°

In Table 3 the following observations are made:

1. The stability margins decrease with increasing T_{reac}.

2. Except at $T_{\text{reac}} = 35$ °C, where the stability margins are almost independent of F_{feed}, the stability margins decrease with decreasing F_{feed}.

From these observations, the following general guideline is proposed, at least for T_{reac} less than 35 °C: The critical operating point regarding controller tuning is maximum T_{reac} and minimum F_{feed}. A PI controller with fixed tuning should be tuned in this operating point. (At $T_{\text{reac}} = 35$ °C, the controller tuning seems to become independent of F_{feed}.)

Below is an attempt to explain the above two observations using the mathematical reactor model.

1. Regarding observation 1: Figure 12 shows the steady-state F_{meth} as a function of constant F_{feed} for different T_{reac}. The static process gain is defined with eq. (16). At least for $F_{\text{feed}} = 10$ L/d

and 25 L/d which are assumed above, K_p increases with T_{reac}, and hence, a reduction of control system stability margins can be expected.

An alternative explanation may be found directly from the modified Hill model: From model eqs. (25), (27), (28) in Haugen et al. (2013a), it is seen that F_{meth} becomes more sensitive to S_{vfa} as the temperature increases, hence the process gain increases. This increased sensitivity may explain the reduced stability (margins) as T_{reac} is increased.

2. Regarding observation 2: From Figure 12, K_p becomes larger, and hence the control system stability margins are reduced, if F_{feed} is reduced.

5. Discussion

Ideally, all the questions stated in the Introduction should be addressed with practical experiments. However, this was not possible of practical reasons, so some questions are addressed using simulations only. Since the modified Hill model has shown to represent the pilot AD reactor well, Haugen et al. (2013a), it is assumed that the results obtained from simulations hold qualitatively, and to some extent, quantitatively.

Both on-off control and PI control are found being successful for controlling the methane gas flow, on a simulated reactor as well as on the practical reactor. For PI controller tuning, the Skogestad method, which is an open loop tuning method, is identified as the favoured tuning method. Also the R-ZN method, which is a closed loop method based on relay oscillations, works well. It is believed that the identification of these tuning methods can reduce time and efforts in controller tuning for AD processes.

Dairy waste as AD feedstock has large buffering capacity, and its composition is relatively constant. If the feedstock is more complex, as with poultry and swine waste and food waste, a richer mathematical model able to predict other AD variables than those of the Hill model, e.g. pH, alkalinity, partical alkalinity (PA), pH, ammonia, and carbon dioxide may be useful. Two model candidates are the AM2 model by Bernard et al. (2001a) and the ADM1 model, Batstone et al. (2002). Overviews over AD models are given in e.g. Gavala et al. (2003) and Strömberg (2010).

6. Conclusions

Using a mathematical model of the AD reactor and the specific upper limit of the concentration of volatile fatty acids, known from the literature, safe operating conditions for the reactor can be found. These conditions imply an upper limit of the feed rate, and an

upper limit of the gas flow setpoint. This limits are theoretical, and should be adjusted on a practical reactor to avoid non-zero steady state control error.

For the present pilot reactor, both simulatons and practical experiments indicate that on-off control is a viable feedback controller if the oscillation in the feed rate and biogas flow can be tolerated. If smooth control is important, PI control is appropriate. The Skogestad method is favoured as a PI controller tuning method since it is easy to apply and gives good tuning results with the present reactor. Also, the R-ZN closed loop tuning method works well, but the time needed to accomplish the tuning is longer than with the Skogestad method.

Simulations indicate that it is safe for control loop stability to tune a PI controller with fixed parameters at low feed flow.

Acknowledgements

A. Mathematical models

A.1. The modified Hill model

In this paper, simulations are based on the modified Hill model adapted to the pilot AD reactor. The model is derived in Haugen et al. (2013a).

A.2. Linearized model

For linear analysis and design, e.g. frequency response based method, a local linear version of the modified Hill model is used. The model has the standard form:

$$\Delta\dot{x} = A\Delta x + B\Delta F_{\text{feed}} \qquad (17)$$

$$\Delta F_{\text{meth}} = C\Delta x + D\Delta F_{\text{feed}} \qquad (18)$$

where x is the state vector:

$$x = [S_{\text{bvs}}, S_{\text{vfa}}, X_{\text{acid}}, X_{\text{meth}}]^T = [x_1, x_2, x_3, x_4]^T \quad (19)$$

The symbol Δ represents "deviation from operating point", i.e. $\Delta x = x - x_{\text{op}}$, $\Delta F_{\text{feed}} = F_{\text{feed}} - F_{\text{feed}_{\text{op}}}$, and $\Delta F_{\text{meth}} = F_{\text{meth}} - F_{meth_{\text{op}}}$.

In eqs. (17)-(18), A, B, C, and D are Jacobian matrices. Their elements are presented in Haugen et al. (2013c).

A.3. Transfer function model

The transfer function from from ΔF_{feed} to ΔF_{meth} can be calculated from the linear state space model, eqs. (17) and (18), with

$$\frac{\Delta F_{\text{meth}}(s)}{\Delta F_{\text{feed}}(s)} \equiv H_{\text{AD}}(s) = C\left(sI - A\right)^{-1}B + D \quad (20)$$

where matrices A, B, C, and D are given in Section A.2.

In eq. (20), ΔF_{meth} represents the (deviation of) the "raw" CH$_4$ gas flow. In practice, the CH$_4$ gas flow is known from the multiplication of the biogas flow online measurement and the CH$_4$ concentration online measurement. These measurements are smoothed with lowpass filters with the following respective time-constants:

- Time-constant of main biogas flow measurement filter:

$$\tau_{f_1} = 0.2 \text{ d} \qquad (21)$$

- Time-constant of additional biogas flow measurement filter:

$$\tau_{\text{f}_2} = 1400 \text{ min} = 0.0162 \text{ d} \qquad (22)$$

- Time-constant of CH$_4$ concentration measurement filter:

$$\tau_{\text{f}_3} = 1 \text{ h} = 0.0417 \text{ d} \qquad (23)$$

Furthermore, it is observed that there is a time delay in the observed measured responses in the CH$_4$ gas flow which is approximately

$$\tau_d = 0.05 \text{ d} \qquad (24)$$

Taking the above mentioned dynamic elements into account, the following transfer function from the feed flow to the methane gas flow measurement is obtained:

$$\frac{\Delta F_{\text{meth}_{\text{m}}}(s)}{\Delta F_{\text{feed}}(s)} = H_{\text{AD}_{\text{m}}}(s) = H_{\text{AD}}H_{\text{d}}H_{\text{f}_1}H_{\text{f}_2}H_{\text{f}_3} \quad (25)$$

where, for $i = 1, 2$, and 3,

$$H_{\text{d}}(s) = e^{-s\tau_d} \qquad (26)$$

$$H_{\text{f}_i}(s) = \frac{1}{\frac{s}{\tau_{\text{f}_i}} + 1} \qquad (27)$$

Figure 15 illustrates the composition of the resulting transfer function, $H_{\text{AD}_{\text{m}}}(s)$, eq. (25).
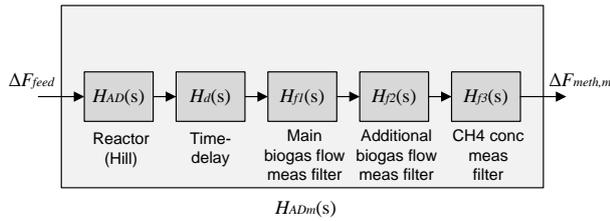
Figure 15: *The composition of the transfer function $H_{AD_m}(s)$, eq. (25).*

B. Abbreviations and nomenclature

B.1. Abbreviations

AD: Anaerobic digestion

BF: Brute force (optimization method)

BVS: Biodegradable volatile solids

COD: Chemical Oxygen Demand

FC: Flow controller

FT: Flow transmitter (sensor)

HRT: Hydraulic retention time

IAE: Integral of absolute value of control error

NTP: Normal Temperature and Pressure: 0 °C, 1 atm

MPC: Model-based predictive control

NLS: Nonlinear least squares

NOC: Normal operating conditions

OP: Operating point

P/A: Proprionic to acetic acid ratio

PID: Proportional-integral-derivate

PWM: Pulse-width modulation

R-ZN: Relaxed Ziegler-Nichols, Haugen and Lie (2013)

TL: Tyreus and Luyben, Tyreus and Luyben (1992)

UASB: Upflow anaerboic sludge blanket

VFA: Volatile fatty acids

VS: Volatile solids

ZN: Ziegler-Nichols, Ziegler and Nichols (1942)

B.2. Nomenclature

In the paper, but not shown in the list below, subindex "s" is used to represent "steady-state" or "static".

The list below contains only symbols which are used in this paper. A complete list of symbols for the modified Hill model is in Haugen et al. (2013a).

A_e: Amplitude of the control error and the process output.

A_u: Amplitude of the on-off control signal.

c: Factor used to define lower limits of biodegraders X_{acid} and X_{meth}.

f_{obj}: Objective function.

F_{feed} [L/d]: Influent or feed flow or load rate, assumed equal to effluent flow (constant volume).

F_{meth} [L CH$_4$/d]: Methane gas flow.

GM: Gain margin.

k_r: Parameter of the Relaxed Ziegler-Nichols tuning method.

K_p [(L CH$_4$/d)/(L/d)] $= \partial F_{\text{meth}_s}/\partial F_{\text{feed}}$: Static process gain.

ω_c [rad/d]: Amplitude crossover frequency, which may be defined as the control system bandwidth.

P_u [d] Period of oscillation.

PM [degrees]: Phase margin.

S_{vfa} [g VFA/L]: Concentration of VFA acids in reactor.

$S_{\text{vfa}_{\text{in}}}$ [g VFA/L]: Concentration of VFA in biodegradable part of influent.

S_{bvs} [g BVS/L]: Concentration of BVS in reactor.

$S_{\text{bvs}_{\text{in}}}$ [g BVS/L]: Concentration of BVS in influent.

$S_{\text{vs}_{\text{in}}}$ [g VS/L]: Concentration of volatile solids in influent.

T_{reac} [°C]: Reactor temperature.

τ_i [d]: Controller integral time.

τ_d [d]: Controller derivative time.

V [L]: Effective reactor volume.

X_{acid} [g acidogens/L]: Concentration of acidogens.

X_{meth} [g methanogens/L]: Concentration of methanogens.

References

Angelidaki, I., Ellegaard, L., and Ahring, B. K. A mathematical model for dynamic simulation of anaerobic digestion of complex substrates: Focusing on ammonia inhibition. *Biotechnology and Bioengineering*, 1993. 42:159–166.

Åstrøm, K. J. and Hägglund, T. *PID Controllers: Theory, Design and Tuning*. ISA, 1995.

Åstrøm, K. J. and Wittenmark, B. *Adaptive Control*. Prentice Hall, 1994.

Batstone, D. J., Keller, J., Angelidaki, I., Kalyuzhnyi, S. V., Pavlovstahis, S. G., Rozzi, A., Sanders, W. T. M., Siegrist, H., and Vavilin, V. A. *Anaerobic Digestion Model No. 1, Scientific and Technical Report 15*. IWA Publising, 2002.

Bernard, O., Hadj-Sadok, Z., Dochain, D., Genovesi, A., and Steyer, J. Dynamical model development and parameter identification for an anaerobic wastewater treatment process. *Biotechnology and Bioengineering*, 2001a. 75(4). doi:10.1002/bit.10036.

Bernard, O., Polit, M., Hadj-Sadok, Z., Pengov, M., Dochain, D., Estaben, M., and Labat, P. Advanced monitoring and control of anaerobic wastewater treatment plants: software sensors and controller for an anaerobic digester. *Water Science and Technology*, 2001b. 43(7).

Deublein, D. and Steinhauser, A. *Biogas from Waste and Renewable Resources*. Wiley, 2010.

Dochain, D. *Bioprocess Control*. Wiley, 2008.

Edgar, T. F., Himmelblau, D., and Lasdon, L. *Optimization of Chemical Processes*. McGraw-Hill, 2001.

Gavala, H. N., Angelidaki, I., and Ahring, B. K. Kinetics and Modeling of Anaerobic Digestion Process. *Advances in Biochemical Engineering/Biotechnology, Springer-Verlag*, 2003. 81.

Haugen, F., Bakke, R., and Lie, B. Adapting dynamic mathematical models to a pilot anaerobic digestion reactor. *Modeling, Identification and Control*, 2013a. 34(2):35–54. doi:10.4173/mic.2013.2.1.

Haugen, F., Bakke, R., and Lie, B. Temperature control of a pilot anaerobic digestion reactor. *Modeling, Identification and Control*, 2013b. 34(3). doi:10.4173/mic.2013.3.1.

Haugen, F., Bakke, R., Vasdal, K., and Bergland, W. Foss Biolab. http://fossbiolab.no, 2013c.

Haugen, F. and Lie, B. Relaxed Ziegler-Nichols Closed Loop Tuning of PI Controllers. *Modeling, Identification and Control*, 2013. 34(2):83–97. doi:10.4173/mic.2013.2.4.

Hill, D. T. Simplified monod kinetics of methane fermentation of animal wastes. *Agric. Wastes*, 1983. 5. doi:10.1016/0141-4607(83)90009-4.

Hill, D. T., Cobb, S. A., and Bolte, J. P. Using volatile fatty acid relationships to predict anaerobic digester failure. *Trans. ASAE*, 1987. 30:496–501.

Husain, A. Mathematical models of the kinetics of anaerobic digestion - a selected review. *Biomass and Bioenergy*, 1998. 14(5/6):561–571.

Johnson, C. D. *Process Control Instrumentation Control Technology*. Prentice-Hall, 2000.

Liu, J., Olsson, G., and Mattiasson, B. Extremum-seeking with variable gain control for intensifying biogas production in anaerobic fermentation. *Water Science and Technology*, 2006. 53(4-5):35–44.

Méndez-Acosta, H. O., Campos-Delgado, D. U., Femat, R., and González-Álvarez, V. A robust feedforward/feedback control for an anaerobic digester. *Computers and Chemical Engineering*, 2005. 29:1613–1623.

Méndez-Acosta, H. O., Palacios-Ruiz, B., Alcaraz-González, V., González-Álvarez, V., and García-Sandoval, J. P. A robust control scheme to improve the stability of anaerobic digestion processes. *Journal of Process Control*, 2010. 20:375–383.

Puñal, A., Palazzotto, L., Bouvier, J. C., Conte, T., and Steyer, J. P. Automatic control of volatile fatty acids in anaerobic digestion using a fuzzy logic based approach. *Water Science and Technology*, 2003. 48(6).

Rodriguez, L., Ruiz, G., Molina, F., Roca, E., and Lema, J. M. A hydrogen-based variable-gain controller for anaerobic digestion processes. *Water Science and Technology*, 2006. 54(2):57–62.

Seborg, D. E., Edgar, T. F., and Mellichamp, D. A. *Process Dynamics and Control*. John Wiley and Sons, 2004.

Simon, D. *Optimal State Estimation*. Wiley, 2006.

Skogestad, S. Simple analytic rules for model reduction and PID controller tuning. *Modeling, Identification and Control*, 2004. 25(2):85–120. doi:10.4173/mic.2004.2.2.

Steyer, J. P., Buffire, P., Rolland, D., and Moletta, R. Advanced control of anaerobic digestion processes through disturbance monitoring. *Water, Science and Technology*, 1999. 33(9):2059–2068.

Strömberg, S. *Development and Evaluation of Numerical Models for Anaerobic Digestion*. M.Sc. thesis. Lund Univ., Sweden, 2010.

Strömberg, S., Possfelt, M. O., and Liu, J. Computer simulation of control strategies for optimal anaerobic digestion. *Water Science and Technology*, 2013. 67(3).

Tchobanoglous, G., Burton, F. G., and Stensel, H. D. *Wastewater Engineering: Treatment and Reuse.* Metcalf and Eddy, McGraw Hill, 2003.

Tyreus, B. D. and Luyben, W. L. Tuning PI Controllers for Integrator/Dead Time Processes. *Ind. Eng. Chem*, 1992. 31(31).

Ziegler, J. and Nichols, N. Optimum settings for automatic controllers. *Trans. ASME*, 1942. 64(3):759–768. doi:10.1115/1.2899060.

Article 4 – State Estimation and Model-based Control of a Pilot Anaerobic Digestion Reactor

Authors: Finn Haugen, Rune Bakke and Bernt Lie.

Authors' roles in the article: Finn Haugen: Main ideas, implementation, and writing. Rune Bakke (co-supervisor) and Bernt Lie (supervisor): Discussions, comments, and proof readings.

Background and methods of the article

Background

A state estimator, also denoted soft sensor, can be useful for monitoring purposes. With the present reactor and the modified Hill model, a continuous measurement of the methane gas flow, the reactor temperature, and the known feed flow, are used to continuously estimate the values of the state variables of the reactor, which in the present research project are the concentrations of biodegradable volatile solids, volatile fatty acids, acidogens, and methanogens, plus the assumed unknown concentration of volatile solids of the influent. Among these states, the concentration of volatile fatty acids is of particular interest since, according to Hill & Barth (1977), a concentration above 0.8 g/L indicates a pending reactor failure.

In most practical applications, an online sensor for this concentration is not available, so an estimator can be an attractive alternative.

A state estimator may also be useful in advanced, model-based control, as in the present article where a predictive controller is used to retain the reactor at a specified operating point defining for example safe reactor operation, and to track a time-varying methane gas flow setpoint. In the predictive controller, the state estimates are used in the controller for prediction of the future process output. This prediction is the basis of the calculation of the optimal control sequence.

Methods

For the state estimator and the model-based controllers presented in this article, the modified Hill AD model presented in Article no. 1, is used. As an AD process model this model is relatively simple, yet it is sufficiently comprehensive for the aforementioned purposes.

As state estimator, the Unscented Kalman Filter (UKF), Julier & Uhlmann (1997) is used. The UKF algorithm implemented is the same as presented in Simon (2006). An alternative is the well-known Extended Kalman Filter (EKF), but the UKF is selected to avoid the linearization needed in the EKF. Simulations based on the modified Hill model have shown that the UKF and the EKF have almost the same performance.

The model-based controllers used in different control problems, include a PI controller based on feedback from the concentration of volatile fatty acids as estimated with the UKF, and a predictive controller for retaining the methane gas flow at its setpoint.

As predictive controller, a relatively simple, straightforward, implementation is made, using the function fmincon() in Optimization Toolbox in MATLAB to calculate the optimal future control sequence that minimizes the optimization objective of the controller. fmincon() uses simulations of the nonlinear model in its search for the optimal control sequence. Although alternative model-based controller functions exist, e.g. the linear quadratic controller and the pole placement controller – both based on state feedback, we see no reason to select any of these instead of the nonlinear predictive controller.

The predictive controller algorithm has been tested on a simulated laboratory-scale air heater where the air temperature is to be controlled, Haugen (2013), then on the real air heater. The algorithm was then tested

on a simulated AD reactor using the modified Hill model. As expected, some errors were observed, but eventually the test were completed successfully. Finally, the algorithm was applied successfully to the real reactor. This approach to testing, i.e. starting with a simple simulated application, then the simple real application, and finally a simulated full application, has turned out to be very effective. This approach of testing is depicted using general terms in Figure 12.
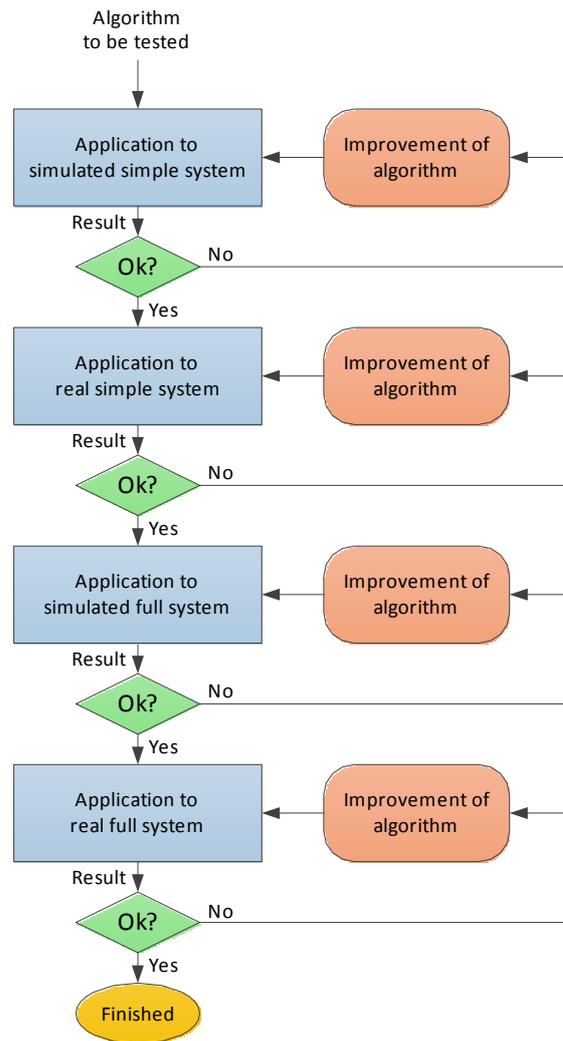
Figure 12: The applied procedure of algorithm testing.

To analyze the control systems in simulation applications, both performance and stability robustness measures are calculated. As performance measures, the IAE index (Integral of Absolute value of control

Error) is calculated for setpoint changes and for disturbance changes. As stability robustness measures, the gain margin (GM) and the phase margin (PM) are calculated from experimental simulations with the nonlinear model by introducing a gain, ΔK, and a time delay, $\Delta\tau$, in the control loop. Initially, $\Delta K = 1$ and $\Delta\tau = 0$. From the gain increase, ΔK_u, and the time delay increase, $\Delta\tau_u$, that (may) bring the control system to the stability limit, i.e. showing sustained oscillations, GM and PM are calculated, as follows:

$$\mathrm{GM} = \Delta K_u \tag{3}$$

$$\mathrm{PM} = \frac{\Delta\tau}{P_u} \cdot 360^{\mathrm{o}} \tag{4}$$

where P_u is the period of the sustained oscillations, Haugen (2012), Appendix A. These GM and PM are equivalent to the GM and PM known from stability analysis of linear feedback systems.

Supplementary material: Implementation of the predictive controller in MATLAB

There are predictive controller algorithms for linear models, Maciejowski (2002), Haber et al. (2011), and for nonlinear models, Grüne & Pannek (2011). Since the modified Hill model is nonlinear, it was decided to try a predictive algorithm for this nonlinear model, and not for the corresponding linear model which can represent the original model only about a given operating point. Furthermore, the implementation will probably be simpler if the linearization can be avoided.

The function fmincon() in MATLAB's Optimization toolbox is used to calculate the optimal future control sequence. fmincon() is a local nonlinear optimizer which can automatically select the most proper optimization algorithm. In general terms, fmincon() calculates the optimal value of objective variables which minimizes the given objective function. In this application, each of the objective variables is each of the elements in the future control signal sequence, $\{u_{\mathrm{opt}}(k)\}$. Since the time step for the predictive controller is 0.025 d and the prediction horizon is 1 d, the number of elements in $\{u_{\mathrm{opt}}(k)\}$ is $1/0.025 = 40$, i.e. the number of optimization variables. The objective function of the predictive controller to be minimized is

$$f_{\mathrm{obj}} = \int_t^{t+\tau_{\mathrm{h}}} \left[e^2\left(\theta\right) + C_{\mathrm{du}}\dot{u}^2\left(\theta\right) \right] d\theta + C_{\mathrm{h}}e^2\left(\tau_{\mathrm{h}}\right) \tag{5}$$

The constraint on u is: $u_{\min} \leq u(t) \leq u_{\max}$. e is the control error. C_{du} and C_{h} are cost (or weight) coefficients. t is the present time. τ_{h} is the prediction horizon.

In Article 4, predictive control is used both for control of F_{meth} and for control of S_{vfa}. Below, the implementation of predictive control of F_{meth} of the simulated reactor is presented in detail, but the implementation of predictive control of S_{vfa} is similar. The algorithm is presented in the MATLAB code excerpt below, however, straightforward details are omitted to save space. The implementation for the real reactor, cf. Article 4, is similar.

Figure 13 shows the function connections in the script implementing nonlinear predictive control of the AD reactor. The reactor is represented with the modified Hill model. The function fmincon() calculates the optimal control sequence (array).
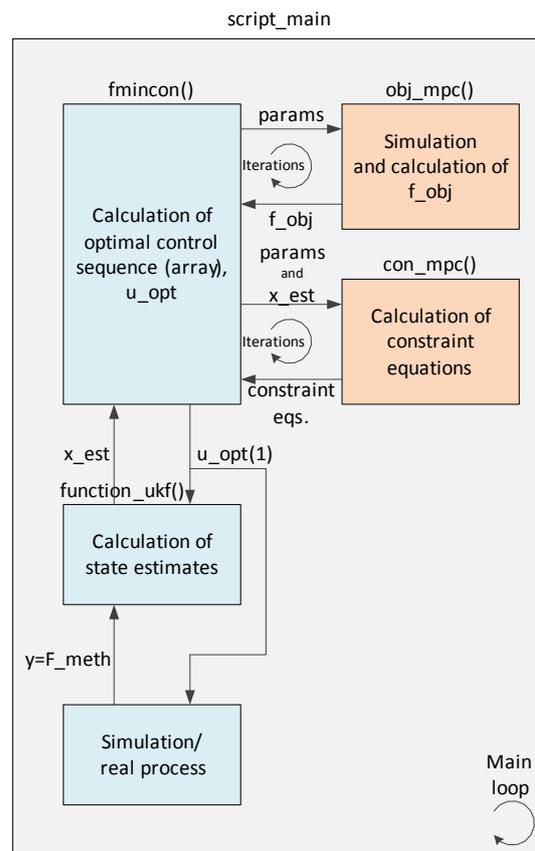
Figure 13: Illustration of the function connections of the program implementing predictive control.

In the code excerpt presented below, the possibility of using different model parameters in the MPC/UKF and the simulator to study the effect of model parameters errors, is implemented. The complete MATLAB script, including the functions involved, is available at Haugen et al. (2013).[6]

The following functions used in the code excerpt below are described after the excerpt:

- fmincon()

- objfun_mpc() (which is invoked by fmincon)

- confun_mpc() (which is invoked by fmincon)

- function_ukf()

```
%Hill params used in MPC and UKF:
b = 2.9;
K_s = 15.5;
...
p_mpc_ukf=[b,K_s,...];

%Hill params representing "real" process,
%which may be set different from p_mpc_ukf:
b_real = 2.9;
K_s_real = 15.5;
...
p_real=[b_real,K_s_real,...];
%-------------------------------------------------
T_reac=35;
std_F_meth_noise=1.2*0;
%-----------------------------------------------
%Time params:
Ts=0.025; %Time-step
t_pred_horizon=1;
Np=t_pred_horizon/Ts;
t_start=0;
t_stop=16;
Nsim=(t_stop-t_start)/Ts;
t=[t_start:Ts:t_stop-Ts]';
%-------------------------------------------------
%Init states:
```

---

[6]The script also contains PI control of F_{meth} for easy comparison with predictive control.

```
S_bvs_init= 3.417;
S_vfa_init= 0.661;
X_acid_init = 2.029;
X_meth_init = 0.387;

F_meth_init = 150;
S_vs_in_init=30.2;
%-------------------------------------------------
%Initial guessed optimal control sequence (u=F_feed):
u_guess=0*zeros(Np,1)+28.19;
%-------------------------------------------------
%State-space model implementing time-delay in "real" process:
Timedelay_real_process=0.2;
nd_real_process=ceil(Timedelay_real_process/Ts);
Ad_real_process=diag([ones(nd_real_process-1,1)],-1);
Bd_real_process=[nd_real_process>=1;zeros(nd_real_process-1,1)];
Cd_real_process=[zeros(1,nd_real_process-1),nd_real_process>=1];
Dd_real_process=[nd_real_process==0];
x_delay_real_process_k=zeros(length(Ad_real_process),1)+u_const;


%State-space model implementing time-delay in MPC:
Timedelay_mpc=0.2;
nd_mpc=ceil(Timedelay_mpc/Ts);
Ad_mpc=diag([ones(nd_mpc-1,1)],-1);
%...Similar to above (details not shown here).
%---------------------------------------------------
%Creating future setpoint profile, assumed known for MPC:
F_meth_sp=...  (details not shown here)
%---------------------------------------------------
%Creating S_vs_in profile for simulation
%(S_vs is still assumed unknown for UKF and MPC):
S_vs_in=...  (details not shown here)
%-------------------------------------------------

%%%%%%%%%%%%%%%%%%%%%%

% MPC with UKF

%%%%%%%%%%%%%%%%%%%%%%%%

%Tuning of UKF:
%Giving values to x_init, x_apost_k_minus_1, Q, R
(Details omitted here.)
%-----------------------------------------
```

```
%Preallocation of arrays:
S_bvs=zeros(Nsim-Np,1)+S_bvs_init;
...  (similar details omitted here)
%-------------------------------------------
%Matrices defining linear constraints for use in fmincon:
A=[];B=[];Aeq=[];Beq=[];
%-------------------------------------------
%Lower and upper limits of optim variable for use in fmincon:
lb=u_guess*0;
ub=u_guess*0+40;
%-------------------------------------------
%MPC costs:
c_e=1;
c_u=0;
c_du=0.01;
c_final=0;
costs=[c_e c_u c_du c_final];
%-------------------------------------------

%For-loop for calculating optimal control sequence applied to
simulated process:

for k=1:Nsim-Np

%Updating future setpoint profile as time elapses:
F_meth_sp_to_optim=F_meth_sp(k:k+Np);
%Time-shift of state:
x_mpc_init=x_apost_k_minus_1;

 %Defining fun handle for fmincon:
fun_handle=@(u) objfun_mpc(Ad_mpc,Bd_mpc,Cd_mpc,...
Dd_mpc,u,T_reac,F_meth_sp_to_optim,p,costs,x_mpc_init,Np,Ts);

 %Using fmincon for Calculating optimal future control
sequence:
optim_options=optimset('Algorithm','active-set','LargeScale','on',...
'MaxIter',10000,'MaxFunEvals',1000*length(u_guess),'Display','off');
[u_opt,fval,exitflag,output,lambda,grad,hessian] =...
fmincon(fun_handle,u_guess,A,B,Aeq,Beq,lb,ub,...
@confun_mpc,optim_options);
%Using optimal control sequence as guessed optim solution
%in next iteration:
u_guess=u_opt;
%Applied controller output set as first sample
```

```
%of optimal control sequence:
u(k)=u_opt(1);

%----------------------------------------------------
%Applying optimal control signal to simulated "real" process:
mu_m=0.013*T_reac-0.129;
mu_mc=mu_m;
mu=mu_m/(K_s_real/S_bvs(k)+1+0*S_vfa(k)/K_i_real);
mu_c=mu_mc/(K_sc_real/S_vfa(k)+1+0*S_vfa(k)/K_ic_real);
in_delay_real_process_k=u(k);
x_delay_real_process_k_plus_1=Ad_real_process*...
x_delay_real_process_k+Bd_real_process*in_delay_real_process_k;
out_delay_real_process_k=Cd_real_process*x_delay_real_process_k+...
Dd_real_process*in_delay_real_process_k;
F_feed(k)=out_delay_real_process_k;


 %Time-derivatives of state variables:
dS_bvs_dt=(B0_real*S_vs_in(k)-S_bvs(k))*...
F_feed(k)/V_real-mu*k1_real*X_acid(k);
dS_vfa_dt=(Af_real*B0_real*S_vs_in(k)-S_vfa(k))*F_feed(k)/V_real+...
mu*k2_real*X_acid(k)-mu_c*k3_real*X_meth(k);
dX_acid_dt=(mu-K_d_real-(F_feed(k)/b_real)/V_real)*X_acid(k);
dX_meth_dt=(mu_c-K_dc_real-(F_feed(k)/b_real)/V_real)*X_meth(k);


 %Euler forward step:
S_bvs(k+1)=S_bvs(k)+Ts*dS_bvs_dt;
...  (similar details omitted here)
F_meth(k)=V*k5_real*mu_c*X_meth(k);
x_delay_real_process_k=x_delay_real_process_k_plus_1;
%----------------------------------------------------
%UKF:
y_k=F_meth(k)+std_F_meth_noise*randn;
F_feed_k=F_feed(k);
[P_apost_k,x_apost_k,y_pred_k,K_k]=...
function_ukf(y_k,P_apost_k_minus_1,x_apost_k_minus_1,Ts,...
F_feed_k,p,T_reac,Q,R);
F_meth_est(k)=y_pred_k;
%----------------------------------------------------
%Time shift:
x_apost_k_minus_1=x_apost_k;
P_apost_k_minus_1=P_apost_k;
S_bvs_est(k)=x_apost_k(1);
```

```
...  (similar details omitted here)
```

```
end %for loop
```

Functions used in the code excerpt above are described in the following.

fmincon()

The function fmincon() in MATLAB's Optimization toolbox is used to calculate the optimal future control sequence. fmincon() is a local nonlinear optimizer which can automatically select the most proper optimization algorithm. In general terms, fmincon() calculates the optimal value of objective variables which minimizes the given objective function. In this application, each of the objective variables is each of the elements in the future control signal sequence, $\{u_{\mathrm{opt}}(k)\}$. Since the time step for the predictive controller is 0.025 d and the prediction horizon is 1 d, the number of elements in $\{u_{\mathrm{opt}}(k)\}$ is $1/0.025 = 40$, i.e. the number of optimization variables. The objective function of the predictive controller to be minimized is

$$f_{\mathrm{obj}} = \int_{t}^{t+\tau_{\mathrm{h}}} \left[e^2\left(\theta\right) + C_{\mathrm{du}}\dot{u}^2\left(\theta\right)\right] d\theta + C_{\mathrm{h}}e^2\left(\tau_{\mathrm{h}}\right) \qquad (6)$$

The constraint on u is: $u_{\min} \le u(t) \le u_{\max}$. e is the control error. C_{du} and C_{h} are cost (or weight) coefficients. t is the present time. τ_{h} is the prediction horizon.

objfun_mpc()

fmincon() invokes objfun_mpc() which calculates f_{obj}, eq. (6), to be minimized by fmincon(). A portion of objfun_mpc() is shown below.

```
function f =
objfun_mpc_kf_pi_delay(Ad_mpc,Bd_mpc,Cd_mpc,Dd_mpc,...
u,T_reac,F_meth_sp,p,costs,x_mpc_init,Np,Ts)
%Params:
b=p(1);
K_s=p(2);
%...(similar details omitted here).

%Costs:
c_e=costs(1);c_u=costs(2);c_du=costs(3);c_final=costs(4);
```

```
%Preallocation and initialization:
S_bvs=zeros(1,Np)+x_mpc_init(1);
%...(similar details omitted here).
x_delay_mpc_k=zeros(length(Ad_mpc),1)+u(1);
F_meth=zeros(1,Np);
e=zeros(1,Np);
J1=zeros(1,Np);
u_k_minus_1=u(1);

for k=1:Np
mu_m=0.013*T_reac-0.129;
mu_mc=mu_m;
mu=mu_m/(K_s/S_bvs(k)+1+0*S_vfa(k)/K_i);
mu_c=mu_mc/(K_sc/S_vfa(k)+1+0*S_vfa(k)/K_ic);
input_delay_mpc_k=u(k);

x_delay_mpc_k_plus_1=Ad_mpc*x_delay_mpc_k+Bd_mpc*input_delay_mpc_k;
output_delay_mpc_k=Cd_mpc*x_delay_mpc_k+Dd_mpc*input_delay_mpc_k;
F_feed(k)=output_delay_mpc_k;

dS_bvs_dt=(B0*S_vs_in(k)-S_bvs(k))*F_feed(k)/V-mu*k1*X_acid(k);
dS_vfa_dt=(Af*B0*S_vs_in(k)-S_vfa(k))*F_feed(k)/V+...
mu*k2*X_acid(k)-mu_c*k3*X_meth(k);
dX_acid_dt=(mu-K_d-(F_feed(k)/b)/V)*X_acid(k);
dX_meth_dt=(mu_c-K_dc-(F_feed(k)/b)/V)*X_meth(k);

S_bvs(k+1)=S_bvs(k)+Ts*dS_bvs_dt;
S_vfa(k+1)=S_vfa(k)+Ts*dS_vfa_dt;
X_acid(k+1)=X_acid(k)+Ts*dX_acid_dt;
X_meth(k+1)=X_meth(k)+Ts*dX_meth_dt;

F_meth(k)=V*k5*mu_c*X_meth(k);

e(k)=F_meth_sp(k)-F_meth(k);
du_dt_k=(u(k)-u_km1)/Ts;
%Updating objective:
J1(k+1)=J1(k)+Ts*(c_e*e(k)*e(k)+c_u*u(k)*u(k)+c_du*du_dt_k*du_dt_k);
%Time shift:
u_k_minus_1=u(k);
x_delay_mpc_k=x_delay_mpc_k_plus_1;
end %for loop

%Calculating the objective function:
J=J1(end)+c_final*e(end)*e(end);
```

```
f = J;

end %function
```

confun_mpc()

fmincon() invokes confun_mpc() in which the user can define equality and inequality contstraints. However, in the present application, no such constraints are implemented. Upper and lower limits on the optimization variables, i.e. $\{u(k)\}$, is instead defined with the pertinent arguments of fmincon().

function_ukf()

function_ukf(), developed for the present application, implements the Unscented Kalman Filter (UKF) algorithm presented in Simon (2006) which estimates the augmented state vector,

$$x = [S_{\mathrm{bvs}}, S_{\mathrm{vfa}}, X_{\mathrm{acid}}, X_{\mathrm{meth}}, S_{\mathrm{vs_{in}}}]^T \tag{7}$$

using the modified Hill model summarized in Appendix A of Article 4. The UKF state estimate is used in objfun_mpc() as the initial state in the simulation used to calculate the steady state value of F_{meth}.

State Estimation and Model-based Control of a Pilot Anaerobic Digestion Reactor

Finn Haugen, Rune Bakke and Bernt Lie*

February 12, 2014

Abstract

A state estimator and various model-based control systems have been designed for a real anaerobic digestion (AD) pilot reactor fed with dairy manure. The model used is a modified Hill model which is a relatively simple dynamical AD process model. The state estimator is an Unscented Kalman Filter (UKF) which uses only methane gas flow measurement to update its states. The model and the state estimates are used in different control systems. One of the control systems aims at controlling the methane gas flow to a setpoint. Simulations indicate that the setpoint tracking performance of a predictive control system is considerably better comparing with PI control, while disturbance compensation is not much better. Consequently, assuming the setpoint is constant, the PI controller competes well with the predictive controller. A successful application of predictive control of the real reactor is presented. Also, three different control systems aiming at retaining the reactor at an operating point where the volatile fatty acids (VFA) concentration has a maximum, safe value are designed. A simulation study indicates that the best control solution among the three alternatives is PI control based on feedback from estimated VFA.

Keywords: Anaerobic digestion, bioreactor, gas flow control, state estimation, Kalman Filter, predictive control, PI control.

---

*All authors are with Telemark University College, Norway. Address: Telemark University College, Kjolnes ring 56, 3918 Porsgrunn, Norway. E-mail address of contact person (first author): finn.haugen@hit.no.

1 Introduction

Anaerobic digestion (AD) of organic substrates can produce biogas which consists mainly of methane and carbondioxide, [40], [7], [42]. In a well-operated AD reactor, the methane content is sufficiently large to make the biogas combustible, i.e. the AD process produces applicable energy. Moreover, the reactor digestate is often high in nutrients and can be used in fertilization. Animal waste, in many cases combined with e.g. food waste, is a typical feedstock of AD reactors. A presentation of AD of animal wastes, from dairy, beef, poultry, and swine, is provided e.g. in [23].

UASB (upflow anaerobic sludge blanket) type reactors are effective AD reactors as they allow for relatively high load rates (feed rates) and/or small reactor volumes, [25], [40]. The effectiveness is due to relatively large solids retention time (SRT), which is the retention time of the micro-organisms which degrades the substrate and generates e.g. methane, compared with the hydraulic retention time (HRT) of the reactor. The AD reactor studied in the present article is an UASB reactor.

Anaerobic digestion a complex and nonlinear dynamic process and most plants suffer from a lack of robust online-measurement systems for online process monitoring [42]. Therefore, automatic plant control is a challenging task. The present article presents an attempt to using a mathematical dynamic model to estimate, online, non-measured AD state variables, and to using these estimates in a model-based control system. Results of the application of state estimation and model-based control to a real pilot AD reactor using dairy waste as feedstock are shown. The reactor is situated at Foss Farm, Skien, Norway. The results from the pilot reactor are assumed to be transferable to a planned full-scale reactor at the farm.

In this article, state estimates are used both in industry-standard PI controllers and in predictive controllers. The only online measurement used by the estimator, and thus by the controllers, is the methane gas flow. The reactor temperature is retained at a constant setpoint by means of a temperature control system [17].

Several control systems are designed and applied to the reactor: One aims at retaining the produced methane flow at a setpoint which can stem from a specified power production. Another control system aims at retaining the reactor at a safe operating point, where the concentration of the VFA (volatile fatty acids) is not above a certain value.

The model-based design and the simulations are based on the modified Hill model adapted to the pilot reactor [15]. This model is summarized in Section 3.3.

This paper is organized as follows. Section 2 gives a literature review. Section 3 provides a system description, including the mathematical reactor model used as the basis for state estimation and model-based control. In Section 4, safe reactor operation conditions is defined in terms of an acceptable range of VFA (volatile fatty acids). Section 3.2 presents a general structure of a model-based optimization and control system, applicable to the reactor. Application of the Unscented Kalman Filter (UKF) to estimate the state variables of the reactor and its main disturbance, namely $S_{vs_{in}}$, is described in Section 5. These estimates are used for control of F_{meth}, which is described in Section 6, which includes both simulated and real results. The estimates are also used for control of S_{vfa}, which is described in Section 7, which is simulation study. Conclusions are given in Section 8.

MATLAB and SIMULINK (MathWorks, Inc.) are used for numerical computations and simulations. The real control system is implemented in LabVIEW (National Instruments, Inc.) running on a laptop PC. In the LabVIEW program, the algorithms of the UKF and the predictive controller are implemented in a Matlab Script Node.

2 Literature review

State estimators for AD reactors

Literature about state estimators applied to AD reactors fed specifically with dairy manure have not been found. Below are references to state estimators applied to reactors fed with other types of substrates, assumed being relevant also for the present application.

In a simulation study, Jones *et al.* [24] apply an Ex-

tended Kalman Filter (EKF) to estimate four states of a simplified version of the AD model by Hill and Barth [21], using five online measurements.

Bernard *et al.* [5] estimate the six states of a real AD reactor fed with effluents from a wood processing plant using an asymptotic observer [2]. Available online measurements were CH_4 gas flow and CO_2 gas flow. Influent concentrations are assumed known. The estimator is based on a state variable transformation leading to a model having auxiliary state variables where the reaction rates are eliminated. These rates are then estimated from the state estimates. The estimator is designed so that the estimation errors converge towards zero with dynamics of the mass balances of the model, determined by e.g. the feed rate. The asymptotic observer is an open loop estimator, and has no tuning parameters, contrary to a Luenberger observer and a Kalman Filter which are closed loop, or feedback, estimators with parameters which can readily be used for performance adjustment.

Alcaraz-Gonzalez *et al.* [1] estimate four out of six states of a real AD reactor fed with industrial wine distillery vinasses, namely the methanogens and acidogens concentrations, COD (chemical oxygen demand), and alkalinity, by using online measurements of CO_2 gas flow, VFA, and TIC (total inorganic carbon). The AD process model is as in [5]. The estimator is an interval observer based on the structure of an asymptotic observer. An important property of an interval observer is that the estimates are guaranteed to be within bounds given by uncertainty bounds of model parameters and AD process inputs.

In a study based on real data, Theilliol *et al.* [41] estimate the six state variables, and three unknown inflow concentrations, namely COD, VFA and TIC, of an AD reactor fed with industrial wine distillery vinasses, using five online measurements: COD, VFA, alkalinity, CH_4 gas flow and CO_2 gas flow. The estimator is based on manipulating the original state space model using SVD (singular value decomposition) to a find an observable subsystem insensitive to unmeasured inputs. Then, a Luenberger observer based on this subsystem is used to estimate the state and the unmeasured inputs.

In a simulation study based on a full-scale agricul-

tural biogas plant, Gaida *et al.* [10] uses discriminant analysis and classification based pattern recognition methods to find the static mapping function between the measurement data, which are biogas flow, CH_4 and CO_2 gas concentrations, pH in the reactor, and the amount of each substrate, and the state of the AD process. The state variables are those of the ADM1 model (Anaerobic Digestion Model No. 1) [3]. The various substrates considered are maize silage, grass, manure and manure solids.

Dochain [8] and Bogaerts *et al.* [6] give an overview over various state estimators suitable for bio-processes, including the estimators applied in the references above.

In the applications referred to above, the estimators use two or more online measurements. In the present paper, only one measurement is used, namely F_{meth} (CH_4 gas flow). Furthermore, in the present paper the Unscented Kalman Filter (UKF) is used. The UKF can be used without any linearization or model manipulation, i.e. it uses the nonlinear state space model directly in the algorithm. We have not found literature on application of the UKF to AD reactors.

Model-based control of AD reactors

We have not found literature on model-based control systems of AD reactors fed specifically with dairy waste. Below are references to model-based control systems of reactors fed with other types of substrates, assumed being relevant also for the present application.

Bernard *et al.* [5] have implemented a model-based adaptive linearizing controller and a fuzzy controller designed to maintain the intermediate alkalinity (VFA, volatile fatty acids) and the total alkalinity within specified limits to ensure stable process conditions and avoid VFA accumulation despite organic load disturbances. The so-called AM2 model, [4], is used for design and simulation.

Puñal *et al.* [31] have designed an automatic fuzzy logic-based control system to maintain the online measured VFA concentration at a proper setpoint.

Méndez-Acosta *et al.* [28] have designed a model-based controller for maintaining the COD (chemical

oxygen demand) of the reactor effluent at its setpoint, using the AM2 model, [4].

Méndez-Acosta *et al.* [29] have designed a multivariable control system for controlling the concentration of VFA in the reactor to its setpoint using the feed rate, and controlling the total alkalinity to its setpoint using the addition of an alkali solution.

Strömberg *et al.* [39] has identified, using simulations, three controllers for AD processes to be the most suitable ones for maximizing gas production while being able to react properly to process disturbances due to variations in pH, ammonia, and concentration in the reactor feed. The simulations use the ADM1 model [3]. All of the controllers have the feed rate as control variable (controller output). The controllers resemble an expert system, with logics (if-clauses) in the control function. The three controllers are: 1. The extremum-seeking variable gain controller by Liu *et al.* [26]. 2. The disturbance monitoring controller by Steyer *et al.* [38]. 3. The hydrogen-based variable gain controller by Rodrigues *et al.* [33]. Strömberg *et al.* note that no uniform tuning method could be derived to tune the three controllers. Instead, trial-and-error procedures are used.

In a simulation study, Gaida *et al.* [9] have implemented a nonlinear predictive controller to control a simulated ADM1, assuming all states are available, and therefore, a state estimator is not used. The controller allows alternative optimization criteria, e.g. economical optimization and minimum methane concentration of the biogas. The plant is the same as in [10], cf. the above section about state estimation.

In a simulation study, Ordace *et al.* [30] have implemented a predictive controller based on transfer functions adapted to the ADM1 model to control the ADM1. The optimization criterion of the controller contains the square of the control error, while the control signal usage is not included, i.e. it has no cost in the criterion.

3 System description

3.1 AD reactor with control system

Figure 1 depicts the AD reactor with its control system. The reactor type is UASB (upflow anaerobic sludge blanket). The reactor is a part of a pilot biological plant for nutrient and energy recovery named Foss Biolab, situated at Foss farm, Skien, Norway. Input to the plant is dairy manure diluted with 25% water and filtered with a sieve, and outputs are fertilizer and biogas consisting of approximately 70% methane. The reactor temperature is kept fixed at its setpoint with an automatic temperature control system.

In Figure 1, the block denoted "Model-based Controller" may comprise a state estimator and alternative controller functions (predictive controller and PI controller with feedback from state estimates). The model-based controller uses an online measurement of F_{meth} which is provided by sensor FT. This measurement is obtained by multiplying the online biogas flow measurement from a thermal gas flow sensor and the online methane concentration measurement from an IR-based sensor. The raw measurement signals
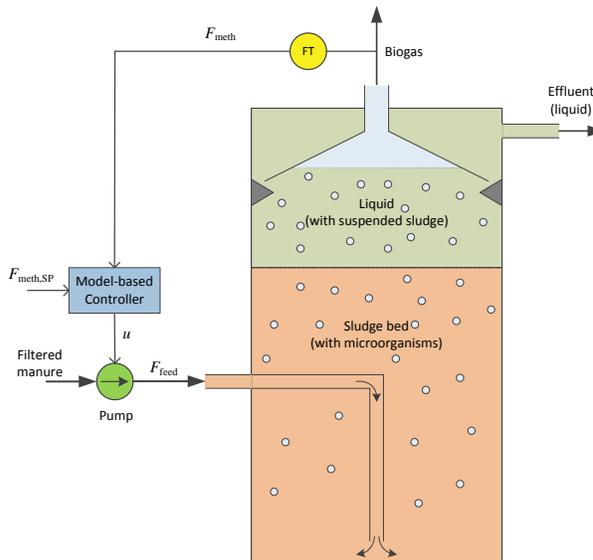

Figure 1: Control system of the AD reactor

4

are smoothed using software filters.

F_{feed} is used as control variable. The demanded flow is obtained with a peristaltic feed pump operated with PWM (Pulse Width Modulation) with a cycle time of 700 sec.

In principle, also T_{reac} is a candidate as control variable since it has a clear impact on F_{meth}, but in [16] we argue why T_{reac} is not considered a usable control variable.

An online measurement of T_{reac} is used by the controller, since T_{reac} is an important model variable. T_{reac} is retained at its (fixed) setpoint with a separate temperature control system where the controller is a PI (proportional plus integral) controller [17].

In this article, T_{reac} is kept at 35 °C because this is a typical temperature at which AD reactors are operated (mesophile conditions). However, this temperature is not necessary optimal. In [18] we show how the temperature can be specified using model-based optimization.

3.2   Control system structure

Figure 2 shows the structure of the control system.
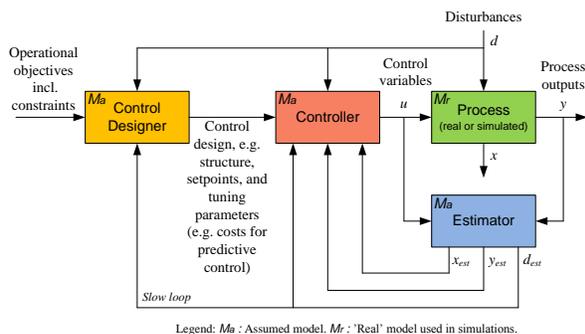
Figure 2: Block diagram of model-based optimization and control system. (Terms and variables are defined in the text.)

In the block diagram: $u = F_{\text{feed}}$, and $d = S_{\text{vs}_{\text{in}}}$. x comprises here the four state variables of the modified Hill model, cf. Section 3.3: $x = [S_{\text{bvs}}, S_{\text{vfa}}, X_{\text{acid}}, X_{\text{meth}}]^T$. Depending on the applications in this paper, $y = F_{\text{meth}}$, cf. Section 6, or $y = S_{\text{vfa}}$, cf. Section 7. Furthermore: The Process is the reactor. The Controller implements predictive control or PI control or manual control. The Estimator is an Unscented Kalman Filter (UKF). The Control Designer is the algorithm or strategy used to transform the specifications of the optimal operation into (optimal) setpoints and/or control signals. The Control Designer may also set parameters for controller tuning, e.g. cost factors in the optimization criterion of a predictive controller, or it may be an optimization algorithm to calculate optimal setpoints.

The symbol M_a in various blocks in Figure 2 represents the assumed mathematical model used in the block. The M_r symbol in the Process block is the model representing the real system (process). Only if model errors are assumed zero, M_a and M_r are identical.

The connections from d and/or d_{est} to the Control Designer are due to d being an input to the process, and the value of d or d_{est} is included in the model-based optimization. For example, the value of $S_{\text{vs}_{\text{in}}}$ in the feed of the reactor have an impact on the specific value of F_{feed} needed to produce a specified F_{meth} which in turn is closely related to the power production in the reactor.

In general, the operational objectives, which are the inputs to the Control Designer in Figure 2, may be adjusted based on results of an evaluation of the factual process operation, but this possible adjustment is not depicted in Figure 2.

A large number of model-based controllers exists [11]. In this paper, a predictive controller [12] [32] is selected.[1] The selection of a predictive controller is due to its popularity (as model-based controller) in the process industry [13], and due to our view that it implements most of important controller features which would otherwise require a number of special solutions, i.e. feedback, feedforward, integrator anti windup, constraints handling, and time delay compensation. When nonlinear predictive control is used, as in this paper, process nonlinearites are taken into account naturally and without approximations. Fur-

---

[1]A predictive controller is also denoted model-based predictive controller (MPC).

thermore, a predictive controller is relatively easy to tune, if the process model is accurate.

3.3 AD process model

The mathematical model of the AD processes in the reactor is a modification of the Hill model [20] adapted to the pilot reactor [15]. The model is based on material balances of biodegradable volatile solids, volatile fatty acids, acidogens and methanogens, and a calculation of the produced methane gas flow. The model is summarized below.

Material balances:

$$\dot{S}_{\mathrm{bvs}} = (B_0 S_{\mathrm{vs_{in}}} - S_{\mathrm{bvs}}) \frac{F_{\mathrm{feed}}}{V} - \mu k_1 X_{acid} \qquad (1)$$

$$\dot{S}_{\mathrm{vfa}} = (A_{\mathrm{f}} B_0 S_{\mathrm{vs_{in}}} - S_{\mathrm{vfa}}) \frac{F_{\mathrm{feed}}}{V} \qquad (2)$$
$$+ \mu k_2 X_{\mathrm{acid}} - \mu_c k_3 X_{\mathrm{meth}} \qquad (3)$$

$$\dot{X}_{\mathrm{acid}} = \left(\mu - K_{\mathrm{d}} - \frac{F_{\mathrm{feed}}/b}{V}\right) X_{\mathrm{acid}} \qquad (4)$$

$$\dot{X}_{\mathrm{meth}} = \left(\mu_c - K_{\mathrm{dc}} - \frac{F_{\mathrm{feed}}/b}{V}\right) X_{\mathrm{meth}} \qquad (5)$$

Methane gas production:

$$F_{\mathrm{meth}} = V \mu_c k_5 X_{\mathrm{meth}} \qquad (6)$$

Reaction rates:

$$\mu = \mu_{\mathrm{m}} \frac{S_{\mathrm{bvs}}}{K_{\mathrm{s}} + S_{\mathrm{bvs}}} \qquad (7)$$

$$\mu_c = \mu_{\mathrm{mc}} \frac{S_{\mathrm{vfa}}}{K_{sc} + S_{\mathrm{vfa}}} \qquad (8)$$

$$\mu_{\mathrm{m}} = \mu_{\mathrm{mc}} = 0.013 T_{\mathrm{reac}} - 0.129 \qquad (9)$$
$$\text{for } 20°\mathrm{C} < T_{\mathrm{reac}} < 60°\mathrm{C}$$

Table 1 shows model parameter values as adapted to AD reactor at Foss Farm, [15].

One example of a set of steady-state values of the AD process variables is given in Table 2.

Table 1: Parameters in the modified Hill model adapted to the AD reactor at Foss Farm

Parameter	Value	Unit
A_f	0.69	(g VFA/L)/(g BVS/L)
b	2.90	d/d
B_0	0.25	(g BVS/L)/(g VS/L)
k_1	3.89	g BVS/(g acidogens/L)
k_2	1.76	g VFA/(g acidogens/L)
k_3	31.7	g VFA/(g methanogens/L)
k_5	26.3	L/g methanogens
K_d	0.02	d^{-1}
K_{dc}	0.02	d^{-1}
K_s	15.5	g BVS/L
K_{sc}	3	g VFA/L
V	250	L

4 Safe operation condition

The various control systems proposed in this paper are designed to retain the reactor at a safe reactor operation condition, defined below. Hill *et al.* [22] have found, from a comprehensive study of literature reporting operational data for reactors fed with swine and beef manure and confirmed by their own laboratory experiments, that $S_{\mathrm{vfa}} > 0.8$ g/L indicates an impending reactor failure, causing a reduction of methane production. Hence, it is here stated that

$$S_{\mathrm{vfa}} \leq 0.8 \text{ g/L} = S_{\mathrm{vfa}}^{\mathrm{max}} \qquad (10)$$

defines safe operation conditions for the reactor. For practical reasons, we have not been able to conduct our own experiments to verify ineq. (10), or to identify a different $S_{\mathrm{vfa}}^{\mathrm{max}}$. However, a new value of $S_{\mathrm{vfa}}^{\mathrm{max}}$ will not change the principal results of this article.

Hill *et al.* found that also the proprionic to acetic acid (P/A) ratio is a good indicator of health. However, this ratio can not be calculated from the mathematical model used in this paper, and therefore, the analysis here is not based on this ratio.

Hill *et al.* did not use dairy manure in their analysis since reliable data for such manure were not available. Nevertheless, it is here assumed that the aforementioned safe range of S_{vfa} applies approximately also for reactors fed dairy manure. A support for this as-

sumption is that the validated AD reactor model by Hill [20] has the same parameters describing the AD process for dairy, swine, poultry, and beef manure, except for parameters expressing the fraction of the organic feed that is degradable, but the AD process dynamics are independent of the latter parameters.

Figure 3 shows simulated static (steady-state) responses in a number of variables to a range of constant feed rates (F_{feed}). The cyan horizontal line in the S_{vfa} plot represents $S_{\text{vfa}} = 0.8$ g/L. The green intervals on the abscissas indicate safe reactor operation, and conversely, the red interval indicate unsafe operation.

Table 2 shows the values of several variables at the ultimate safe steady state operating point. The set of three corresponding values, (S_{vfa}, F_{feed}, F_{meth}), constitutes the ultimate safe steady state operating point of the reactor. Table 2 also shows, for completeness, values of other model parameters and variables than those discussed here.

Table 2: The ultimate safe steady state operating point.

Variable	Value	Unit
S_{vfa}	0.8	g/L
F_{feed}	35.3	L/d
$F_{\text{feed}}/V = D$	0.14	(L/d)/L
$V/F_{\text{feed}} = \text{HRT}$	7.1	d
F_{meth}	174.2	L CH_4/d
F_{meth}/V	0.70	(L CH_4/d)/L
S_{bvs}	4.14	g/L
X_{acid}	1.80	g/L
X_{meth}	0.39	g/L
$S_{\text{vs}_{\text{in}}}$	30.2	g/L
T_{reac}	35	°C

One question arises about the applicability of the modified Hill model to predict safe/unsafe operation of the reactor: Is it necessary to include $S_{\text{vfa}}^{\text{max}} = 0.8$ g/L explicitly to find the ultimate (maximum) safe operating point? Assuming the reactor model is accurate, safe operating points should be implicit in the model, i.e. they can be calculated from the model, e.g. by simulations. The modified Hill model used in the present paper is relatively simple. It is not

clear, because appropriate experiments have not be run here, to what extent the model is able to predict a possible failure of the real reactor due to high concentration of VFA. Therefore, as long as this simple model is chosen, it will be safer to define $S_{\text{vfa}}^{\text{max}}$ explicitly instead of relying on the model alone to predict a possible failure.

Defining explicit limits on model variables for safe operation is consistent with the approaches in e.g. [5] and [29] where limits on VFA and TA (total alkalinity) are set explicitly.

5   State estimation

State estimation is used in the control systems described in Sections 6 and 7. State estimators can also be useful solely for monitoring purposes, i.e. for estimation of state variables in the lack of sensors. The state estimator used in the present article is a Kalman Filter [35] algorithm based on the modified Hill model presented in Section 3.3. While there exist several state estimation algorithms, cf. Section 2, we select here the Kalman Filter because it has a relatively simple and straightforward structure, and because it can be easily fine-tuned.

The modified Hill model is a nonlinear model. The Extended Kalman Filter (EKF) is a commonly used extension of the basic Kalman Filter for nonlinear models. The EKF involves linearization of the process model. An alternative to the EKF is the Unscented Kalman Filter (UKF) [35]. Two benefits of the UKF, compared to the EKF, are that no linearization is necessary, and that the estimates are more accurate as the propagation of the estimation covariances, needed to calculate the optimal state estimates, are calculated more accurately. Because of these two benefits, the UKF is selected as state estimator in this paper.

Variables and parameters of the model

The state variables of the modified Hill model are, cf. Section 3.3, S_{bvs}, S_{vfa}, X_{acid}, and X_{meth}. They are estimated with the UKF. It is decided to also estimate $S_{\text{vs}_{\text{in}}}$ with the UKF since it it assumed that its
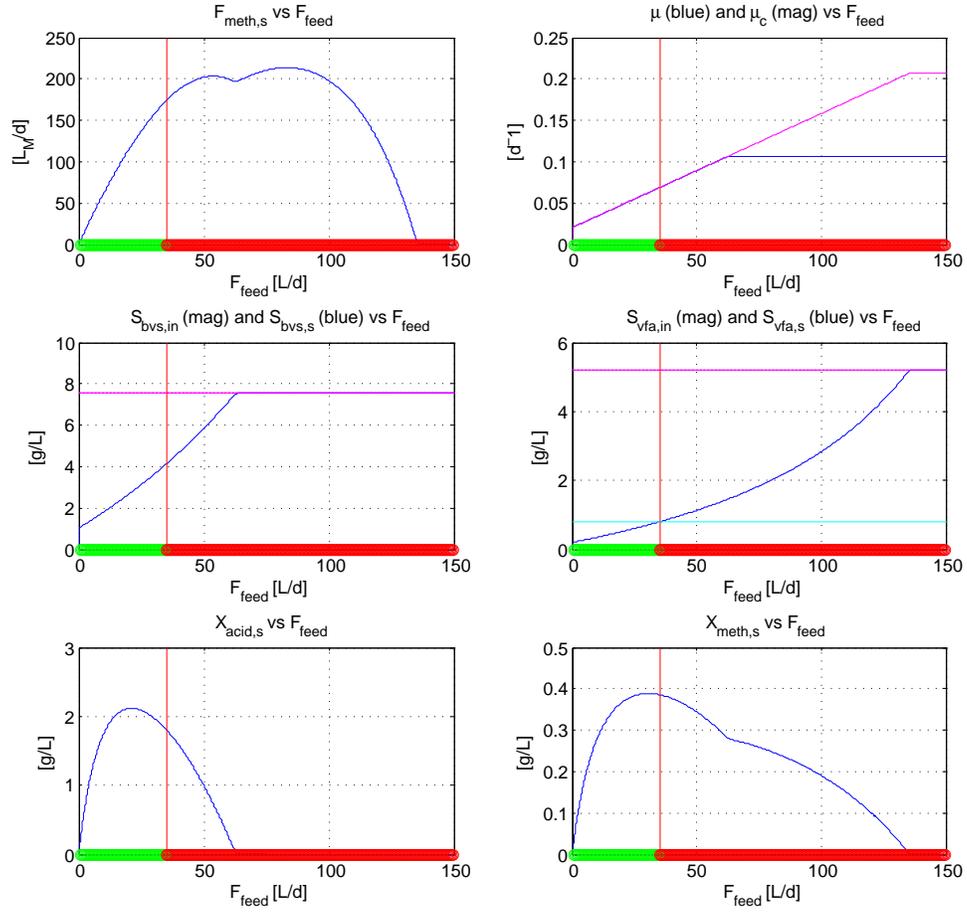
Figure 3: Simulated static (steady-state) values of a number of variables versus F_{feed} (constant) at $T_{\text{reac}} = 35^{\circ}$C. The green intervals on the abscissas indicate safe reactor operation as defined in ineq. (10). Conversely, the red intervals represent unsafe reactor operation.

8

value may vary, though slowly. As is common, $S_{vs_{in}}$ is modelled as a "random walk": $\dot{S}_{vs_{in}} = w$ where w is a random disturbance. Thus, the augmented state vector to be estimated by the UKF is

$$x = [S_{bvs}, S_{vfa}, X_{acid}, X_{meth}, S_{vs_{in}}]^T \qquad (11)$$

F_{feed} is regarded as an input variable to the UKF. F_{feed} is the control variable, which is always known.

The model parameters are known from model adaptation [15]. T_{reac} may vary, but is always known as it is measured continuously.

The process measurement, y, used by the UKF is F_{meth} available from sensor FT in Figure 1. Hence, $y = F_{meth}$ in the UKF.

Observability

The linearized reactor model, augmented with $S_{vs_{in}}$, is found observable at a number of typical operating points using the obsv function of the MATLAB Control System Toolbox (further details are not shown here).

Tuning of the UKF

The tuning parameters of the UKF are as follows $\hat{x}(t_0|t_0)$ (initial estimated state; the initial aposteriori estimate), $\hat{P}(t_0|t_0)$ (initial state estimation error covariance), R (measurement noise covariance), and Q (process noise covariance). Ideally, these parameters are set equal to their known values, but some of them may not be available. Good tuning guidelines are actually hard to find. Even an otherwise thorough book as [35] gives little advice. In this paper the tuning is done as follows.

- $\hat{x}(t_0|t_0)$ is set equal to the values from laboratory analysis at the start of the pertinent time interval. This applies ideally to S_{bvs}, S_{vfa}, and $S_{vs_{in}}$. However, for $S_{vs_{in}}$ we impose on for the purpose of demonstration, a large initial estimation error by setting the initial estimate of $S_{vs_{in}}$ equal to 20% of the value known from laboratory analysis.

- X_{acid} and X_{meth} are not known, but their initial values are calculated from the model assuming

steady state (details of the calculation can be found in [15]).

- $\hat{P}(t_0|t_0)$ is set as a diagonal matrix as follows:

$$\hat{P}_{ii}(t_0|t_0) = [k_P \hat{x}_i(t_0|t_0)]^2 \qquad (12)$$

with $k_P = 0.01$.

- R is a diagonal matrix, which, since the number of measurements is one (F_{meth}), is reduced to a scalar – the measurement variance. From a representative real time series,

$$\text{var}(F_{meth}) = 1.44 = R \qquad (13)$$

- Q is typically set as a constant matrix (diagonal). Assuming that $\hat{x}(t_0|t_0)$, $\hat{P}(t_0|t_0)$ and R are set, Q can be used as final tuning parameter:

  - Increasing $Q_{i,i}$ makes the estimate for state variable x_i converge faster to the assumed true value, but with the drawback that the estimate for x_i becomes more noisy (caused by the increased propagation of the measurement noise, via the Kalman Filter gain(s)).

  - Reducing $Q_{i,i}$ has the opposite effects.

It is proposed to relate the diagonal element (i.e., the process noise variance) to the magnitude of the pertinent state variable:

$$Q_{i,i} = [k_Q m_i x_i(t_0|t_0)]^2 \qquad (14)$$

With the initial setting of $m_i = 1$, it is found that $k_Q = 0.0005$ is a proper value. Then the ultimate tuning is made by adjusting m_i. By trial-and-error, $\{m_i\} = \{10, 1, 1, 1, 10\}$.

Results and discussion

Figure 4 shows estimates with the UKF together with real data from online sensors and laboratory analysis over a time interval of 85 days. (This time interval includes the interval where the UKF is applied to the real reactor as a part of the predictive controller, cf.
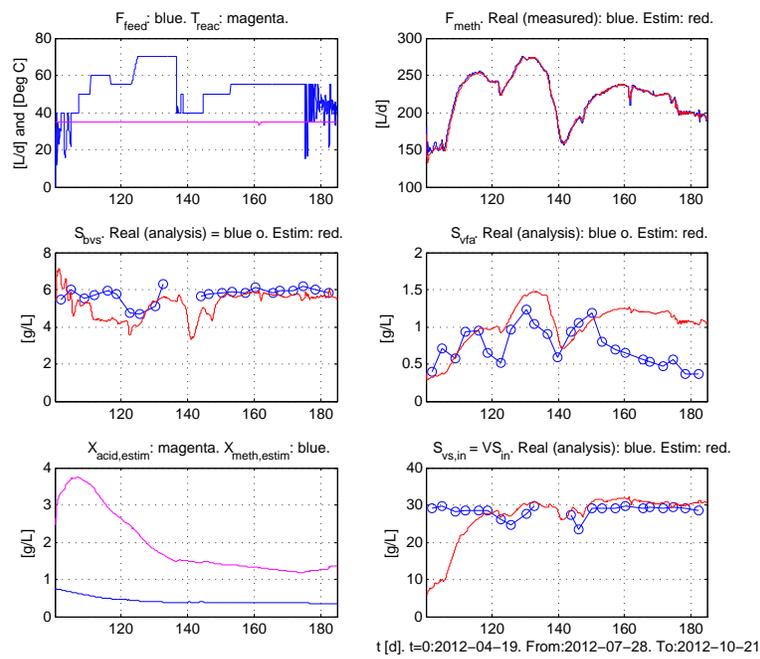
Figure 4: Estimates and real data from laboratory analysis with UKF. Standard deviations of estimation errors: S_{bvs}: 0.62 g/L. S_{vfa}: 0.32 g/L. $S_{\mathrm{vs_{in}}}$: 1.02 g/L. (For $S_{\mathrm{vs_{in}}}$, the standard deviation is calculated from $t = 120$ d, since a relatively large initial estimation error is imposed on purpose).

Section 6.5.) The process measurement used by the UKF is F_{meth}.

Overall, the UKF gives reasonably good estimates (real values of X_{acid} and X_{meth} are not known).

The large initial estimation error $S_{\mathrm{vs_{in}}}$ imposed on purpose is effectively reduced during approximately 15 days.

From $t = 150$ d, there is a noticeable difference between the estimate and the laboratory analysis of S_{vfa}. It is not clear what is the cause of this difference. If the model is trusted, the difference may indicate an inaccuracy of the laboratory analysis.

6 Control of methane gas production

6.1 The effect of feedback control

To demonstrate the effect of feedback (or automatic or closed loop) control of F_{meth}, Figure 5 shows, for the real pilot reactor, experimental time-series of F_{meth} and F_{feed} (and T_{reac}) with feedback control and without control. It is clear that F_{meth} varies less with control than without control. F_{meth} remains close to $F_{\mathrm{meth_{sp}}}$ even after the setpoint is changed. The variations are due to inevitable disturbances. In the case of feedback control, F_{feed} is of course varying, while it is constant in the case of no control (i.e. open loop control). T_{reac} is actually different in the two cases, but it is assumed the difference between the two cases is independent of the temperature difference.

Whether the variations in F_{meth} in open loop control is acceptable or not, must be decided in each specific application. A comparison of the performance of closed loop control and open loop control when disturbances are assumed, can be made using simulations with the AD model presented in Section 3.3.

6.2 Operational objective and control strategy

It is here assumed that a sufficient rationale for feedback control of F_{meth} exists. The operational objective is stated as producing a demanded methane gas flow. A specific value of F_{meth} is related to the power,
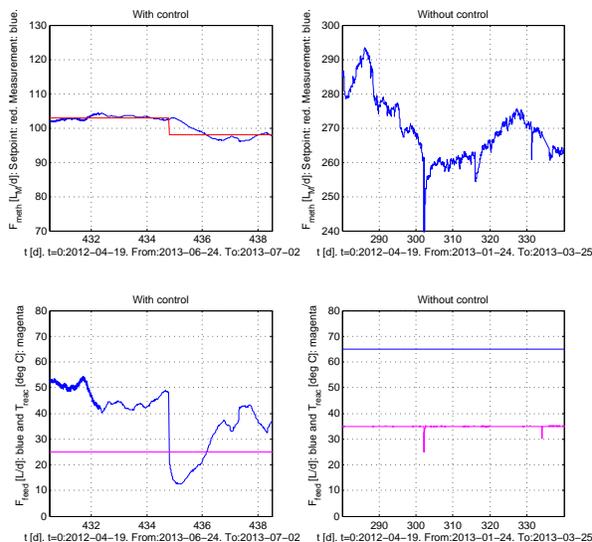
Figure 5: F_{meth} and F_{feed}, and T_{reac}, for the real reactor, with (automatic) control and without control. (The length of each of the time intervals for these two cases are different.) [Reprinted from [16] by permission.]

P [kW], as the energy content of methane gas is 9.95 kWh/m^3 at NTP.

The methane gas flow setpoint must be feasible. The feasibility can be checked with steady state simulations. More specificly, it can be checked using the upper-left plot in Figure 3.

Furthermore, safe reactor operation must be ensured, which here means that ineq. (10) is satisfied.

Relating to Figure 2, the above specifications concerning F_{meth}, the limitation of variations of F_{feed}, and the condition ineq. (10) are inputs to the Control Designer. Outputs from the Control Designer are $F_{\mathrm{meth}}^{\mathrm{sp}}$ and C_{du}. The latter is the cost factor of the control signal variations of a predictive controller.

6.3 Control functions

In control system design, the PI(D) controller should normally be taken into account when different con-

trollers are evaluated. If oscillations can be tolerated, even the on-off controller should be considered. Using on-off controllers and PI controllers for F_{meth} control of the pilot reactor is discussed in detail in [16].

In many cases, advanced controllers can give improved control compared with the simple PI(D) controller and the on-off controller, but typically the implementation is considerably more demanding. As argued in Section 3.2, a predictive controller is used as advanced controller in this paper. A predictive controller to retain F_{meth} at its setpoint is implemented both on a simulator of the reactor and on the real reactor. The model is the modified Hill model, cf. Section 3.3. A time-delay of $\tau_d = 0.2$ d is included at the control input of the model:

$$F_{\text{feed}}(t) = u(t - \tau_{\text{d}}) \tag{15}$$

where F_{feed} is the feed rate of the modified Hill model and u is the control signal. This time-delay accounts approximately for the dynamics not included in the modified Hill model presented in Section 3.3. The optimization objective of the predictive controller is

$$\min_{u} \; f_{\text{obj}} \tag{16}$$

where

$$f_{\text{obj}} = \int_{t}^{t+\tau_{\text{h}}} \left[e^2 \left(\theta \right) + C_{\text{du}} \dot{u}^2 \left(\theta \right) \right] d\theta \tag{17}$$

with constraint $u_{\text{min}} \leq u(t) \leq u_{\text{max}}$ which is included in the optimization problem formulation, i.e. it is an input argument in the fmincon function call in MATLAB. t is the present time instance. e is the control error, $e = F_{\text{meth}}^{\text{sp}} - F_{\text{meth}}$. The time derivative, $\dot{u}$, represents the control signal changes. The larger C_{du}, the smoother control actions.

In implementations, the discretized version of f_{obj} is minimized, giving an optimal control sequence, $\{u\}_{\text{opt}}$, over the prediction horizon. The first element of this sequence, i.e. $u(t_0)_{\text{opt}}$, is applied as control signal at the present time point. The prediction horizon is receding, and the procedure of obtaining $\{u\}_{\text{opt}}$ and $u(t_0)_{\text{opt}}$ is repeated as time evolves.

The prediction made by the controller is based on the modified Hill model discretized with the Euler explicit (forward) method. $\{u\}_{\text{opt}}$ is calculated with the nonlinear optimization function fmincon in the Optimization toolbox of MATLAB. The present state, $x(t)$, needed for the prediction, is calculated with the augmented Unscented Kalman Filter presented in Section 5.

6.4   Simulations

Controller settings

The settings of the predictive controller in the simulations are as follows.

A time-step of $\tau_{\text{s}} = 0.025$ d is used in the discrete-time version of the modified Hill model used for prediction. This is also the time step of the discretization of f_{obj}. τ_{h} corresponds to $1/0.025 = 40$ time steps, which is then the prediction horizon in number of time-steps.

$C_{\text{du}} = 0.01$ in eq. 17 is found by trial-and-error on a simulator. A proper value of the prediction horizon is found as $\tau_{\text{h}} = 1$ d (with $\tau_{\text{h}} < 0.5$ d, a change in performance can be observed).

In the simulations, the predictive controller is compared with the predictive controller. The PI controller is tuned at the operating point shown in Table 2 using the Skogestad method [36], with the modification of the τ_{i} setting as proposed in [19]. The PI settings are $K_{\text{c}} = 0.89$ [(L CH4/d)/(L feed/d)] and $\tau_{\text{i}} = 0.8$ d.

Performance and robustness measures

The control system performance and robustness measures applied in the simulations, are described in the following.

IAE (performance)

The IAE index (Integral of Absolute Error) is commonly used measure of control system performance. IAE_{s} measures the setpoint tracking:

$$\text{IAE}_{\text{s}} = \int_{t_{\text{i}_{\text{s}}}}^{t_{\text{f}_{\text{s}}}} |e| \, dt \tag{18}$$

The IAE_{d} measures the disturbance compensation:

$$\text{IAE}_{\text{d}} = \int_{t_{\text{i}_{\text{d}}}}^{t_{\text{f}_{\text{d}}}} |e| \, dt \tag{19}$$

Control signal variations (performance)

As measures of the variation of the control signal, both the standard deviation, σ_u, and the mean of the absolute value of the rate of changes, $\mu_{|\dot{u}|}$, are calculated.

Stability margins (robustness)

The traditional measure for robustness of linear control systems are the gain margin (GM) and the phase margin (PM). The predictive controller is a nonlinear controller, and the (reactor) is a nonlinear process. Thus, the predictive control system and the PI control system are nonlinear systems. We propose here to expand the use of GM and PM as stability margins also for these nonlinear system, as explained in the following.

An adjustable gain, ΔK, is inserted into the loop (between the controller and the process), see Figure 6. Normally, $\Delta K = 1$. The (ultimate) value, ΔK_u,
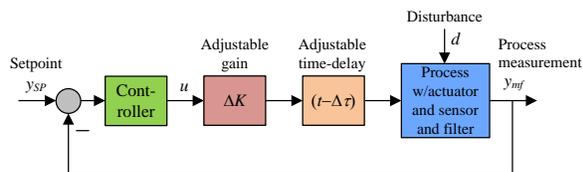

Figure 6: An adjustable gain and time-delay are inserted into the loop to find the stability margins (gain margin and phase margin) experimentally.

that brings the (simulated) control system to the stability limit, with sustained oscillations, is found by trials. Then,

$$\mathrm{GM} = \Delta K_\mathrm{u} \qquad (20)$$

To calculate the PM, an adjustable time-delay, $\Delta\tau_\mathrm{delay}$, is inserted into the loop, see Figure 6. Normally, $\Delta\tau_\mathrm{delay} = 0$. The value $\Delta\tau_{\mathrm{delay}_\mathrm{u}}$ that brings the control system to the stability limit, i.e. causing a sustained oscillation, is found experimentally on the simulator. Denote the period the oscillation as P_u [s]. As shown in [14] (Appendix 1),

$$\mathrm{PM}\ [\mathrm{deg}] = 360^\mathrm{o}\,\frac{\Delta\tau_{\mathrm{delay}_\mathrm{u}}}{P_\mathrm{u}} \qquad (21)$$

Seborg *et al.* [34] propose the following ranges for appropriate values of the stability margins: $1.7 = 4.6$ dB $\leq$ GM $\leq 4.0 = 12.0$ dB, and $30^\mathrm{o} \leq$ PM $\leq 45^\mathrm{o}$.

Relating to Figure 2, ΔK and $\Delta\tau_\mathrm{delay}$ are included before the Process block, after the branch from u to the Estimator.

Simulations

Figure 7 shows simulated time-series with predictive control and, for comparison, PI control. The initial operating point of the reactor is as shown in Table 2, which is the ultimate (maximum) safe steady state operating point. The setpoint $F^\mathrm{sp}_\mathrm{meth}$ is varied as a sequence of two ramps of slope ± 2 (L CH$_4$/d)/d each lasting for 1 d. The disturbance $S_{\mathrm{vs}_\mathrm{in}}$ is varied as a ramp of slope 2 (g/L)/d during 1 d which is a realistic variation [16].

The simulations shown in Figure 7 are without measurement noise. To measure the control signal variations, simulations have been run with measurement noise in the form of a normally distributed random signal with zero mean and standard deviation $\sigma_\mathrm{n} = 1.2$ L CH$_4$/d, which is realistic for the present reactor. The simulations are run over 10 d with a constant setpoint and a constant disturbance (simulations are not shown here).

Results and discussion

Table 3 shows performance and robustness measures with predictive control and with PI control. The IAE indexes, eqs. 18 and 19, are calculated with $t_{\mathrm{i}_\mathrm{s}} = 1$ d, $t_{\mathrm{f}_\mathrm{s}} = 7$ d, $t_{\mathrm{i}_\mathrm{d}} = 7$ d, and $t_{\mathrm{f}_\mathrm{d}} = 14$ d.

Table 3: Performance and robustness measures for predictive control and PI control.

	Predictive	PI	Ratio: Pred./PI
IAE$_\mathrm{s}$	0.093	0.72	0.13
IAE$_\mathrm{d}$	1.46	2.20	0.66
σ_u	0.69	1.29	0.67
$\mu_{|\dot{u}|}$	7.07	25.2	0.28
GM	$\approx \infty$	2.6	N/A
PM	63.9^o	47.6^o	1.34

Comments to the results shown in Table 3:
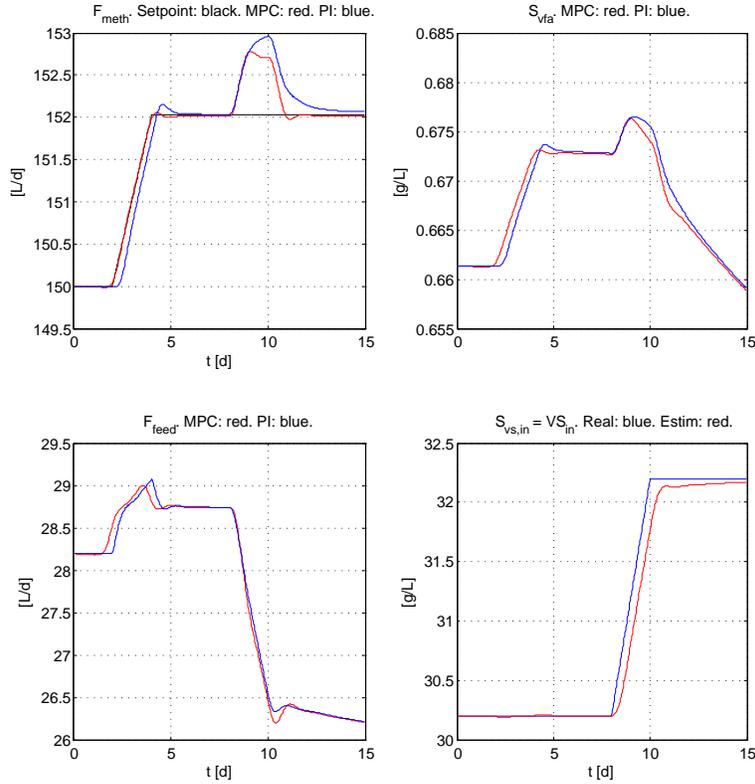
Figure 7: Simulated responses with predictive control and PI control.

- IAE_s with predictive control is 13% of IAE_s with PI control. Hence, predictive control is clearly best.

- IAE_d with predictive control is 66% of IAE_d with PI control. Again, predictive control is best, but the improvement compared with PI control is not large.

- σ_u with predictive control is approximately 67% of the value with PI control, while $\mu_{|\dot{u}|}$ with predictive control is approximately 28% of the value with PI control. These numbers vary with the realization of the random processes generated in the simulation, but they are representative.

By detuning the PI controller for more relaxed control (reducing K_c and increasing τ_i according

to Skogestad's formulas), both σ_u and $\mu_{|\dot{u}|}$ are reduced. By a proper retuning, either of them can become approximately equal to the value with predictive control. The consequence of such a retuning is that the IAE measures with PI control will increase. In one simulated example, the PI controller was retuned so that $\mu_{|\dot{u}|}$ with predictive control and PI control was approximately equal. The IAE_d with PI control then increased 4.5 times, i.e. the control performance became radically worse.

The smoother control actions with predictive control compared with PI control has been observed on experiments on the real reactor.

- GM is acceptable with PI control. With predictive control the notion of GM is questionable,

14

since the simulated control system does not actually become unstable for any gain increase at the process input. Rather, the gain increase is seen by the UKF as a change in the disturbance, or, more specifically, as an increase in $S_{vs_{in}}$. Consequently, the estimate of $S_{vs_{in}}$ is increased, which in turn is used in the prediction by the predictive controller, causing a large overshoot or undershoot in F_{meth} before it eventually reaches F_{meth}^{sp} (plots of simulations not shown). From simulations it is found that F_{meth}^{sp} is back at its setpoint during 1-2 d for $0.5 \leq \Delta K_u \leq 4$.

- PM is larger with predictive control (63.9º) compared with PI control (47.6º).

Concluding remarks

Above, the predictive controller has been compared with the PI controller tuned using a standard method, namely the Skogestad method [36]. Simulations indicate that predictive control has better performance and better robustness than the PI controller. It can also be claimed that the predictive controller, here including the state estimator, is more intuitive to adjust since its parameters have a direct relation to practical factors such as measurement noise and control signal variation. The drawbacks with predictive control is that a mathematical model of the reactor is required, and that it is more complicated to implement.

The setpoint tracking performance of the predictive controller is considerably better than with the PI controller, while the improvement in disturbance compensation is not large. Taken into account that the PI controller is much easier to implement, it may be claimed that the PI controller is the preferred controller if the setpoint is constant.

6.5 Experiments on the real reactor

Predictive control has been applied to the real reactor. Some of the settings in the practical experiment differ from those used in the simulation study presented in Section 6.4, which has been accomplished approximately one year after the practical experiment. (However, simulations were used to test the

control system before the practical implementation.) The differences in settings are:

- In the practical experiments, $\tau_s = 0.05$ d, and $\tau_p = 2$ d. In the simulations in Section 6.4, $\tau_s = 0.025$ d, and $\tau_p = 1$ d. $\tau_s = 0.05$ d has been tested in simulations, giving a slight change in performance, probably due to less accurate numerical integration (explicit Euler is used). $N_p = \tau_p/\tau_s = 40$ is the same both in the practical experiments and in the simulations.

- F_{feed} is limited to 40 L/d, which is also used in the simulations in Section 6.4. This limit is reached in the practical experiment, but is not reached in the simulations since the perturbations are relatively small there.

- No time delay term is included in the model used by the predictive controller in the practical experiment, while it is found appropriate to include a time delay in the simulation study as the model analysis in [15] indicate that a time delay is present.

- The cost factor C_{du} in eq. (17) was set to 0.8 in the practical experiment, while 0.01 is found appropriate in the simulation study, cf. Section 6.4. The smaller C_{du} in the simulations may be due to dynamic phenomena of the real reactor not encapsulated by the model. In any case, C_{du} is typically a tuning parameter.

Results and discussion

Figure 8 shows the time-series of the practical experiments. Below are comments to this figure.

- At $t = 99.8$ d, F_{meth}^{sp} was reduced instantly from 190 to 150 L/d. Since the reduction was instant, the predictive controller could not take any control action in advance. The response in the gas flow is stable and shows acceptable stability, but the stability is reduced compared with the simulated response. The control error is less than 3 L/d after approximately 1 d.

    A possible explanation of the damping of the real response being less than in the simulated
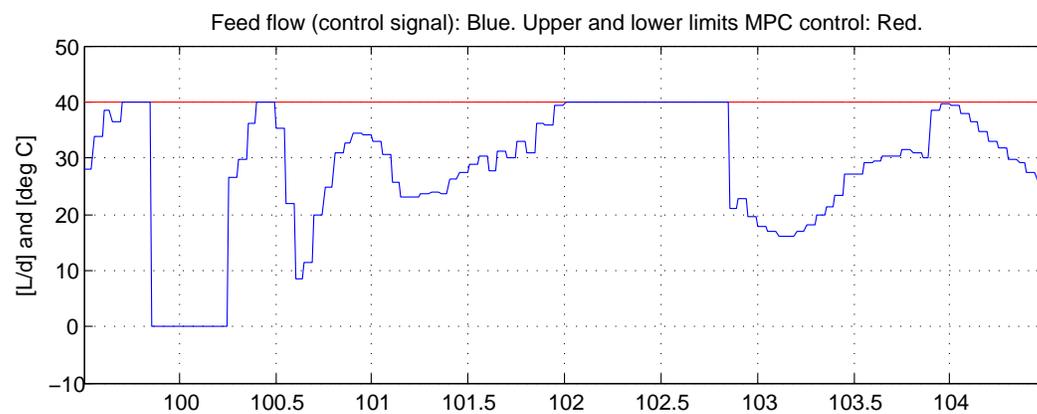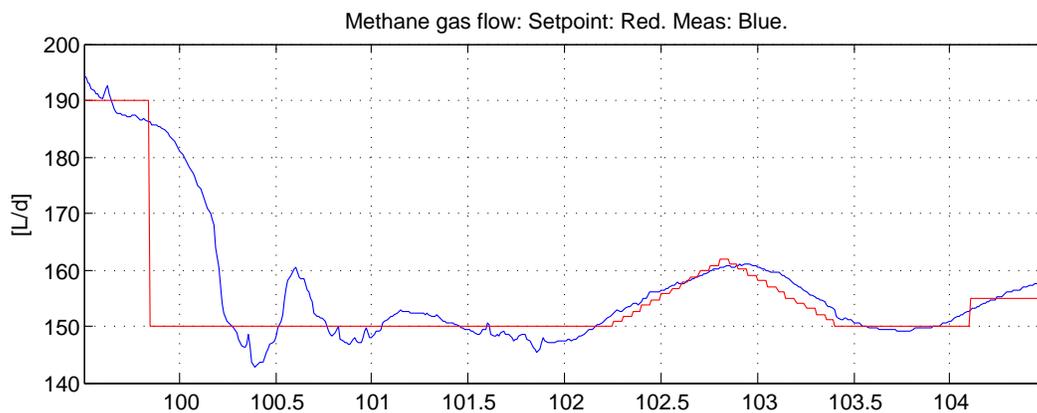
15

Figure 8: Time-series from application of predictive control of F_{meth} on the real reactor.

16

response, is that the predictive controller does not include any process model time delay while, as pointed out above, there is actually a time delay in the real process.

- At $t = 102.3$ d, a preset ramped setpoint profile started. The predictive controller adjusts F_{feed} before $F_{\text{meth}}^{\text{sp}}$ starts increasing. The tracking is accurate. The upper bound of F_{feed} of 40 L/d is eventually reached, causing the rate of change of F_{meth} to become less than the rate of change of $F_{\text{meth}}^{\text{sp}}$.

- At $t = 102.8$ d, the rate of change of $F_{\text{meth}}^{\text{sp}}$ is instantly adjusted from $+20$ (L CH$_4$/d)/d to -20 (L CH$_4$/d)/d. The observed lag in F_{meth} can be explained with the instant change of $F_{\text{meth}}^{\text{sp}}$ which prevents predictive control action.

- At $t = 104.1$ d, a preset step change of $F_{\text{meth}}^{\text{sp}}$ from 150 to 155 L CH$_4$/d is applied. The predictive adjustment of F_{feed} is obvious. F_{meth} shows a clear overshoot, but it is expected that the response will stabilize.

- At $t = 104.4$ d, the predictive control experiment had to be stopped as other experiments were scheduled to start at this point of time. The controller was actually set to manual mode. The saved future control signal sequence generated by the predictive control shows a declining behaviour, indicating that F_{meth} eventually would have been brought back to its setpoint.

As pointed out earlier, the methane gas flow setpoint must be feasible. For the above experiments, the feasibility can be checked using the upper-left plot in Figure 3. According to this plot, the setpoint values used in the experiments, cf. Figure 8, are actually feasible.

7 Control for safe reactor operation

7.1 Objective and control strategies

Here, the operational objective of the reactor is defined as retaining the reactor at the ultimate safe steady state operating point given in Table 2 (this is the input to the Control Designer in Figure 2). To this end, the following three alternative control strategies are tested (they comprise the "output" from the Control Designer in Figure 2):

1. F_{feed} is controlled to a setpoint of $F_{\text{feed}}^{\text{sp}}$, which is 35.3 L/d, assuming the operating point shown in Table 2. This control strategy is described in Section 7.2.

2. S_{vfa} is controlled to a setpoint of $S_{\text{vfa}}^{\text{sp}}$, which is 0.8 g/L according to Table 2. In principle, this control requires feedback from the measurement of S_{vfa}. Such sensors do exist [37] [27], but it is not in use on the present reactor. Instead, the estimate of S_{vfa} calculated continuously with a state estimator (Kalman Filter) is used, cf. Section 5. This control strategy is described in Section 7.3.

3. F_{meth} is controlled to a setpoint of $F_{\text{meth}}^{\text{sp}}$, which is 174 L CH$_4$/d according to Table 2. This control requires feedback from the measurement of F_{meth}. This control strategy is described in Section 7.4, where also PI control is applied for comparison.

In each of the control strategies, the feed rate is used as control variable, $u = F_{\text{feed}}$, cf. Section 3.2.

The applicability of the three control strategies described above is demonstrated with simulations in the following subsections. In each of the simulations, a disturbance in $S_{\text{vs}_{\text{in}}}$ is applied.

7.2 Control of F_{feed}

F_{feed} is held constant at 35.3 L/d, cf. Table 2. On the real reactor, this can be implemented easily since

the feed pump is a peristaltic pump which gives the demanded flow without feedback (flow) control.

Figure 9 shows the simulated response with constant F_{feed}. Table 4 shows performance measures.

7.3 Control of S_{vfa}

S_{vfa} is controlled to its setpoint, $S_{\text{vfa}}^{\text{sp}} = S_{\text{vfa}}^{\text{max}}$, using feedback from $S_{\text{vfa}}^{\text{est}}$ from the Kalman Filter, cf. Section 5. Both predictive control and PI control are tested.

Predictive control

The optimization criterion of the predictive controller is selected as

$$\min_{u} \quad f_{\text{obj}} \tag{22}$$

where

$$f_{\text{obj}} = \int_{t}^{t+\tau_{\text{h}}} \left[e^2 \left(\theta \right) + C_{\text{du}} \dot{u}^2 \left(\theta \right) \right] d\theta + C_{\text{h}} e^2 \left(\tau_{\text{h}} \right) \tag{23}$$

with constraint $u_{\text{min}} \leq u(t) \leq u_{\text{max}}$. The control error is $e = S_{\text{vfa}}^{\text{sp}} - S_{\text{vfa}}^{\text{est}}$. Comparing with the criterion of predictive control of F_{meth}, eq. (17), the term $e^2 \left(\tau_{\text{h}} \right)$, which is e^2 at the end of the prediction horizon, is now included. The term brings $e(t + \tau_{\text{h}})$ approximately to zero. Without this term, $e(t + \tau_{\text{h}})$ is 0.1 g/L, and the control signal is actually constant. It is found that $C_{\text{du}} = 0.2$ and $C_{\text{h}} = 20$ are proper settings.

It is found that the predictive control is considerably smoother with $\tau_{\text{h}} = 4$ d than with $\tau_{\text{h}} = 1$ d which is used in Section 6. Increasing τ_{s} from 0.025 d, which is used in Section 6, to 0.1 d, here, has very little impact on the control system performance over the simulation time interval used here, while the computational burden is noticeably less.

PI control

PI controller is also applied. The PI settings are $K_{\text{c}} = 50.9$ (L/d)/(g VFA/L) and $\tau_{\text{i}} = 0.9$ d found using the Relaxed Ziegler-Nichols closed loop method based on relay oscillations [19] which is a quick method to use on a simulator.

Simulations

The initial operating point is as shown in Table 2. The setpoint is $S_{\text{vfa}}^{\text{sp}} = S_{\text{vfa}}^{\text{max}} = 0.8$ g/L. At $t = 10$ d, the disturbance $S_{\text{vs}_{\text{in}}}$ is changed as a ramp of slope 2 (g/L)/d during 1 d, which is the same variation as in F_{meth} control, cf. Section 6. This is a reasonable variation for the real reactor. Measurement noise is not included in simulations.

Figure 9 shows simulated responses in S_{vfa}, F_{meth}, F_{feed} and $S_{\text{vs}_{\text{in}}}$ with predictive control and PI control, and with constant F_{feed}. Table 4 shows performance measures.

Results and discussion

Table 4 shows performance and robustness measures with the three control strategies above. IAE$_{\text{d}}$, defined by eq. (19), is calculated over the simulated time interval. $|e|_{\text{max}}$ is the maximum control error. GM and PM are found as explained in Section 6.4.

Table 4: Performance measures for three control strategies for controlling S_{vfa}.

Measure	Const. F_{feed}	Predictive	PI
IAE$_{\text{d}}$	1.52	0.20	0.090
GM	N/A	$\approx \infty$	5.5
PM	N/A	$\approx \infty$	71.0º

Comments:

- In Figure 9 it is seen that the setpoint tracking works for both predictive control and PI control. However, the PI controller gives a more smooth response in S_{vfa}.

- The lower right plot in Figure 9 shows the manipulated F_{feed} which is adjusted by the controllers. The control action is smoother with PI control than with predictive control.

- The performance measures shown in Table 4 indicate that PI control of S_{vfa}, based on feedback from UKF is the best control strategy here.

- Also using a constant F_{feed} can be regarded acceptable with the disturbance change simulated.
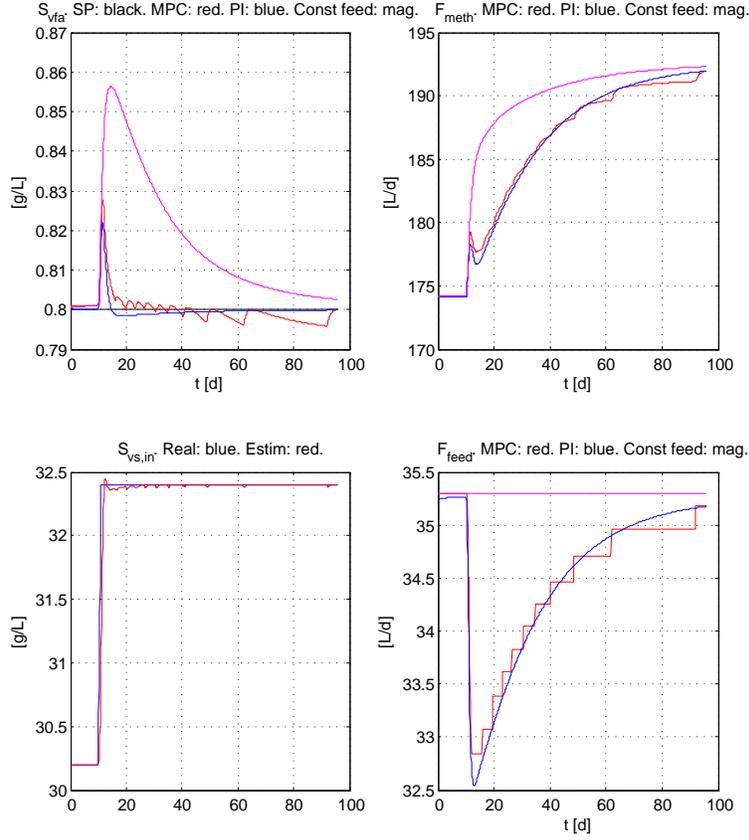
Figure 9: Control of S_{vfa} with different control functions: Constant F_{feed}, predictive control (MPC), and PI control. Simulated responses in S_{vfa}, F_{meth}, F_{feed} and $S_{\text{vs}_{\text{in}}}$ are shown.

- The upper right plot in Figure 9 illustrates that F_{meth} is not under control. Although not shown here, F_{meth} settles at steady state at approximately $t = 120$ d.

- GM is large with PI control. With predictive control, the notion of GM is questionable, since the simulated control system does not actually become unstable for any gain increase at the process input. Rather, the gain increase is seen by the UKF as an increase in $S_{\text{vs}_{\text{in}}}$. The relatively large estimate of $S_{\text{vs}_{\text{in}}}$ is used in the prediction by the predictive controller, causing a large overshoot in F_{meth} before it eventually reaches $F_{\text{meth}}^{\text{sp}}$ (plots are not shown here). This behaviour is the

same as with predictive control of F_{meth}, cf. Section 6.4.

- PM is large with PI control. With predictive control, no limit was found, i.e. the controller handles unmodelled time delays in the controlled process even as large as 10 d.

7.4   Control of F_{meth}

Controllers

The third control strategy proposed in Section 7.1 is controlling F_{meth} to a setpoint, $F_{\text{meth}}^{\text{sp}}$, set equal to the value of F_{meth} at the ultimate operating point,

19

cf. Table 2. Both predictive control based on feedback from UKF estimates and PI control based on measurement of F_{meth} are simulated.

Simulations

The simulation scenario differs from the scenario of the simulations in Section 7.3 as $S_{\text{vs}_{\text{in}}}$ is now decreased instead of increased. Decreasing $S_{\text{vs}_{\text{in}}}$ is here selected because in the corresponding response, S_{vfa} increases (in steady state), and an increase of S_{vfa} is more critical than a decrease.

In the predictive controller, τ_{s} is set as 0.05 d, and τ_{h} is 1 d.

Figure 10 shows simulated responses in S_{vfa}, F_{meth}, F_{feed} and $S_{\text{vs}_{\text{in}}}$ with predictive control based on feedback from UKF estimates, and PI control based on measurement of F_{meth}.

Results

- As seen in Figure 10, F_{meth} is much closer to $F_{\text{meth}}^{\text{sp}}$ with predictive control than with PI control.

- With both predictive control and PI control, S_{vfa} increases. Simulations over 400 d shows that S_{vfa} goes toward approximately 1.05 g/L, which is 0.25 larger than the critical value of 0.8 g/L. This makes this control strategy questionable.

What is the best control strategy for safe reactor operation?

From the results in Sections 7.3, 7.2 and 7.4 it can be concluded that the best control strategy for safe reactor operation is controlling S_{vfa} to a (fixed) setpoint using feedback from the state estimator (UKF). In the aforementioned control strategy, PI control is evaluated as better than predictive control. These two controllers give a similar disturbance compensation, but the control signal is smoother with PI control than with predictive control.

8 Conclusions

The original four states of the modified Hill model, S_{bvs}, S_{vfa}, X_{acid}, X_{meth}, and the assumed unknown organic content, $S_{\text{vs}_{\text{in}}}$, of the feedstock of a real pilot AD reactor have been mainly successfully estimated with an Unscented Kalman Filter (UKF), but with an estimation error for S_{vfa} in a part of the time interval.

These estimates, together with the model, have been applied in two different model-based control systems: The first system aims at retaining F_{meth} at a possibly time-varying setpoint, which may originate from a demanded power production by the reactor. Simulations indicate that the setpoint tracking performance of the predictive controller is considerably better while disturbance compensation, assuming that the disturbance has an unknown value, is not much better compared with PI control, confirming a well-known fact, cf. e.g. [13]. Consequently, assuming the setpoint is constant, the PI controller competes well with the predictive controller. A successful application of predictive control of the real reactor is reported.

The second control system aims at retaining the reactor at an ultimate, safe operating point where S_{vfa} has a critical maximum value. This operating point is characterized by three corresponding values of F_{feed}, S_{vfa} and F_{meth}, as found from steady state simulations of the reactor model. These operating point values can be used as setpoints in pertinent control systems. Simulations indicate that the best control solution among the three alternatives is PI control based on feedback of S_{vfa} estimated by Kalman Filter.

The results of this paper indicate that a model-based control system, using a relatively simple mechanistic dynamical reactor model, can be designed and implemented on real AD reactors.

A Abbreviations

AD: Anaerobic digestion.

BVS: Biodegradable volatile solids.

20
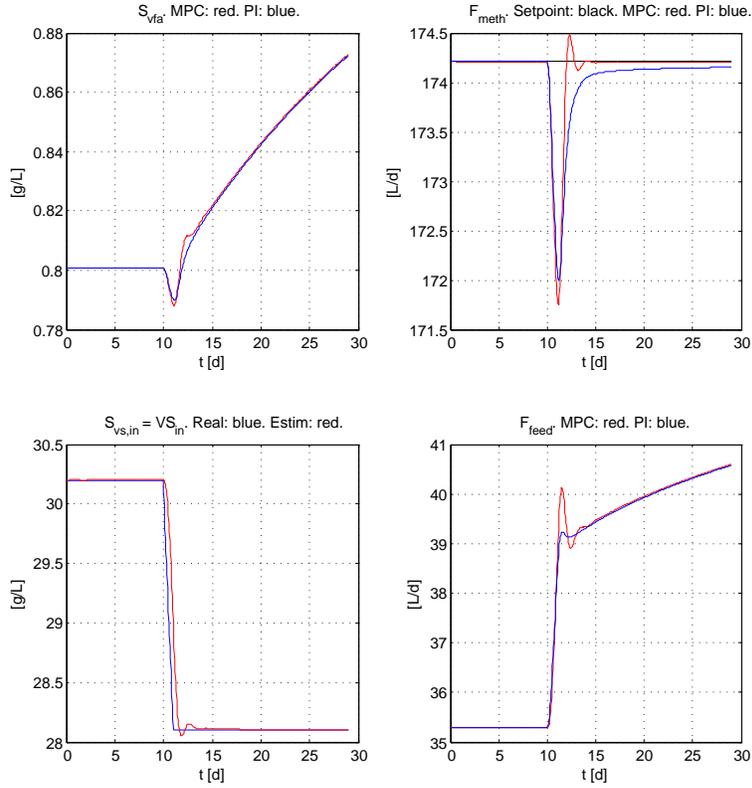
Figure 10: Predictive control and PI control of F_{meth}. The process perturbation is a change in $S_{vs_{in}}$. Simulated responses in S_{vfa}, F_{meth}, F_{feed} and $S_{\mathrm{vs_{in}}}$ are shown.

COD: Chemical oxygen demand.

EKF: Extended Kalman Filter.

FC: Flow controller.

FT: Flow transmitter (sensor).

HRT: Hydraulic retention time.

IAE: Integral of absolute error.

MPC: Model-based predictive control.

NTP: Normal Temperature and Pressure: 0 °C, 1 atm.

PI: Proportional plus integral (control).

PWM: Pulse width modulation.

TIC: Total inorganic carbon.

UKF: Unscented Kalman Filter.

VFA: Volatile fatty acids.

VS: Volatile solids.

B   Nomenclature

A_e: Amplitude of the control error and the process output (measurement).

A_{f} [(g VFA/L)/(g BVS/L)] is acidity constant.

A_u: Amplitude of the on-off control signal.

B_0 [(g BVS/L)/(g VS/L)] is biodegradability constant.

C_{du}: Cost (weight) factor of $\dot{u}^2$ in predictive control.

C_{h}: Cost (weight) factor of $e^2(\tau_{\mathrm{h}})$ in predictive control.

D [d^{-1}]: Dilution rate.

e: Control error.

f_{obj}: Objective function.

F_{feed} [L/d]: Influent or feed flow or load rate, assumed equal to effluent flow (constant volume).

F_{meth} [L CH$_4$/d]: Methane gas flow.

$F_{\mathrm{meth}}^{\mathrm{sp}}$ [L CH$_4$/d]: Setpoint of F_{meth}.

GM: Gain margin.

k: Discrete-time index.

k_1 [g BVS/(g acidogens/L)] is a yield constant.

k_2 [g VFA/(g acidogens/L)] is a yield constant.

k_3 [g VFA/(g methanogens/L)] is a yield constant.

k_5 [L/g methanogens] is a yield constant.

K_s [g BVS/L] is Monod half-velocity constant for acidogens.

K_{sc} [g VFA/L] is Monod half-velocity constant for methanogens.

K_{d} [d^{-1}] is specific death rate of acidogens.

K_{dc} [d^{-1}] is specific death rate of methanogens.

μ [d^{-1}] is reaction (growth) rate of acidogens.

μ_{c} [d^{-1}] is reaction (growth) rate of methanogens.

μ_{m} [d^{-1}] is the maximum reaction rate for acidogens.

μ_{mc} [d^{-1}] is the maximum reaction rate for methanogens.

P [kW]: Power.

P_{u} [d]: Period of oscillation.

$\hat{P}$: State estimation error covariance.

PM [degrees]: Phase margin.

Q: Process noise covariance.

R: Measurement noise covariance.

S_{vfa} [g VFA/L]: Concentration of VFA acids in reactor.

$S_{\mathrm{vfa}}^{\mathrm{est}}$ [g VFA/L]: Estimate of S_{vfa}.

$S_{\mathrm{vfa_{in}}}$ [g VFA/L]: Concentration of VFA in biodegradable part of influent.

$S_{\mathrm{vfa}}^{\mathrm{max}}$ [g VFA/L]: Upper limit of safe range of concentration of VFA in reactor.

$S_{\mathrm{vfa}}^{\mathrm{sp}}$ [g VFA/L]: Setpoint of S_{vfa}.

S_{bvs} [g BVS/L]: Concentration of BVS in reactor.

$S_{\mathrm{bvs_{in}}}$ [g BVS/L]: Concentration of BVS in influent.

$S_{\mathrm{vs_{in}}}$ [g VS/L]: Concentration of volatile solids in influent.

σ_u [L/d]: Standard deviation of control signal.

T_{reac} [°C]: Reactor temperature.

τ_{h}: Prediction horizon.

τ_{i} [d]: Controller integral time.

θ [d]: Integration variable in predictive control criterion.

V [L]: Effective reactor volume (assumed filled with liquid).

$\hat{x}$: Estimated state vector.

X_{acid} [g acidogens/L]: Concentration of acidogens.

X_{meth} [g methanogens/L]: Concentration of methanogens.

Declaration about possible conflict of interests

The authors declare that there is no conflict of interests regarding the publication of this paper.

Acknowledgements

References

[1] V. Alcaraz-Gonzalez, J. Harmand, A. Rapaport, J.P. Steyer, V. Gonzalez-Alvarez, and C. Pelayo-Ortiz. Software sensors for highly uncertain WWTPs: A new approach based on interval observers. *Water Research*, 36, 2002.

[2] G. Bastin and D. Dochain. *On-line Estimation and Adaptive Control of Bioreactors*. Elsevier, 1990.

[3] D. J. Batstone, J. Keller, I. Angelidaki, S. V. Kalyuzhnyi, S. G. Pavlovstahis, A. Rozzi, W. T. M. Sanders, H. Siegrist, and V. A. Vavilin. *Anaerobic Digestion Model No. 1, Scientific and Technical Report 15*. IWA Publising, 2002.

[4] O. Bernard, Z. Hadj-Sadok, D. Dochain, A. Genovesi, and J.P. Steyer. Dynamical model development and parameter identification for an anaerobic wastewater treatment process. *Biotechnology and Bioengineering*, 75(4), 2001.

[5] O. Bernard, M. Polit, Z. Hadj-Sadok, M. Pengov, D. Dochain, M. Estaben, and P. Labat. Advanced monitoring and control of anaerobic wastewater treatment plants: software sensors and controller for an anaerobic digester. *Water Science and Technology*, 43(7), 2001.

[6] Ph. Bogaerts and A. Vande Wouwer. Software sensors for bioprocesses. *ISA Transactions*, 42:2515–2524, 2003.

[7] D. Deublein and A. Steinhauser. *Biogas from Waste and Renewable Resources*. Wiley, 2010.

[8] D. Dochain. *Bioprocess Control*. Wiley, 2008.

[9] D. Gaida, A. L. S. Brito, C. Wolf, T. Back, M. Bongards, and S. McLoone. Optimal control of biogas plants using nonlinear model predictive control. In *22nd IET Irish Signals and Systems Conference (ISSC)*, 2011.

[10] D. Gaida, C. Wolf, C. Meyer, A. Stuhlsatz, J. Uppel, T. Back, M. Bongards, and S. McLoone. State estimation for anaerobic digesters using the adm1. *Water Science and Technology*, 66(5), 2012.

[11] G. C. Goodwin, S. F. Graebe, and M. E. Salgado. *Control System Design*. Prentice-Hall, 2001.

[12] L. Grüne and J. Pannek. *Nonlinear Model Predictive Control*. Springer-Verlag, London, 2011.

[13] R. Haber, R. Bars, and U. Schmitz. *Predictive Control in Process Engineering*. Wiley-VCH, 2011.

[14] F. Haugen. The Good Gain method for simple experimental tuning of PI controllers. *Modeling, Identification and Control*, 33(4):141–152, 2012.

[15] F. Haugen, R. Bakke, and B. Lie. Adapting dynamic mathematical models to a pilot anaerobic digestion reactor. *Modeling, Identification and Control*, 34(2):35–54, 2013.

[16] F. Haugen, R. Bakke, and B. Lie. On-off and pid control of methane gas production of a pilot anaerobic digestion reactor. *Modeling, Identification and Control*, 34(3), 2013.

[17] F. Haugen, R. Bakke, and B. Lie. Temperature control of a pilot anaerobic digestion reactor. *Modeling, Identification and Control*, 34(3), 2013.

[18] F. Haugen, R. Bakke, B. Lie, K. Vasdal, and J. Hovland. Optimization of Design and Operation of an Anaerobic Digestion Reactor. *Submitted to Computers and Electronics in Agriculture*, 2013.

[19] F. Haugen and B. Lie. Relaxed Ziegler-Nichols Closed Loop Tuning of PI Controllers. *Modeling, Identification and Control*, 34(2):83–97, 2013.

[20] D. T. Hill. Simplified monod kinetics of methane fermentation of animal wastes. *Agric. Wastes*, 5, 1983.

[21] D. T. Hill and C. L. Barth. A dynamic model for simulation of animal waste digestion. *J. Water Pollution Control Federation*, 49(10), 1977.

[22] D. T. Hill, S. A. Cobb, and J. P. Bolte. Using volatile fatty acid relationships to predict anaerobic digester failure. *Trans. ASAE*, 30:496–501, 1987.

[23] A. Husain. Mathematical models of the kinetics of anaerobic digestion - a selected review. *Biomass and Bioenergy*, 14(5/6):561–571, 1998.

[24] R. M. Jones, J. F. MacGregor, and K. L. Murphy. State estimation in wastewater engineering: Application to an anaerboic process. *Environmental Monitoring and Assessment*, 12:271–282, 1989.

[25] G. Lettinga, A. F. M. van Velsen, S. W. Hobma, W. de Zeeuw, and A. Klapwijk. Use of the upflow sludge blanket (USB) reactor concept for biological wastewater treatment, especially for anaerobic treatment. *Biotechnology and Bioengineering*, 22(4):699–734, 1980.

[26] J. Liu, G. Olsson, and B. Mattiasson. Extremum-seeking with variable gain control for intensifying biogas production in anaerobic fermentation. *Water Science and Technology*, 53(4-5):35–44, 2006.

[27] M. Madsen, J. B. Holm-Nielsen, and K. H. Esbensen. Monitoring of anaerobic digestion processes: A review perspective. *Renewable and Sustainable Energy Reviews*, 15:3141–3155, 2011.

[28] H. O. Méndez-Acosta, D. U. Campos-Delgado, R. Femat, and V. González-Álvarez. A robust feedforward/feedback control for an anaerobic digester. *Computers and Chemical Engineering*, 29:1613–1623, 2005.

[29] H. O. Méndez-Acosta, B. Palacios-Ruiz, V. Alcaraz-González, V. González-Álvarez, and J. P. García-Sandoval. A robust control scheme to improve the stability of anaerobic digestion processes. *Journal of Process Control*, 20:375–383, 2010.

[30] A. Ordace, C. M. Ionescu, Th. P. W. Vannecke, E. I. P. Volcke, I. Nascu, and R. De Keyser. Predictive control of anaerobic digestion of wastewater sludge. In *Proc of the 16th Int Conf on System Theory, Control and Computing, Romania, Oct. 12-14*, 2012.

[31] A. Puñal, L. Palazzotto, J. C. Bouvier, T. Conte, and J. P. Steyer. Automatic control of volatile fatty acids in anaerobic digestion using a fuzzy logic based approach. *Water Science and Technology*, 48(6), 2003.

[32] S. J. Qin and Th. A. Badgwell. A survey of industrial model predictive control technology. *Control Engineering Practice*, 11:733–764, 2003.

[33] L. Rodriguez, G. Ruiz, F. Molina, E. Roca, and J. M. Lema. A hydrogen-based variable-gain controller for anaerobic digestion processes. *Water Science and Technology*, 54(2):57–62, 2006.

[34] D. E. Seborg, Th. F. Edgar, and D. A. Mellichamp. *Process Dynamics and Control*. John Wiley and Sons, 2004.

[35] D. Simon. *Optimal State Estimation*. Wiley, 2006.

[36] S. Skogestad. Simple analytic rules for model reduction and PID controller tuning. *Modeling, Identification and Control*, 25(2):85–120, 2004.

[37] J. P. Steyer, J. C. Bouvier, T. Conte, P. Gras, J Harmand, and J. P. Delgenes. On-line measurements of COD, TOC, VFA, total and partial alkalinity in anaerobic digestion processes using infra-red spectrometry. *Water, Science and Technology*, 45, 2002.

[38] J. P. Steyer, P. Buffire, D. Rolland, and R. Moletta. Advanced control of anaerobic digestion processes through disturbance monitoring. *Water, Science and Technology*, 33(9):2059–2068, 1999.

[39] S. Strömberg, M. O. Possfelt, and J. Liu. Computer simulation of control strategies for optimal anaerobic digestion. *Water Science and Technology*, 67(3), 2013.

[40] G. Tchobanoglous, F. G. Burton, and H. D. Stensel. *Wastewater Engineering: Treatment and Reuse*. Metcalf and Eddy, McGraw Hill, 2003.

[41] D. Theilliol, J.-C. Ponsart, J. Harmand, C. Joina, and P. Gras. On-line estimation of unmeasured inputs for anaerobic wastewater treatment processes. *Control Engineering Practice*, 11:10071019, 2002.

[42] P. Weiland. Biogas production: current state and perspectives. *Appl Microbiol Biotechnol*, 85:849860, 2010.

Article 5 – Optimal Design and Operation of a UASB Reactor for Dairy Cattle Manure

Authors: Finn Haugen, Rune Bakke, Bernt Lie, Jon Hovland and Knut Vasdal.

Authors' roles in the article: Finn Haugen: Main ideas, implementation, and writing. Rune Bakke (co-supervisor), Bernt Lie (supervisor), Jon Hovland, and Knut Vasdal: Discussions, comments, and proof readings.

Background and methods of the article

Background

The specific aim of this article it to determine the optimal design and steady state operation of a planned full-scale AD reactor at Foss dairy farm, Norway. The optimization is based on steady state simulations of the modified Hill AD process model originally adapted to the real pilot reactor combined with models of the reactor temperature and heat exchanger temperatures based on energy balances. Alternative optimization problems are solved, i.e. alternative objective optimization functions, f_{obj}, are defined, namely maximization of produced methane gas flow, minimization of reactor volume, and maximization of power surplus. Although a specific

case is studied in the article, it can be assumed that the results obtained are useful also for other cases.

The article does not address economical optimization, which would involve constructional, capital, and operational cost. In economical optimization, the value of the reactor effluent may also be taken in to consideration. The models and results of the present paper may, however, constitute a part of the total model used in economical optimization.

Methods

The value of f_{obj} is calculated from the steady-state values of the dynamic simulations of the modified Hill model of the AD process combined with the steady-state models of the reactor temperature and the heat exchanger temperatures based on energy balances. The simulator is based on the Euler explicit numerical method implemented in for-loops. Tests indicates that a simulation using this simple implementation is executed a few hundreds times faster than an implementation in e.g. SIMULINK or with an ODE-solver. Hence, the total execution time needed to get the results in MATLAB, is dramatically reduced with the simple implementation.

The optimization problems are solved using the straightforward "brute force" (BF) method where the objective function, f_{obj}, is calculated over a grid of the optimization variables, here denoted x. The optimal value, x_{opt}, is found by searching the matrix of stored values of f_{obj} for the optimum. For each of the optimization variables, a reasonable range of each of the optimization variable is guessed. The grid resolution is adapted (manually) to each of the optimization problems, typically 1/100 of the range of the pertinent optimization variable. For illustration, Figure 14 shows a 3-D of a $f_{\text{obj}} = P_{\text{sur}}$ (power surplus) as a function of the two optimization variables, $x_1 = T_{\text{reac}}$ (reactor temperature) and $x_2 = V$ (reactor volume) for optimization problem P_{P_1} in the article. In the article, the resolution is 1/100 both for x_1 and x_2, but is 1/25 in Figure 14 to make the plot clearer. The optimum is $P_{\text{sur}}^{\max} = 55.4$ MWh/year corresponding to $x_1^{\text{opt}} = T_{\text{reac}}^{\text{opt}} = 24.9$ °C and $x_2^{\text{opt}} = V^{\text{opt}} = 137$ m^3.

The BF method can detect the global maximum (with reasonable precision), while a local optimizer like fmincon() in MATLAB may get stuck in a local maximum if the initial guess of x is unfortunate. The plot in Figure 14 shows no local optimum, however.

In general, precise solutions are desired. To obtain more precise solutions, the following alternative approaches were tested on some of the
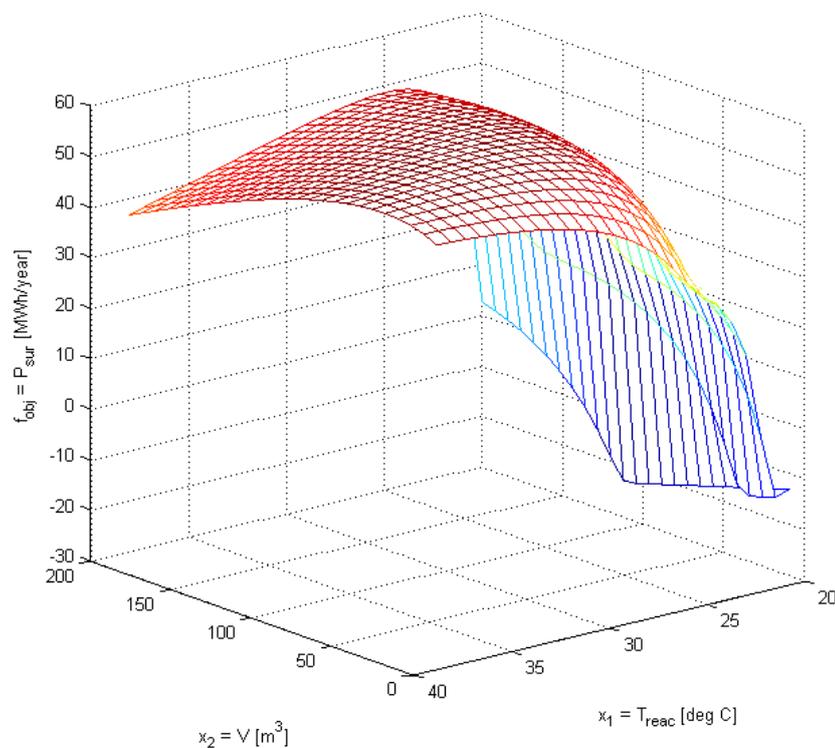
Figure 14: A 3-D plot of $f_{\mathrm{obj}} = P_{\mathrm{sur}}$ (power surplus) as a function of the two optimization variables, $x_1 = T_{\mathrm{reac}}$ (reactor temperature) and $x_2 = V$ (reactor volume) for optimization problem P_{P_1} in the article.

optimizations problems: Reducing the range, improving the resolution by increasing number of grid intervals, and applying a local optimizer, namely fmincon() in MATLAB, with the global optimal solution found with the BF method as the initial (guessed) optimal solution. The fmincon in MATLAB was used as local optimizer. It was found that the difference between using a local optimizer and the other two alternative approaches were negligible.

Several methods for global optimization exist, Edgar et al. (2001). For the present article, the BF method is considered sufficient.

Optimal Design and Operation of a UASB Reactor for Dairy Cattle Manure

F. Haugen[a,*], R. Bakke[a], B. Lie[a], J. Hovland[b], K. Vasdal[c]

[a]*Telemark University College, Kjolnes Ring 30, N-3918 Porsgrunn, Norway*
[b]*Tel-Tek, N-3918 Porsgrunn, Norway*
[c]*Telemark University College, Porsgrunn, and Foss Farm, Skien, Norway*

Abstract

Optimal design and operation of a planned full-scale UASB reactor at a dairy farm are determined using optimization algorithms based on steady state simulations of a dynamic AD process model combined with models of the reactor temperature and heat exchanger temperatures based on energy balances. Available feedstock is 6 m^3/d dairy manure produced by the herd. Three alternative optimization problems are solved: Maximization of produced methane gas flow, minimization of reactor volume, and maximization of power surplus. Constraints of the optimization problems are an upper limit of the VFA concentration, and an upper limit of the feed rate corresponding to a normal animal waste production at the farm. The most proper optimization problem appears to be minimization of the reactor volume, assuming that the feed rate is fixed at its upper limit and that the VFA concentration is at its upper limit. The optimal result is a power surplus of 49.8 MWh/y, a hydraulic retention time of 6.1 d, and a reactor temperature of 35.9 °C, assuming heat recovery with an heat exchanger, and perfect reactor heat transfer insulation. In general, the optimal solutions are improved if the ratio of the solids (biomass) retention time to the hydraulic retention time is increased.

Keywords: Anaerobic digestion, UASB reactor, Biogas, Mathematical models, Optimization, Design, Operation.

1. Introduction

The aim of this paper is to optimize the design and steady-state operation of a planned full-scale upflow anaerobic sludge blanket (UASB) reactor fed with dairy cattle waste with 6 m^3/d available feedstock. The optimization is based on a mathematical model of the reactor comprising a dynamic AD process

---

*Corresponding author
Email addresses:* `finn.haugen@hit.no` (F. Haugen), `rune.bakke@hit.no` (R. Bakke), `bernt.lie@hit.no` (B. Lie), `jon.hovland@tel-tek.no` (J. Hovland), `knut@vasdal.no` (K. Vasdal)

model combined with models of the reactor temperature and the heat exchanger temperatures based on energy balances. The biological parameters of the AD process model was estimated from experiments on a real pilot reactor using the same feedstock as the planned full-scale reactor.

Three sets of optimization problems are studied: Maximization of the produced methane gas flow, minimization of the reactor volume, and maximization of the power surplus. The biological product considered in the optimization problems is the produced methane gas. The value of the liquid effluent is not taken into account.

An early attempt to use a dynamic AD model for optimization of anaerobic digestion (AD) reactors was made by Hill (1983a). In that study, a series of simulations based on the model presented by Hill (1983b) were used to detect the optimum hydraulic retention time (HRT) that maximized the volumetric methane productivity defined as steady-state volumetric methane gas flow divided by reactor volume. The solids retention time (SRT) was assumed equal to the HRT, as in a continuous stirred tank reactor (CSTR). In the present study, the reactor is a UASB type reactor, making SRT larger than HRT.

Poels et al. (1983) reported experiences from AD processing of swine waste on a farm of typical size for Belgium. They emphasized the importance of insulation and preheating the (cold) influent by the (warm) influent was emphasized.

Bozinis et al. (1996) showed in a simulation study of a hypothetical centralized wastewater treatment plant based on co-digestion of a number of wastewater streams how optimization methods, namely nonlinear programming (NLP), can be used to identify the optimal number of CSTR AD reactors and their volumes that minimize costs. They also showed how to identify the optimal mixing of the wastewater streams that maximize the total COD (chemical oxygen demand) conversion of the plant. Simple steady-state AD process models based on Monod kinetics were assumed.

Ciotola et al. (2011) used emergy analysis to evaluate biogas production and energy generation from small-scale AD reactors. While emergy is a useful concept, we decided not to consider emergies in the present paper to keep the analysis simple.

The methods of formulation and solution of optimization problems for technical systems and industrial plants presented in (Edgar et al., 2001) have been useful for the present paper as they are applicable also to biological plants.

The outline of this paper is as follows. A description of the planned AD reactor and the optimization method used are described in Section 2. Optimization results are presented in Section 3. A discussion is given in Section 4, and conclusions are given in Section 5. Mathematical models are presented in Appendix Appendix A.

Notation

Unless otherwise stated, the numerical values of variables presented in this paper are steady-state values.

Computing tool

MATLAB (The MathWorks, Inc.) is used for numerical computations.

2. Materials and methods

2.1. The AD reactor

The AD reactor is a part of a (planned) full-scale biological plant for nutrient and energy recovery, named Foss Biolab, situated at Foss farm, Skien, Norway. A small-scale pilot plant has been in operation for about two years. The feed to the pilot reactor, which has 250 L liquid volume, is dairy waste diluted with approximately 25% water and filtered with a sieve to remove larger particles to avoid technical problems. The produced biogas consists of approximately 70% methane. A description of the pilot plant, including its monitoring and control system, is in (Haugen et al., 2013a).

Figure 1 depicts the planned full-scale reactor. (The pilot reactor has no heat exchanger.)
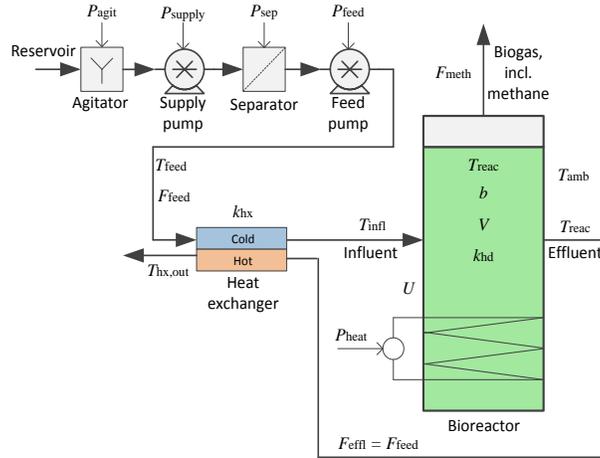
Figure 1: Planned full-scale AD reactor. (Nomenclature is in Appendix Appendix C.)

2.2. Mathematical models

The mathematical model used for optimization of the planned full-scale reactor comprises the following sub-models:

1. The modified Hill model of the AD processes adapted to the pilot reactor (Haugen et al., 2013a). For easy reference, this model is summarized in Appendix Appendix A.1.
2. A model of the reactor liquid temperature based on energy balance (Haugen et al., 2013a), summarized in Appendix Appendix A.2.
3. A model of the temperatures of heat exchanger based on energy balances. The model is derived in Appendix Appendix A.3.

2.3. Optimization objectives and variables

Figure 2 shows alternative optimization variables and objective variables. In the various optimization problems discussed in Sections 3.2 – 3.4, various subsets of these variables are used.
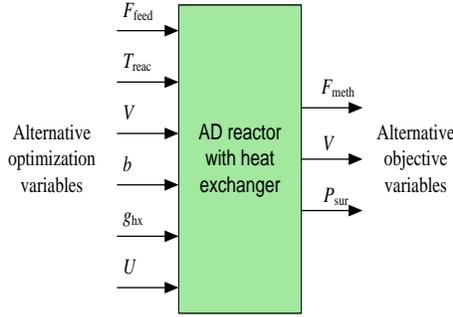

Figure 2: Alternative optimization variables and objective variables.

Optimization objectives

Figure 2 defines alternative optimization objective variables (the outputs in the block diagram):

F_{meth}, to be maximized, which is an appropriate objective if the gas is supplied (sold) to a gas grid.

V, to be minimized, which is an appropriate objective to save space and constructional and installation costs.

P_{sur}, to be maximized, which is an appropriate objective if the gas is applied for heating within the farm.

Optimization variables and their constraints

In the following, the optimization variables are characterized as either operational or design optimization variables. The former can be changed while the reactor is being operated, while design optimization variables can be changed in the design or constructional phase.

The various optimization variables shown in Figure 2, and their constraints, are described in the following.

F_{feed}: The livestock of the pertinent farm counts approximately 60 cows, each producing approximately 0.1 m^3 diluted raw waste per day. The wet fraction which remains after the separation, amounts to approximately 0.7 (weight base), which is fed to the reactor. Thus, feasible values of F_{feed} is

$$0 \leq F_{\mathrm{feed}} \leq 4.2 \mathrm{m^3/d} = F_{\mathrm{feed}}^{\mathrm{max}} \tag{1}$$

F_{feed} is an operational optimization variable.

4

T_{reac}: According to Tchobanoglous et al. (2003), most AD reactors are operated in the mesophilic temperature range which is 30–38 °C. For the planned reactor, it is of interest to also investigate temperatures below this range mainly because of the relatively cold climate in Norway. The modified Hill model is applicable for T_{reac} in the range $20 \leq T_{\mathrm{reac}} \leq 60$ °C, cf. Appendix Appendix A.1. The following range of T_{reac} is considered in this paper:

$$T_{\mathrm{reac_{min}}} = 20 \leq T_{\mathrm{reac}} \leq 38^{\mathrm{o}}\mathrm{C} = T_{\mathrm{reac}}^{\mathrm{max}} \tag{2}$$

T_{reac} is an operational optimization variable.

V: Above, it is defined as an optimization objective, but it is also used as an optimization design variable in some of the optimization problems.

b: In (Haugen et al., 2013a), the retention times ratio is defined as

$$b = \frac{\mathrm{SRT}}{\mathrm{HRT}} \tag{3}$$

where SRT is the solids (biomass) retention time, and HRT is the hydraulic retention time (HRT) which is defined as (Tchobanoglous et al., 2003):

$$\mathrm{HRT} = \frac{V}{F_{\mathrm{feed}}} \tag{4}$$

SRT can not be less than HRT. Therefore, b is lower bounded to 1. It is assumed that b does not have a larger value than 20, i.e.

$$b_{\mathrm{min}} = 1 \leq b \leq 20 = b_{\mathrm{max}} \tag{5}$$

This assumption is supported by simulations: Figure 3, plot 3a, indicates that the sensitivity of F_{meth} to b is relatively small for b above 20.

b is a design optimization variable, but may be changed after the reactor has been set into operation. As shown in Section 3, it is beneficial in the optimization scenarios that b is as large as possible. Dairy waste is relatively rich on particles, making it difficult to obtain a large b. For the real pilot reactor, b is estimated from time-series as 2.9 (Haugen et al., 2013a).

g_{hx}, the heat exchanger coefficient, is defined with eq. (A.14) in Appendix Appendix A. g_{hx} is a design optimization variable. In the optimization problems, g_{hx} has value either ∞ (perfect heat exchange) or 0 (no heat exchange). On a real heat exchanger, perfect heat exchange can of course not be obtained, corresponding to a limited value of g_{hx}. Still, it is decided to assume an ideal heat exchanger to avoid complicating the analysis. Also, the principal difference between applying heat exchange and not, is expected to be principally the same for a real heat exchanger as for an ideal heat exchanger.

U, the specific heat transfer coefficient of the reactor, is calculated from the value of the real pilot reactor as explained in Appendix Appendix A. $U = 0$ implies perfect thermal insulation of the reactor walls. U is a design optimization variable.

Although not an optimization variable, the constraints on S_{vfa} is an important optimization constraint. According to the discussion in (Haugen et al., 2013b) based on the results in (Hill et al., 1987), the range of S_{vfa} for safe reactor operation is

$$S_{\text{vfa}} \leq 0.8\text{g/L} = S_{\text{vfa}}^{\max} \tag{6}$$

2.4. Optimization algorithm

The optimization problems are solved using the straightforward "brute force" (BF) method where the objective function, f_{obj}, is calculated over a grid of the optimization variables, here x. The optimal value, x_{opt}, is found by searching the matrix of stored values of f_{obj} for the optimum. For each of the optimization variables, a reasonable range is guessed. The grid resolution is adapted (manually) to each of the optimization problems. For optimization variable x_i, the resolution is typically selected as $1/N_{x_i}$ where $N_{x_i} = 100$ (number of grid intervals).

In general, precise solutions are desired. To obtain more precise solutions, the following alternative approaches were tested on some of the optimizations problems: Reducing the range, improving the resolution by increasing number of grid intervals, and applying a local optimizer (Edgar et al., 2001) with the global optimal solution found with the BF method as the initial (guessed) optimal solution. The fmincon in MATLAB was used as local optimizer. It was found that the difference between using a local optimizer and the other two alternative approaches were negligible. The computer program implementation of the BF method is considerably simpler and more flexible (scalable) than an implementation using fmincon. Therefore, the BF method, without any local optimizer, is the selected method in this paper.

The value of f_{obj} is calculated from the steady-state of the dynamic simulations of the modified Hill model of the AD process combined with the steady-state models of the reactor temperature and the heat exchanger temperatures based on energy balances. The simulator is based on the Euler explicit numerical method implemented in for-loops. This approach to find f_{obj} is similar to that in (Rivas et al., 2008) where a wastewater treatment plant is optimized. There, the GRG2[1] algorithm implemented in Microsoft Excel is used.

3. Results

3.1. Summary

Table 1 summarizes the results of the optimization problems presented in the following sections. Units of the table entries are defined in Appendix Appendix

---

[1]Generalized Reduced Gradient

C. Underlines denote values of the optimization variables. Frames denote objective variables.

The optimization problems are categorized as follows:

- In problems P_{F_i}, F_{meth} is maximized.[2]

- In problems P_{V_j}, V is minimized.

- In problems P_{P_k}, P_{sur} is maximized.

The power surplus, P_{sur}, is calculated with eq. (A.20), where all power terms are in units of MWh/y.

In Table 1, γ_{meth} is the gas productivity:

$$\gamma_{meth} = \frac{F_{meth}}{F_{feed}} \tag{7}$$

and γ_P is here defined as the power surplus productivity:

$$\gamma_P = \frac{P_{sur}}{N_{LU}} \tag{8}$$

In Table 1, $g_{hx} = \infty$ corresponds to using an ideal heat exchanger for preheating the feed, while $g_{hx} = 0$ corresponds to no such preheating (no heat exchanger).

In each of the optimization problems, both T_{amb} and T_{feed} are set to 10 °C.[3]

Implementation of optimal solutions

Due to inevitable disturbances, the optimal solutions should be retained with feedback control. Control of the pilot reactor is studied in (Haugen et al., 2013b) and (Haugen et al., 2013c).

The implementation of feedback control may not be trivial. For example, in the optimization problems P_{V_1}-P_{V_5}, cf. Table 2, S_{vfa} is assumed being retained at $S_{vfa}^{max} = 0.8$ g/L, its setpoint. Since S_{vfa} is not measured online, the control feedback can not be based on a measurement. Instead, feedback can be made from an estimate of S_{vfa} calculated by a state estimator (Kalman filter), which requires a dynamic model of the AD processes (Haugen et al., 2013a).

3.2. Maximization of F_{meth}

To maximize F_{meth}, the following variables are considered as optimization variable candidates in the optimization problems discussed in the following sections: F_{feed}, T_{reac}, b, and V. To provide insight into the steady-state behaviour of the reactor when these variables are varied, Figure 3 shows F_{meth} and S_{vfa} vs.

---

[2]P_{F_5} is actually not an optimization problem, but is included for demonstration purposes, cf. Section 3.2.

[3]In an online system for optimal reactor operation, online temperature measurements may be used as inputs to the optimizer.

each of these variables.[4] S_{vfa} is plotted since its value determines whether the reactor is in a safe operation condition, or not, cf. Section 2.3. The simulations are based on the modified Hill model adapted to the pilot reactor applied to the planned full-scale reactor. The reactor volume is set as $V = 10$ m^3 which is assumed a possible, but not necessarily optimal, volume of an AD reactor fed with animal waste at Norwegian farms. The magenta circle with star in each plot corresponds to the steady-state operating point given in Table 2. This operating point is more or less randomly chosen, but so that ineq. (6) is satisfied: $S_{\mathrm{vfa}} = 0.66$ g/L $\leq S_{\mathrm{vfa}}^{\mathrm{max}} = 0.8$ g/L. Along the abscissa axes in Figure 3, green color represents safe operation, i.e. $S_{\mathrm{vfa}} \leq S_{\mathrm{vfa}}^{\mathrm{max}}$ there, ineq. (6). Conversely, red color along the abscissa axes corresponds to $S_{\mathrm{vfa}} > S_{\mathrm{vfa}}^{\mathrm{max}}$, i.e. unsafe operation. The red vertical lines in Figure 3 correspond to $S_{\mathrm{vfa}} = S_{\mathrm{vfa}}^{\mathrm{max}}$.

Comments to the plots of Figure 3 regarding each of the four optimization variables:

- F_{feed}: Plot 1a shows that the maximum F_{meth} is obtained with $F_{\mathrm{feed}} = 3.34$ m^3/d. However, this maximum is regarded as non-feasible since ineq. (6) is violated, cf. plot 1b.

  As F_{feed} is increased beyond $F_{\mathrm{feed}} = 3.34$ m^3/d, F_{meth} decreases, which can be explained by a "wash-out" of the methanogens. For F_{feed} beyond 5.5 m^3/d, no methane gas is produced.

- T_{reac}: Plot 2a shows that F_{meth} is monotonically increasing with T_{reac}. Plot 2b shows that a reduction of T_{reac} increases S_{vfa}. If T_{reac} is too small, ineq. (6) is violated.

- b: Plot 3a shows that F_{meth} is monotonically increasing with b. Plot 3b shows that a relatively small b will violate ineq. (6). Although b can be regarded as an optimization variable, it is rather a design parameter than an operational parameter.

- V: Plot 4a shows that F_{meth} is monotonically increasing with V. Plot 4b shows that a relatively small V will violate ineq. (6). Manipulating the reactor volume during reactor operation is theoretically possible, but hardly a practical option.

Optimization problems:
$\mathbf{P_{F_1}}$:

$$\max_{F_{\mathrm{feed}}, T_{\mathrm{reac}}} F_{\mathrm{meth}}$$

b and V are fixed. Results are: The optimal F_{feed} of 1.63 m^3/d is less than $F_{\mathrm{feed}}^{\mathrm{max}}$, which is due to the limitation by ineq. (6). The optimal T_{reac} is 38 °C which is the maximum acceptable value.

---

[4]The simulations are run over a time interval of 1000 d which is sufficient for the dynamic $F_{\mathrm{meth}}(t)$ to get into an approximate steady state.

Table 1: Results of various optimization problems. Underlines denote values of the optimization variables. Frames denote objective variables. ($6.5\text{e}4 = 6.5 \cdot 10^4$.)

	P_{F_1}	P_{F_2}	P_{F_3}	P_{F_4}	P_{F_5}	P_{V_1}	P_{V_2}	P_{V_3}	P_{V_4}	P_{V_5}	P_{P_1}	P_{P_2}	P_{P_3}	P_{P_4}	P_{P_5}
F_{feed}	1.63	4.2	4.2	4.2	4.2	4.2	4.2	4.2	4.2	4.2	4.2	4.2	4.2	1.63	1.14
T_{reac}	38	38	38	25	25	38	38	35.9	35.9	32.1	24.9	25.5	21.5	38	27.9
V	10	10	700	10	10	25.5	25.5	28.3	28.3	5.2	137	39.5	58.5	10	10
b	2.9	20	2.9	20	2.9	2.9	2.9	2.9	2.9	20	2.9	20	20	2.9	2.9
g_{hx}	∞	∞	∞	∞	∞	0	∞	∞	∞	∞	∞	∞	0	∞	0
U	6.5e4	6.5e4	6.5e4	6.5e4	6.5e4	6.5e4	6.5e4	6.5e4	0	6.5e4	6.5e4	6.5e4	6.5e4	6.5e4	6.5e4
S_{vfa}	0.80	0.38	0.19	0.79	5.2	0.80	0.80	0.80	0.80	0.80	0.56	0.43	0.56	0.80	0.80
F_{meth}	8.09	25.6	27.8	20.8	0	20.7	20.7	20.7	20.7	20.7	23.5	25.0	23.6	8.09	5.61
HRT	6.1	2.4	167	2.4	2.4	6.1	6.1	6.7	6.7	1.23	32.5	9.4	13.9	6.1	8.8
γ_{meth}	4.96	6.1	6.62	4.96	0	4.94	4.94	4.94	4.94	4.94	5.60	5.96	5.61	4.96	4.94
P_{meth}	29.4	93.0	101	75.6	0	75.3	75.3	75.3	75.3	75.3	85.5	91.0	85.5	29.4	20.4
P_{heat}	14.5	29.8	105.6	15.6	15.6	58.9	33.9	32.0	23.2	22.2	27.8	20.4	26.9	14.5	14.1
P_{agit}	0.57	1.46	1.46	1.46	1.46	1.46	1.46	1.46	1.46	1.46	1.46	1.46	1.46	0.57	0.39
P_{supply}	0.057	0.15	0.15	0.15	0.15	0.15	0.15	0.15	0.15	0.15	0.15	0.15	0.15	0.057	0.040
P_{sep}	0.28	0.73	0.73	0.73	0.73	0.73	0.73	0.73	0.73	0.73	0.73	0.73	0.73	0.28	0.20
P_{feed}	0.0038	0.010	0.040	0.010	0.010	0.013	0.013	0.014	0.014	0.0078	0.014	0.015	0.018	0.0038	0.0026
P_{sur}	14.0	60.9	-7.0	57.3	-18	14.1	39.1	41.0	49.8	50.8	55.4	68.2	56.3	14.0	5.7
γ_{P}	0.23	1.02	-0.12	0.96	-0.3	0.24	0.65	0.68	0.83	0.85	0.92	1.14	0.94	0.23	0.095

Table 2: Steady-state operating point of the AD reactor used in simulations, as explained in the text. Units are defined in Appendix Appendix C.

Variable	Value
V	10
T_{reac}	35
b	2.9
$S_{\text{vs}_{\text{in}}}$	30.2
F_{feed}	1.13
F_{meth}	6.00
S_{bvs}	3.42
S_{vfa}	0.66
X_{acid}	2.03
X_{meth}	0.39
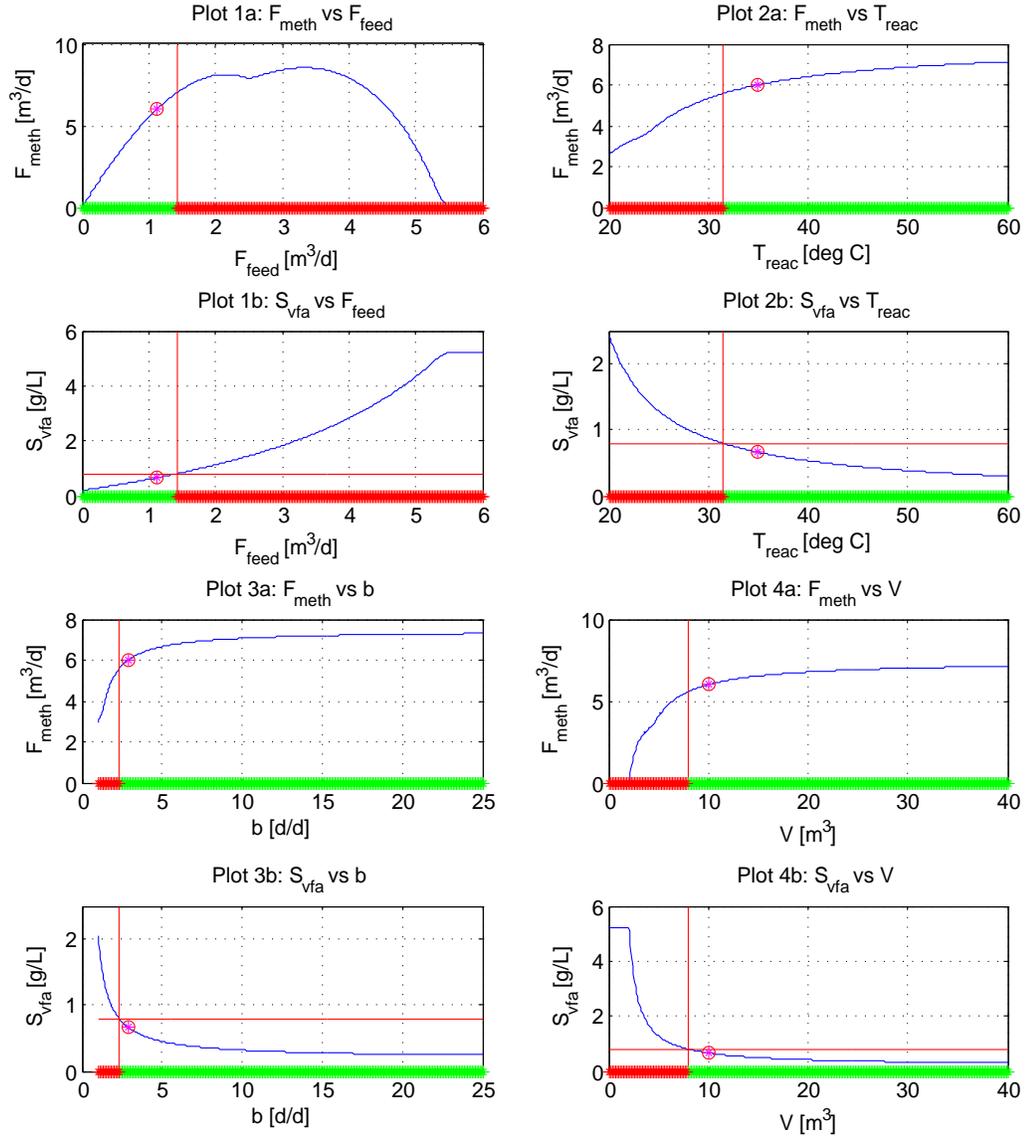
Figure 3: F_{meth} and S_{vfa} as function of F_{feed}, T_{reac}, b and V. Along the abscissa axes, green colour represents safe operation, i.e. $S_{\mathrm{vfa}} \leq S_{\mathrm{vfa}}^{\mathrm{max}}$. Red colour corresponds to $S_{\mathrm{vfa}} > S_{\mathrm{vfa}}^{\mathrm{max}}$, i.e. unsafe operation. The red vertical lines correspond to $S_{\mathrm{vfa}} = S_{\mathrm{vfa}}^{\mathrm{max}}$.

$\mathbf{P_{F_2}}$:

$$\max_b F_\text{meth}$$

F_feed is fixed at F_feed^max. Results are: The optimal b is 20, its upper limit. F_meth is $25.6/8.09 = 3.2$ times larger than in the previous case. P_sur is $60.9/14.0 = 4.4$ times larger than in the previous case.

$\mathbf{P_{F_3}}$:

$$\max_V F_\text{meth} \tag{9}$$

F_feed is set to F_feed^max. The upper limit of V is set to 700 m^3, a very large value. Results are: The optimal V is 700 m^3, its upper limit, corresponding to HRT $= 167$ d, a very large value. This optimal V is probably impractical to implement. Furthermore, P_sur is negative, due to the large heat loss, seen indirectly in the large P_heat.

$\mathbf{P_{F_4}}$:

$$\max_b F_\text{meth} \tag{10}$$

T_reac is fixed at 25 °C, which is a temperature in the lower end of the mesophilic range, but assumed a plausible temperature for AD reactor operation. This optimization problem is similar to P_{F_2}, except T_reac is there fixed at 38 °C. Results are: The optimal b is 20, its upper limit, as in P_{F_2}. Both F_meth and P_sur are comparable with the respective values for P_{F_2}. Hence, it is demonstrated that it is beneficial to have a large b since it allows for a lower reactor temperature.

$\mathbf{P_{F_5}}$:

This scenario is actually not an optimization problem as all parameters are fixed. Its purpose is to demonstrate the importance of parameter b. The conditions are as in P_{F_4}, except b is now set as 2.9, which is the value estimated for the real pilot reactor. Simulations show that reactor failure can be expected since $S_\text{vfa} = 5.2$ g/L, which is (much) larger than the critical limit $S_{vfa}^\text{max} = 0.8$ g/L. Simulations (not represented in Table 1) show that, also with T_reac set as 38 °C, and other parameters being the same, reactor failure can be expected. Comparing with P_{F_4}, where $b = 20$, these simulations demonstrate the importance of having a large b. This scenario also demonstrates that care must be taken when selecting V for a given b and a fixed F_feed, to prevent reactor failure.

Conclusions (maximization of F_meth):

- In general, T_reac should be set to $T_\text{reac}^\text{max} = 38$ °C, and b should be as large as possible.

- Furthermore, V should be set to its maximum value. However, large V decreases P_sur due to increased thermal loss. Of course, increasing V also increases constructional and capital costs, but these factors are not discussed in this paper.

- In most cases, increasing F_feed gives increasing F_meth. However, the limitation $S_\text{vfa} \leq S_\text{vfa}^\text{max}$ sets an upper limit of F_feed. This upper limit of F_feed may be less than F_feed^max, the (normal) animal waste production.

11

- Assuming $F_{\text{feed}} = F_{\text{feed}}^{\max}$. By selecting a sufficient large T_{reac}, V and/or b, $S_{\text{vfa}} \leq S_{\text{vfa}}^{\max}$ can be maintained. However, If T_{reac} and b are fixed, the optimal V may become very large.

- Maximization of F_{meth} is a questionable optimization problem since there it may have two unfortunate results: (1) Assuming limited T_{reac}, V and/or b, the F_{feed} that maximizes F_{meth} may become less than $F_{\text{feed}}^{\max}$ implying that only a part of the bioresource volume is utilized. (2) Assuming $F_{\text{feed}} = F_{\text{feed}}^{\max}$, the "optimal" V may become impractically large.

- Assuming specifically $V = 10$ m^3 which is a plausible reactor size for Norwegian farms: Assuming $F_{\text{feed}} = F_{\text{feed}}^{\max} = 4.2$ m^3/d, and $T_{\text{reac}} = 25$ °C, it is necessary that b has a large value, here 20, for the reactor to operate safely. With $b = 20$, the difference in F_{meth} and P_{sur} between $T_{\text{reac}} = 25$ °C and $T_{\text{reac}} = 38$ °C is not large. However, if $b = 2.9$ as estimated for the real pilot reactor, reactor failure may occur both with $T_{\text{reac}} = 25$ °C and $T_{\text{reac}} = 38$ °C. Consequently, a large b is very important.

3.3. Minimization of V

Although constructional and capital costs are not included explicitly in the optimization problems discussed in this paper, it is, beneficial to minimize the reactor volume, V. Figure 3, plots 4a and b, show that, for a given F_{feed}, there is a lower limit of V while satisfying ineq. (6). In the present section, the optimization problems aim at finding the minimum V under various conditions, while satisfying ineq. (6). In each of the problems, F_{feed} is set $F_{\text{feed}}^{\max}$. Note that minimizing V assuming that F_{feed} is constant, is equivalent to minimizing HRT, cf. the definition of HRT, eq. (4). Neither F_{meth} nor P_{sur} are included in theses optimization problems, but their values are presented, cf. Table 1.

Optimization problems:

P_{V_1}:

$$\min_{V} V, \text{ without heat exchanger} \tag{11}$$

Here, heat exchanger is not used. T_{reac} is fixed at $T_{\text{reac}}^{\max}$. Result: $P_{\text{sur}} = 14.1$ MWh/y.

P_{V_2}:

$$\min_{V} V, \text{ with heat exchanger} \tag{12}$$

Here, a heat exchanger is used. This problem is otherwise similar to P_{V_1}, and V is therefore the same. Result: P_{sur} becomes 39.1 MWh/y, a considerable increase comparing with P_{V_1}. This indicates that using a heat exchanger is beneficial.

P_{V_3}:

$$\min_{V, T_{\text{reac}}} V, \text{ with heat exchanger} \tag{13}$$

12

T_{reac} is now an optimization variable (in addition to V). The results in this problem are to be compared with P_{V_3}, see below.

P_{V_4}:

$$\min_{V, T_{\text{reac}}} V, \text{ with heat exchanger and full insulation} \qquad (14)$$

This problem is similar to P_{V_3}, but with full thermal insulation of the reactor walls, i.e. $U = 0$, which corresponds to $G = 0$ in eqs. (A.10) and (A.17). Results: The optimal V becomes 28.3 m^3, the same as in P_{V_3}. The optimal T_{reac} is 35.9 °C, as in P_{V_3}. However, P_{sur} becomes larger, 49.8 vs. 41.0 MWh/y, indicating that good insulation is beneficial.

P_{V_5}:

$$\min_{V, T_{\text{reac}}} V, \text{ with heat exchanger and full insulation} \qquad (15)$$

This problem is similar to P_{V_3}, but now b is set to $b_{\max} = 20$. Results: The optimal T_{reac} is 32.1 °C. The minimum V is 5.2 m^3, which is considerably smaller than in the other optimization problems. This indicates that it is (very) beneficial to have a large b.

Conclusions (minimization of V):

Assuming $b = 2.9$ as for the real pilot reactor, the following conditions (P_{V_4}) is recommended for design: Assuming $F_{\text{feed}} = F_{\text{feed}}^{\max}$, $V = 28.3$ m^3 is appropriate, corresponding to HRT = 6.7 d. Furthermore, the optimal T_{reac} is 35.9 °C.

The larger b, the smaller the minimum V.

3.4. Maximization of P_{sur}

The power surplus, P_{sur}, is calculated with eq. (A.20). In optimization problems P_{P_1}, P_{P_2} and P_{P_3}, F_{feed} is set to $F_{\text{feed}}^{\max}$.

Optimization problems:

P_{P_1}:

$$\max_{V, T_{\text{reac}}} P_{\text{sur}}$$

Results are: The optimal V is 137 m^3, giving HRT = 32.5 d, a relatively large value. The optimal T_{reac} is 24.9 °C, a relatively small value.

P_{P_2}:

$$\max_{b, V, T_{\text{reac}}} P_{\text{sur}}$$

F_{feed} is set to $F_{\text{feed}}^{\max}$. Comparison is made with Problem P_{P_3}, see below.

P_{P_3}:

$$\max_{V, T_{\text{reac}}} P_{\text{sur}}, \text{ without heat exchanger}$$

This problem is the same as P_{P_2}, but now without heat exchanger. Results are: Comparing P_{P_3} and P_{P_2} shows that by using an heat exchanger, P_{sur} is increased by 21% and V is reduced by 32%.

P_{P_4}:

$$\max_{F_{\text{feed}}, T_{\text{reac}}} P_{\text{sur}}, \text{ with heat exchanger}$$

V is fixed at 10 m^3, and b at 2.9. Thus, P_{P_4} is the same as P_{P_1}, except in P_{P_1}, F_{meth} is to be maximized. Results are: Comparing P_{P_4} and P_{P_1} shows that when an heat exchanger is installed, maximizing P_{sur} or F_{meth} gives the same optimal solution. Only (1.63 m^3/d)/(4.2 m^3/d) = 39% of the available feedstock is used, which may make this solution unacceptable.

P_{P_5}:

$$\max_{F_{\text{feed}}, T_{\text{reac}}} P_{\text{sur}}, \text{ without heat exchanger}$$

This problem is the same as P_{P_4}, but now without heat exchanger. Result: Comparing P_{P_5} and P_{P_4} shows that using an heat exchanger increases P_{sur}. Only (1.14 m^3/d)/(4.2 m^3/d) = 27% of the available feedstock is used, which may be unacceptable.

Conclusions (maximization of P_{sur})

P_{sur} increases considerably if b is increased and if a heat exchanger is used.

Assuming $b = 2.9$ as for the present pilot reactor and F_{feed} fixed at $F_{\text{feed}}^{\max}$, a maximum P_{sur} is obtained with $V = 137$ m^3, corresponding to HRT = 32.5 d. However, this large value of V may be impractical to realize.

With V fixed at 10 m^3, assumed a plausible reactor size, and b assumed 2.9, as for the pilot reactor, P_{sur} is maximized by F_{feed} equal to only 39% of $F_{\text{feed}}^{\max}$. Hence, only a small part of biological resources is utilized.

The maximum P_{sur} is 68.2 MWh/y is obtained in P_{P_2}, corresponding to power surplus productivity $\gamma_P = 1.14$ (MWh/y)/LU. This is also the maximum over all of the optimization problems reported in Table 1.

3.5. Summary of results

Below is a summary of the results of the three optimization problems discussed in Sections 3.2-3.4.

Maximization of F_{meth}:

T_{reac} and b should have values as close as possible to their assumed upper limits, 38 °C and 20, respectively.

If F_{feed} is fixed at $F_{\text{feed}}^{\max}$, the maximum F_{meth} is obtained with a very large V, which may be impractical to implement.

In most cases, increasing F_{feed} gives increasing F_{meth}. However, the limitation $S_{\text{vfa}} \leq S_{\text{vfa}}^{\max}$ sets an upper limit of F_{feed}. This upper limit of F_{feed} may be less than $F_{\text{feed}}^{\max}$, the (normal) animal waste production.

The two conclusions above imply that maximization of F_{meth} is a questionable optimization problem.

Assuming specifically $V = 10$ m^3 which is a plausible reactor size for Norwegian farms: Assuming $F_{\text{feed}} = F_{\text{feed}}^{\max} = 4.2$ m^3/d, and $T_{\text{reac}} = 25$ °C, it is necessary that b has a large value, e.g. 20, for the reactor to operate safely.

14

With $b = 20$, the difference in F_{meth} and P_{sur} between $T_{\text{reac}} = 25$ °C and $T_{\text{reac}} = 38$ °C is not large. However, if $b = 2.9$ as estimated for the real pilot reactor, reactor failure may occur both with $T_{\text{reac}} = 25$ °C and $T_{\text{reac}} = 38$ °C.

Minimization of V:

The minimization assumes the following equality constraints: $S_{\text{vfa}} = S_{\text{vfa}}^{\text{max}}$, and $F_{\text{feed}} = F_{\text{feed}}^{\text{max}}$. Assuming $b = 2.9$ as for the real pilot reactor, the minimum V is 28.3 m^3, corresponding to HRT = 6.7 d. Furthermore, the optimal T_{reac} is 35.9 °C.

With a larger b, the minimum V is reduced.

Maximization of P_{sur}:

P_{sur} increases considerably if b is increased and if a heat exchanger is used.

Assuming $b = 2.9$ as for the present pilot reactor and F_{feed} fixed at $F_{\text{feed}}^{\text{max}}$, a maximum P_{sur} is obtained with $V = 137$ m^3, corresponding to HRT = 32.5 d. However, this large value of V may be impractical to realize.

With V fixed at 10 m^3, assumed a plausible reactor size, and b assumed 2.9, as for the pilot reactor, P_{sur} is maximized with F_{feed} equal to only 39% of $F_{\text{feed}}^{\text{max}}$, which may be an unacceptable solution as not all of the biological resources is utilized.

4. Discussion

The optimization results in this paper are based on three mathematical models – the AD process model, the model of the reactor temperature, and model of the heat exchanger temperatures. The first two models have been adapted quite successfully to the real pilot reactor (Haugen et al., 2013a). The latter has not been adapted to a physical heat exchanger, and therefore its accuracy can not be stated. However, the underlying modeling principles are assumed reasonable. Thus, although it can not be claimed that the optimization results found are accurate, it can be expected that the results provide useful knowledge about optimal reactor design and operation.

The modified Hill model, presented in Appendix Appendix A.1, is a relatively simple AD process model. In this model, S_{vfa} is the only variable which can be used to define the conditions for safe reactor operation, and $S_{\text{vfa}}^{\text{max}} = 0.8$ g/L has been used as a constraint in the optimization problems discussed in this paper. In other applications, e.g. AD reactors fed with swine waste, it may be important to take other constraints taken into account, e.g. maximum ammonia concentration, minimum pH, maximum propionic to acetic acid ratio, and maximum ratio of intermediate alkalinity over total alkalinity. To these ends, more comprehensive AD models are needed. Overviews of various AD models are given by e.g. Gavala et al. (2003), Lyberatos and Skiadas (1999), and Strömberg (2010). A short discussion of relevant models are also given by (Haugen et al., 2013a). Although the model used in the present paper is relatively simple, we think that the approach to optimization used is applicable to alternative AD models.

The present study does not address economical optimization, which, in general, involves constructional, capital, and operational cost. The models and results of the present paper may, however, constitute a part of the total model used in economical optimization.

5. Conclusions

Optimal design and operation of a planned full-scale UASB reactor at a dairy farm have been determined using optimization algorithms based on steady state simulations of a dynamic AD process model combined with models of the reactor temperature and the heat exchanger temperatures based on energy balances. Available feedstock is 6 m^3/d dairy waste.

The optimization solutions have been found using the straightforward "brute force" (BF) method which is based on a scan for the global optimal solution over a grid of the optimization variables. The grid resolution is typically selected as 1/100 of the range of the pertinent variable, giving a sufficient precision of the optimal solution.

For the given AD reactor and its mathematical model, alternative optimization objectives are maximizing F_{meth}, minimizing V, and maximizing P_{sur}. Optimization variables candidates are F_{feed}, T_{reac}, b, V, g_{hx}, and U. The optimization algorithm takes into account the following constraints: $S_{\text{vfa}} \leq S_{\text{vfa}}^{\max}$, and $F_{\text{feed}} \leq F_{\text{feed}}^{\max}$.

The results indicate that any optimal solution is improved, for example, the maximum P_{sur} is increased, if b is increased, if energy is recovered with a heat exchanger, and if the reactor is well insulated.

Evaluated over all of the optimization problems studied, the maximum P_{sur} is 68.2 MWh/y, corresponding to power surplus productivity $\gamma_{\text{P}} = 1.14$ (MWh/y)/LU.

Appendix A. Mathematical models

Values of model parameters having constant values are given in Appendix Appendix C.

Appendix A.1. Model of the AD process

The mathematical model of the AD processes in the reactor is a modification of the model in (Hill, 1983b), adapted to the pilot reactor (Haugen et al., 2013a). The model is based on material balances of biodegradable volatile solids, volatile fatty acids, acidogens and methanogens, and a calculation of the produced methane gas flow. The model is summarized below.

Material balances:

$$\dot{S}_{\text{bvs}} = (B_0 S_{\text{vs}_{\text{in}}} - S_{\text{bvs}}) \frac{F_{\text{feed}}}{V} - \mu k_1 X_{\text{acid}} \tag{A.1}$$

$$\dot{S}_{\text{vfa}} = (A_{\text{f}} B_0 S_{\text{vs}_{\text{in}}} - S_{\text{vfa}}) \frac{F_{\text{feed}}}{V} + \mu k_2 X_{\text{acid}} - \mu_c k_3 X_{\text{meth}} \tag{A.2}$$

$$\dot{X}_{\text{acid}} = \left(\mu - K_d - \frac{F_{\text{feed}}/b}{V} \right) X_{\text{acid}} \tag{A.3}$$

$$\dot{X}_{\text{meth}} = \left(\mu_c - K_{dc} - \frac{F_{\text{feed}}/b}{V} \right) X_{\text{meth}} \tag{A.4}$$

Methane gas production:

$$F_{\text{meth}} = V \mu_c k_5 X_{\text{meth}} \tag{A.5}$$

Reaction rates:

$$\mu = \mu_m \frac{S_{\text{bvs}}}{K_s + S_{\text{bvs}}} \tag{A.6}$$

$$\mu_c = \mu_{mc} \frac{S_{\text{vfa}}}{K_{sc} + S_{\text{vfa}}} \tag{A.7}$$

$$\mu_m = \mu_{mc} = 0.013 T_{\text{reac}} - 0.129 \quad (20°\text{C} < T_{\text{reac}} < 60°\text{C}) \tag{A.8}$$

Appendix A.2. Model of reactor temperature

The mathematical model able to predict T_{reac} is based on energy balance model of the pilot reactor (Haugen et al., 2013a). For easy reference in the present paper, the model is reviewed here:

$$\dot{T}_{\text{reac}} = \frac{1}{c\rho V} [P_{\text{heat}} + c\rho F_{\text{feed}} (T_{\text{infl}} - T_{\text{reac}}) + G (T_{\text{amb}} - T_{\text{reac}})] \tag{A.9}$$

The corresponding steady-state version of this model is

$$P_{\text{heat}} = c\rho F_{\text{feed}} (T_{\text{reac}} - T_{\text{infl}}) + G (T_{\text{reac}} - T_{\text{amb}}) \tag{A.10}$$

which is combined with the heat exchanger model as described below.

In eq. (A.10), G is calculated assuming that the reactor is a vertical cylinder of diameter d and height h. Their ratio is $k_{\text{hd}} = h/d$, which can be regarded as an optimization variable. In the context of selected optimization problems described in previous sections, it was found that $k_{\text{hd}} = 1$ is optimal, and therefore $k_{\text{hd}} = 1$ is used throughout this paper.

For simplicity, it is assumed that the heat conduction takes place at all sides of the cylinder. The area-specific heat transfer conductivity, U, is assumed equal to that of the pilot reactor (Haugen et al., 2013a).

Appendix A.3. Model of heat exchanger temperatures

The mathematical modelling of the heat exchanger shown in Figure 1 assumes that the liquid flows are equal to the feed flow, F_{feed}, in all pipelines.

It is assumed that the heat exchanger consists of two homogeneous volumes: the product volume and the heating medium volume, respectively. The energy balances are:

$$c\rho V_{\mathrm{p}}\dot{T}_{\mathrm{infl}} = c\rho F_{\mathrm{feed}}\left(T_{\mathrm{feed}} - T_{\mathrm{infl}}\right) + G_{\mathrm{hx}}\left(T_{\mathrm{hx_{out}}} - T_{\mathrm{infl}}\right) \tag{A.11}$$

$$c\rho V_{\mathrm{h}}\dot{T}_{\mathrm{hx_{out}}} = c\rho F_{\mathrm{feed}}\left(T_{\mathrm{reac}} - T_{\mathrm{hx_{out}}}\right) + G_{\mathrm{hx}}\left(T_{\mathrm{infl}} - T_{\mathrm{hx_{out}}}\right) \tag{A.12}$$

In this paper, the steady-state version of this model is used in the analysis, i.e. the time-derivatives are set to zero. Eliminating $T_{\mathrm{hx_{out}}}$ from the resulting steady-state equations yields

$$T_{\mathrm{infl}} = \frac{1 + g_{\mathrm{hx}}}{1 + 2g_{\mathrm{hx}}}T_{\mathrm{feed}} + \frac{g_{\mathrm{hx}}}{1 + 2g_{\mathrm{hx}}}T_{\mathrm{reac}} \tag{A.13}$$

where

$$g_{\mathrm{hx}} = \frac{G_{\mathrm{hx}}}{c\rho F_{\mathrm{feed}}} \tag{A.14}$$

Some special cases of eq. (A.13) are:

- $g_{\mathrm{hx}} = 0$, i.e. no heat exchange:

$$T_{\mathrm{infl}} = T_{\mathrm{feed}} \tag{A.15}$$

- $g_{\mathrm{hx}} = \infty$, i.e. an extremely high, or ideal, heat exchange:

$$T_{\mathrm{infl}} = \frac{1}{2}\left(T_{\mathrm{feed}} + T_{\mathrm{reac}}\right) \tag{A.16}$$

Combining eq. (A.13) with eq. (A.10) gives

$$P_{\mathrm{heat}} = \frac{1 + g_{\mathrm{hx}}}{1 + 2g_{\mathrm{hx}}}c\rho F_{\mathrm{feed}}\left(T_{\mathrm{reac}} - T_{\mathrm{feed}}\right) + G\left(T_{\mathrm{reac}} - T_{\mathrm{amb}}\right) \tag{A.17}$$

where P_{heat} is in J/d.

Power savings due to using preheating with heat exchanger

The saving in P_{heat} due to using an heat exchanger can be calculated as the difference in P_{heat} given by eq. (A.17) with $g_{\mathrm{hx}} = 0$ and with the assumed value of g_{hx}. Assuming T_{reac} is the same in both cases, the saving is

$$\Delta P_{\mathrm{heat}} = \frac{g_{\mathrm{hx}}}{1 + 2g_{\mathrm{hx}}}c\rho F_{\mathrm{feed}}\left(T_{\mathrm{reac}} - T_{\mathrm{feed}}\right) \tag{A.18}$$

Considering the special case of $G = 0$ (perfect reactor insulation) and $g_{\mathrm{hx}} = \infty$ (perfect heat exchange),

$$\Delta P_{\mathrm{heat}} = \frac{1}{2}c\rho F_{\mathrm{feed}}\left(T_{\mathrm{reac}} - T_{\mathrm{feed}}\right) \tag{A.19}$$

18

Compared with eq. (A.17), the savings is *half* of the power demand without preheating. In other words, for a perfectly insulated reactor, preheating with a perfect heat exchanger halves the external power needed to retain the reactor at a given T_{reac}.

Appendix A.4. Power calculations

The power surplus is calculated as

$$P_{\text{sur}} = P_{\text{meth}} - P_{\text{heat}} - P_{\text{agit}} - P_{\text{supply}} - P_{\text{sep}} - P_{\text{feed}} \tag{A.20}$$

where P_{sur} is in MWh/y. The individual terms in eq. (A.20) are:

$$P_{\text{meth}} = E_{\text{meth}} F_{\text{meth}} [\text{kWh/y}] \tag{A.21}$$

$$P_{\text{supply}} = k_{\text{supply}} F_{\text{feed}_{\text{raw}}} [\text{kWh/y}] \tag{A.22}$$

$$P_{\text{sep}} = k_{\text{sep}} F_{\text{feed}_{\text{raw}}} [\text{kWh/y}] \tag{A.23}$$

$$P_{\text{feed}} = \rho g h F_{\text{feed}} \ [\text{J/d}] \tag{A.24}$$

where

$$F_{\text{feed}} = k_{\text{s}} F_{\text{feed}_{\text{raw}}} \tag{A.25}$$

$$P_{\text{agit}} = k_{\text{agit}} F_{\text{feed}_{\text{raw}}} \ [\text{kWh/y}] \tag{A.26}$$

Appendix B. Abbreviations

AD = Anaerobic digestion.

BVS = Biodegradable volatile solids.

CSTR = Continuous stirred tank reactor.

HRT = Hydraulic retention time.

LU = Livestock unit (head or cow).

NLP = Nonlinear programming.

SRT = Solids retention time.

STP = Standard temperature and pressure; 0 °C, 1 bar.

UASB = Upflow anaerobic sludge blanket.

VFA = Volatile fatty acids.

VS = Volatile solids.

Appendix C. Nomenclature and values of constants

The nomenclature is in alphabetical order.

$A_f = 0.25$ (g VFA/L)/(g BVS/L) is acidity constant.

$b = \text{SRT/HRT}$ [d/d] is retention time ratio.

$B_0 = 0.69$ (g BVS/L)/(g VS/L) is biodegradability constant.

$c = 1000$ J/(kg K) is specific heating capacity of reactor liquid.

$E_{\text{meth}} = 9.95$ kWh/m^3 is specific energy contents of methane gas at STP conditions (calculated from the ideal gas law).

F_{feed} [m^3/d] is influent or feed flow or load rate, assumed equal to effluent flow (constant volume).

$F_{\text{feed}_{\text{raw}}}$ [m^3/d] is raw diluted dairy waste fed to the separator.

F_{meth} [L CH$_4$/d] is methane gas flow.

$g = 9.81$ kgm/s^2 is gravity constant.

g_{hx} [1] is defined as the heat transfer conductivity coefficient of the heat exchanger.

G [(J/d)/K] is thermal conductivity of the reactor.

G_{hx} [(J/d)/K)] is thermal conductivity between the heating medium side and the product side of the heat exchanger.

γ_{meth} [m^3 CH$_4$/d)/(m^3/d)] is gas productivity.

γ_{P} [(MWh/y)/LU] is power surplus productivity.

h [m] is lift height of reactor influent.

$\text{HRT} = F_{\text{feed}}/V$ [d] is hydraulic retention time.

$k_{\text{agit}} = 243.3$ (kWh/y)/(m^3/d) is power coefficient of agitator.

k_{hd} [m/m] is ratio of reactor height to reactor diameter.

k_{f} [1] is wet fraction of raw (non-separated) feed passing through the separator and being fed to the reactor.

k_{w} [MWh/y] is energy conversion constant.

$k_{\text{s}} = 0.70$ (m^3/d)/(m^3/d) is separation constant.

$k_{\text{supply}} = 24.33$ (kWh/y)/(m^3/d) is power coefficient of supply pump.

$k_{\text{sep}} = 121.7$ (kWh/y)/(m^3/d) is power coefficient of separator.

$k_1 = 3.89$ g BVS/(g acidogens/L) is a yield constant.

$k_2 = 1.76$ g VFA/(g acidogens/L) is a yield constant.

$k_3 = 31.7$ g VFA/(g methanogens/L) is a yield constant.

$k_5 = 26.3$ L/g methanogens is a yield constant.

$K_s = 15.5$ g BVS/L is Monod half-velocity constant for acidogens.

$K_{sc} = 3.0$ g VFA/L is Monod half-velocity constant for methanogens.

$K_d = 0.02$ d^{-1} is specific death rate of acidogens.

$K_{dc} = 0.02$ d^{-1} is specific death rate of methanogens.

L CH$_4$ is litres of methane gas at STP (standard temperature and pressure), i.e. temperature 0 °C and pressure 1 bar.

L is litres of liquid.

μ [d^{-1}] is reaction (growth) rate of acidogens.

μ_c [d^{-1}] is reaction (growth) rate of methanogens.

μ_m [d^{-1}] is the maximum reaction rate for acidogens.

μ_{mc} [d^{-1}] is the maximum reaction rate for methanogens.

N_{LU} is number of lifestock units (LU).

N_{x_i} [1] is number of grid intervals, or subintervals, for optimization variable x_i.

P_{agit} [kWh/y] is power consumption of the agitator.

P_{heat} [kWh/y] is power consumption of the electrical heater, i.e. power supplied to the reactor by the electrical heater.

P_{meth} [kWh/y] is usable power of the methane gas.

P_{feed} [kWh/y] is power consumption of the feed pump related to lifting the feed up to the reactor inlet, typically provided by a displacement pump.

P_{supply} [kWh/y] is power consumption of the supply pump, which is typically a monopump.

P_{sep} [kWh/y] is power consumption of the feed separator.

P_{sur} [MWh/y] is power surplus.

ρ [kg/m^3] is density of reactor liquid.

S_{vfa} [g VFA/L] is concentration of VFA acids in reactor.

T_{amb} [°C] is ambient (air) temperature.

T_{feed} [°C] is temperature of reactor feed.

T_{h} [°C] is "hot" side temperature of the heat exchanger.

T_{infl} [°C] is temperature of reactor feed.

T_p [°C] is "cold" side temperature of the heat exchanger.

T_{reac} [°C] is reactor temperature.

$U = 6.50 \cdot 10^4$ ((J/d)/K)/m² is specific thermal conductivity of the reactor, assumed equal to that of the pilot reactor. In Haugen *et al.* (2013b), U is denoted G_s.

V [m³] is effective volume of reactor liquid.

y is year.

References

Bozinis, N. A., Alexiou, I. E., Pistikopoulos, E. N., 1996. A mathematical model for the optimal design and operation of an anaerobic co-digestion plant. Water Science and Technology 34 (5-6).

Ciotola, R. J., Lansing, S., Martin, J. F., 2011. Emergy analysis of biogas production and electricity generation from small-scale agricultural digesters. Ecological Engineering 37, 1681–1691.

Edgar, T. F., Himmelblau, D., Lasdon, L., 2001. Optimization of Chemical Processes. McGraw-Hill.

Gavala, H. N., Angelidaki, I., Ahring, B. K., 2003. Kinetics and Modeling of Anaerobic Digestion Process. Advances in Biochemical Engineering/Biotechnology, Springer-Verlag 81.

Haugen, F., Bakke, R., Lie, B., 2013a. Adapting dynamic mathematical models to a pilot anaerobic digestion reactor. Modeling, Identification and Control 34 (2), 35–54.

Haugen, F., Bakke, R., Lie, B., 2013b. On-off and pid control of methane gas production of a pilot anaerobic digestion reactor. Modeling, Identification and Control 34 (3).

Haugen, F., Bakke, R., Lie, B., 2013c. State estimation and model-based control of a pilot anaerobic digestion reactor. Submitted to Journal of Control Science and Engineering.

Hill, D. T., 1983a. Design Parameters and Operating Characteristics of Animal Waste Anaerobic Digestion Systems. Dairy Cattle. Agric. Wastes 5, 219–230.

Hill, D. T., 1983b. Simplified monod kinetics of methane fermentation of animal wastes. Agric. Wastes 5.

Hill, D. T., Cobb, S. A., Bolte, J. P., 1987. Using volatile fatty acid relationships to predict anaerobic digester failure. Trans. ASAE 30, 496–501.

Lyberatos, G., Skiadas, I. V., 1999. Modeling of anaerobic digestion - a review. Global Nest: the Int. J. 1 (2), 63–76.

Poels, J., Neulermans, G., van Assche, P., Debruyckere, M., Verstraete, W., 1983. Performance, operation and benefits of an anaerobic digestion system on a closed piggery farm. Agric. Wastes 8, 233–249.

Rivas, A., Irizar, I., Ayesa, E., 2008. Model-based optimisation of wastewater treatment plants design. Environmental Modelling and Software 23, 435–450.

Strömberg, S., 2010. Development and Evaluation of Numerical Models for Anaerobic Digestion. M.Sc. thesis. Lund Univ., Sweden.

Tchobanoglous, G., Burton, F. G., Stensel, H. D., 2003. Wastewater Engineering: Treatment and Reuse. Metcalf and Eddy, McGraw Hill.

Article 6 – Relaxed Ziegler-Nichols Closed Loop Tuning of PI Controllers

Authors: Finn Haugen and Bernt Lie.

Authors' roles in the article: Finn Haugen: Main ideas, implementation, and writing. Bernt Lie (main supervisor): Discussions, comments, and proof readings.

Background and methods of the article

Background

During the tuning of both the reactor temperature PI controller in Article no. 2 and the methane gas flow PI controller control loop in Article no. 3, it was found that the standard Ziegler-Nichols closed loop PI settings, Ziegler & Nichols (1942), gave poor control system stability. This was observed both on the real reactor and on the simulated reactor. Also, the gain margin and the phase margin as calculated from the frequency response showed small values. The Tyreus-Luyben modification of the Ziegler-Nichols PI settings, Tyreus & Luyben (1992), improved the stability, but with unnecessarily slow disturbance compensations. Improved PI settings were then derived by combining the Ziegler-Nichols closed loop method with the successful Skogestad method, Skogestad (2004), for open loop PI tuning of "integrator with time delay" processes.

Method

The proposed PI settings are tested on various simulated processes and on a real laboratory scale air heater, Haugen (2013). To analyze the control systems in simulation applications, both performance and stability robustness measures are calculated. As performance measures, the IAE index is calculated for setpoint changes and for disturbance changes. As stability robustness measures, the GM and the PM are calculated. In the simulated cases, they are calculated from the open loop frequency response. In the practical case with the air heater, the GM and PM are calculated from experiments, as explained in the article.

Relaxed Ziegler-Nichols Closed Loop Tuning of PI Controllers

Finn Haugen [1]   Bernt Lie [1]

Telemark University College, Kjolnes ring 56, 3918 Porsgrunn, Norway. E-mail contact: {*finn.haugen,bernt.lie*}*@hit.no*

Abstract

A modification of the PI setting of the Ziegler-Nichols closed loop tuning method is proposed. The modification is based on a combination of the Skogestad SIMC tuning formulas for "integrator plus time-delay" processes with the Ziegler-Nichols tuning formulas assuming that the process is modeled as an "integrator plus time-delay" process. The resulting PI settings provide improved stability margins compared with those obtained with the original Ziegler-Nichols PI settings. Compared with the well-known Tyreus-Luyben PI settings, the proposed PI settings give improved disturbance compensation. For processes with zero or a negligible time-delay, but with some lags in the form of time-constants, tuning based on ultimate gain and ultimate period may give poor results. Successful PI settings for such processes are proposed.

Keywords: PI controller, tuning, open loop, closed loop, Ziegler-Nichols, Tyreus-Luyben, Skogestad, relay-tuning, performance, stability, robustness.

1. Introduction

The PI (proportional plus integral) controller is probably the most frequently used controller function in practical applications. The PI controller stems from a PID controller with the D-term (derivative) deactived to reduce the propagation of amplified random measurement noise via the controller, thereby limiting variations in the control signal due to noise.

Ziegler and Nichols (1942) presented two, now famous, methods for tuning P, PI, and PID controllers: The closed loop, or ultimate gain, method, and the open loop, or process reaction curve, method. In the present paper, focus is on closed loop tuning of PI controllers.

The PI settings with the Ziegler and Nichols closed loop method are:

$$K_c = 0.45 K_{c_u} \tag{1}$$

$$T_i = \frac{P_u}{1.2} \tag{2}$$

where K_{c_u} is the ultimate gain, and P_u is the ultimate period to be found by the user. A practical, experimental way to find K_{c_u} and P_u is using relay oscillations, Åstrøm and Hägglund (1995), cf. Appendix A.

It is well-known that Ziegler and Nichols closed loop PI tuning in many cases give relatively fast process disturbance compensation, but unfortunately poor stability margins, seen as poorly damped oscillatory responses. This is demonstrated in several examples in Section 3. Tyreus and Luyben (1992) proposed a now well-known modification of the Ziegler-Nichols PI settings which typically give improved control system stability:

$$K_c = 0.31 K_{c_u} \tag{3}$$

$$T_i = 2.2 P_u \tag{4}$$

In the present paper, another modification of the Ziegler-Nichols PI settings is proposed to provide acceptable stability margins and improved disturbance compensation compared to the Tyreus and Luyben settings. The proposed tuning rules, here denoted the Relaxed Ziegler-Nichols (R-ZN) PI settings, are based

on the open loop tuning rules in the SIMC method (Simple Internal Model Control) by Skogestad (2004) applied to an "integrator plus time-delay" process estimated from the ultimate gain and the ultimate period, Yu (1999).

The outline of this paper is as follows: In Section 2, the R-ZN PI settings are derived. In Section 3, the original Ziegler-Nichols (ZN) PI settings, the Relaxed Ziegler-Nichols PI settings, and the Tyreus-Luyben (TL) PI settings are applied to two simulation cases and to a practical temperature control system of an air heater. In Section 4 an adjustable parameter of the R-ZN method is used to tune processes without time-delay, but with lags. Section 5 contains a discussion, and conclusions are given in Section 6.

Appendix A reviews the relay experiment of finding the ultimate gain and the ultimate period from both sinusoidal and triangular oscillations. Appendix B presents a modification of the Skogestad PI settings for improved disturbance compensation, used in the derivation of the proposed PI controller setting. Appendix C shows abbreviations and nomenclature.

In this paper, the same symbol (letter) will be used for variables in time-domain as in the Laplace domain. This simplifies the notation. It is assumed that the meaning of the symbol is clear from the context.

MATLAB and SIMULINK (MathWorks, Inc.) are used for numerical computations and simulations. LabVIEW (National Instruments, Inc.) is used to implement the temperature control system for the real air heater.

2. Relaxed Ziegler-Nichols PI tuning

2.1. Derivation of the tuning formulas

The following PI controller function is assumed:

$$u(t) = u_{\mathrm{man}} + K_c e(t) + \frac{K_c}{T_i} \int_0^t e(\tau)\, d\tau \qquad (5)$$

Skogestad (2004) has provided PI settings for a number of different types of process dynamics, among which are "integrator plus time-delay" and "time-constant plus time-delay". Assuming that Skogestad's rule-of-thumb about setting the user-specified closed loop time-constant, T_c, equal to the process time-delay, τ, his PI settings for these two process types are actually identical as long as the relation between the time-constant of the "time-constant plus time-delay" process and the time-delay satisfies

$$T \geq 8\tau \qquad (6)$$

In the following, it is assumed that eq. (6) is satisfied for the process to be controlled. Thus, an "integrator plus time-delay" process is assumed, with the following transfer function:

$$\frac{\Delta y(s)}{\Delta u(s)} = H_p(s) = \frac{K_{i_p}}{s} e^{-\tau s} \qquad (7)$$

The Skogestad PI settings for this process are:

$$K_c = \frac{1}{K_{i_p}(T_c + \tau)} \qquad (8)$$

$$T_i = c_s(T_c + \tau) \qquad (9)$$

The parameter c_s is introduced here. The original PI settings in Skogestad (2004) correspond to $c_s = 4$ in eq. (9). For "integrator plus time-delay" processes with an "input" process disturbance, the disturbance compensation appears as unnecessarily slow with $c_s = 4$. To obtain a faster disturbance compensation while retaining acceptable stability margins, a value of c_s smaller than 4 can be used. It is found that values around 2 are proper values. Thus, $c_s = 2$ is proposed. The implications of various values of c_s are investigated in Appendix B.

The user must select a proper value of T_c in eqs. (8) and (9). Skogestad provides the following rule-of-thumb:

$$T_c = \tau \qquad (10)$$

With $c_s = 2$ and the rule-of-thumb eq. (10), eqs. (8) and (9) become

$$K_c = \frac{1}{2K_{i_p}\tau} \qquad (11)$$

$$T_i = 4\tau \qquad (12)$$

which may be denoted the modified Skogestad PI settings for "integrator plus time-delay" processes.

The Skogestad PI settings, also with $c_s = 2$, typically yield acceptable stability of the control system, while Ziegler and Nichols PI settings often give poor stability, with oscillatory responses (as demonstrated in several applications in Section 3). The PI settings, eqs. (11) and (12), will now be exploited to relax the original ZN PI settings, eqs. (1)-(2).

For an "integrator plus time-delay" process, K_{i_p} and τ can be estimated from K_{c_u} and P_u as follows, Yu (1999), DiRuscio (2010):

$$K_{i_p} = \frac{2\pi}{K_{c_u} P_u} \qquad (13)$$

$$\tau = \frac{P_u}{4} \qquad (14)$$

As pointed out in Seborg et al. (2004), process parameters K_{i_p} and τ can be used in any model-based controller tuning method. Here, the (modified) Skogestad

PI settings, eqs. (11) and (12), are used. Inserting eqs. (13) and (14) into eqs. (11) and (12) gives

$$K_c = \frac{K_{c_u}}{\pi} = 0.32 K_{c_u} \qquad (15)$$

$$\underline{T_i = P_u} \qquad (16)$$

which will be referred to as the (default) Relaxed Ziegler-Nichols (R-ZN) PI settings.

Comparing with ZN and TL

Compared with the (original) ZN PI settings, eqs. (1)-(2), the gain is smaller and the integral time is somewhat larger in the R-ZN PI settings, indicating improved stability.

Compared with the TL PI settings, eqs. (3)-(4), the R-ZN gain is almost the same, while the R-ZN integral time is smaller, indicating faster integral action, i.e. the control error is brought faster to zero, however, somewhat reduced stability can be expected.

Enhanced relaxation

Above, the closed loop time-constant is set equal to the (estimated) process time-delay, cf. eq. (10). Particularly in applications where the process has zero or negligible time-delay but some lag, the default R-ZN PI settings may result in poor stability (and the ZN settings may even give instability). Acceptable stability can be obtained with enhanced relaxation of the PI settings. To this end, we propose

$$\underline{T_c = k_r \tau} \qquad (17)$$

where $k_r \geq 1$ is a relaxation parameter to be set by the user. The default PI settings, eqs. (6) and (6), are obtained with $k_r = 1$. Enhanced relaxation of the PI settings is obtained with $k_r > 1$. Using eq. (17) in eqs. (8) and (9), and setting $c_s = 2$ in (9), give

$$K_c = \frac{2}{\pi (k_r + 1)} K_{c_u} \qquad (18)$$

and

$$\underline{T_i = \frac{k_r + 1}{2} P_u} \qquad (19)$$

The usefulness of enhanced R-ZN tuning is demonstrated in Section 4.

One question may arise: Why not just apply original ZN settings and adjust K_c and T_i directly? While this is of course an option, we think that it better to use a meaningful single parameter, k_r, to obtain the PI settings. The benefit of reducing the number of controller parameters to adjust from two to one is actually substantial. Skogestad's tuning method is an excellent

example of this: From the user's perspective, adjusting T_c, which has a meaningful interpretation, to obtain the PI settings is a much simpler task than adjusting K_c and T_i directly.

2.2. Some derived results

Estimation of control system response-time

The control system response-time, T_r, can be estimated from the ultimate period, P_u, as explained in the following. The typical setting of $k_r = 1$ is here assumed. Then the PI settings are eqs. (6) and (6). Assume that the setpoint is changed as a step. Then the response in the process output reaches 63% of its final value at time (approximately)

$$T_r \approx \tau + T_c = \frac{P_u}{4} + \frac{P_u}{4} = \frac{P_u}{2} \qquad (20)$$

T_r is here the 63% rise-time, or response-time, of the control system. As an example of eq. (20), see Figure 9 where the response in air heater temperature due to a setpoint step is plotted. In that example, $P_u = 15$ s, giving $T_r \approx P_u/2 = 7.5$ s, which is in good accordance with the plotted response in Figure 9.

Retuning the PI controller

Equations (18) and (19) can be used to retune a PI controller safely. Note that the factor $(k_r + 1)$ appears in the denominator of eq. (18) and in the numerator of eq. (19). For example, assume that it is desired to decrease the present value of K_c by a factor of 2 (to obtain a smoother control signal). This gain reduction should be acccompanied by an increase of T_i by a factor 2. (This inversely proportional adjustment also follows directly from Skogestad's formulas, eqs. (8) and (9).)

3. Applications

3.1. Overview

In the following subsections, PI settings with the (original) Ziegler-Nichols closed loop method, the R-ZN closed loop method, and the TL method are applied to the following three cases:

- A simulated control system for an "integrator with time-delay" process (Section 3.3).

- A simulated control system for a "time-constant with time-delay" process (Section 3.4).

- A practical temperature control system for a laboratory air heater (Section 3.5). The process dynamics is roughly "time-constant with time-delay".

The PI settings will be compared using quantitive measures of performance and robustness defined in Section 3.2.

For easy reference, the various PI settings formulas are summarized in Table 1. In the examples, K_{c_u} and P_u are found from the method of relay oscillations described in Appendix A.

Table 1: PI settings formulas.

	ZN	R-ZN	TL
K_c	$0.45K_{c_u}$	$0.32K_{c_u}$	$0.31K_{c_u}$
T_i	$\frac{P_u}{1.2}$	P_u	$2.2P_u$

3.2. Measures of performance and robustness

The measures used in this paper for comparing the various methods of PI controller tuning can be grouped into performance and robustness measures described in the detail in the following.

3.2.1. Performance

IAE at setpoint change

In the tests the setpoint is changed as a step. The setpoint tracking is measured with the IAE (Integral of Absolute Error) index calculated over a proper time interval as

$$\text{IAE}_s = \int_{t_i}^{t_f} |e| \, dt \qquad (21)$$

where e is the control error, t_i is the initial time, selected as the time of the step change, and t_f is a proper final time. A reduced IAE_s value indicates improved setpoint tracking.

IAE at process disturbance change

In the tests a process disturbance is changed as a step. The disturbance compensation is measured with

$$\text{IAE}_d = \int_{t_i}^{t_f} |e| \, dt \qquad (22)$$

A reduced IAE_d value indicates improved disturbance compensation.

Response time

The response time, T_r [s], is here defined as the inverse of the bandwidth defined as the amplitude crossover frequency, ω_c [rad/s]:

$$T_r = \frac{1}{\omega_c} \qquad (23)$$

T_r indicates the speed of the response of the control system due to a setpoint step change. T_r is approximately the time-constant of the control system. ω_c is equal to the phase crossover frequency, ω_{180_d}, of the loop brought to marginal stability by a reduction of the phase of the loop while the amplitude is retained, as by an increase of the loop time-delay:

$$T_r = \frac{1}{\omega_{180_d}} = \frac{P_u}{2\pi} \qquad (24)$$

where P_u [s] is the (ultimate) period of the oscillations at marginal stability.

Setpoint tracking versus disturbance compensation

For systems where the setpoint is constant, which is the case in many practical process control systems, it can be claimed that good disturbance compensation is more important than good setpoint tracking. In the examples presented in the following sections, disturbance compensation is emphasized.

3.2.2. Stability robustness (stability margins)

Gain margin, GM

For the cases based on simulations GM is calculated from the loop transfer function, $H_L(s)$, using the `margin` function in MATLAB. $H_L(s)$ is

$$H_L(s) = H_c(s)H_p(s) \qquad (25)$$

where $H_c(s)$ is the controller transfer function, and $H_p(s)$ is the process transfer function.

For the practical case (air heater) an adjustable gain, ΔK, is inserted into the loop (between the controller and the process), see Figure 1. Initially, $\Delta K = 1$. The
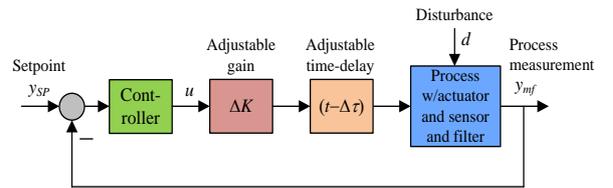

Figure 1: An adjustable gain and time-delay are inserted into the loop to find the stability margins (gain margin and phase margin) experimentally.

(ultimate) value ΔK_u that brings the control system to the stability limit so that the responses are sustained oscillations, is found experimentally (by trials). The gain margin is then

$$\text{GM} = \Delta K_u \qquad (26)$$

Phase margin, PM

For the cases based on simulations PM is calculated from the loop transfer function using the margin function in MATLAB.

For the practical case (air heater) an adjustable time-delay, $\Delta\tau$ [s], is inserted into the loop (between the controller and the process), see Figure 1. Initially, $\Delta\tau = 0$. For each of the tuning methods, the value $\Delta\tau_u$ that brings the control system to the stability limit, i.e. causing sustained oscillations, is found experimentally. The period, P_u [s], of the oscillations is measured. The corresponding phase margin is

$$\text{PM [deg]} = 360 \frac{\Delta\tau_u}{P_u} \tag{27}$$

Equation (27) is derived in Haugen (2012) (Appendix 1).

Proper values of GM and PM

Seborg et al. (2004) propose the following ranges for proper values of the stability margins:

$$1.7 = 4.6 \text{ dB} \leq \text{GM} \leq 4.0 = 12.0 \text{ dB} \tag{28}$$

and

$$30^{\circ} \leq \text{PM} \leq 45^{\circ} \tag{29}$$

Since poor control system stability must be avoided, the lower limits of GM and PM can be regarded as critical, while the upper limits are not.

3.3. Application: Simulated "integrator plus time-delay" process

3.3.1. Process description

The process to be controlled is an "integrator plus time-delay" process:

$$\dot{y}(t) = K_{i_p}u(t - \tau) + K_d d(t) \tag{30}$$

which has transfer function as in eq. (7). The process parameter values are: $K_{i_p} = 1 \text{ s}^{-1}$, $K_d = 1$, $\tau = 1$ s.

3.3.2. PI controller tuning from relay oscillations

K_{c_u} and P_u are found from relay oscillations. Figure 2 shows plots of the sustained oscillations during the relay tuning, cf. Appendix A. From the plots, $A_{\text{tri}} = 1.0$. The square wave in the control signal has amplitude $A_{\text{sq}} = 1$.

Equation (47) in Appendix A gives

$$K_{c_u} = \frac{\pi A_{sq}}{2A_{tri}} = \frac{\pi \cdot 1}{2 \cdot 1} = 1.57 \tag{31}$$
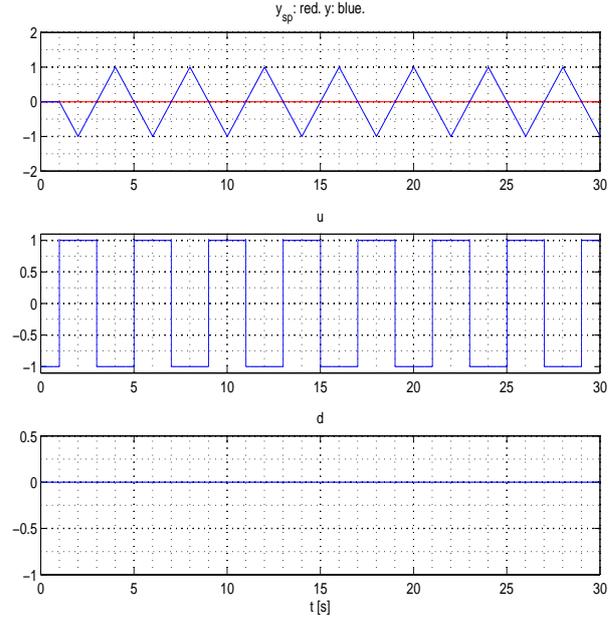
Figure 2: Responses during relay tuning

It is interesting that the ultimate gain using a P controller also gives $K_{c_u} = 1.57$. Hence, the Fourier-series approximations used to derive eq. (47) give a very precise result in this case.

Furthermore, from the plots,

$$P_u = 4.0 \text{ s} \tag{32}$$

Various PI settings are calculated from the above values of K_{c_u} and P_u using the formulas in Table 1. The PI settings are shown in Table 2.

3.3.3. Performance and stability robustness of the control system

Figure 3 shows responses in the process output variable (y) and the controller output (u) with a step change of the temperature setpoint (y_{sp}) and a step change of the disturbance (d) for the three different PI settings shown in Table 2.

GM, PM and T_r are calculated from the model. IAE_s is calculated time-series over the interval $t = [2 \text{ s}, 40 \text{ s}]$. IAE_d is calculated over $t = [40 \text{ s}, 80 \text{ s}]$. Table 2 summarizes the performance and robustness measures.

Below are a number of observations made in Table 2 (the abbreviations are as in Table 2):

- *Setpoint tracking*:

  IAE_s: ZN and TL are the best, and almost equal, but ZN suffers from large overshoot.

87
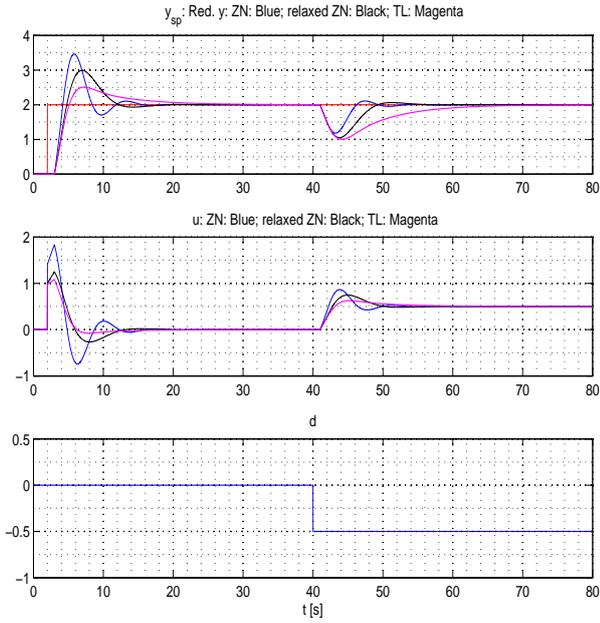
Figure 3: Responses with various PI settings.

Table 2: Controller settings and performance and robustness measures for simulated control system for "integrator plus time-delay" process with different PI settings.

	ZN	R-ZN	TL
K_c	0.71	0.50	0.49
T_i [s]	3.3	4.0	8.8
IAE_s	7.9	8.1	8.0
IAE_d	2.8	4.5	9.0
GM	1.9	2.7	3.1
GM [dB]	5.4	8.8	9.7
PM [deg]	24.9	34.1	48.6
T_r [s]	1.3 s	1.8	2.0

T_r: ZN is the best, while R-ZN and TL do not differ much.

- *Disturbance compensation*:

  IAE_d: ZN is clearly best. R-ZN is in turn clearly better than TL as the R-ZN has a value which is 50% of the value of TL.

- *Stability robustness (margins)*:

  GM: ZN is poor, and actually below the lower limit in ineq. (28). R-ZN and TL do not differ much and have acceptable values.

  PM: Again ZN is poor, and below the lower limit in ineq. (29). R-ZN gives a somewhat small, but acceptable, value. TL gives large value, possibly

unnecessarily large as it is larger than the higher limit in ineq. (29).

The low stability margins with ZN are apparent in the oscillatory responses with the ZN settings, see Figure 3.

Comments and conclusions

The Ziegler-Nichols PI settings give poor control loop stability margins. The TL and the R-ZN settings give acceptable stability margins. With emphasis on disturbance compensation rather than setpoint tracking, the R-ZN settings are better than the TL settings.

3.4. Application: Simulated "time-constant plus time-delay" process

3.4.1. Process description

The process to be controlled is a "time-constant plus time-delay" process (assuming the time-delay is at the input-side):

$$T\dot{y}(t) = -y(t) + Ku(t - \tau) + K_d d(t) \qquad (33)$$

The process parameter values are: $K = 8, K_d = 8, \tau = 1$ s.

The time-constant being 8 times the time-delay makes the Skogestad PI settings for a "time-constant plus time-delay" process become identical with the settings for an "integrator plus time-delay" process. Therefore, the condition for using Skogestad tuning for "integrator plus time-delay" processes, ineq. (6), is satisfied.

3.4.2. PI controller tuning from relay oscillations

The ultimate gain and the ultimate period are found from relay oscillations. Figure 4 shows plots of the sustained oscillations during the relay tuning. The response in y are approximately triangular, so eq. (47) is used to calculate K_{c_u}. From Figure 4, $A_{\text{tri}} = 0.94$, $A_{\text{sq}} = 1$. Equation (47) gives

$$K_{c_u} = \frac{\pi A_{\text{sq}}}{2A_{\text{tri}}} = \frac{\pi \cdot 0.94}{2 \cdot 1} = 1.48 \qquad (34)$$

The ultimate gain using a P controller gives $K_{c_u} = 1.65$ which differs somewhat from 1.48. Still, $K_{c_u} = 1.48$ is used to stick to relay tuning, and using 1.48 rather than 1.65 is safe (conservative) regarding control loop stability.

Furthermore, from Figure 4,

$$P_u = 3.78 \text{ s} \qquad (35)$$
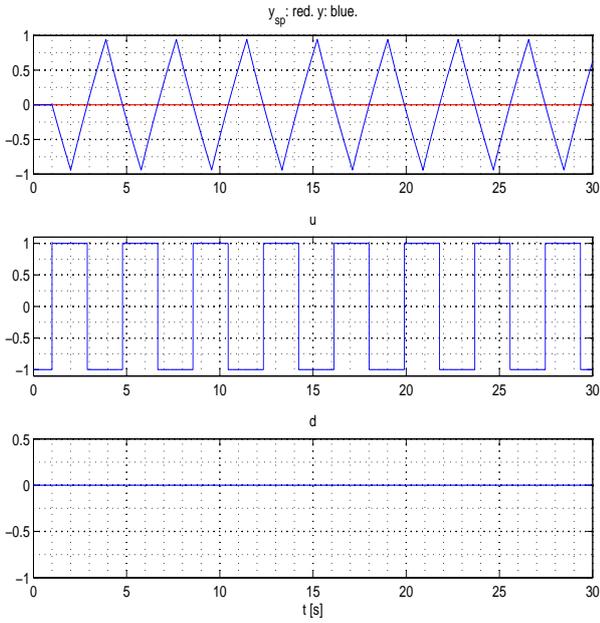
Figure 4: Responses during relay tuning
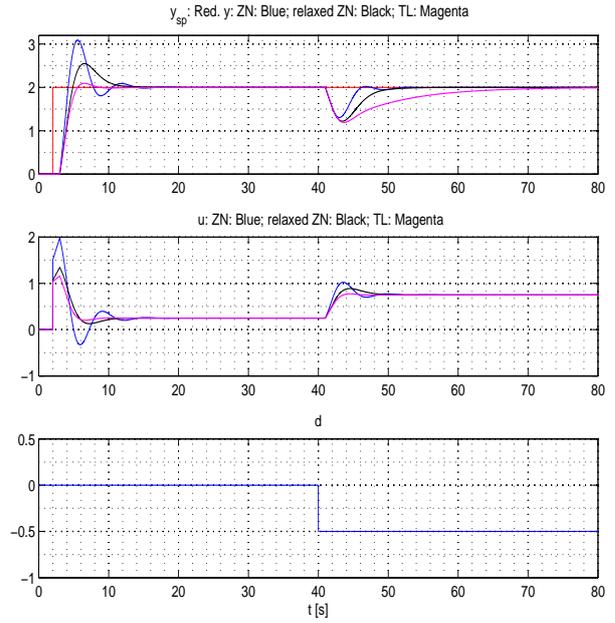
Figure 5: Responses with various PI settings.

Various PI settings are calculated from the above values of K_{c_u} and P_u using the formulas in Table 1. The PI settings are shown in Table 2.

3.4.3. Performance and stability robustness of the control system

Figure 5 shows responses in the process output variable (y) and the controller output (u) with a step change of the temperature setpoint (y_{sp}) and a step change of the disturbance (d) for the three different PI settings shown in Table 3.

GM, PM and T_r are calculated from the model. IAE_s is calculated over the interval $t = [2 \text{ s}, 40 \text{ s}]$. IAE_d is calculated over $t = [40 \text{ s}, 80 \text{ s}]$. Table 3 summarizes the performance and robustness measures.

Table 3: Controller settings and performance and robustness measures for simulated control system for "time-constant plus time-delay" process with different PI settings.

	ZN	R-ZN	TL
K_c	0.75	0.53	0.52
T_i [s]	3.2	3.8	8.3
IAE_s	6.1	5.8	4.3
IAE_d	2.1	3.6	7.9
GM	1.7	2.6	3.0
GM [dB]	4.8	8.1	9.7
PM [deg]	22.3	32.2	60.1
T_r [s]	1.2	1.7	1.9

Below are a number of observations made in Table 2 (the abbreviations are as in Table 2):

- *Setpoint tracking*:

  IAE_s: TL is best.

  T_r: ZN is best, while R-ZN and TL do not differ much.

- *Disturbance compensation*:

  IAE_d: ZN is clearly best. R-ZN is in turn clearly better than TL. R-ZN has a value which is 45 % of the value of TL.

- *Stability robustness (margins)*:

  GM: Strictly, all settings give acceptable values, but ZN is on the lower limit.

  PM: ZN is poor, and below the lower limit in ineq. (29). R-ZN gives a somewhat small, but acceptable, value. TL gives a large value, possibly unnecessarily large as it is larger than the higher limit in ineq. (29).

Comments and conclusions

The Ziegler-Nichols PI settings give poor control loop stability as the PM is too small. The rest of the comments are identical with those for the "integrator plus time-delay" case in Section 3.3: The TL and the R-ZN settings give acceptable stability margins. With emphasis on disturbance compensation rather than setpoint tracking, the R-ZN settings are better than the TL settings.

3.5. Application: Practical temperature control system

3.5.1. Process description

Figure 6 shows an air heater laboratory station. The
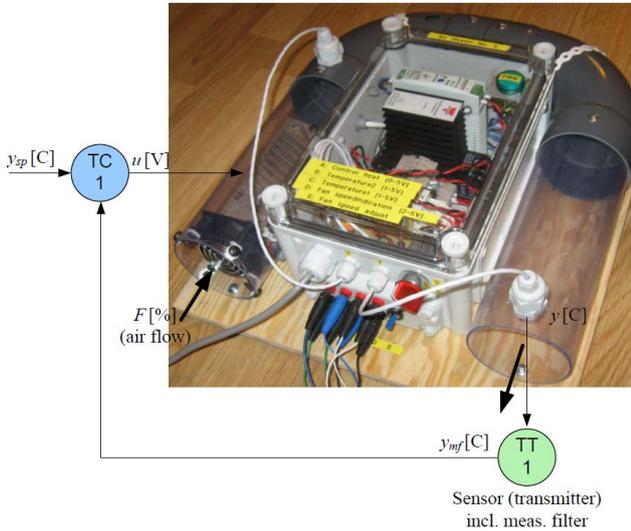
Figure 6: Temperature control system for an air heater (laboratory rig)

temperature of the air outlet is controlled by adjusting the control signal (voltage) to the heater. The temperature is measured with a Pt100 element. A measurement filter with time-constant 0.5 s is used to attenuate measurement noise. The National Instruments USB-6008 is used as analog I/O device. The control system is implemented in LabVIEW (National Instruments) running on a PC. The fan rotational speed, and the air flow, can be adjusted manually with a potentiometer. Changes of the air flow comprises a process disturbance giving an impact on the temperature. The measured voltage drop across the potensiometer is represented by the variable F in percent. Thus, F represents the air flow disturbance.[1]

The nominal operating point of the system is temperature at 35 °C and air flow $F = 50$ %.

Figure 7 shows the open loop, or process, step response in the filtered temperature, y_{mf}, due to a step in the heater control signal, u. The response indicates that the process dynamics is roughly "time-constant with time-delay", with time-constant ≈ 37 s and time-delay ≈ 3 s which is about 8% of the time-constant.

---

[1] Additional information about the air heater is available at Haugen (2013).
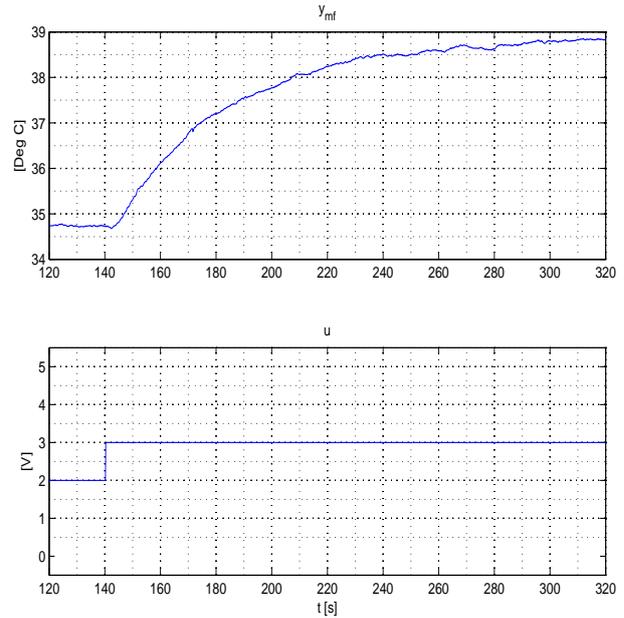

Figure 7: Open loop step response in filtered temperature, y_{mf}, due to a step in the heater control signal, u.

3.5.2. PI controller tuning from relay oscillations

K_{c_u} and P_u are found from relay oscillations. Figure 8 shows plots of the sustained oscillations during the relay tuning. The oscillations in temperature (process measurement) looks more sinusoidal than triangular. Therefore, K_{c_u} is calculated using eq. (45).

From Figure 8, $A_{sin} = 0.75$ °C and $A_{sq} = 2.5$ V. Equation (45) gives

$$K_{c_u} = \frac{4A_{sq}}{\pi A_{sin}} = \frac{4 \cdot 2.5 \text{ V}}{\pi \cdot 0.75 \text{ °C}} = 4.24 \ \frac{\text{V}}{\text{°C}} \qquad (36)$$

From Figure 8,

$$P_u = 15.0 \text{ s} \qquad (37)$$

Various PI settings are calculated from the above values of K_{c_u} and P_u using the formulas in Table 1. The PI settings are shown in Table 4. Both standard R-ZN and enhanced R-ZN tuning are applied, with $k_r = 1$ and $k_r = 2$, respectively.

3.5.3. Performance and stability robustness of the control system

Figures 9, 10, 11, and 12 show responses in the air temperature (y_{mf}) and the controller output (u) due to a step change of the temperature setpoint (y_{sp}) and a step change of the disturbance (d) for the four different PI settings shown in Table 4.
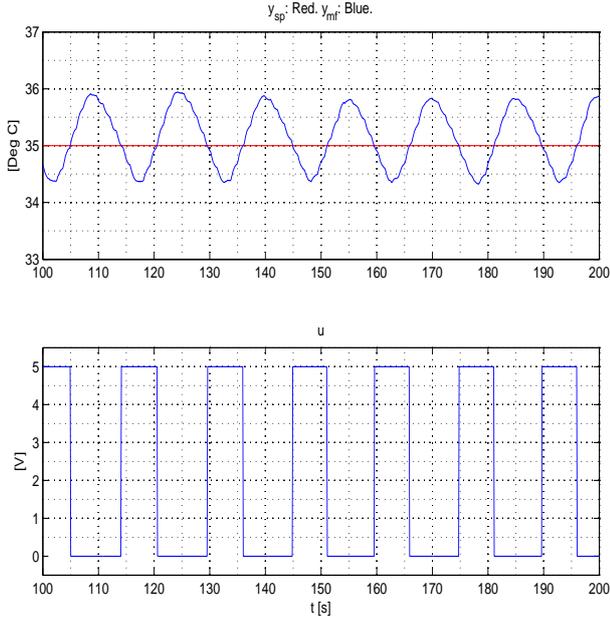
Figure 8: Responses during relay tuning

Figure 9: Responses with Ziegler-Nichols PI settings

Performance and stability robustness measures are calculated from the time-series as explained in Section 3.2. IAE$_s$ is calculated over the interval $t = [100 \text{ s}, 180 \text{ s}]$. IAE$_d$ is calculated over $t = [200 \text{ s}, 280 \text{ s}]$. Table 4 summarizes the performance and robustness measures.

Table 4: Controller settings and performance and robustness measures for practical temperature control system for different PI settings.

	ZN	R-ZN $k_r = 1$	R-ZN $k_r = 2$	TL
K_c	1.91	1.35	0.90	1.32
T_i [s]	12.5	15.0	22.5	33.0
IAE$_s$	16.2	12.3	10.6	10.3
IAE$_d$	4.3	4.9	7.5	11.8
GM	1.5	1.8	2.8	2.6
GM [dB]	3.5	5.1	8.9	8.3
$\Delta\tau_u$ [s]	1.6	2.6	7.7	5.7
P_u [s]	24.0	31.0	50.0	39.0
PM [deg]	24.0	30.2	55.4	52.6
T_r [s]	3.8	4.9	8.0	6.2

Below are a number of observations made in Table 4 (the abbreviations are as in Table 4):

- *Setpoint tracking*:

  IAE$_s$: TL and R-ZN with $k_r = 1$ and with $k_r = 2$ do not differ much and are clearly better than ZN which is due to the large overshoot and oscillatory response with ZN.

T_r: ZN is clearly best. It gives fast control. R-ZN with $k_r = 1$ is also relatively fast.

- *Disturbance compensation*:

  IAE$_d$: ZN and R-ZN with $k_r = 1$ are much better than both R-ZN with $k_r = 2$ and TL. R-ZN with $k_r = 1$ give only 36% of that of TL. Relaxed ZN with $k_r = 2$ is also clearly better than TL.

- *Stability robustness (margins)*:

  GM: ZN is poor, and actually below the lower limit in ineq. (28). R-ZN with $k_r = 1$ is small, but just within the limits.

  PM: Again ZN is poor, and below the lower limit in ineq. (29). R-ZN with $k_r = 1$ is small, but just within the limits. TL has a large value, possibly unnecessarily large since it is larger than the higher limit in ineq. (29). R-ZN with $k_r = 2$ has a very large value.

  The low stability margins with ZN are apparent in the oscillatory responses with the ZN settings. R-ZN with $k_r = 1$ seems to give acceptable stability as seen from time-series. R-ZN with $k_r = 2$ and TL both give smooth, but slow, responses.

Comments and conclusions

The Ziegler-Nichols PI settings give poor control loop stability. The TL and the R-ZN settings both with $k_r = 1$ and $k_r = 2$ give acceptable stability margins, though R-ZN with $k_r = 1$ gives small margins. R-ZN

91
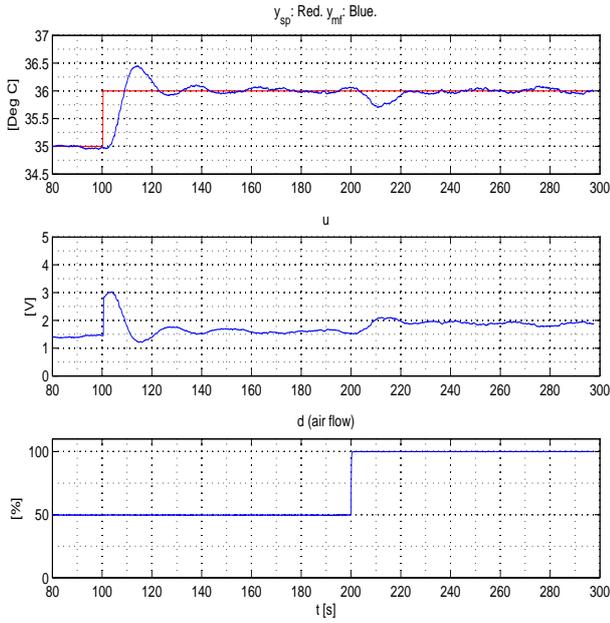
Figure 10: Responses with R-ZN PI settings with $k_r = 1$.
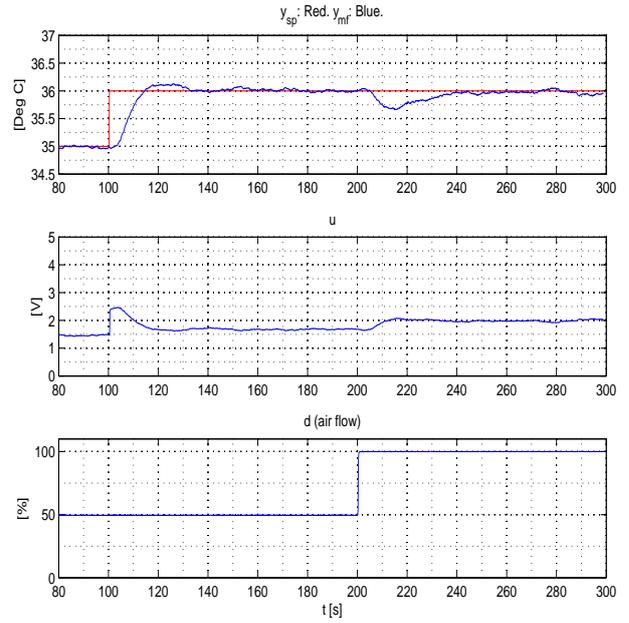
Figure 11: Responses with R-ZN PI settings with $k_r = 2$.

with $k_r = 1$ give clearly the best disturbance compensation, and since the stability margins are within the acceptable limits, it gives the prefered PI settings in this application.

If it is important with smooth responses, both TL and R-ZN with $k_r = 2$ can be used. Among these two, we prefer the latter because it gives best disturbance compensation, and because the R-ZN settings are adjustable, while the TL settings are fixed.

4. Relaxed tuning for processes with no time-delay but with lags

Closed loop PI tuning with the standard Ziegler-Nichols method, the TL method, or even the R-ZN tuning method with the default setting $k_r = 1$ may not work well if the process has no, or negligible time-delay, however, some lag is assumed. The resulting stability may be very poor. Such cases may occur in e.g. temperature control, Haugen et al. (2013) and biogas flow control of bioreactors, Haugen and Lie (2013). However, enhanced R-ZN tuning with a proper $k_r > 1$ seems to work well. An explanation of the resulting poor stability is that, due to the lack of a time-delay, the phase characteristic is relatively flat around the critical frequencies, making the phase margin small.

Now, an extreme case is assumed, and enhanced R-ZN PI tuning is used. The value of k_r that is found useful in this case may be used in other less extreme

cases to obtain proper stability. Note that for processes with a noteable time-delay the R-ZN PI settings with the default value $k_r = 1$, i.e. eqs. (6)-(6), should be used.

Assume that the process is an integrator without any time-delay but with two lags in the form of time-constant terms where one of the time-constants is one tenth of the other. Specifically, the following process transfer function model is assumed:

$$y(s) = \frac{1}{s(T_1 s + 1)(T_2 s + 1)} \left[K_{i_p} u(s) + K_d d(s) \right] \quad (38)$$

where u is control variable and d is disturbance. Time-constant T_1 may represent a process lag due to e.g. dynamics of a heating element or a valve or a pump or represent inhomogeneous conditions in a tank, while T_2 may represent the time-constant of a measurement filter. The integrator, $1/s$, may represent e.g. energy or material balance. The following parameter values are assumed: $K_{i_p} = 1$ s^{-1} $K_d = 1$, $T_1 = 1$ s, and $T_2 = 0.1$ s. In less extreme cases the difference between the two time-constants are less, and there may also be a non-zero time-delay.

The relay method is used, giving $K_{c_u} = 10.24$ and $P_u = 2.02$ s. The three PI tuning methods mentioned in the beginning of the present section are tested. Figure 13 shows their responses. With TL tuning and R-ZN tuning with $k_r = 1$ the control system is stable, but the stability is poor. With Ziegler-Nichols tuning, the system is unstable!
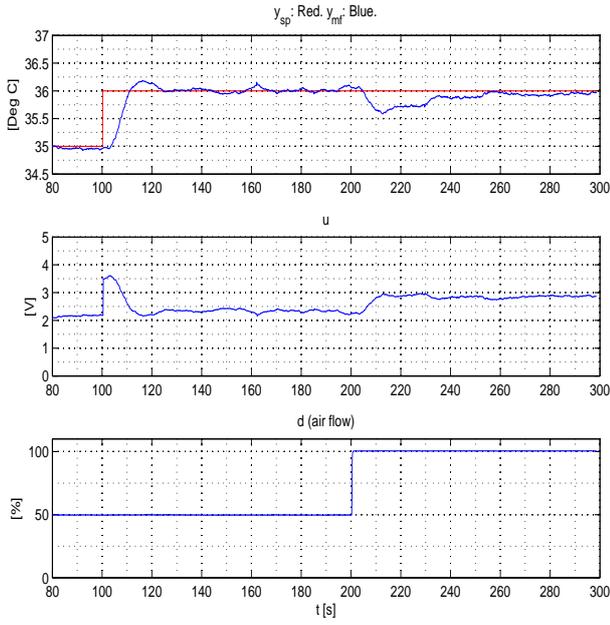
Figure 12: Responses with TL PI settings
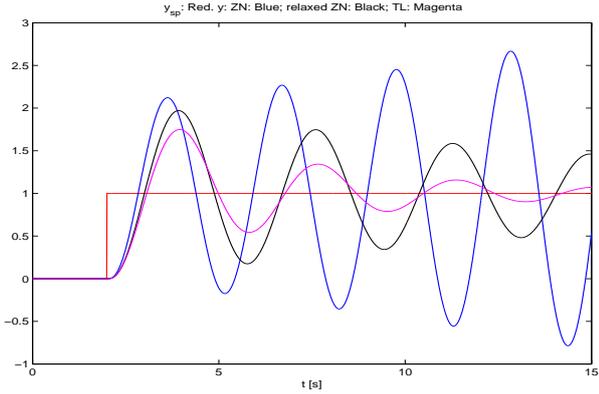
Figure 13: Responses with various PI settings.

By trial-and-error it is found that R-ZN tuning with $k_r = 4$ works well. Hence, with $k_r = 4$ in (18) and (19) the PI settings become

$$K_c = 0.13 K_{c_u} \qquad (39)$$

and

$$T_i = 2.5 P_u \qquad (40)$$

Figure 14 shows simulated responses. Table 5 shows PI settings and stability margins.

Comments and conclusion:

- GM is large, but is accepted here.

- PM is small and just outside the acceptable range where 30.0° is the critical limit, cf. ineq. (29).
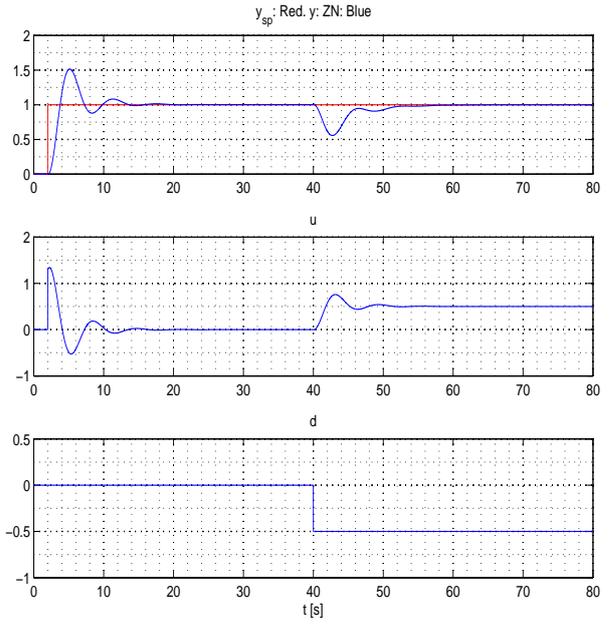
Figure 14: Responses with PI controller tuned with the R-ZN method with $k_r = 4$.

Table 5: Controller settings and performance and robustness measures for simulated PI control system for an "integrator with two lags" process with R-ZN tuning with $k_r = 4$.

K_c	1.3
T_i [s]	5.2
GM	6.7
GM [dB]	16.5
PM [deg]	29.4

However, the value of 29.4° is here regarded as acceptable since it is for an assumed extreme case. With $k_r = 5$ PM = 34.3° which is within the range given by ineq. (29), but simulations indicate that the control system becomes unnecessarily sluggish with $k_r = 5$ applied for less extreme cases.

- How can one know that a process has one or more lags and no or negligible time-delay, so that the enhanced relaxed tuning should be applied? Physical insight may be useful: If the sensor or actuator is located close to the main process (which can be e.g. a reactor vessel), the time-delay may be negligible compared to time-constant lags. A process step response test is also an option, but then an open loop controller tuning method, as the Skogestad method (2003, 2004), may be applied directly.

93

5. Discussion

The proposed new set of PI settings are based on tuning rules derived by Ziegler and Nichols (1942), tuning rules derived by Skogestad (2004), and the modeling of the process as an "integrator plus time-delay" according to Yu (1999). The validity and applicability of the proposed PI settings rely on assumptions made by these authors. The sensitivity of the present results with respect to such assumptions has not been investigated here. However, two simulation tests and one practical test indicate that the proposed tuning works as assumed.

In the simulations it is assumed that the process disturbance is an input disturbance as it acts on the process at the same place, dynamically, as the control signal does. In most practical processes the main disturbances are actually input disturbances. We have not investigated the consequences for our results of moving the disturbance to the process output.

It is found that for processes with no, or a negligible time-delay, but with some lags in the form of time-constants, R-ZN tuning with $k_r = 1$ may give poor stability (This applies to ordinary ZN and TL tuning, too). However, proper stability may be obtained with enhanced relaxation of the tuning, and $k_r = 4$ seems to be a proper value at least for processes without time-delay but with two lags with one being one tenth of the other. The conditions that make the selection $k_r = 4$ unsuccessful have not been investigated, but for processes where the time-constants are closer, the PI settings with $k_r = 4$ will certainly be safe (conservative).

6. Conclusions

The main result of this paper is a proposed new set of PI settings which uses the same information as in the Ziegler-Nichols closed loop method, namely knowledge about the ultimate gain, K_{c_u}, and the ultimate period, P_u: The proposed settings are:

$$K_c = 0.32 K_{c_u}$$

$$T_i = P_u$$

These settings are modifications, or relaxations, of the original Ziegler-Nichols PI settings, and they give improved control system stability. In this paper, the proposed setting have been successfully applied to two simulated control systems and to a practical temperature control system of an air heater.

Comparing with the TL PI settings, which also are based on knowledge of the ultimate gain and the ultimate period, the proposed PI settings give clearly better disturbance compensation.

The proposed PI settings have an adjustable parameter which can be used to obtain enhanced relaxation which is useful for processes with zero or negligible time-delay but some lags (time-constants).

Acknowledgments

A. Finding the ultimate gain and period from relay oscillations

In the original Ziegler-Nichols closed loop method the user must find, typically by trial-and-error, the ultimate controller gain value, K_{c_u}, of a P controller which makes the responses in the control system become sustained oscillations. The user must also read off the ultimate period, P_u, of the oscillations. K_{c_u} and P_u are then used to calculate the PI settings with the following formulas:

$$K_c = 0.45 K_{c_u} \tag{41}$$

$$T_i = \frac{P_u}{1.2} \tag{42}$$

Åstrøm and Hägglund (1995) introduced a relay, or on-off, controller to replace the P controller in the tuning phase, thereby avoiding the possibly time-consuming trial-and-error procedure as the oscillations come automatically. During the relay tuning the control signal is a square wave.

K_{c_u} can be estimated from the relay oscillations as follows. Assume that the amplitude of the square wave is

$$A_{\text{sq}} = \frac{u_{\text{on}} - u_{\text{off}}}{2} \tag{43}$$

where u_{on} and u_{off} are the values of the controller output when the relay is in the on- and off-state, respectively. The square wave is approximated by its fundamental sinusoidal component of its Fourier series. The fundamental sinusoid is known to have amplitude

$$A_{\text{sq,F}} = \frac{4 A_{\text{sq}}}{\pi} \tag{44}$$

Sinusoidal oscillations

With relay-based oscillations, for many practical processes the filtered process measurement is approximately sinusoidal. Assume that the measurement has amplitude A_{sin}. The control error, which is the input

to the relay, then also has amplitude $A_{\sin}$. The equivalent gain of the relay function, which is used as the ultimate gain in eq. (41), is

$$K_{c_u} = \frac{A_{\text{sq,F}}}{A_{\sin}} = \frac{4A_{\text{sq}}}{\pi A_{\sin}} = 1.27\frac{A_{\text{sq}}}{A_{\sin}} \qquad (45)$$

The ultimate period, P_u, needed in eq. (42) is the period of the oscillations.

Triangular oscillations

If the process dynamics is pure "integrator plus time-delay" the relay-based oscillations in the process measurement are not sinusoidal, but triangular. Let A_{tri} be the amplitude of these triangular oscillations. The fundamental sinusoidal component of the triangular oscillation is known to have amplitude

$$A_{\text{tri,F}} = \frac{8A_{\text{tri}}}{\pi^2} \qquad (46)$$

The equivalent gain of the relay function, which is used as the ultimate gain in eq. (41), is

$$K_{c_u} = \frac{A_{\text{sq,F}}}{A_{\text{tri,F}}} = \frac{\pi A_{\text{sq}}}{2A_{\text{tri}}} = 1.57\frac{A_{\text{sq}}}{A_{\text{tri}}} \qquad (47)$$

The ultimate period, P_u, in eq. (42) is the period of the oscillations.

If the process dynamics is "time-constant plus time-delay" with the time-constant being much larger than the time-delay, and without other process dynamics (lags), the relay-based oscillations appear more triangular than sinusoidal. In these cases, eq. (47) can be used.

B. Impact of the proposed parameter c_s in the modified Skogestad PI settings

Simulations are used to investigate the implications of using various values of parameter c_s in eq. (9).

The process to be controlled is an "integrator with time-delay" process given by eqs. (30) with $K_{i_p} = 1$ s^{-1}, $K_d = 1$ and $\tau = 1$ s. The PI controller is tuned with the (modified) Skogestad tuning formulas, eqs. (8) and (9).

Figure 15 shows simulations for the following values of c_s:

- $c_s = 1.5$ which is the the value corresponding to the IMC settings for an "integrator with time-delay" process by Chien and Fruehauf (1990).

- $c_s = 2$ which is the value used in the present paper.
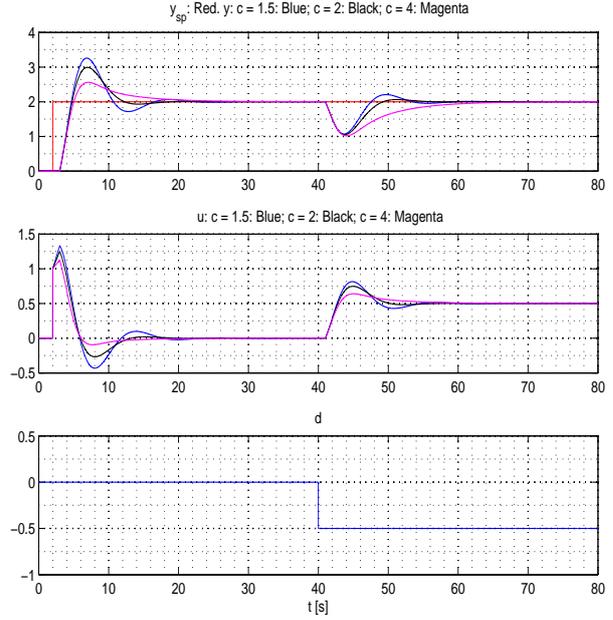
Figure 15: Simulations of control systems for an "integrator with time-delay" process with Skogestad controller tuning with $c_s = 1.5$, $c_s = 2$, and $c_s = 4$.

- $c_s = 4$ which is Skogestad's original value.

Table 6 shows a number of characteristics of the simulated control system for the three values of c_s. GM, PM and T_r are calculated from the model, cf. Section 3.2. IAE$_s$ is calculated time-series as explained in Section 3.2 over the interval $t = [2\ \text{s},\ 40\ \text{s}]$. IAE$_d$ is calculated over $t = [40\ \text{s},\ 80\ \text{s}]$.

Table 6: Results with $c = 1.5$, $c = 2$, and $c = 4$ in the (modified) Skogestad PI tuning formulas for an "integrator with time-delay" process.

	$c_s = 1.5$	$c_s = 2$	$c_s = 4$
K_c	0.5	0.5	0.5
$T_i[s]$	3	4	8
IAE$_s$	9.6	8.1	7.8
IAE$_d$	4.5	4.5	8.0
GM	2.6	2.7	3.0
PM [deg]	26.9	34.1	46.9
T_r [s]	1.7	1.8	1.9

Comments and conclusions

In Table 6, PM = 26.9 for $c_s = 1.5$ which is regarded as a poor value since it is lower than the lower limit in ineq. (29).

With $c_s = 2$ and $c_s = 4$ the stability margins are acceptable.

IAE_d with $c_s = 2$ is 56% of IAE_d with $c_s = 4$, indicating a considerable improved disturbance compensation with $c_s = 2$. This is also clearly seen in the simulations.

We prefer $c_s = 2$ over $c_s = 4$ in the Skogestad PI settings formulas for "integrator plus time-delay" processes since the disturbance compensation is improved.

C. Abbreviations and nomenclature

C.1. Abbreviations

GM: Gain margin.

IAE: Integral of absolute error.

PI: Proportional plus integral (control).

PM: Phase margin.

R-ZN: Relaxed Ziegler-Nichols.

ZN: Ziegler-Nichols (original method).

TL: Tyreus-Luyben.

SIMC: Simple Internal Model Control.

C.2. Nomenclature

A_{sin}: Amplitude of sinusoidal wave in control error or in process (output) measurement.

A_{sq}: Amplitude of square wave in control signal.

A_{tri}: Amplitude of triangular wave in control error or in process (output) measurement.

A_u: Amplitude of the on-off control signal.

c_s: Parameter introduced in the integral time settings in the Skogestad method.

d is process disturbance.

Δ: Deviation from operating point.

e: Control error. $e = y_{sp} - y$.

k_r: The relaxation parameter in the Relaxed Ziegler-Nichols method.

K is process gain.

K_c [s]: Controller proportional gain.

K_d is disturbance gain.

K_{i_p} [s]: Process integrator gain.

P_u [s]: Period of sustained oscillations.

T [s]: Process time-constant.

T_c [s]: Closed loop time-constant.

T_i [s]: Controller integral time.

T_r [s]: Response-time, or 63% rise time of step response.

τ [s]: Process time-delay.

u: Control signal (controller output).

u_{man}: Manual control signal (control bias).

y: Process output measurement.

y_{sp}: Setpoint

References

Åstrøm, K. J. and Hägglund, T. *PID Controllers: Theory, Design and Tuning*. ISA, 1995.

Chien, I. L. and Fruehauf, P. S. Consider IMC Tuning to Improve Controller Performance. *Chem. Eng. Progress*, 1990. Oct:33–41.

DiRuscio, D. On Tuning PI Controllers for Integrating Plus Time Delay Systems. *Modeling, Identification and Control*, 2010. 31(4):145–164. doi:10.4173/mic.2010.4.3.

Haugen, F. The good gain method for simple experimental tuning of pi controllers. *Modeling, Identification and Control*, 2012. 33(4):141–152. doi:10.4173/mic.2012.4.3.

Haugen, F. Air heater. http://home.hit.no/~finnh/air_heater, 2013.

Haugen, F., Bakke, R., and Lie, B. Temperature control of a pilot anaerobic digestion reactor. *Submitted to Modeling, Identification and Control*, 2013.

Haugen, F. and Lie, B. On-off and pid control of methane gas production of a pilot anaerobic digestion reactor. *Submitted to Modeling, Identification and Control*, 2013.

Seborg, D. E., Edgar, T. F., and Mellichamp, D. A. *Process Dynamics and Control*. John Wiley and Sons, 2004.

Skogestad, S. Simple analytic rules for model reduction and pid controller tuning. *Modeling, Identification and Control*, 2004. 25(2):85–120. doi:10.4173/mic.2004.2.2.

Tyreus, B. D. and Luyben, W. L. Tuning PI Controllers for Integrator/Dead Time Processes. *Ind. Eng. Chem*, 1992. 31(31).

Yu, C. C. *Autotuning of PID Controllers*. Springer Verlag, 1999.

Ziegler, J. and Nichols, N. Optimum settings for automatic controllers. *Trans. ASME*, 1942. 64(3):759–768. doi:10.1115/1.2899060.